Near Field Channel Modelling through Large Aperture Massive Array Systems and Low-Complexity Pre-processing Robust to Local Mobility

Authors:
Pelayu Cadenas Buelga
Rasmus Birkelund Nielsen

A thesis presented for the degree of
Master of Science

AALBORG UNIVERSITY
DENMARK

Department of Electronic Systems

June 4, 2014

Department of Electronic Systems
Electronic Engineering
Fredrik Bajers Vej 7
9220 Aalborg Ø
Telefon 99 40 86 00
http://es.aau.dk

Title:
Near Field Channel Modelling through Large Aperture Massive Array Systems and Low-Complexity Pre-processing Robust to Local Mobility

Subject:
Multi Agent Wireless Systems

Project period:
WCS 9–10, 2014

Group:
Group 953

Authors:
Pelayu Cadenas Buelga
Rasmus Birkelund Nielsen

Supervisors:
Elisabeth de Carvalho

Copies: 4

Page count: 164

Appendix: 11

Completed: June 4^{th}, 2014

Synopsis:

This Master's thesis's goal is two-fold. On the first hand, an adequate Point-to-Point (P2P) MIMO channel model for a large-aperture array consisting of a massive number of elements is to be constructed. The large aperture forces a Near Field (NF) focus. On the other hand, a low-complexity pre-processing design is to be carried out as a means of MU-access method. Robustness on the users' local mobility is sought. Beamformers both considering inst. CSIT and statistical channel information on the users' local movement are considered.
The P2P channel model is developed through a simplified COST2100 approach. Among other simplifications, a 2D downgrade, a narrowband channel and a NF focus are allowed. The resulting model, tested with relevant metrics, is consistent and goes in accordance with similar channel models.
Two approaches on beamforming were executed. Firstly, linear precoders based on inst. CSIT were considered in order to reveal optimality of a MF precoder, optimal according to literature under the asymptotically large number of antennas. However, discrepancies on inter-user correlation due to the massive array's configuration were unveiled, which motivated an extensive study hereof. Lastly, two sets of statistical precoders were proposed. While most of them are suboptimal with respect to the full CSIT case, it is shown that, at least, performance equivalent to the MF based on inst. CSIT may be obtained. Interestingly, one of the proposed statistical approaches is able to outperform the latter case under some specific circumstances.

Preface

The main concerns of this master thesis, has been the modelling and analysis of a Near Field Channel through a Large Aperture Massive Array System (LA-MASS) while employing low-complexity pre-processing. The thesis has been completed as a long running master thesis during the period from 16^{th} of September, 2013, to 4^{th} of June, 2014. It has been produced by graduate students Pelayu Cadenas Buelga and Rasmus Birkelund Nielsen, under the supervision of assoc. prof. Elisabeth de Carvalho, at the section Antennas, Propagation, & Radio Networking, under the Department of Electronic System at Aalborg University.

The report was been written in LaTeX, and consists of 13 chapters and 11 appendices. Simulations have been performed in MATLAB.

References to literature are denoted in the content as a number, enclosed of square brackets, i.e. [1]. References to chapters, sections, equations, and so on, are appended by their corresponding short hand notation.

Pelayu Cadenas Buelga

Rasmus Birkelund Nielsen

Acknowledgements

We would like to thank our supervisor, Elisabeth de Carvalho, for the extensive support that has been given during the entire course of this Master's Thesis.

A special thanks is given to our families and friends, who have supported us throughout this project.

Besides family and friends, the following people have constituted special support during the development of this thesis.

Patrick Claus F. Eggers *Associate Professor, Department of Electronic Systems, Aalborg University, Aalborg*
General technical counselling, especially discussions regarding channel modelling.

Àlex Oliveras Martínez *Research Assistant, Department of Electronic Systems, Aalborg University, Aalborg*
Continuous technical discussion all over the progression of this thesis.

Inés Cartón Llorente *Graduate student, Wireless Communication Systems, Department of Electronic Systems, Aalborg University*
Discussions regarding results and more general issues.

Andrés Buendía Gil *Graduate student, Wireless Communication Systems, Department of Electronic Systems, Aalborg University*
Discussions regarding results and more general issues.

Enrique Saez Gil *Graduate student, Wireless Communication Systems, Department of Electronic Systems, Aalborg University*
Discussions regarding results and more general issues.

Table of Contents

List of Abbreviations

AOA	Angle of Arrival
AOD	Angle of Departure
BD	Block Diagonalization
BS	Base Station
CCW	counterclockwise
CDF	Cumulative Distribution Function
CDMA	Code Division Multiple Access
CIR	Channel Impulse Response
CN	Condition Number
CSI	Channel State Information
CSIR	Channel State Information at the Receiver
CSIT	Channel State Information at the Transmitter
CW	clockwise
DOA	Direction of Arrival
DOD	Direction of Departure
DoF	Degrees of Freedom
DPC	Dirty Paper Coding
DS	Delay Spread
EGC	Equal-Gain Combining
FC	Far Cluster
FDMA	Frequency Division Multiple Access
FSPL	Free-space path loss
GSCM	Geometry-based Stochastic Channel Model
ISI	Inter-Symbol Interference
LA-MASS	Large Aperture Massive Array System
LC	Local Cluster

LHP	Left Half Plane
LOS	Line Of Sight
LSP	Large Scale Parameter
MBC	Multiple Bounce Cluster
MF	Matched Filter
MIMO	Multiple Input Multiple Output
MISO	Multiple Input Single Output
MMSE	Minimum Mean Square Error
MPC	Multipath component
MRC	Maximum Ratio Combining
MT	Mobile Terminal
MUI	multi-user interference
MU-MIMO	Multi-User MIMO
NF	Near Field
NPCG	Normalised Parallel Channel Gain
NLOS	Non Line Of Sight
P2P	Point-to-Point
PAP	Power Angular Profile
PDP	Power Delay Profile
RBD	Regularized Block Diagonalization
RHP	Right Half Plane
RMS	Root Mean Square
RMSE	Root Mean Square Error
SBC	Single Bounce Cluster
SC	Sum Capacity
SD	Selection Diversity
SDMA	Space Division Multiple Access
SIMO	Single Input Multiple Output
SINR	Signal to Interference plus Noise Ratio
SIR	Signal to Interference Ratio
SISO	Single Input Single Output
SNR	Signal to Noise Ratio

SR	Sum Rate
SVD	Singular Value Decomposition
TDD	Time Division Duplex
TDMA	Time Division Multiple Access
ULA	Uniform Linear Array
VR	Visibility Region
ZF	Zero Forcing

List of Figures

List of Tables

Chapter 1

Introduction

This chapter is aimed at providing full account of the main characterising features of both Multiple Input Multiple Output (MIMO) and Massive-MIMO systems. It is divided into two main sections, covering MIMO and Massive-MIMO, respectively.

1.1 Multiple Input Multiple Output (MIMO)

This section addresses the significance of Multiple Input Multiple Output (MIMO) systems nowadays. It is mainly based on [11].

1.1.1 MIMO framework

A desire to access the Internet wirelessly has grown dramatically over the past years. The reasons for this are founded on two key facts: first of all, mobile communications have experienced an unprecedented increase over the recent years; second, the Internet itself and its applications have expanded tremendously. Consequently, a demand for a much higher data volume has appeared. This implies a serious challenge with respect to the currently deployed technology. MIMO systems are considered to be a possible solution to this challenge as possessors of the ability to provide with this enhanced service and to meet the challenges that wireless communications will potentially face. Briefly, MIMO systems are a promising technology to achieve high data rates.

1.1.2 Single Input Single Output (SISO) links

Single Input Single Output (SISO) systems constitute the simplest wireless scenario. They consist of a single antenna at each end (receiver and transmitter), as shown in fig. 1.1 on the next page. However, if we assume that one of the ends is a Base Station and the another one is a user, we could presume that in a real scenario there would be a number of users and not only one of them. In a simple scenario, each user would have a single antenna. Consequently, multiple users would have to share the same medium to simultaneously perform their transmissions. This could lead to signal cross, which might eventually yield a communication breakdown. This problem is tackled via multiple access techniques to separate users, being the fundamental ones Time Division Multiple Access (TDMA), Frequency Division Multiple Access (FDMA) and Code Division Multiple Access (CDMA).

- TDMA separates users forcing them not to transmit/receive simultaneously. To that purpose, users are assigned a time slot in which they control the channel. Assigned time slots have the same duration for all of the users.
- FDMA separates users allocating them in different parts of the spectrum (different frequencies). Users transmit simultaneously.

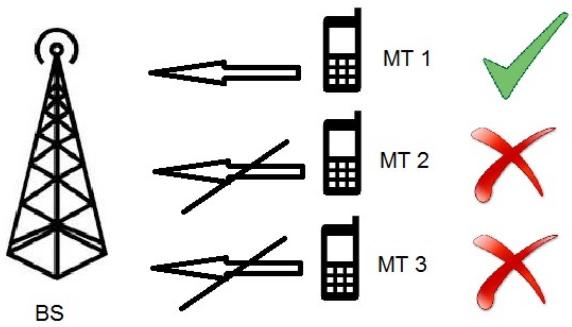

Figure 1.1 *SISO system, assuming single-antenna Tx (BS) and single-antenna Rx antenna. A TDMA scenario is featured with three Mobile Terminals (MT) and a BS. Only MT1 has access to the BS in the depicted scenario (graphical depiction of MT1's TDMA slot in a given TDMA frame.)*

- CDMA separates each user's signal with a code specific to that user and orthogonal to the codes used by the rest of the users. Users transmit/receive simultaneously and they use the same frequency.

1.1.3 Single Input Multiple Output (SIMO)/Multiple Input Single Output (MISO) links

In the SISO case, the received signal is sometimes too weak, which leads to unacceptable error rates or simply communication failure. To combat this problem, a technique called diversity can be employed. Diversity relies on the use of multiple copies of the same signal, that the receiver selects or combines. The idea is that even if one copy of the signal is weak (in a fade), it is expected that not all of them are. To minimise the probability of all the signals facing bad propagation conditions simultaneously, the copies of the signal should be independent to each other. In other words, the links through which those copies travel should be orthogonal to each other.
There are three main domains of diversity:

1. Time: copies are generated transmitting the signal numerous times. Requires only one antenna at each end.

2. Frequency: copies are generated transmitting the signal at different parts of the spectrum. Requires only one antenna at each end.

3. Space: Copies are generated simultaneously and at the same frequency by many antennas, that can be located at the Base Station (BS) (in this case diversity is called large-scale diversity) or/and at the terminal (small-scale diversity). In case of large-scale diversity with a single user having only one antenna, the system is known as Multiple Input Single Output (MISO). In the case of small-scale diversity, having the BS only one antenna, the system would be called Single Input Multiple Output (SIMO).

There are in turn three main diversity techniques:

1. Selection Diversity (SD). The idea is to select the best of the incoming signals. The criterion used to determine which of the signals is the best one corresponds to the largest channel coefficient, which translates into the largest arriving signal's SNR.

2. Equal-Gain Combining (EGC). The idea is to add the incoming signals coherently. Thus, their phases need being aligned previously. This phase alignment is done applying phase weights to each of the incoming signals. In the optimal case, twice as much signal could be retrieved.
3. Maximum Ratio Combining (MRC). The idea is to first scale the incoming signals suitably so that stronger signals have a higher weight and them add them coherently employing phase weights again. If the scaling factors are selected adequately, MRC is the technique that yields the best results.

Diversity weighting and beamforming: glimpse on MIMO spatial exploitability

In general, application of weights to signals received or transmitted by multiple antennas is called beamforming, being those weightings applied for diversity purposes or not. This document will refer to beamforming as *weighting* or *diversity weighting* when it is for diversity purposes and *beamforming* otherwise. Diversity optimal weighting for the reverse link is still valid for the forward link (assuming an invariant and reciprocal channel at the instants when weighting is applied on each). It must be noted that diversity benefits come at a cost since they require more system resources. Another disadvantage is that diversity is a process of diminishing returns: the gain resulting from two antennas is lesser that the gain resulting from three of them in relative terms and so on.
Finally, it must remarked that in a general purpose situation (taking beamforming as a wide sense antenna weighting term and not only for diversity purposes), the application of weights at multiple antennas or beamforming principle allows the radiating station to point the energy into specific directions (which potentially means that more than one user can be accommodated) and/or to null the energy in some others (which could yield interference suppression).

1.1.4 Multiple Input Multiple Output (MIMO)

Spatial diversity relied on the use of multiple antennas at one of the ends of the link. When this is applied at both ends, an additional benefit on top of diversity gain appears. That is called **spatial multiplexing gain** and responds to the ability to send several data streams simultaneously and independently. Data streams should travel along orthogonal paths. These might be created via beamforming if the beams are sufficiently separated. In general, though, they are created as per the Singular Value Decomposition (SVD) of the channel matrix, via pre-coding at the transmitter and post-coding at the receiver. When beamforming is built like that, it is known as eigen-beamforming, as will be seen later in this section.

MIMO spatial exploitability. [1, 2, 5, 11, 12]

Diversity and beamforming had already been reviewed in the SIMO/MISO section (sec. 1.1.3 on the facing page). A new spatial domain enters the picture now: multiplexing.
A MIMO channel can then be exploited in three different domains: beamforming, diversity and multiplexing.

- **Beamforming** refers to directing the power in a specific angular direction so that an increase of the gain (antenna pattern) at that specific angular direction occurs. The maximum beamforming gain that can be achieved is $M \cdot N$, being M the number of transmit antennas and N the number of receive ones.[1] The result of beamforming can be:
  - A higher SNR by focusing the energy towards intended users (if there is LOS) or even significant scatterers. This results in an antenna gain.

[1] All trhoughout this project, the number of antennas at the base station can be either written as M or M and the number of antennas at the user, as eiterh N or N.

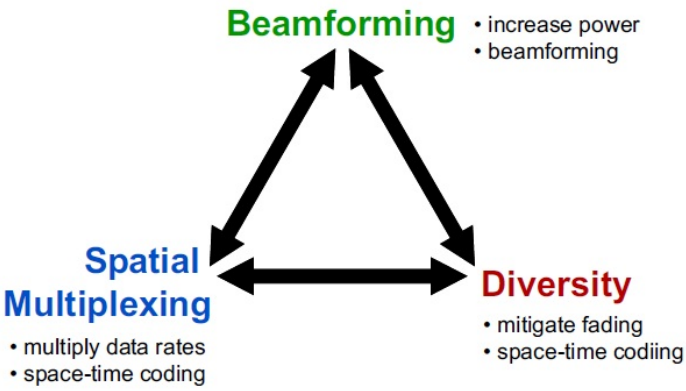

Figure 1.2 *Three MIMO domains and their benefits. [1]*

  - A higher SINR by focusing nulls to unintended directions, which results in interference suppression.
  - Space Division Multiple Access (SDMA) as an alternative to conventional multiple access techniques.

  In any case, users (if LOS), significant scatterers or interferers need to be localised via localisation algorithms. Examples of those are the ESPRIT, MUSIC, SAGE or CAPON algorithms.
  Improved SNR or SINR levels can be either be used to **decrease error rates** (thanks to the increase in power) or to **increase the data rate** (switching to higher-order modulations). Normally, Channel State Information (CSI) is taken for granted at the receiver, but not at the transmitter. However, if CSI is known at both the receiver (Channel State Information at the Receiver (CSIR)) and the transmitter (CSIT), then beamforming can be done as per the SVD of the channel matrix **H** (via pre-coding and post-coding). In this case, beamforming is renamed as eigen-beamforming. In eigen-beamforming, the concepts of beamforming and multiplexing blend together. In eigen-beamforming, normally an optimal power allocation is performed (waterfilling is generally carried out).

- **Diversity** responds to sending several replicas of the same signal expecting to increase the fading channel's reliability (**decrease error rates**). The degree of diversity is limited by the number of channel coefficients in the channel matrix, and so, by $M \cdot N$.

- **Multiplexing** refers to the capability in MIMO to send several substreams of information simultaneously and orthogonally (independently). The maximum number of multiplexed substreams is, under the best channel conditions, $min(M, N)$ (since usually in MIMO $N < M$, N is normally limiting). Otherwise, the maximum number of data streams that can be sent simultaneously lowers according to the environment's capability to support such transmission. In a scattering environment, that relates directly to the *scattering* or *multipath richness*. A scattering environment is rich if it supports multiplexing to a high extent. In any case, the degree of spatial exploitability with respect to multiplexing is given by the channel matrix rank, which includes the three factors given above: M, N and multipath richness. Multiplexing results in a **higher data rate**.

The degree of exploitability is limited, though, so there is a tradeoff between the three domains. If one of the domains is chosen to work at full degree, then the others cannot be invoked. The only exception is the multiplexing domain, since its full degree accounts as much as min(M,N) under the best channel conditions. If working at full multiplexing degree, then beamforming cannot be summoned but diversity can be employed at a reduced extent. Fig. 1.3 features MIMO spatial domains just like fig. 1.2 on the facing page, although benefits are narrowed down.

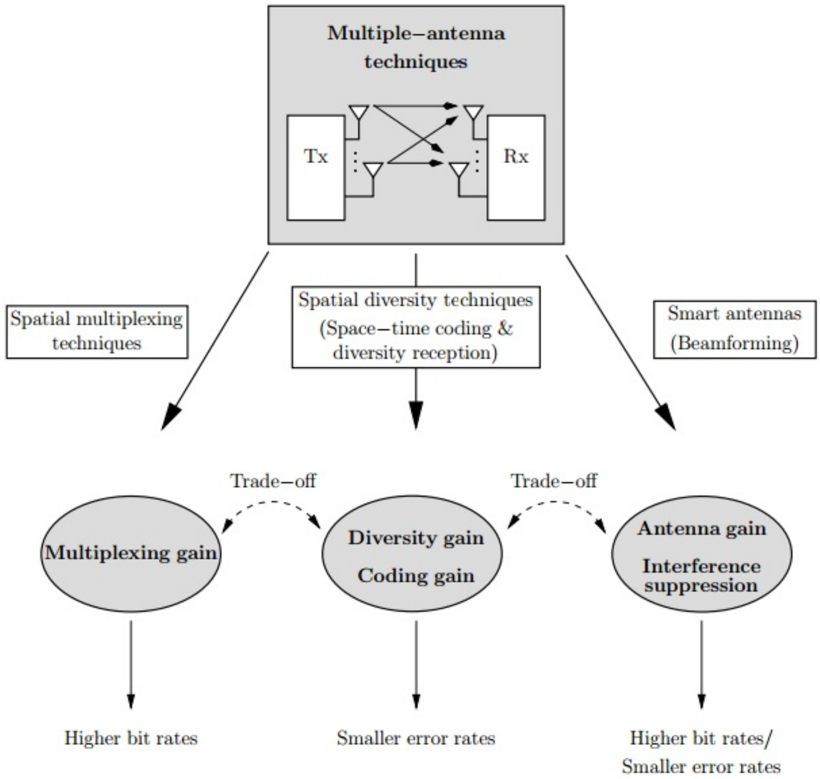

Figure 1.3 *Three MIMO domains and their benefits. [2]*

Multiplexing is the domain that always leads to an increase of the system's data rate; however, this can be done as per beamforming as well under certain focuses as covered above. As explained in chap. 2 on page 11, the initial aim of this project is to analyse the conditions and scenarios in which data rates can be pushed upwards under special MIMO array features (Massive MIMO), and so we will initially narrow down the domain exploitability to the multiplexing realm. Multiplexing does not consume the total MIMO spatial expolitability, so it is a suitable option for future work on others: if working at full degree, only diversity can be invoked; otherwise, both diversity and beamforming can be summoned. Multiplexing+beamforming is the sought context (p.eg., eigen-beamforming). Ideally and in the optimal case, techniques that do not use multiplexing at full degree allowing the possibility to use beamforming are to be combined with techniques that at the same time optimise the maximum achievable data rate. Both goals are met at the same time by using waterfilling, an optimal power allocation technique at the transmitter, which potentially cuts down the non-powerful subchannels (lowering the multiplexing exploitability degree of use) and yields at the same time the maximum achievable rate. This will be fully detailed in subsequent chapters.

1.1.5 Multiplexing and beamforming context: single-user and multi-user perspective

The lines above account for the three domains of spatial exploitability of MIMO systems, being multiplexing the domain that could yield higher data rates. The multiplexing domain, if not at full degree, might leave space for beamforming application. In that case, benefits might be categorised under a single-user and a multiple-user framework, as reviewed below: MIMO can improve the performance of a communication channel from two viewpoints.

Single user perspective

MIMO is able to increase the data rate of the transmitted data without increasing the transmit power and without increasing the radio frequency bandwidth (multiplexing).

Multiple user perspective

In a communication system, there are normally several users transmitting at the same time and using the same frequency. Conventionally in SISO systems, users were separated using one of the multiple access techniques: TDMA, FDMA or CDMA. However, MIMO is able to accommodate users simultaneously without making use of any of these techniques via beamforming. One of the beamforming techniques employed by MIMO is the Space Division Multiple Access (SDMA), which separates each of the users' transmitted signals. In fig. 1.4, after an adequate beamforming, y_{out_1} is only dependant on x_1 and y_{out_2} is in turn only dependant on x_2, respectively.

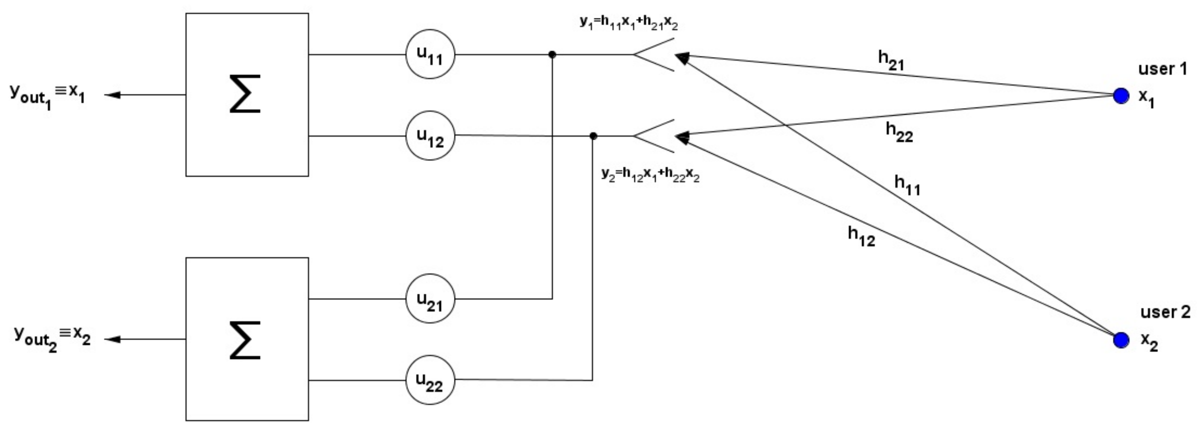

Figure 1.4 *Two-user SDMA with a BS consisting of two antennas.*

Conditions for work under a multiplexing and beamforming perspective

Conditions for MIMO to work are given by the algebraic solutions of the linear system of equations that involves the channel coefficients and is made to create beams. These conditions translate into requirements to the channel. Two channel situations can be told apart: link in the free space and with obstacles in the middle. In the free space case, the requirement specifies that antennas at both ends should be separated enough so that independent links can be established. If there are obstacles in the volume that the link covers, those should be appropriately located so that multipath components are successfully created. Multiplexing can be understood as taking advantage of the multipath created by those obstacles as a controlled multipath to make the different signals reach the receiver. Obstacles are usually called scatterers. Scattering richness refers to the ability of scatterers to successfully create adequate multipath and support multiplexing. It is related to their location and density. In the free space case, if there is insufficient separation between ends, multipath created by scatterers can constitute a solution.

1.1.6 MIMO research and development

The concept of MIMO was first introduced in 1987 although it is still a topic under analysis and research. The main areas to cover are:

- Radio
- Signal processing

- Coding
- Networking
- Hardware

1.2 Massive MIMO

This section reviews the key points of Massive MIMO [2] systems and emphasises its potential advantages and challenges. This section is based mainly on [13, 14, 3].

1.2.1 MIMO future outlook

MIMO technology is thought to be the basis for the future 5G architecture. The three main candidates are the following deployments:

- Coordinated MIMO. Also, Network MIMO or Cooperative MIMO. Its concept lies on a coordinated transmission from multiple Base Stations.
- Massive-MIMO. Conceptually, Massive-MIMO is Multi-User MIMO (MU-MIMO) having the Base Stations a high number of antennas and assuming that the number of users to be served is much smaller than the number of antennas at the BSs. Massive MIMO fundamentals will be fully reviewed in the forthcoming pages.
- Millimetric MIMO. It involves work in the millimetric band.

The next pages will address Massive-MIMO systems.

1.2.2 Concept of Massive-MIMO

The concept of Massive MIMO relies basically on the MU-MIMO notion with a very high number of antennas at the Base Station (see fig. 1.5) In practice, a ratio of at least ten for the number of antennas at the Base Station and the number of users is taken in Massive MIMO systems [13], constituting this an excess of BS antennas. This excess together with the fact that the total number of BS antennas is very high contributes to provide Massive-MIMO systems with unique advantages as next pages will elaborate.

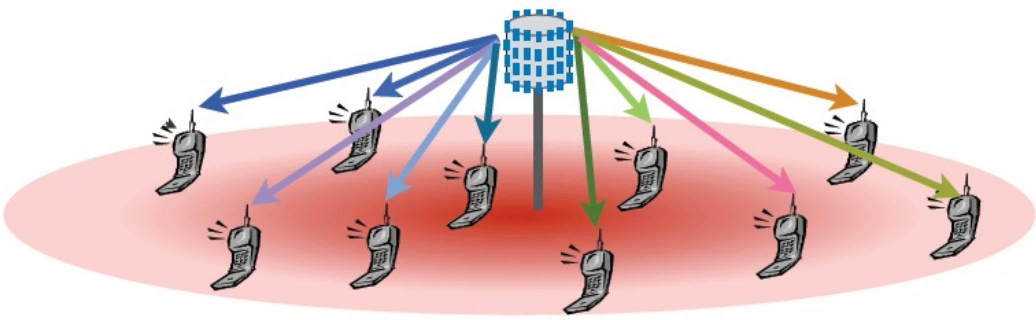

Figure 1.5 *Massive-MIMO deployment [3].*

[2]Massive MIMO will be also be written in this project like massive MIMO, uncapitalised

1.2.3 Advantages of Massive-MIMO systems

Massive-MIMO systems possess unique and singular characteristics that other systems do not have. This is mainly due to the high number of antennas at the BS, since that high number of antennas constitutes an excess number of antennas at the BS to cover all the links to the users and because a beamforming technique (normally equivalent to an MRC's matched filter [13, 15, 16]) is employed.
If we assume the BS has M antennas and is serving K users within its cell, then the channel matrix **H** can be written as in eq. 1.1.

$$\mathbf{H} = \begin{bmatrix} h_{11} & h_{12} & \cdots & h_{1M} \\ h_{21} & h_{22} & \cdots & h_{2M} \\ \vdots & \vdots & \ddots & \vdots \\ h_{K1} & h_{K2} & \cdots & h_{KM} \end{bmatrix} \tag{1.1}$$

In this situation and if $M \gg K$, then:

- The fact there is an excess M-K number of antennas provides the system with M-K unused Degrees of Freedom (DoF). Those can be used to invoke other MIMO spatial domains. If not working at full multiplexing, beamforming can also be employed, for instance, for inter-cell interference elimination.

- (Optimal) MRC beamforming makes the power per link be approximately constant for all links. For the $\mathrm{j^{th}}$ channel:

  $$P_i = \frac{\sum_{1 \leq j \leq M} \parallel h_{ij} \parallel^2}{M} \approx \text{constant} \tag{1.2}$$

  where $\parallel \; \parallel$ is the absolute value operator.

- The fact the number of antennas in the BS is very large (↑↑M) implies:
  - That the thermal noise and the small-scale fading can be averaged out, due to the Law of Large Numbers and presuming the former have zero mean.
  - That the transmit power can be lowered making use of inexpensive low-power components, improving the radiation efficiency. If this is combined with a very-large aperture MIMO system, then Near Field (NF) operation with less transmit power is possible. That power save can be of an order of magnitude or even more for Very Large arrays according to [13].
  - That the employment of a matched filter precoder is assumed to behave optimally, making possible that energy is focused on smaller regions in space, where components add up constructively.
  - That throughput improvements are achieved because of the multiplexing gain inherent in MIMO systems, provided the creation of orthogonal paths for the independent data links. From the Multi-User perspective, techniques like SDMA are employed to this purpose. Moreover, a massive number of antennas can be used under the perspective of both an increase of transmit power or reduction of the total transmit power employing less powerful elements. If the former is opted, then the Signal to Noise Ratio (SNR) at the users is lifted considerably, which results into a higher throughput.

1.2.4 Challenges of Massive-MIMO systems

The same way Massive MIMO has some unique features that make it different to other systems, it also involves some challenges. Those are accounted for below:

- Links should be (nearly) orthogonal so that MIMO work conditions are satisfied. In literature [13, 14]. this is said to happen under favourable propagation conditions. In the multi-user case, if $\mathbf{H}_i$ is the channel matrix related to the ith user and $\mathbf{H}_j$ is the channel matrix related to the jth user, then both links are (nearly) orthogonal to each other if:

$$\mathbf{H}_i{}^{\mathrm{H}} \cdot \mathbf{H}_j \approx 0, i \neq j$$

- The fact beamforming is looked for for users' spatial division (and to yield a beamforming gain on those being targeted) requires some spatial multiplexing techniques like SDMA, which in turn requires some form of knowledge about the channel in the form of CSI. Application occurs at both the uplink and the downlink. CSI is in practice acquired at the uplink and reciprocity for the downlink is applied (this is because estimation at the BS, being proportional to the number of users, would cause too much overhead and delay; at the users, it is proportional to their own number of antennas, thus much less computationally demanding). Correct CSI acquisition is then an issue. Besides, CSI acquisition forces to Time Division Duplex (TDD) operation.
  Uplink CSI acquisition can be done from either pilots or data itself. Pilot contamination might happen when users from neighbouring cells are considered to be part of the set of users of a specific BS, which can impair CSI acquisition. This lies behind the limited training sequences used per cell, which forces reuse in neighbouring cells, yielding the possibility of contamination at the BS from users in neighbouring cells. A possible solution for the pilot contamination problem lies in coordination.

- As already mentioned, the excess number of antennas at the BS provides the system with some extra DoF. The exploitation of those unused DoF is also an issue. As already hinted, those could be used for inter-cell interference cancellation.

Chapter 2

Project Goal

As discussed in the previous chapter, MIMO technology is becoming more mature, and incorporation into emerging wireless standards is more prevalent e.g. LTE, 802.11n (WiFi), 802.16 (WiMAX), etc. MIMO technology incorporation has been applied mainly to outdoor scenarios. Such has has been the case of Massive MIMO. The scenario tackled in this project is in turn a large venue, in which a Large Aperture Massive Array System (LA-MASS) array is to be deployed. The fact the aperture of the considered array is very large determines some special features which will be thoroughly review throughout this report.

2.1 Problem definition

The eventual aim of this project tackles a multi-user simultaneous access to the channel, being the BS a LA-MASS array with an aperture of tens of metres or even more.
Current assumptions for scenario modelling allow for simplified channel models. Therefore, simulations might be unrealistic in some scenarios . Channel modelling with very-large aperture arrays is to be done within the Near Field Region, since very large apertures bring about large Near Field Regions, inside which the coverage area is found. An array's Near-Field analysis will be presented in Chap. 4 on page 27. This is the area that has been considered to apply the spherical-wave model, since propagation in the Near Field does not allow to model transmitted waves as planar (like ordinarily under a Far Field scope).
Finally, and in regards to channel modelling as well, it must be remarked that models will vary according to a single-user or multiple-user scenario. In the first case, we will refer to a *Point-to-Point model*, while in the second and more reality-representational case, we will address a *multi-user case*. Mainly, the multi-user problem address simultaneous user access to the channel, which requires some form of pre-processing design or beamforming. The focus in this thesis is set upon a low-complexity beamformer robust to users' local mobility.

Course of action summary

The main issues to be researched in this project are,

- *Channel characterisation for a large-aperture BS with a massive number of antennas in the Near Field and in a realistic scattering environment.*
- *Low-complexity beamforming design under the scope of robustness to the users local mobility.*

2.2 State of the art and motivation.

MIMO transmission utilises several antennas at both ends of a communication link. In single-user transmission and in highly scattering environments, the scatterers make the signal from each individual transmitter appear highly uncorrelated at each receive antenna, which allows to differentiate each transmitted signal if the correct processing is carried out. This yields an extremely spectrum-efficient technology [17, 18]. In reality, the achievable spectral efficiency is limited by the number of uncorrelated paths between the transmitter and receiver that can be obtained (relates to multipath richness) and the relative powers of the corresponding communication subchannels. This results in a requirement on the minimum number of scatterers. In NLOS scenarios, this responds to the will to achieve capacities predicted by the i.i.d Rayleigh fading model. In contrast, for environments with a strong dominant LOS component, the effective spectral efficiency is usually very low due to the linear dependency on the phases for the LOS ray [19, 20] which are yielded by the planar-wave transmission assumed in conventional MIMO systems. In some scenarios, though, the presence of a dominant LOS component can be turned into advantage ([7]), as elaborated below.

However and in any case, conclusions are to be confirmed under a wide range of different scenarios for both the LOS and the NLOS cases. To this purpose, scenario-sensitive realistic MIMO channel models are to be employed. Those are mainly given by the scattering models and the wave transmission models.

- The scattering models include factors such as disposition of the scatterers, interaction of the scatterers with the environment, etc, which eventually result in a scattering channel matrix. The scattering environment may or may not be rich (supporting multiplexing), which translates into the capacity obtained as per the scattering channel matrix.

- Wave transmission models, namely plane-wave models or spherical-wave models (the latter indicated for short-range scenarios, [7]) describe the transmission of the wave through the environment and are related to the location of the receive antenna with respect to the transmit antenna (Far Field or Near Field). Short-range models bring along the problem of inter-element spacing at the arrays at both ends. Again in [7]), it is claimed that in such scenarios, a larger antenna spacing than ordinarily is sought to achieve full-rank.

MIMO systems have been studied deeply for outdoor scenarios and so Far Field and in turn planar-wave transmission has been assumed (in order to reduce complexity). Research has not been done at such a high extent when it comes to large-aperture arrays (working under a Near Field focus), which are the main concern in this project ([21]). In such scenarios, the presence of a strong LOS component is a reasonable assumption. When this happens, it is stated in [7] that full rank might be obtained, but that this requires some non-customary features, namely larger inter-element separations yielding larger apertures.

Regarding the scattering models that have been commonly employed, many factors which may significantly degrade the overall MIMO system performance have been revealed. For example, [22] and [23] have shown that among such factors, multipath richness, correlation of channel coefficients or keyhole effects are critical. Furthermore and as stated above, sometimes the presence of a strong LOS component is taken as a degradation. The reason for this is because a strong LOS component usually results in a unity-rank channel and such a channel is unable to support multiple parallel streams. However, as already mentioned above, investigation on this is provided in [7], concluding that with the adequate wave model and a large aperture array, the LOS problem might not be such and the presence of a LOS might even be beneficial in terms of capacity. This is of substantial importance with respect to this project, since it tackles directly the scenario to be examined. Thus, it is one of the main motivations for this project.

MIMO technology has matured to such a state that it is already being incorporated into standards such as LTE. Yet, this type of MIMO system accommodates up to four antenna ports at e.g. the Base Station ([24]). Whether it being Point-to-Point MIMO or Multiuser-MIMO, there are limitations on capacity and performance.

Extending the notion of MIMO, large aperture MIMO systems with a massive number of

elements at the BS many more antenna elements than classical MIMO systems. That number could reach hundreds of antennas, constituting an excess number of antennas, which brings along the benefits but also the challenges accounted for in chap. 1 on page 1 and in this same chapter.
Mainly, the motivation for this project is brought by the following factors:

- Lack of short-range (Near Field) scenario models for large-aperture arrays with a massive number of elements, which yield promising advantages in terms of performance with the inherent presence of LOS components in those scenarios.
- Massive-MIMO potential benefits in terms of data rates and simultaneous multiuser-energy focusing through adequate beamforming, which would potentially yield a larger coverage range, an enhanced energy efficiency due to energy focusing and a reduction of the inter-cell interference due to the lack of energy spill-over.

Part I

Channel modelling

Chapter 3

Channel model basics

The aim of the first part of this project is to define the channel characterisation under a large-aperture array scope, which will in turn determine multi-user access. This definition will eventually result in the definition of the channel elements as per the proposed modelling.
This chapter contains the milestones of this channel model and grants is main features. The subsequent chapters will refine and narrow down these initial channel pillars in order to complete the definition of the channel matrix. Once the channel matrix is completely determined, performance metrics will be introduced. These performance metrics will serve to evaluate a large-aperture massive MIMO system's expected benefits (see previous chapters).

3.1 Aim

The aim of this chapter is to give account of the milestones of a practical short-range channel model, in the form of a generic channel matrix and an input-output relation. The basic measure of performance, namely channel capacity, will also be briefly introduced.

3.2 Scenario features

As proposed in [21], the scenario in which this project is to be focused has the following features:

- Is a large venue.
- Contains a single Base Station serving a number of K users, where $M \gg K$. The Base Station is made up of a single antenna, namely a large-aperture array consisting in turn of a very large number of elements M. The large-aperture array may hereinafter be called large-aperture array, very large-aperture array or simply massive array, case-insensitively.
- Each user terminal is assumed to be made up of an array containing N antennas, where $N \ll M$.
- The Massive Array is thought to serve all the users within its coverage area simultaneously.
- Due to the nature of the Massive Array, a LOS component between the array and the users is a reasonable assumption.
- The large venue where the massive array is deployed contains scatterers: building elements, furniture, other users, etc. Thus, the channel will contain multipath components. See section below on channel assumptions in this matter.
- Users are assumed to suffer local mobility, something that tackles the second part of this thesis, i.e. pre-processing design. In the Point-to-Point case, that is to say, in the first part of this project, the channel's performance does not take mobility into account.

Fig. 3.1 features a stadium, which is a possible scenario that fits the description above. The massive array is located at the ceiling and can be seen at the bottom right-hand corner of the image. An intended user (red person icon) receives a LOS component (red line) and numerous multipath components due to the scatterers; in this case, some scattering components as per other users (black lines) and the stadium itself (blue lines) have been represented. Only one of the massive array's elements has been selected to easily depict the system. By extension, all the other elements would have a similar behaviour.
This is only an example aimed at representing the type of scenario this project tackles and in any case restricts the scenario to the case it features. Other proposed scenarios are a shopping centre, a concert site or an airport hall [21].

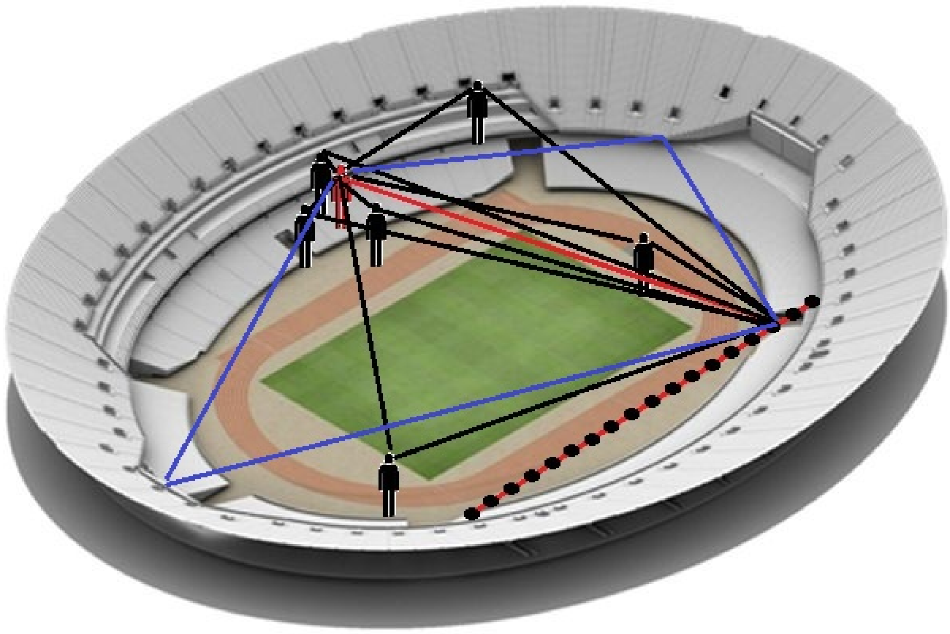

Figure 3.1 *Example of a representational scenario. Stadium picture: [4]*

3.3 Channel type I: Wave transmission model

A plane-wave transmission model is widely employed for wireless communications systems, due to simplicity reasons. This normally fits the scenarios which are to be analysed, including MIMO systems. However, in the case of the current project, a Massive MIMO short-range scenario is examined. Due to this, users are likely to be located within the massive array's Near Field region, although there are parts of the service area that fall outside this region, as yielded by results in chap 4 on page 27. This makes the plane-wave transmission model be inadequate and, according to [7] it can even lead to pessimistic results in terms of performance. This source claims as well that for short-range MIMO systems (being Massive-MIMO or not), a spherical-wave transmission is to be used instead. The spherical-wave model is further elaborated in chap. 5 on page 37. In this chapter, the inter-relation that a spherical-wave transmission model has with the presence of LOS components in the channel, which is again the case of the scenario in this project, is also covered. In brief, the use of the spherical model for the LOS provides the channel with richness even without the presence of any scatterers whatsoever via a large antenna element spacing that in turn yields a large-aperture array.
It is also claimed in [7] that in the presence of multipath, the spherical model should still be applied (being this the case we deal with in this project).
In the same line, it is concluded that, in the presence of LOS and adjusting the array geometries at both ends of communications so that the antenna spacing is high in both, performance can

be dramatically improved, which is one of the main motivations in this project.
Finally, it can be extracted from the same source that the distance limit below which the plane wave cannot be applied any more without making an error higher than 50% in terms of capacity (so forcing to work with the spherical model) is, in a relevant scenario to this project, lower than the Far Field distance. In other words, the short-range as defined in [7] is contained within the Near Field Region of the array. As argued in chap. 5 on page 37, the short-range region will be approximated by the Near Field Region of the massive array, in which the spherical wave-model will be applied. This motivates the study of the Near Field Region of an array, done in chap. 4 on page 27. The study will be narrowed down to a Uniform Linear Array (ULA) (array with a linear geometry).

3.4 Channel type II: Space-time channel. MIMO Models.

Wireless communication channels response $\mathbf{H}$ varies in the most general case according to three phenomena [5]:

- **Time t $\rightarrow$ H$\equiv$H(t).**
  Channel response may change over time. Time dependency can categorise channels into time-invariant and fading channels. In the latter case, fading can be fast or slow. (see subsec. 3.4.4 on page 22).

- **Angular direction $\varphi \rightarrow$ H$\equiv$H(φ).**
  Channel response varies according to the angular directions along which energy is expected to travel, given by the energy angular distribution. This angular distribution might be calculated as per the Directions of Departure/Arrival (DOD and DOA, respectively), which would yield a Power Angular Profile (PAP), which would in turn yield an angular spread. The environment might significantly influence the angular distribution.
  The angular direction is a two-fold variable. In 3D environments, it is usually defined by the azimuth angle (ϕ) and the elevation angle (θ):

  $$\varphi \equiv (\phi, \theta) \tag{3.1}$$

- **Delay $\tau \rightarrow$ H$\equiv$H(τ).**
  Channel response will also depend on the delayed incoming signals, should the environment cause multipath. This is given by the delay (or temporal) distribution. Like with the angular case, the temporal distribution can be calculated as per the incoming signal's delay, which can build a Power Delay Profile (PDP) and eventually a delay spread. Needless to say, the environment plays an essential role here. The delay distribution together with the transmit signal's symbol period branches out channels into Narrowband and Wideband channels, as explained in subsec. 3.4.2 on page 21

Fig. 3.2 on the following page shows the angular and delay domains of some channel response and serves to grasp the space-time concept.

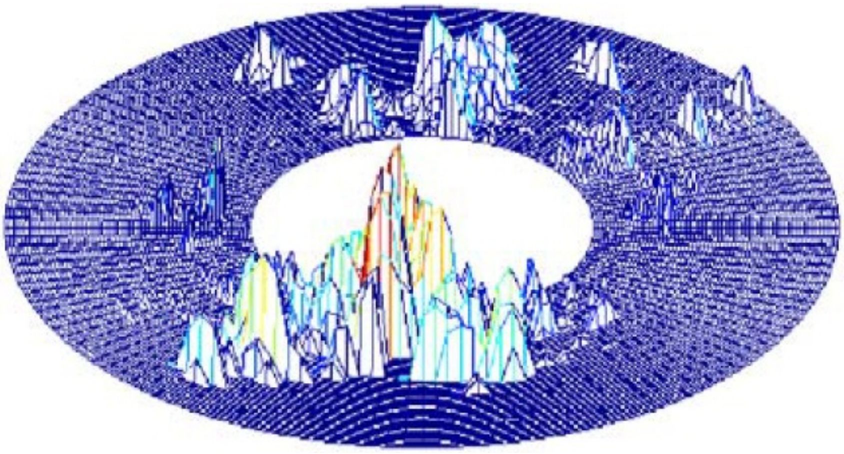

Figure 3.2 *Space-time channel response. Angular response (azimuth axes) and delay response (radial axes). [5]*

The angular and delay distributions are generally given by a joint distribution function $p(\tau, \varphi)$, since they both depend on each other. In principle they cannot be split into differentiated distribution functions. However, in practice some environments allow to do so. In general, this is the case outdoors. Indoors mutual influence is more intuitive (signal might enter a room through a window, or be guided along a hallway, for instance). Since the joint distribution depends on the environment at a high extent and is inherently given by the model being used, a correct and accurate scattering channel model has to be carried out.
Regarding the MIMO case exclusively, typically models can be categorised into two types. Let [5, 11, 8] serve as some reference samples to this. These two types are:

1. **Deterministic** - Time consuming and complex. Only used in small indoor environments. Examples: Ray-tracing based models.

2. **Stochastic** - Based on realisations of the channel. They rely on a limited number of parameters to effectively describe the channel statistics in different domains. According to [8], stochastic models can be sub-categorised into two groups: analytical and physical.

   i **Analytical** models characterise the channel mathematically and include the antenna effects (antenna+environment).

   ii **Physical** models characterise the channel matrix as per the radio waves' delay, the Direction of Departure (DOD), the Direction of Arrival (DOA) and the complex path weight. They do not include the antenna effects (environment, only).
   A subgroup of MIMO stochastic physical models is constituted by the **Geometry-based Stochastic Channel Model (GSCM)** types. The COST family models (259, 273 and 2100) are GSCM.

   Examples of stochastic models can be the COST family (already mentioned), the Kronecker model (correlation-based, analytical) or the Weichselberger and Brown & Eggers models (eigenmode-based, analytical).

3.4.1 Space-time channel definition: MIMO model selection.

MIMO model selection: simplified COST2100.

Eventually, space-time models yield a channel response $\mathbf{H}$ that depends on time, angular direction and delay:

$$\mathbf{H} \equiv \mathbf{H}(t, \varphi, \tau) \tag{3.2}$$

These dependencies are given by the channel model that best fits the scenario to be tackled and are still impaired by its accuracy. As argued in chap. 6 on page 43, COST2100 model is the one that would best fit the scenario proposed for this project. This scenario is accounted for in sec. 3.2 on page 17 in this chapter. However, as also elaborated in chap. 6 on page 43, implementation of the model as per COST2100 is impaired, among other factors, by the lack of relevant mathematical public information existing on this model. It is mainly for this reason that a simplified version of the COST2100 model will be implemented in this project. On top of this, the channel type will be narrowed down (see next subsection), which will in turn downscale the already simplified COST2100 model.

3.4.2 Delay domain downscale: Narrowband channel.

Channel types in the delay domain.

Channels can be either narrowband or wideband according to the relation between the channel's Delay Spread (DS) due to multipath (given by the delay distribution) and the arriving signal's symbol period (T_s).

- If the arriving signal's symbol period is much greater than the delay spread (DS $\ll T_s$), then the response in frequency is considered approximately constant due to the narrow frequency band a large period symbol brings about. In other words, the channel is flat in frequency (if it fades in the frequency domain, fade is not frequency-selective but flat). Channels like these are called **Narrowband Channels** due to this issue. Narrowband channels are unable to resolve the different incoming multipath components, and so, can do away with the delay dependency.

$$\mathbf{H} \equiv \mathbf{H}(t, \varphi) \tag{3.3}$$

  Narrowband channels might suffer from signal temporal dispersion in the form of Inter-Symbol Interference (ISI), although it can be avoided with techniques like the guard interval.

- If the delay spread due to multipath is much greater than the arriving signal's symbol period ($T_s \ll$ DS), then the channel will suffer from frequency-selective fading. This is due to the large bandwidth a signal with a very short symbol duration has. Accordingly, channels like these are called **Wideband Channels**. Wideband channels can differentiate the different multipath arrivals, and so general delay dependency in the channel response remains.

$$\mathbf{H} \equiv \mathbf{H}(t, \varphi, \tau) \tag{3.4}$$

Channel determination: Narrowband.

Since the scenario this project deals with is a short-range one, being the users located within the massive array's Near Field Region, it is reasonable to assume that the incoming signals at the receiver will suffer moderate delays. This is for instance done in [19] for an indoor MIMO scenario with the presence of LOS, which is similar to the case of this project barring the very large aperture and then, the enlarged range we deal with, apart from the fact the venue considered in this thesis is not necessarily indoors. Thus, the system covered is this project will be considered to be narrowband and consequently, delay dependency is ignored:

$$\mathbf{H} \equiv \mathbf{H}(t, \varphi) \tag{3.5}$$

In Narrowband MIMO systems, each channel coefficient between the m^{th} transmit antenna and the n^{th} receive antenna is a complex scalar at a time instant [11].
Even in the case the channels under modelling can be wideband, the narrowband study is of crucial interest in any case since a wideband channel can always be split into numerous narrowband ones (e.g., via OFDM [12]).

3.4.3 Angular domain downscale: 2D, azimuth angle only.

Angular domain dependency recap.

As already stated in 3.4 on page 19, an angular direction has a two-variable dependence, normally being those two variables in 3D systems the azimuth angle ϕ and the elevation angle θ, and so $\varphi \equiv (\phi, \theta)$.

2D analysis.

The current project will evaluate a scenario like the one described in sec. 3.2 on page 17. As a delimitation due to complexity reasons, the scenario will be evaluated from a two-dimensional (2D) perspective. This will allow to disregard the elevation angle θ and consider the azimuth angle ϕ, only. Consequently, the channel response's variation with the angular direction will respond to the following expression:

$$\mathbf{H}(\varphi) = \mathbf{H}(\phi, \theta) \xrightarrow{2D} \mathbf{H}(\varphi) = \mathbf{H}(\phi) \tag{3.6}$$

3.4.4 Time domain downscale: time-invariant or fast fading channel.

Channel types in the time domain

Basically, two channel categories exist with respect to the time domain [11]:

- **Time-invariant**. The channel remains constant at all time instants. Time dependency disappears.

  $$\mathbf{H}(t) \equiv constant \rightarrow \mathbf{H} \not\equiv \mathbf{H}(t) \tag{3.7}$$

  Both instantaneous CSIR and CSIT are known.
  If the channel is narrowband, the channel coefficients will be complex scalars.

- **Fading channel**. The channel does not remain constant in time. The channel matrix will be different at each time instant, thus time dependence remains:

  $$\mathbf{H}(t_1) \neq \mathbf{H}(t_2) \neq \cdots \mathbf{H}(t_i) \rightarrow \mathbf{H} \equiv \mathbf{H}(t) \tag{3.8}$$

  Instantaneous CSIR is known but instantaneous CSIT might or might not. In the latter case, however, the distribution of the CSIT can be achieved.
  If the channel is narrowband, at each time instant, the channel matrix coefficients will be complex scalars.
  There are two fading channel groups. They depend on the relation between the channel coherence time (which can be understood as the time duration before the channel suffers significant variation) and the coding delay (understood as the effective time duration of a codeword):

  (a) If the channel coherence time is shorter than the coding delay, then a single codeword will suffer from many channel variations, from many fades. The channel appears to vary fast compared to the duration of the codeword. Thus, the channel is **fast fading**.

  (b) If the channel coherence time is larger than the coding delay, then a single codeword experiences no significant fades. The channel appears to vary slowly compared to the duration of the codeword. Thus, the channel is **slow fading**.

Channel determination: time-invariant or fast fading channel.

Two aspects are to be considered with respect to channel determination in the time domain.

1. According to the channel's basic features, users suffer mobility, but this is only local. However, given an instantaneous CSIT case, their location can be considered to be known for each realisation of the channel (Monte Carlo simulation). It is also then a reasonable assumption to consider that the degree of mobility of scatterers is reduced, i.e., a high number of the scatterers is constituted by the other users, the building's elements, etc. (Another aspect is the fact that, as chap. 6 on page 43 states, given a user's location, not all scatterers have an impact on the user but just a few). Thus, it could be argued that the channel is time-invariant for each snapshot of the model, in other words, for each realisation of the model (Monte Carlo simulation). If we take the LOS-only case (no scatterers or impactless scatterers in the environment), the channel is undoubtedly time-invariant for all realisations.
   In brief: At each realisation of the model, both users and scatterers can be considered to remain still, CSIT is assumed and thus, time-invariance.

2. Notwithstanding the solidity of the arguments in the last lines, barring the LOS case with no scatterers, the approach above fails to represent the channel if all scatterers are at the same approximate location for all realisations unless they introduce different incoherency at each realisation and those changes can be determined instantaneously (instantaneous CSIT). This addresses mainly the introduction of amplitude and phase randomness in the channel matrix coefficients, being the phase randomness introduction the inherent definition of the scatterers' behaviour. Stating the obvious, this happens even if the scatterers' location remained perfectly constant for every realisation of the channel.
   In brief: At each realisation of the model the scatterers are assumed to introduce different incoherency (via amplitude and phase contributions).

Conclusively, for each realisation, the channel can be interpreted to be time-invariant. Each realisation should contain a different incoherency impingement due to the scatterers. Accounting for all realisations of the channel, if those are thought of as time lapses, the previous makes the channel be forcefully **fast-fading**. In any case, instantaneous CSIT is assumed at each realisation of the channel, unless otherwise is stated (we refer mainly to the second part of this project tackling users mobility with no instantaneous CSIT).

As introduced below, the performance metric that is employed to measure the channel's benefit is capacity, the maximum achievable rate. It happens that capacity for a time-invariant channel has a simple closed-form expression. Conversely, capacity for a fast fading channel is no longer analytical but an averaged capacity over several realisations. This averaged capacity is now called ergodic capacity.
Capacity's expression simplicity for a time-invariant channel is the triggering fact to assume instantaneous CSIT at each realisation and then, average over all realisations. The averaging, thus, occurs over the scatterers' amplitude and phase shifts, hereinafter also referred to as simply *weighting*. This applies in the first part of this thesis, but not in the whole second part (beamforming), as will be reviewed. This will be reaccounted for below (sec. 3.6 on the next page).

3.5 Channel type determination

According to discussion in sections 3.3 on page 18 and 3.4 on page 19, the MIMO channel response given in the form of the channel matrix $\mathbf{H}$ will be narrowed down so that its expression reduces to

$$\mathbf{H}(t, \phi)$$

if the channel is fast fading. The timeline can be thought as being simulated as for different channel realisations. The channel matrix will be defined as per the COST2100 MIMO model, simplified as explained on the pages above. Since the channel is considered to be narrowband, each channel matrix coefficient will be a complex scalar at each realisation.
Finally, it must be remarked that the channel response $\mathbf{H}$ will vary according to the scenario being modelled from a single-user or multiple-user perspective (Point-to-Point model and Multi-User models, respectively.)

3.6 Performance metric brief introduction: capacity.

This section is to briefly introduce the concept of capacity, which will be further elaborated in subsequent chapters. Evaluation of the potential benefits that the system in this project would have will be done according to the capacity of the channel, the maximum achievable data rate in the system. Other metrics will also be employed, although they will mainly serve as holders of underlying information which results in some capacity value.

Capacity is computed differently according to the channel being analysed, Point-to-Point or Multi-User. In the latter case, we rather talk about *Sum Capacity* or *Sum Rate*, instead [13, 10, 25]. Point-to-Point MIMO capacity has a different definition depending on the knowledge of the instantaneous CSIT or only its distribution. In brief:

- If instantaneous CSIT is known, then the course of action involves optimal power allocation (normally via waterfilling) and capacity results in a closed-form expression. This is always the case in time-invariant channels.

- When instantaneous CSIT is ignored its distribution can usually still be found. In this situation, the course of action excludes optimal power allocation since an optimal power allocation is unknown a priori (real performance). Capacity results in an averaged form. In fast-fading channels, in which this is likely to happen, capacity is averaged over the channel fades during a codeword (so long codewords are preferred) so that fades are averaged out since performance of the codes converges towards a mean performance. Capacity is renamed as *ergodic capacity.* This out-averaging can only be done if fading is modelled as an ergodic process (which is an ordinary assumption), hence ergodic capacity.

As we have already hinted, computation of capacity will follow the procedure detailed in the lines above. At a given realisation, since the channel has been argued to be time-invariant, the closed-formed expression of capacity including optimal power allocation will be calculated. Yet, given the fast-fading nature of the channel in the form of the scatterers' different weighting from realisation to realisation, an averaging must be carried out; this average will be done for a set of realisations over the scatterers' weighting.

Once again, we remind the reader that chap. 7 on page 55 on Performace Metrics gives detailed account for capacity computation.

3.7 Input-output relation of a Narrowband MIMO Point-to-Point channel

The discrete baseband input-output relation of a narrowband MIMO Point-to-Point channel in which the transmitter has M antennas and the receiver N antennas, follows the expression given below ([11, 25, 2, 26, 10], to name just some):

- For a *time-invariant* channel:

$$\mathbf{y} = \mathbf{H}(\phi)\,\mathbf{x} + \mathbf{n} \tag{3.9}$$

  where:

- $\mathbf{y}$ is an Nx1 matrix containing each output signal at each receive antenna. $\mathbf{y}^{\mathrm{T}} = [y_1 \cdots y_N]$.
- $\mathbf{H}(\phi)$ is an NxM matrix containing the channel coefficients, which depend on the scenario geometry, exclusively (ϕ).

$$\mathbf{H}(\phi) = \begin{bmatrix} h_{11} & \cdots & h_{1M} \\ \vdots & \ddots & \vdots \\ h_{N1} & \cdots & h_{NM} \end{bmatrix} \tag{3.10}$$

  Each channel coefficient h_{nm} depends on the angular geometry seen from both m$^{\mathrm{th}}$ transmit antenna and the n$^{\mathrm{th}}$ receive antenna according to the selected simplified COST2100 model, given by the angular geometry. To ease the reading, angular dependency has not been incorporated in the coefficients. This model requires the aid of the wave-transmission model, as well. We remind the reader that wave transmission was determined to be spherical. Finally, the reader is also reminded that, since the channel is assumed narrowband, each coefficient is a complex scalar.
- $\mathbf{x}$ is an Mx1 matrix containing each input signal at each transmit antenna. $\mathbf{x}^{\mathrm{T}} = [x_1 \cdots x_M]$
- $\mathbf{n}$ is an Nx1 noise vector, the n$^{\mathrm{th}}$ component being the channel noise the n$^{\mathrm{th}}$ receive antenna would suffer from.

• For a *fast fading* channel:

$$\mathbf{y(t)} = \mathbf{H(t}, \phi)\ \mathbf{x(t)} + \mathbf{n} \tag{3.11}$$

where all the notation is exactly as for the time-invariant channel, barring the newly incorporated time dependence. The noise notation has been eased without a time dependence.
For a specific snapshot at a time instant t_k (given by the respective realisation of the channel), time-invariant definition for the channel terms applies:

$$\mathbf{y(t_k)} = \mathbf{H(t_k}, \phi)\ \mathbf{x(t_k)} + \mathbf{n} \equiv \text{Time-invariant} \tag{3.12}$$

Chapter 4

Near Field Region of a Massive Uniform Linear Array (ULA)

This chapter is aimed at examining the Near Field Region of an array and narrows down the study to a Uniform Linear Array (ULA). The motivation for this study lies in the short-range channel model that has to effectively be constructed for an indoors Massive-MIMO system with a Very Large aperture (see chap. 2 on page 11), approximated by the Near Field Region of the massive array (see sec. 3.3 on page 18 and chap. 5 on page 37).

4.1 Classic Theory

This section is based on [6].
The space that surrounds an antenna can be divided into two regions, called the Near Field Region and the Far Field or Fraunhofer Region. The Near Field can be subdivided into another two regions, called the Reactive Near Field and the Radiating Near Field regions. As the distance from the antenna increases, the electromagnetic (EM) field changes. How this field changes is what determines the region boundaries, as some terms in the EM field become more or less dominant.
These regions, however, do not have clear boundaries (transition is not abrupt) and they are not unique, although distances shown in fig. 4.1 on the following page are commonly used. Each region is characterised by the following definitions:

1. **Reactive Near Field**
   The Reactive Field predominates.

2. **Radiating Near Field**
   Radiative Fields predominate but the angular field distribution is dependant on the distance from the antenna. The boundary is conventionally taken at a distance $R_{RAD} = 0.62\sqrt{D^3/\lambda}$ [m].

3. **Far Field**
   The angular field distribution is independent on the distance from the antenna (commonly, a phase error of $\pi/8$ [rad] or less is considered to state so). The inner boundary is commonly taken to be the radial distance $R_{FF} = 2D^2/\lambda$ [m] and the outer one, infinity.

The mathematical computation that yields these formulas is provided in appendix A on page 167.

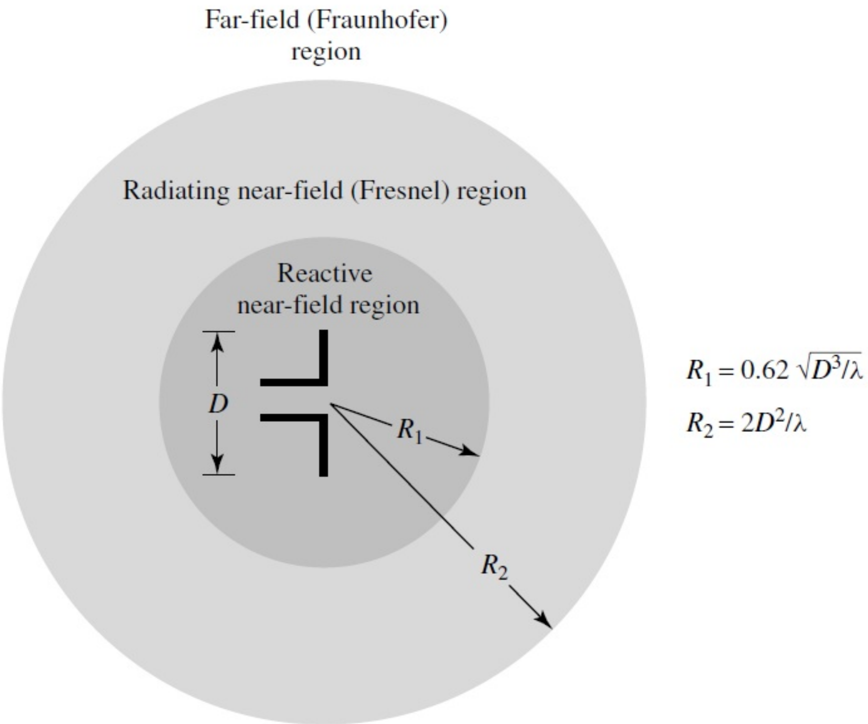

Figure 4.1 *Field Regions. D [m] is the largest dimension of the antenna. λ [m] is the signal's wavelength. [6]*

4.2 Array Specific Near - Far Field (ULA)

Regarding antenna theory, an array is a set-up consisting of several antennas arranged in a specific electrical and geometrical configuration. The aim is to achieve a radiating pattern that could not be obtained using single elements only. Identical elements are usually employed, but this does not necessarily have to apply. [6]
The simplest array arrangement is the linear one, with its elements being equally or uniformly spaced. This is an Uniform Linear Array (ULA), and it is the one to be tackled in this project. Fig. 4.2 shows a ULA made up of five elements centred in origo and placed along the x axis.

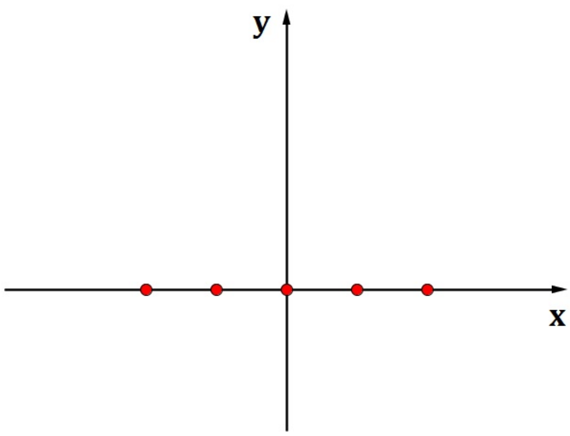

Figure 4.2 *Five-element ULA. elements are red dots.*

4.2.1 Broadside direction

The Near Field-Far Field contour R_{FF} for an array is not only defined by the radial distance given by

$$R_{\text{FF}} = \frac{2D^2}{\lambda} \quad [\text{m}] \tag{4.1}$$

as accounted for in the previous section. This is due to the geometric disposition of an array. It applies on the broadside axis, though, which is the one crossing the array perpendicularly at its middle point. This is the only direction that fits the classic Near-Far Field theory. Fig. 4.3 shows the broadside direction for two different ULAs.
Fig. 4.4 on the following page shows several Far-Field distances (at the broadside direction) for an array of a fixed aperture of D=10 [m] at a variable operating frequency in a range from 100 [MHz] to 10 [GHz] (ten of them were selected linearly).
Fig. 4.5 on page 31 shows in turn several Far-Field distances (at the broadside direction) for an array working at a fixed frequency of f = 2.4 [GHz], which is an ordinary WiFi operating frequency, with several aperture lengths.

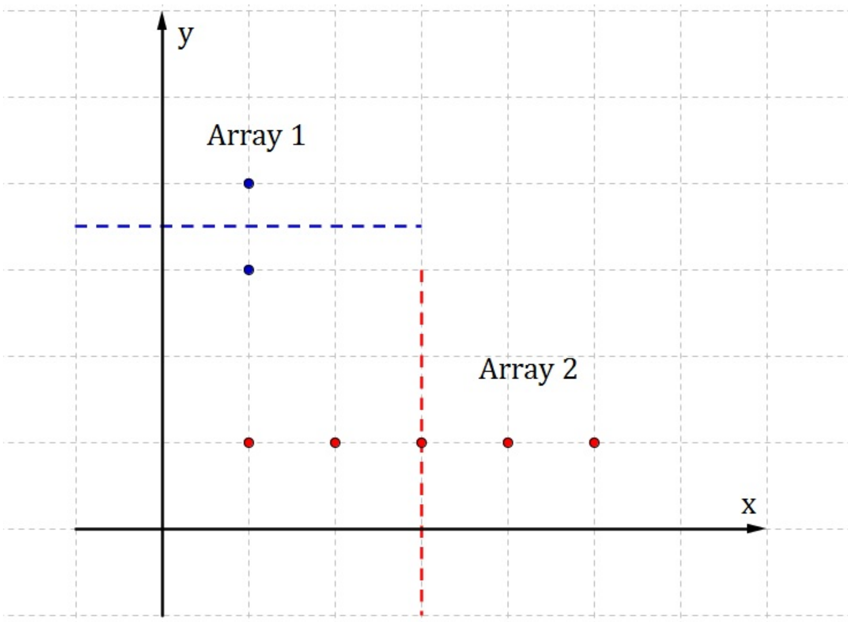

Figure 4.3 *Broadside direction for two ULAs: Array 1, blue; Array 2, red. Broadside direction is shown with a dashed segment, although it is an infinite line.*

4.2.2 Non-broadside direction

At the non-broadside direction, classic theory fails to work, so the Far Field distance will have to be calculated as per different means. In general, though, the resulting Far Field distance will be lower than the classic one ($2{\cdot}D^2/\lambda$).

Two possibilities are to be tackled in the case of the non-broadside direction: echelon and endfire directions. Fig. 4.6 on page 32 exhibits both cases. An array represented by five red dots is placed in origo. Then, a blue point at a distance R_{ech} and angle ϕ representing a direction in echelon is included. Finally, so is done with a green point in the endfire direction, at a distance R_{end} from origo.

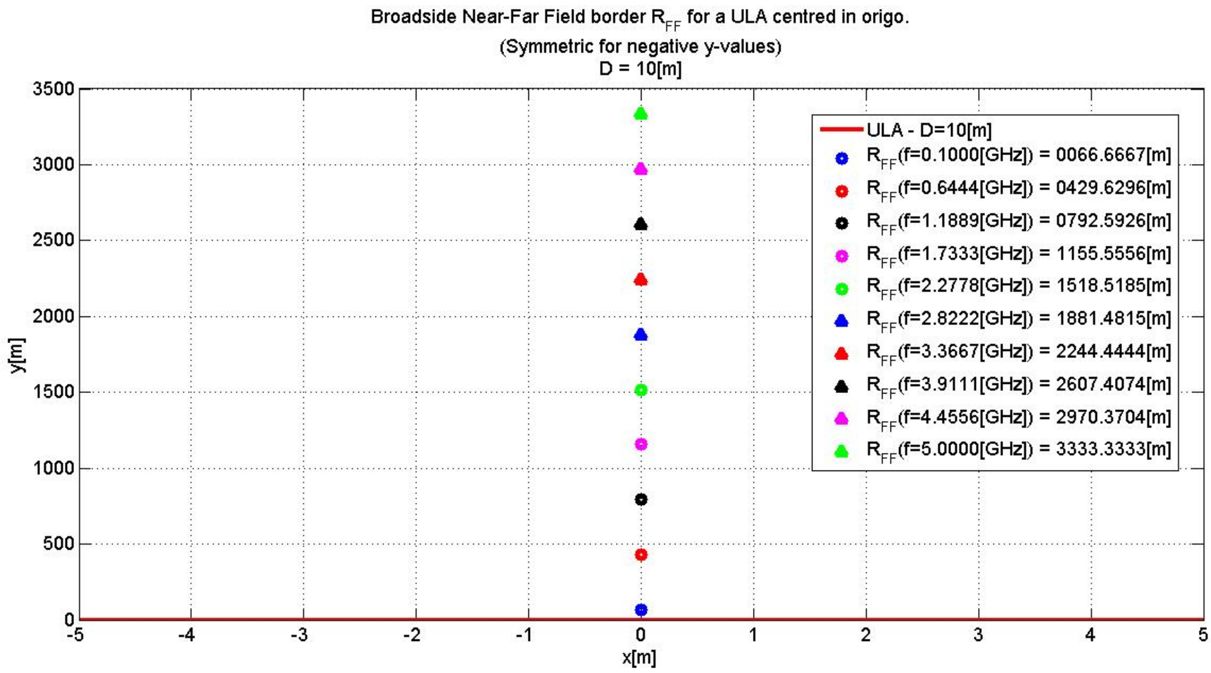

Figure 4.4 *ULA Near-Far Field border at the broadside direction. Variable frequency, fixed aperture length (D=10 [m]).*

Echelon direction

A method to solve the Far Field distance in an echelon direction is to calculate the equivalent broadside array for that particular direction and then to compute the Far Field distance of this equivalent broadside array making use of the classic Far Field formula (eq. 4.1 on the previous page). The issue is that for a particular echelon direction given by the echelon angle ϕ, the equivalent broadside array's aperture varies according to the distance R_{ech}. (Both ϕ and R_{ech} are shown in fig. 4.6 on page 32). Fig. 4.7 on page 33 shows the equivalent broadside array for a set of (R_{ech},ϕ), named point S in that figure.

A way to solve this problem consists of computing the Far Field distance appealing to the mathematical background that provides the Far-Field distance. This computation is detailed in A on page 167. In this case, we would like to make use of them to *solve the Far-Field distance of the equivalent broadside array*. According to them, the aim would be to evaluate the maximum **phase difference** for the equivalent broadside array, as follows:

$$\{\varepsilon_{\mathrm{phase}}\}_{MAX} = \mathrm{k} \cdot (\mathrm{D_m} - \mathrm{R_{eff}}) \leq \frac{\pi}{8} \quad [\mathrm{rad}] \tag{4.2}$$

Where k [rad/m] is the wavenumber and $\mathrm{D_m} = \min(\mathrm{D_1}, \mathrm{D_M})$. (See Fig. 4.7 on page 33)
Fig. 4.8 on page 33 exhibits the Far Field boundary according to eq. 4.2 for a set of three different frequencies and a ULA with a fixed aperture. Notice the significant Near Field Region growth with an in turn increasing frequency.

Endfire direction

The endfire direction is the one occupied by the ULA itself, as shown in fig. 4.6 on page 32. The phase difference criterion is not applicable in this case, due to the fact the aperture of the equivalent broadside array is zero in this direction. Hence, another standard is to be employed in order to calculate the region boundaries. In this section, only the Far Field boundary is tackled (and set aside the radiating near field one).
One of the criteria that can be followed to solve this issue is the **amplitude criterion**. The aim is to calculate all the power differences in the endfire direction due to the disposition of

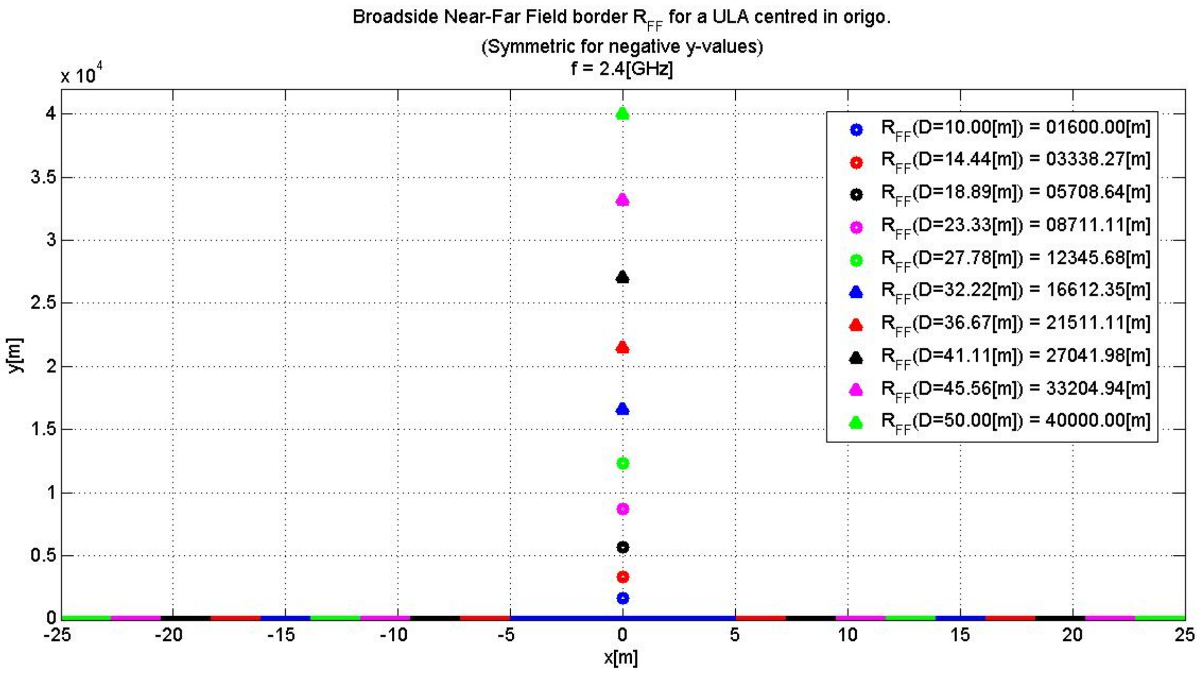

Figure 4.5 *ULA Near-Far Field border at the broadside direction. Fixed frequency, variable aperture length.*

the array and then set a limiting power threshold $(\Delta P)_{MAX}$ (similar to the phase threshold of $\pi/8$ [rad]) to evaluate the Far Field distance. $(\Delta P)_{MAX}$ can be set to 3 [dB], which means a 50 % power difference. Fig. 4.9 on page 34 exhibits the geometry of the endfire case and eq. 4.3 is the mathematical expression of the amplitude criterion.

$$|P(R_M) - P(R_1)| \leq (\Delta P)_{MAX} \quad \text{[dB]} \tag{4.3}$$

The power (in natural units) can be computed as shown in the following equation:

$$P(R) = \frac{1}{R^n} \quad \text{[W]} \tag{4.4}$$

Fig. 4.10 on page 34 shows the Far Field boundaries for an array with aperture D=15 [m] at an operating frequency of 2.4 [GHz]. It has to be noted that the amplitude criterion is not frequency but only geometry-dependant. Fig. 4.11 on page 35 shows the aperture-dependency experienced by the amplitude criterion, exhibiting the Near-Far Field boundary for two arrays with an aperture of D=15 [m] and D=30 [m], respectively, working at the same frequency.

Resulting Near-Field Region.

It can easily be presumed that the amplitude criterion can be applied not only in the endfire direction but in all of them. I might happen that, for some areas, both criteria might overlap (meaning they both agree to consider those areas to be within the Near-Field Region) but might not for some others (meaning the criteria yield dissimilar results). Fig. 4.12 on page 35 shows the overlapping areas of both criteria for a ULA with an aperture of $D = 15[m]$ at a frequency of $f = 800[MHz]$.

The conflicted areas might be treated differently. Basically, a decision ought to be made on whether the different sets yielded by both criteria are to be united (*union operation*, meaning the final Near-Field Region is the *union* of both Near-Field Regions) or rather whether one of them is to be discarded. The optimal operation, though would include the vectorial combination

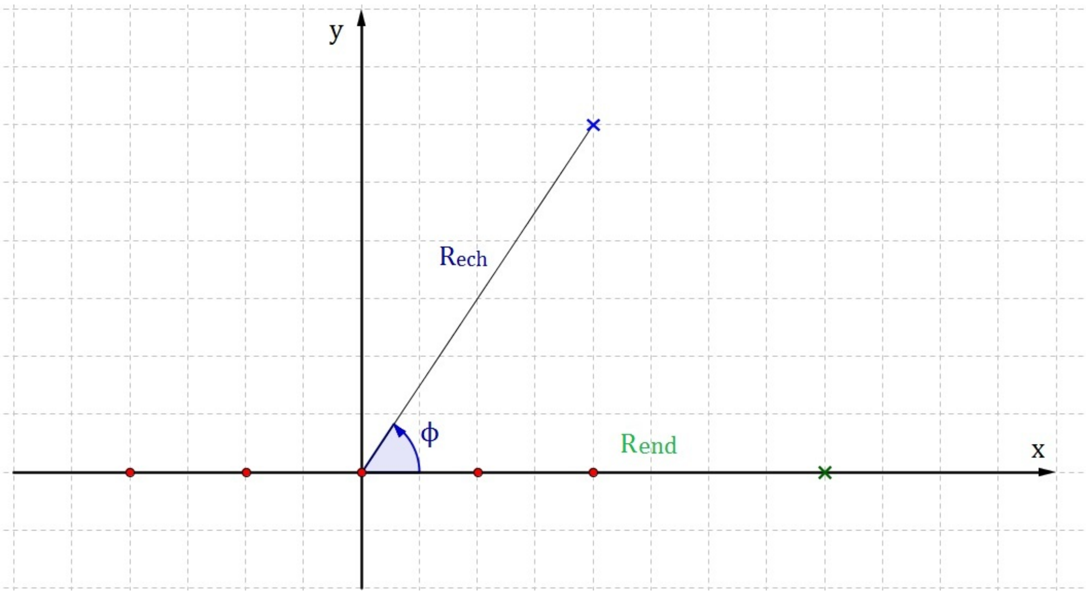

Figure 4.6 *Echelon direction and endfire direction. The array is represented by red dots. A blue cross at the echelon direction (given by the echelon angle ϕ) at a distance R_{ech} from origo is given by the pair (R_{ech},ϕ). A green cross represents a point at the endfire direction at a distance R_{end} from origo. The endfire direction can be understood as an echelon direction with $\phi = 0$.*

of both.
Based on the fact the Near-Field Region shown by the amplitude criterion is tremendously much smaller than the one yielded by the phase criterion, which is clearly dominant, the former was discarded in favour of the phase criterion. The *amount* of Near Field Region done away with if this procedure is carried out is negligible since the discrepant areas are notably reduced in all cases. Thus, will not cause any meaningful changes, let alone when the array has a very-large aperture as is the case of this project.

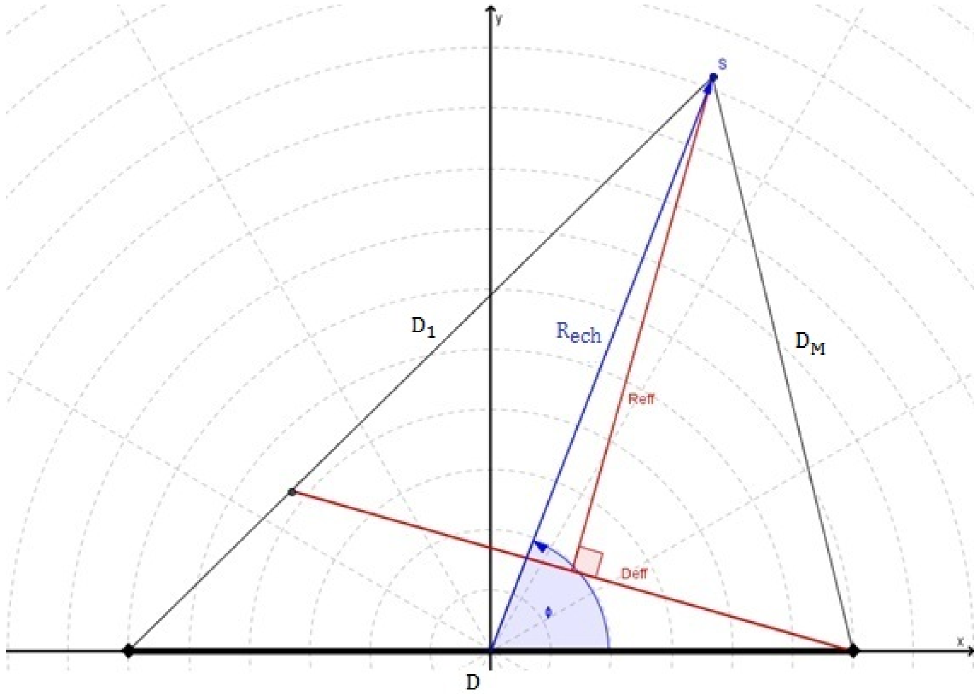

Figure 4.7 *Equivalent broadside array for a set of (R_{ech},ϕ). The real array is placed in origo and has an aperture D. The equivalent broadside array has an aperture D_{eff} and is at an orthogonal distance R_{eff} from point S(R_{ech},ϕ). The distance from point S to the first element of the real array (set to be the leftmost element) is D_1. Likewise, the distance from point S to the last element of the array (set to be the rightmost one) is D_M.*

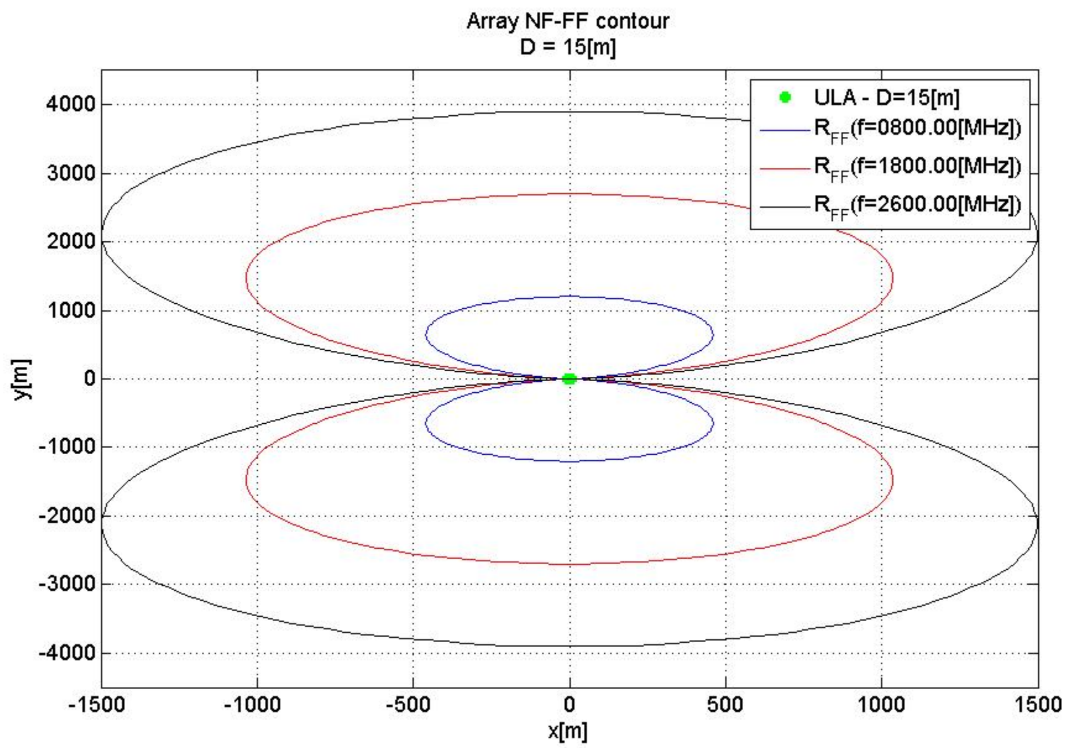

Figure 4.8 *Far Field boundary contour for an array of aperture D=15 [m] for three LTE frequencies used by Danish providers.*

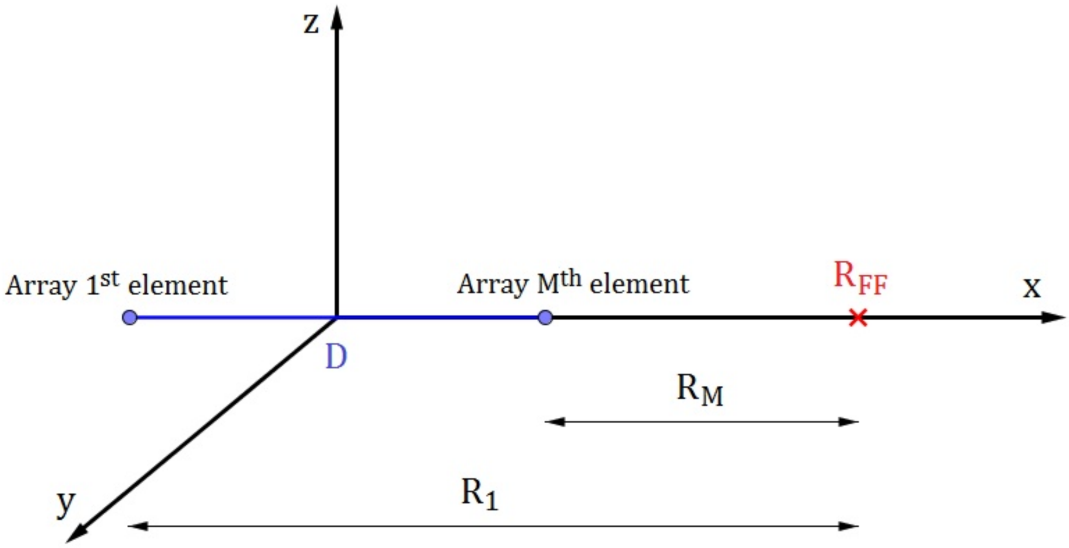

Figure 4.9 *Endfire case scenario. D [m] is the aperture of the array. R_1 and R_M are the distances from the Far Field point to the first (1^{st}) and last (M^{th}) elements of the array, respectively. R_{FF} is the Far Field distance at the endfire direction.*

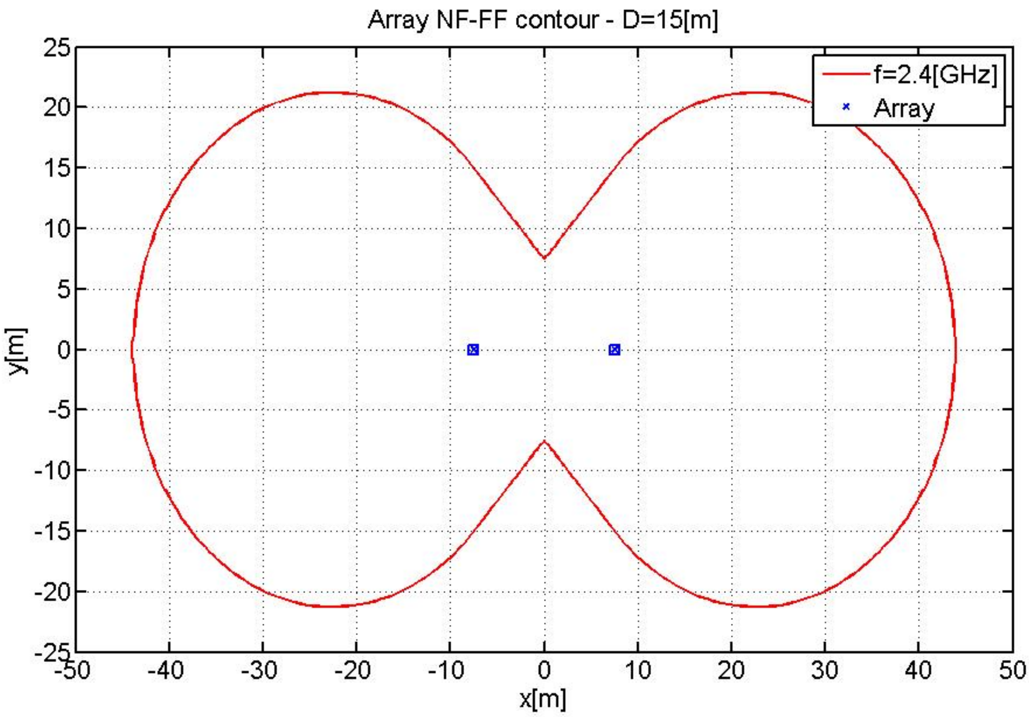

Figure 4.10 *Near-Far Field contour according to the amplitude criterion for a power difference of 3 [dB] and an array of aperture D=15 [m].*

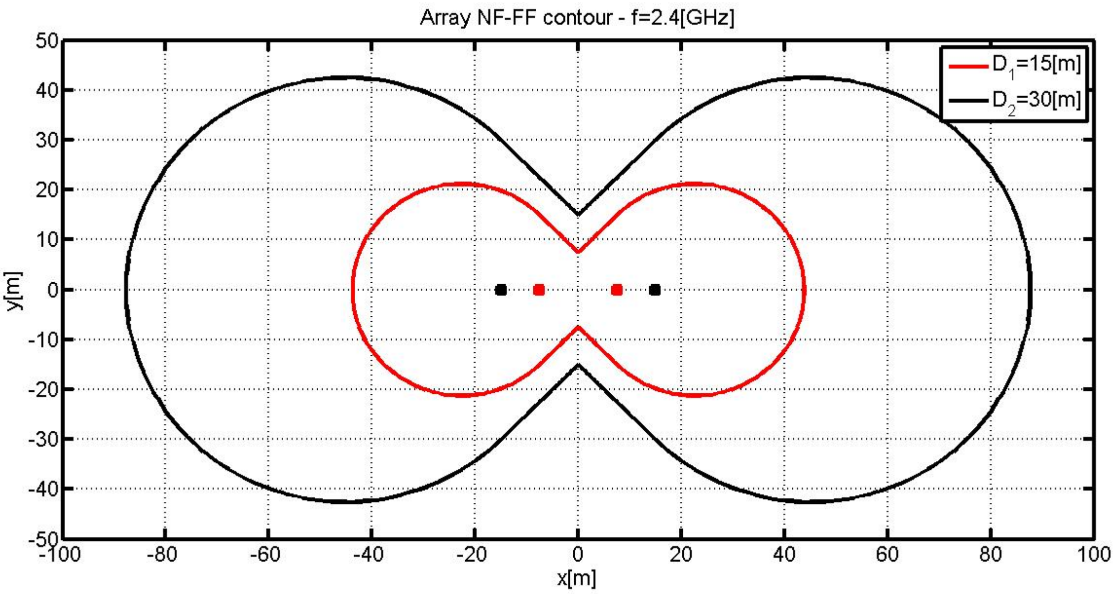

Figure 4.11 *Near-Far Field contour according to the amplitude criterion for a power difference of 3 [dB] and an array of aperture D=15 [m] and another one of aperture D=30 [m]. Both work at a frequency of f=2.4 [GHz]*

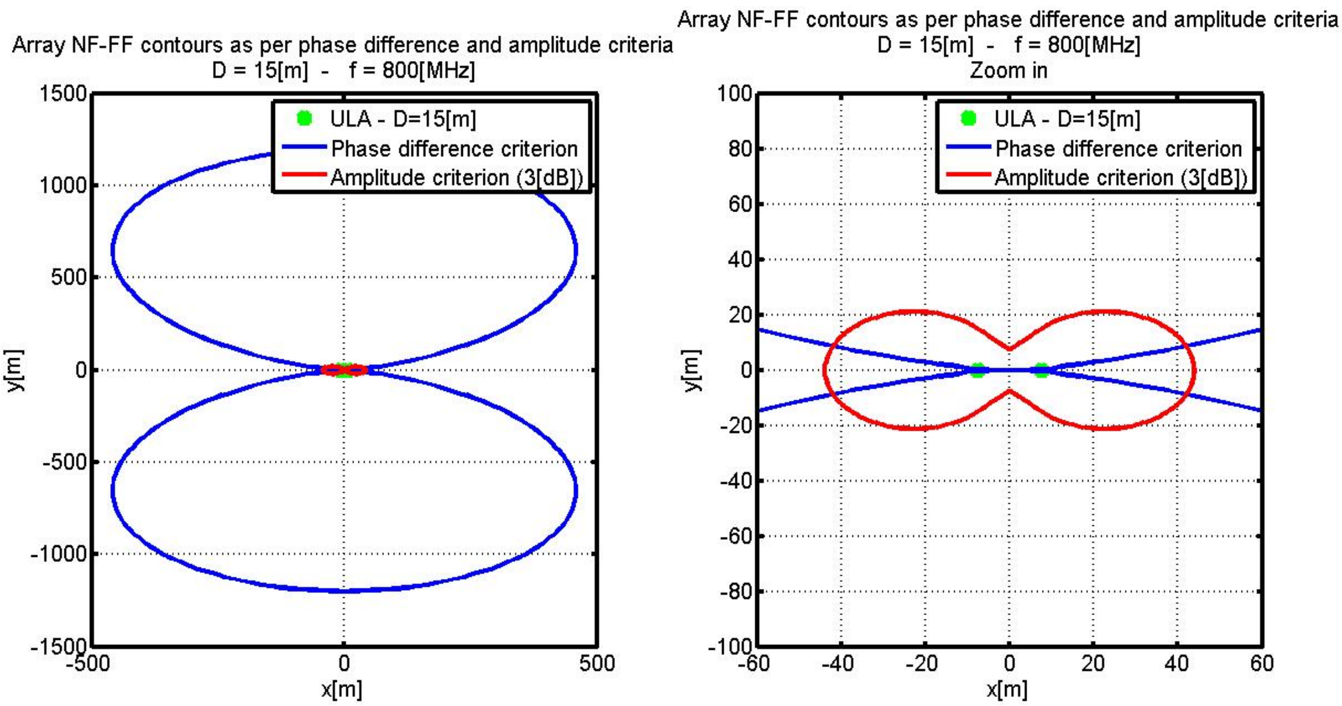

Figure 4.12 *Near-Far Field overlapping contours according to both the phase and the amplitude criterion (for a power difference of 3 [dB]) and an array of aperture D=15 [m] at a frequency of f=800 [MHz]. The conflicted areas are the ones the amplitude criterion establishes to be within the array's Near Field, unlike the phase criterion. They can be found close to the endfire direction. Those areas have been zoomed-in for clarifying purposes (figure below).*

4.3 Conclusions

It has been seen that Far-Field distance contours increase when either (a) the operating frequency increases or (b) the array aperture length increases.
Thus, very large Far-Field distances and then Near Field Regions may be achieved setting one of them or both to sufficiently large values. Therefore, by using Very Large-Aperture arrays, a large amount of the service area could be contained within the Near-Field region.

This phenomenon is specifically accounted for mathematically at the broadside direction via the classic Far-Field distance formula given in 4.1 on page 29 and that we reproduce again below:

$$R_{\mathrm{FF}} = \frac{2D^2}{\lambda} \quad [\mathrm{m}]$$

In fact, the potential to achieve large Far-Field distances is particularly clear at the broadside direction. As an example, according to Fig. 4.5 on page 31, a Far-Field distance of $R_{\mathrm{FF}} = 40.00$ [km] is achieved at the broadside direction at a frequency of $f = 2.4$ [GHz] with an array of aperture $D = 50[m]$.

Regarding the echelon case, it has been seen how the broadside Far Field formula can be applied via the equivalent broadside array computation at each echelon direction. Contour boundaries have been displayed by means of MatLab simulations. It has also been shown that, as well as concluded in the broadside case, the Near-Far Field boundary is frequency-dependant and aperture-dependant, with the same tendency shown at the broadside direction. By extension and as already stated, it was then concluded that larger Near-Field Regions are obtained for larger array apertures and higher frequencies, at all echelon directions.

Finally, the amplitude criterion was employed to deal with the endfire case, for which the phase criterion failed to work. A figure showing the amplitude criterion for a specific case was included (fig. 4.10 on page 34). It was concluded that the amplitude criterion was not frequency-dependant but yet aperture-dependant (fig. 4.11 on the previous page).
However, it was seen that the amplitude criterion can apply to any direction and not only to the endfire one. It was then noted that the Near-Far Field contour given by the amplitude criterion for a power difference of 3 [dB] appears much closer to the array than that given by the phase criterion. In any case, there will be some overlapping areas considered to be within the Near Field area by one of the criteria and outside by the other.
As a simplification, it was stated that the Near-Field Region yielded by the amplitude criterion would be ignored, being the considered Near-Field Region the one resulting from the application of the phase difference criterion, only. However, accuracy would be achieved by an effective combination of both criteria following a vector addition method. This has not been implemented.

Chapter 5

Wave transmission model

When modelling channel propagation, the usual assumption is that T-R separation is large enough to assume each of these ends to be in the Far Field of each other, and thus planar wave incidence. This assumption is used extensively in fields such as array signal processing, parameter estimation and wireless channel modelling [7]. Especially the latter is of most relevance for this chapter.

Several claims are made in [7], which seem to indicate that plane-wave model might underestimate the performance of a MIMO channel in some scenarios, and instead usage of the spherical-wave model would improve results on them. The assertions are as follows:

"*1) that a LOS MIMO channel can achieve full rank and yield the highest possible capacity, 2) that the spherical-wave model is required to properly analyse short-range MIMO, and 3) that large antenna spacing can have a very significant and positive impact at short-range*" [7, p. 1534].

In brief, this chapter will attempt to clarify what the Plane-wave assumption is, before going into the issues of using the plane-wave assumption for a short-range, large-aperture massive MIMO scenario. Next, a description on the effect on capacity will be provided.

5.1 Background

According to [7], the motivation of studying the differences between plane-wave and spherical-wave model was fuelled by discrepancy in measured data on some indicators, and particularly, capacity. A significant difference in capacity between reconstructed MIMO channels and direct measured capacity was found. It was then hinted at that the major reason for this deviation was incorrect modelling of the wave components. It is claimed in this source that by using the spherical-wave model rather than the plane-wave one, it is possible to reduce this discrepancy. Discrepancy was first evaluated in a scenario containing LOS components only, with no scatterers. The spherical modelling of the LOS components allowed to provide "richness" to a scenario as simple as a free-space MIMO channel even with no scatterers in the environment and to dramatically reduce the discrepancy with measured data [7]. A multipath scenario modelled spherically with and without LOS was also tackled, reaching the same results [7].
The next lines will provide with a discussion on the ordinary plane-wave model, which will trigger discussion on the spherical one. Finally, benefits on capacity that the latter model brings along are evaluated, as well as capacity optimisation criteria. It must be reminded that this model fits measurements, so benefits are not as such if the spherical model is to be understood as an approach to real behaviour.

5.2 Plane-wave assumption

Considering only LOS transmission, it is common to model a MIMO channel, assuming the received wavefront is a plane-wave [7, 27]. In this model, the plane-wave is received at some

DOA, indicated by φ_{Rx}. The direction φ_{Rx} consists of angles ϕ_{Rx} and θ_{Rx} in the azimuth and elevation planes, respectively. This plane-wave had been initially transmitted with a DOD given by the angular direction φ_{Tx}, consisting of angles ϕ_{Tx} and θ_{Tx} again in the azimuth and elevation planes, respectively. In this model, the channel is built on the propagation from the transmitter to the receiver. However, each end cannot distinguish between the elements making up each end's antenna, and thus see each other as a point source. There is only a single channel term in the channel matrix. A planar wave's voltage propagation term can be written as, [25]

$$h = \frac{1}{R^{n_v}} e^{-\text{j}kR} \tag{5.1}$$

where:

- R is the distance between the transmit and receive antennas, a function of φ_{Tx} and φ_{Rx}.

$$R \equiv R(\varphi_{\text{Tx}}, \varphi_{\text{Rx}}) \tag{5.2}$$

- n_v is the voltage pathloss exponent. In the Free Space, it is normally taken as one.
- $k = \frac{2\pi}{\lambda}$ [rad/m] is the wavenumber.

5.3 Spherical-Wave model

In [7], several claims are made regarding the application of the plane-wave model. While being suitable for SISO and SIMO systems, the plane-wave assumption affects the channel matrix rank, and the distribution of singular values for short-range MIMO systems with a dominant LOS component.

As mentioned in sec. 5.2, the plane-wave model assumes that the incident wave is plane, and thus simplifies analysis. This means that DOD and DOA for the transmitter and receiver respectively are the same for all elements in their corresponding ends. This is reasonable to be implemented if each end sees each other as a point source, if each end is unable to distinctly differentiate the antenna elements at the another end. This fits reality as long as the ends are not close enough, as long as they are not in short-range to each other.

Consequently, **an issue arises when the transmitter and receiver distances are short or array sizes are large, which is a twist on the same statement**. In principle, **the spherical-wave model should be employed within the array's Near Field region**, issue upon which chap. 4 on page 27 was written. However, authors in [7] give a more restrictive definition according to measurement's discrepancies on capacity. This will be elaborated throughout this chapter.

When waves are considered to be spherical, then DODs and DOAs are different for each pair of transmit and receive antenna elements, and as such represented as, $\theta_{\text{Tx}\,ij}$, $\phi_{\text{Tx}\,ij}$ and $\theta_{\text{Rx}\,ij}$, $\phi_{\text{Rx}\,ij}$ for DOD and DOA respectively. Fig. 5.1, shows how angles are related to each transmitter/receiver pair.

The channel is then written as a matrix, containing gains for each link between the i$^{\text{th}}$ receive antenna ant the j$^{\text{th}}$ transmit one. If there are M transmit antennas and N receive ones, **H** would be written as follows (the channel response matrix written as **H** was already introduced in chap. 3 on page 17):

$$\mathbf{H} = \begin{bmatrix} h_{11} & \cdots & h_{1M} \\ \vdots & \ddots & \vdots \\ h_{N1} & \cdots & h_{NM} \end{bmatrix} \tag{5.3}$$

where h_{ij} are the link-wise channel gains (i$^{\text{th}}$ receive antenna, j$^{\text{th}}$ transmit antenna), and are written as,

$$h_{ij} = \frac{1}{R_{ij}^{n_v}} e^{-\text{j}kR_{ij}} \tag{5.4}$$

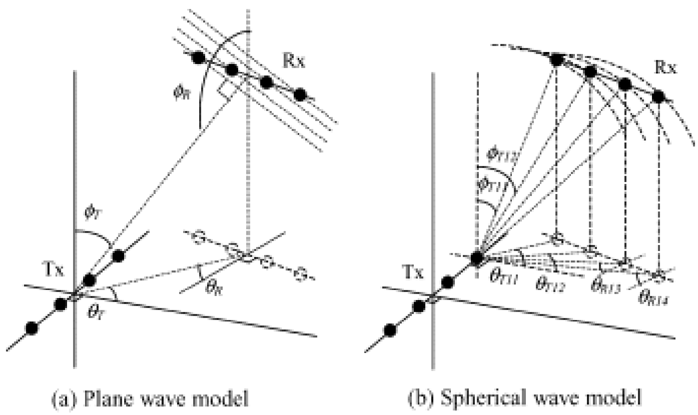

Figure 5.1 *Illustration of the plane-wave and the spherical-wave models. [7]. It must be noted that in this illustration $\theta_{\mathrm{Tx}\,ij}$ and $\theta_{\mathrm{Rx}\,ij}$ are taken as the azimuth angles and $\phi_{\mathrm{Tx}\,ij}$ and $\phi_{\mathrm{Tx}\,ij}$, as the elevation angles. Since notation is more distinct the other way round (due to spherical coordinates logic), it has been opted to work with the already stated ϕ's for the azimuth angles and θ's for the elevation angles, notwithstanding notation employed in [7].*

Similarly, as in eq. 5.1, R_{ij} is a function of $\varphi_{\mathrm{Tx}\,ij}$ and $\varphi_{\mathrm{Rx}\,ij}$.

$$R_{ij} \equiv R_{ij}(\varphi_{\mathrm{Tx}\,ij}, \varphi_{\mathrm{Rx}\,ij}) \tag{5.5}$$

2D approach

$\mathbf{H}$ dependence with the angular direction was set as $\mathbf{H} \equiv \mathbf{H}(\varphi)$ in chap. 3 on page 17. What is more, dependence was downscaled to the azimuth angle if a two-dimensional approach was followed:

$$\mathbf{H}(\varphi) = \mathbf{H}(\phi, \theta) \xrightarrow{2D} \mathbf{H}(\varphi) = \mathbf{H}(\phi) \tag{5.6}$$

In this section it has been stated that the angular dependency was given in the form of the distance between every pair of elements at each end $R_{ij} \equiv R_{ij}(\varphi_{\mathrm{Tx}\,ij}, \varphi_{\mathrm{Rx}\,ij})$. By narrowing these distances down to the 2D case, then R_{ij} will depend on the two azimuth angles seen at each pair:

$$R_{ij} \equiv R_{ij}(\phi_{\mathrm{Tx}\,ij}, \phi_{\mathrm{Rx}\,ij}) \tag{5.7}$$

5.4 Effects on capacity: Usage threshold determination and optimisation factors.

Open-loop capacity assuming equal power allocation at the transmitter may be written as [7]

$$C = \log_2 \left| \mathbf{I}_N + \frac{\rho}{M} \mathbf{H}\mathbf{H}^{\mathrm{H}} \right| \quad \text{[bptx]} \tag{5.8}$$

where $|\cdot|$ is the matrix determinant operator, ρ is the SNR as the total transmit power over the noise power, $\mathbf{H}$ is the channel matrix (unmodified by any pre- or post-coding, hence, open-loop), $^{\mathrm{H}}$ denotes the Hermitian transpose and N and M are number of antennas at the receive and transmit side, respectively. Discussion below will assume LOS paths only to describe performance as stated in sec. 5.1 on page 37. Further discussion on capacity for single- and multi-user cases will follow in chap. 7 on page 55.

5.4.1 Plane wave lower usage threshold distance discussion

Assuming LOS paths only (no multipath) in the scenario, a study was carried out by the authors of [7] to determine where the spherical model should be applied rather than the planar one, **notwithstanding the validity of the spherical-wave model inside the array's Near Field Region**. In other words, authors in [7] look for a threshold for non-usage if the planar-wave is employed inside and outside the Near Field region.
To that purpose, they identified a threshold distance R_{th}, below which capacity based on the spherical-wave model is greater than 1.5 times that of the plane-wave model for a given array size. Rephrasing the wording, at the threshold distance capacity underestimation error due to application of the plane-wave model in lieu of the spherical one is 50 % and much greater when the transmitter and receiver are at a shorter distance. Additionally, authors in [7] discovered that discrepancy between models was maximum when the arrays are broadside to each other (see chap. 4 on page 27 to find account for the broadside direction).

The threshold level at the broadside direction that fits with measurements is given as [7]

$$R_{\text{th}} = \alpha \frac{L^2}{\lambda} \quad [\text{m}] \tag{5.9}$$

where:

- L [m] is the array's aperture size.
- λ [m] is the signal's wavelength.
- α is a fitting constant that ranges from 3.75 to 4.4 for a number of antennas between 3 and 16.

Due to the varying characteristics of α, it is claimed in [7] that $\alpha = 4$ is a reasonable assumption that approximately fits every scenario and so the threshold distance at the broadside direction is given by the expression:

$$R_{\text{th}} = 4 \frac{L^2}{\lambda} \quad [\text{m}] \tag{5.10}$$

Interestingly enough, this expression for the threshold distance has a high degree of similarity to that which marks the Far Field boundary as per a phase mismatch of $\pi/8$ [rad] (see chap. 4 on page 27):

$$R_{\text{FF}} = 2 \frac{L^2}{\lambda} \quad [\text{m}] \tag{5.11}$$

This means that application of the spherical-wave model within the Near Field Region at the broadside direction is correct. Nevertheless, the expression in eq. 5.9 assumes that both the transmit and receive arrays apertures are equal in size (both are L), which is unrealistic in the scenario tackled in this project, since one of the ends is a Very Large Aperture array. Generalisation of the threshold distance would imply taking into account the transmit array aperture L_T [m] and the receive one L_R [m]. This would result in an expression like this:

$$R_{\text{th}} = \alpha \frac{L_T \cdot L_R}{\lambda} \quad [\text{m}] \tag{5.12}$$

If $L_T \gg L_R$, e.g. in a Very Large Aperture MIMO system, then the Far Field distance will be greater than the threshold distance given in eq. 5.12. It must be noted, though, that this does not imply that the spherical wave should not be employed beyond the threshold distance given in eq. 5.12, since *the threshold distance gives the distance under which the plane wave model should no longer be used due to capacity underestimation.* Contrarily, if the spherical wave is maintained beyond the threshold distance no error increment should be expected. It is for this reason that it was decided to use the Near Field Region (bounded by the Far Field distance) as the equivalent delimiter for the short-range region in which the spherical model ought to be applied (in this project).

As a final remark, the non-broadside case was tackled in [7] as per the equivalent broadside aperture, being a generalised formula given by the expression below:

$$R_{\text{th}} = 4L_T L_R \cos\phi_T \cos\phi_R \tag{5.13}$$

where ϕ_T and ϕ_R are the transmit and receive arrays angular displacement, relative to each other (azimuth angles). This procedure of Near Field contour calculation as per the equivalent broadside array at an echelon direction was the one followed as well in this project to solve the Near Field Region of the Massive Array (see chap. 4 on page 27), which gives further endorsement to the arguments above to use the Near Field Region as the short-range spherical-wave model application region.

5.4.2 Optimisation factors

The authors of [7] include as well several optimisation factors that can lead to both a higher and a better behaviour of MIMO capacity in the short-range.
These optimisation factors can be grouped into two sets:

- T-R distance.
  They conclude that, in general, the shorter this distance is, the higher short-range MIMO capacity will be.

- Array geometry.
  In general, a large aperture yields higher capacity. However, antenna geometry (and particularly its spacing) and the azimuth angles are interrelated. This interrelation is given in the form of capacity dependence on both DOD and DOA for a given T-R distance and several spacings. In brief:
  - That dependence makes the shape of capacity curves (capacity vs DOD and DOA) hold up for a spacing within $[1\lambda - 5\lambda]$. In this case, optimality is achieved (curves hit their maximum value) at the broadside direction and when both arrays are parallel to each other, being this condition given by a unique pair of DOD and DOA, i.e. (DOD,DOA)=(0,0).
  - When the spacing is higher than 5λ, then curves get rippled, the maximum direction might not be the broadside direction any more and maxima are obtained for more than one combination of DOD and DOA (several optimal directions exist, rather than only one).

Further discussion on this can be found in appendix B on page 171.

5.5 Conclusion on spherical-wave model for the LOS scenario

In this project, the spherical-wave model is simplified to the two-dimensional case. For this purpose, transmit and receive arrays are projected onto the XY-plane, and thus the Z-dimension is neglected. This results in the elevation angles, θ_T and θ_R being projected onto the XY-plane and then neglected, and the azimuth angles ϕ_T and ϕ_R, only, being considered.

In other terms, capacity can be very much brought to accordance with measurements when the spherical-wave model is applied within a region given by an empirical threshold distance extracted by the authors of [7]. It has been argued in this case to extend that threshold to the one given by the Near-Field Region, since **validity of the spherical-wave model beyond the former threshold is guaranteed**.

Finally, it has been discussed on the capacity optimisation factors, which mainly account for the distance between the transmitter and the receiver (T-R distance) and the array geometry, given by the azimuth angles and the antenna spacing (aperture size). In brief:

- Capacity is higher for a short T-R distance.
- Capacity is higher for a larger aperture (high antenna spacing).
- For a certain T-R distance, capacity shape varies according to both DOD and DOA, achieving the maximum at a single combination of DOD and DOA given by the broadside direction and then being that one the optimal one. However, this does only apply at a spacing within an interval of $[1\lambda - 5\lambda]$. Then, a larger spacing provokes maxima to happen for more than one pair of DOD and DOA via ripples creation, meaning the optimal direction is not unique and might not be at the broadside any more. In any case, though, maximum capacity (for that specific spacing) is always achieved.

Finally, it is claimed that adjusting the array geometry and especially the antenna spacing at both ends, significant capacity increases can be obtained. As a last remark, placing the base station in a place where LOS availability is guaranteed would lead to better performance results.

Chapter 6

Point-to-Point channel model: simplified COST2100.

The COST2100 MIMO channel model is a GSCM, that reproduces the stochastic properties of a MIMO channel over time, frequency and space. Additionally, it can model both multi-user and distributed MIMO scenarios.
This chapter has a two-fold aim. On the one hand, the general properties of the COST2100 model will be covered, including its structure and key modelling aspects. The Channel Impulse Response (CIR) as per COST2100 will be accounted for. On the other hand, this model will be downscaled as already stated in previous chapters. The reasons for this reduction are multiple: simplicity, lack of information on some aspects, considerations on the channel type, etc. All delimitations will be reported. This section is primarily based on [8].

6.1 Point-to-Point MIMO Input-Output relation.

As explained in sec. 3.7 on page 24, the discrete baseband input-output relation of a narrowband MIMO Point-to-Point channel in which the transmitter has M antennas and the receiver N antennas, has the expression below for a time-invariant channel ([11, 25, 2, 26, 10], to name just some):

$$\mathbf{y} = \mathbf{H}(\phi)\, \mathbf{x} + \mathbf{n} \tag{6.1}$$

where ϕ is the azimuth angle.
In a matrix form, this expression is:

$$\begin{bmatrix} y_1 \\ \vdots \\ y_N \end{bmatrix} = \begin{bmatrix} h_{11} & \cdots & h_{1M} \\ \vdots & \ddots & \vdots \\ h_{N1} & \cdots & h_{NM} \end{bmatrix} \begin{bmatrix} x_1 \\ \vdots \\ x_M \end{bmatrix} + \begin{bmatrix} n_1 \\ \vdots \\ n_N \end{bmatrix} \tag{6.2}$$

where:

- $\mathbf{y}$ is an Nx1 matrix containing each output signal at each receive antenna. $\mathbf{y}^{\mathrm{T}} = [y_1 \cdots y_N]$.
- h_{nm} is the channel term as per the m^{th} transmit antenna and the n^{th} receive antenna (azimuth angle dependency has been omitted for readability). As stated in sec. 3.7 on page 24, each of the channel terms will de modelled as per a simplified version of the COST2100 model via a spherical-wave transmission model.
- $\mathbf{x}$ is an Mx1 matrix containing each input signal at each transmit antenna. $\mathbf{x}^{\mathrm{T}} = [x_1 \cdots x_M]$
- $\mathbf{n}$ is an Nx1 noise vector, the n^{th} component being the channel noise the n^{th} receive antenna would suffer from.

The aim of this chapter is to define the simplified COST2100 channel model that will be applied in this project.

6.2 COST2100 model.

6.2.1 Introduction

As stated in chap. 3 on page 17, the system we deal with in the present project is a space-time channel. A space-time channel has three domains (time, angular and delay). The three are defined by a distribution function, being the distribution of the angular and delay domains normally a joint function. In any case, though, the three domains are defined by the selected system model. Thus, choice on which model to use is crucially important. The one that best fits the scenario to be tackled each time is to be chosen. Regarding MIMO systems in particular and as explained as well in chap. 3 on page 17, several types of MIMO models exist, yet these types are mainly split into two groups: deterministic models and stochastic models [11, 8], with the stochastic models being the most widely used ones [8]. They rely on a limited number of parameters to efficiently describe the channel statistics on different domains.
Two approaches to stochastically characterise the channel exist. On the one hand, analytical (or non-physical) models are used to characterise the channel matrix mathematically, by of means a mathematical description; they include antenna effects. On the other hand, channel matrices can be described by using physical models which characterise the propagation radio waves by their delay, DOD, DOA and complex path weight (this is done for different polarisations). However, these models do not include antenna effects, since they are antenna independent. To that purpose, the channel matrix given by the physical model can be directly combined with the antenna array response [8]. Furthermore, a subgroup of stochastic physical MIMO models called **Geometry-based Stochastic Channel Model (GSCM)** constitutes a branch of advanced MIMO channel models, that **statistically describe the properties of the channel via analysis of the geometric distribution of the interacting objects in the environment, called scatterers**. The COST2100 MIMO channel model is a GSCM.

The evolution to the COST2100 model stems from the framework of the earlier COST259 and -273 models. COST259 was the first channel model to consider multi antennas as the base station (MISO), and was then extended upon to cover full MIMO systems in the COST273 version. Later on, this was extended to COST2100 to larger MIMO systems, including multi-user, multicellular and cooperative aspects.

6.2.2 Geometry-based Stochastic Channel Models: Multipath Components (MPCs).

The principle of a GSCM is to model the stochastic properties wireless channels by analysing the geometric distribution of the interacting objects in the environment, known as scatterers.

For a radio channel, this is done by modelling the superposition of all the existing propagation paths, known as Multipath components (MPCs). The MPCs are caused by the interaction of the radio waves with the scatterers, and are characterised by the delay and direction domains. Furthermore, each MPC can result from the interaction of the radio wave with a single object or multiple objects (single or multiple bounces).

Each scatterer results into an MPC, whose delay and angles are calculated geometrically. The delay of an MPC is the sum of all partial delays: from the BS to the scatterer, cluster-link delay (if it exists) and from the scatterer to the Mobile Terminal (MT).

In case there is LOS, like in this project, that is treated as a special cluster that results in only one MPC.

In brief, the main feature a scatterer has is its introduction of fading in the channel due to the incoherency provided by their random phase.

6.2.3 Key modelling concepts: Visibility Regions, Clusters and Scatterers.

COST2100 is a cluster-based model: each MPC generated by each cluster is modelled as per its stochastic properties. A cluster is defined by a group of scatterers with (quasi-)common features (see last subsection). COST2100 defines three types of clusters:

- Local clusters.
- Single-bounce clusters (far clusters).
- Multiple-bounce clusters (far clusters).

Each cluster will bring along modelling its Visibility Region, its own shape and location and the Scatterers belonging to it.
A complete account for this is included as a reference guide in appendix C on page 173.

COST2100 key modelling concepts will be summarised next.

Visibility Regions

A cluster's Visibility Region (VR) is a region in the environment where the scatterers within the cluster contribute with their MPCs to the channel matrices of the users lying within this region. In other words, it is a region in space where users see the cluster whose VR they are within. They are circular and are uniformly distributed in the simulation area. The VR gain is a model of how powerful the cluster is at a specific location of the MT. Thus, it varies as the MT moves.

Clusters

Clusters themselves are modelled as 3D ellipsoids. These ellipsoids must have a specific position and orientation, and those are determined by the values that make their spatial spreads match their corresponding delay and angular spreads. This is seen in fig. 6.1, where h_c is height, b_c is width, and a_c is length. These parameters correspond to elevation spread, azimuth spread and

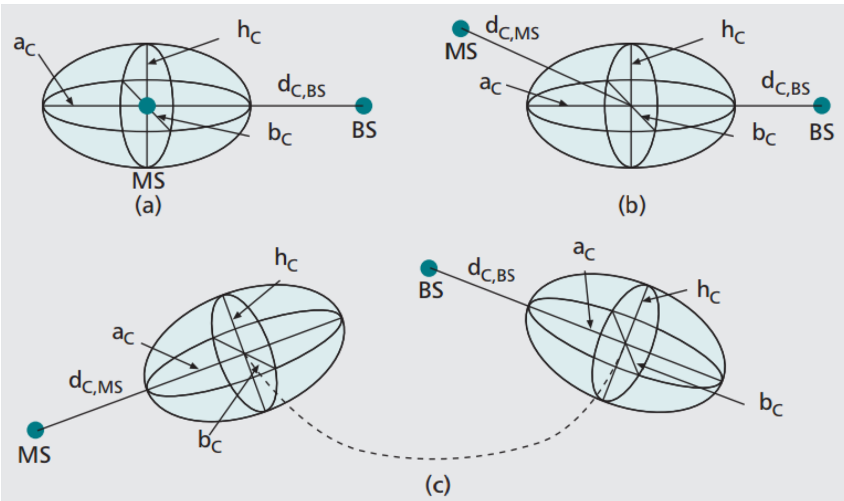

Figure 6.1 *Clusters are modelled as 3D ellipsoids with parameters h_c = height, b_c = width and a_c = length, corresponding to elevation, azimuth and delay spread, respectively. (a)Local Cluster, (b)Single-bounce-cluster and (c)Multiple-bounce cluster. [8]*

delay spread, respectively. In the following, the three types of clusters are described. First, local clusters are described following single-bounce clusters and twin clusters. Finally other cluster parameters are described.

In **local clusters**, the azimuth spread is omnidirectional; the spatial spread is therefore only given by its delay and elevation spread. Scatterers inside are uniformly distributed in the azimuth plane to account for omnidirectionality in this plane.

Single-bounce clusters have independent delay and azimuth spreads. To that purpose, they are rotated towards the BS so that its spatial spreads adequately fit the delay and angular spreads as viewed from the BS. To that purpose, the position of the single-bounce cluster is determined by a random vector originating from the BS. Its length follows a lower-bounded non-negative distribution. Furthermore, that vector is rotated with an angle relative to the imaginary line between the BS and the centre of its corresponding VR. This angle is Gaussian distributed.

In the case of **multiple-bounce clusters or twin clusters**, to determine the position of each of the two twin clusters, the method for a single-bounce cluster is applied twice. First for the BS side, and afterwards for the MT side. A cluster link delay has to be modelled as a non-negative random variable. Its minimum value is the LOS delay between both of the twin clusters' centres.

All and all, each cluster c is modelled according to the following parameters,

- Visibility gain V_c: accounts to how powerful the cluster is depending on the MT's position.
- Shadow fading (large-scale fading) S_c: cluster shadow fading.
- Attenuation L_c: due to the difference between the maximum cluster delay and the LOS delay.
- Inter-link delay τ_c: Inter-cluster delay. Multiple-bounce clusters, only.

Scatterers

Each MPC p created by a scatterer having the same index p is modelled according to the following parameters:

- Complex fading introduced by the p-th scatterer (complex fading suffered by the p-th MPC): $a_{c,p}$, Gaussian complex variable.
- Delay $\tau_{c,p}$: Delay due to distance BS-scatterer p-MT.
- DOD of the p-th MPC in cluster n $\Omega_{c,p}$
- DOA of the p-th MPC in cluster n $\Psi_{c,p}$.

We warn the reader that the angular direction, given as φ in previous chapters is split into Ω and Ψ in COST2100 for the departure and arrival directions, respectively. Then, each has an azimuth ϕ and an elevation θ dependence:

- Departure, DOD: $\Omega \equiv (\phi^T, \theta^T)$.
- Arrival, DOA: $\Psi \equiv (\phi^R, \theta^R)$

where the super-indexes T and R stand for Transmitter and Receiver, respectively, since it is the transmitter that sees the direction of departure the same way it is the receiver that sees the direction of arrival.

6.2.4 Channel impulse response CIR as per COST2100.

Due to the inherent nature of stochastic physical models, the scattering modelling has to be combined with the antenna effects to achieve a complete characterisation of the CIR. The CIR is given in the form of the channel matrix **H**, as already stated multiple times.
The Point-to-Point MIMO channel matrix according to these statements is given below:

$$\mathbf{H} = \mathbf{H}(t,\varphi,\tau) = \mathbf{H}(t,\Omega,\Psi,\tau) = \frac{1}{L}\sum_{c\in\aleph} V_c\sqrt{\frac{S_c}{L_c}}\left[\sum_{p=1}^{N_s^c} a_{c,p}\cdot s_T(\Omega_{c,p})\cdot s_R(\Psi_{c,p})\cdot\delta(\tau-\tau_c-\tau_{c,p})\right] \tag{6.3}$$

where the new parameters are:

- L is the overall pathloss between the BS and the MT.
- $\aleph$ is the set of visible clusters according to the MT's location.
- N_s^c is the number of scatterers in cluster c.
- $s_T(\Omega_{c,p})$ is the steering vector of the transmit antenna in the DOD provided by $\Omega_{c,p}$.
- $s_R(\Psi_{c,p})$ is the steering vector of the receive antenna in the DOA provided by $\Psi_{c,p}$.
- $\delta(\cdot)$ is the Dirac function.

In a general fashion, the steering vectors are defined for the whole array, fixing an axis and a spatial point of reference for both ends, which in turn define the DOD and DOA, which are projected into the fixed axis at both ends. This is a Far Field focus. Definition of the steering vectors in the Far Field may be found in [25, chap. 7]

6.3 Simplified COST2100 model.

6.3.1 Spherical-model application (short range).

As explained in chap. 3 on page 17, the Point-to-Point MIMO scope implied that the channel response **H** be a matrix containing NxM entries, since M is the number of transmit antennas and N is the number of receive antennas. This is already considered by the COST2100 model, that states that the CIR is given in the form of a matrix. However, COST2100's channel matrix is not defined element-wise as the spherical-wave model would require, due to the definition of the steering vectors.
Yet, if the spherical model is applied to COST2100, then element-wise distinction is to be done and thus, some of COST2100's parameters having a collective influence may be now split into each of the contributors'. For instance, the overall pathloss L, accounting for the overall T-R pathloss will now be able to be split into *all of the elements' individual pathlosses, term-wise.* In the same line and more importantly, the steering vectors are to be defined element-wise (see subsec. 6.3.5 on page 50). It has then been decided that the expression given in eq. 6.3 be included in each term of the channel matrix **H**:

$$\mathbf{H} = \begin{bmatrix} h_{11} & \cdots & h_{1M} \\ \vdots & \ddots & \vdots \\ h_{N1} & \cdots & h_{NM} \end{bmatrix} \tag{6.4}$$

each term h_{nm} is proportional to the expression given in eq. 6.3. We note this with a *proportional to* symbol:

$$h_{nm} \propto \frac{1}{L_{nm}}\sum_{c\in\aleph} V_c\sqrt{\frac{S_c}{L_c}}\left[\sum_{p=1}^{N_s^c} a_{c,p}\cdot s_m(\Omega_{c,p}^m)\cdot s_n(\Psi_{c,p}^n)\cdot\delta(\tau-\tau_c-\tau_{c,p})\right] \tag{6.5}$$

where:

- L_{nm} is the pathloss between the m$^{\text{th}}$ transmit antenna and the n$^{\text{th}}$ receive antenna (spherical-wave model).
- The transmit and receive antenna steering vectors s_T and s_R are no longer unique (for a specific MPC in a cluster), but vary according to which pair (m$^{\text{th}}$ transmit antenna, n$^{\text{th}}$ receive antenna) we are dealing with, hence s_m and s_n. Thus, the steering vectors fail to be such and can no longer be defined as in the Far Field.
- The angular directions of the transmitter and receiver are no longer unique (for a specific MPC in a cluster), but vary according to which pair (m$^{\text{th}}$ transmit antenna, n$^{\text{th}}$ receive antenna) we are dealing with, hence (Ω^m, Ψ^n). This goes in line with the abandoning of the Far Field in favour of the Near Field focus, which does not allow any more any projection of DOD and DOA.

All the other parameters are still dependent on the MT as a whole and not antenna element-wise.

6.3.2 Space-time model application

The channel under scope was argued to be narrowband, on a reduced two-dimensional angular domain and fast-fading due to the presence of scatterers, but argued to be time-invariant realisation-wise thanks to the assumption of instantaneous CSIT acquisition(see chap. 3 on page 17).

- The fact it is narrowband, removes the delay dependency in eq. 6.5 on the preceding page.
- The fact the angular domain is two-dimensional and in the azimuth plane only, as discussed in chap. 3 on page 17, narrows down both the DOD and the DOA in eq. 6.5 on the preceding page to the azimuth angles.
- The fact it is fast-fading forces time dependency to remain, at least to account for a general expression.

According to this, an initial downgrade in the channel response would result in the dependencies below:

$$\mathbf{H} = \mathbf{H}(t, \phi^T, \phi^R) \tag{6.6}$$

Eq. 6.7 accounts for the downgraded expression of each term:

$$h_{nm}(t, \phi^m, \phi^n) \propto \frac{1}{L_{nm}} \sum_{c \in \aleph} V_c \sqrt{\frac{S_c}{L_c}} \left[\sum_{p=1}^{N_s^c} a_{c,p} \cdot s_m(\phi_{c,p}^m) \cdot s_n(\phi_{c,p}^n) \right] \tag{6.7}$$

It is important to remark that discarding the delay domain dependence under the assumption of a narrowband channel brings about discarding in turn the presence of multiple-bounce clusters due to their inherent inter-link delay, (necessary to map them geometrically), as long as their delay spread is lower than the duration of a symbol, which we assume. Their contribution was then omitted in eq. 6.7. In other words, a zero inter-delay makes a multiple-bounce cluster collapse into a single-bounce one since both twin single-bounce clusters would overlap (and we remind the reader they are mirror-like clusters). A narrowband channel requires that neither cluster in the environment be multiple-bounce.

In other terms, it must be noted that the cluster attenuation due to the cluster excess delay term L_c does not apply either due to the above arguments.

Finally, it must be remarked that the 2D downgrade as per the space-time channel model makes clusters become ellipses rather than ellipsoids, i.e. their height is zero. Fig. 6.2 on the next page accounts for that.

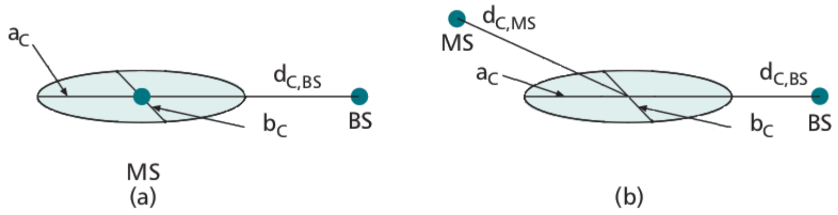

Figure 6.2 *Clusters are modelled as 2D ellipses with parameters b_c = width and a_c = length, corresponding to azimuth and delay spread, respectively. (a)Local Cluster, (b)Single-bounce-cluster. Fig. modified from [8]*

6.3.3 Definition of Visibility Regions at the Massive Array.

One of the key aspects to achieve a good model, able to cover a scenario with dynamic users, is to consider Visibility Regions not only at the users, but also at the massive array [9], as shown in fig. 6.3.

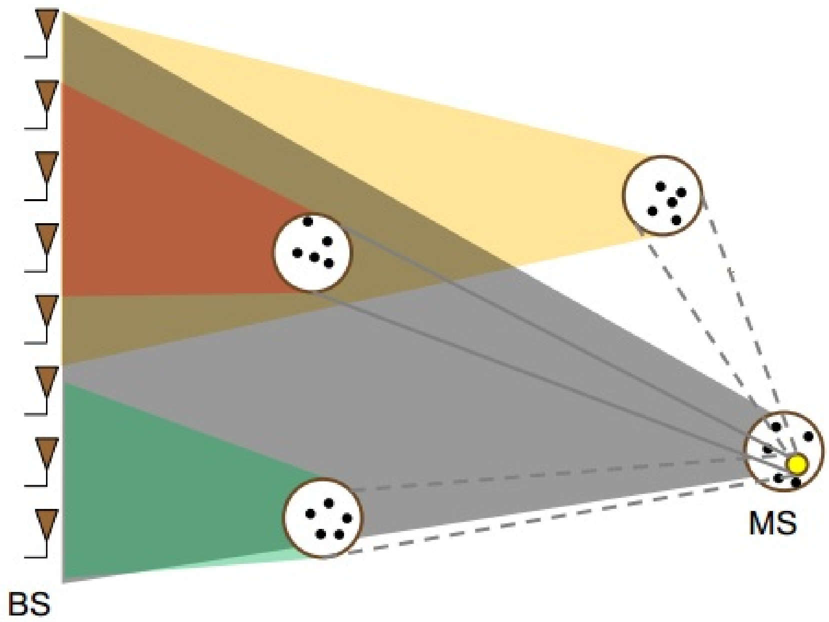

Figure 6.3 *Visibility regions seen from the massive array (BS) and the user (MS). The local cluster to the user (the one surrounding it) is always visible to both the user and the array. [9]*

The mathematical definition and modification of the channel term given in eq. 6.7 on the preceding page will be done in the lines below.

Terms extractions. Cluster visibility gain dualised and defined via pathloss components.

It was stated lines above that should there be a LOS component, that could be treated as a special type of MPC originated in a cluster that does not *give birth* to any other component. Applying superposition inversely, we could extract this cluster from the set of clusters $\aleph$ in the form of the LOS component and write it separately, taking for granted the LOS component is always visible. Should this not be the case hereinafter, specific remark will be made.
Similarly, the local cluster to the receiver, which is always visible to it, could as well be extracted. Both extractions would result into the following general expression for each term:

$$h_{nm}(t, \phi^m, \phi^n) = h_{nm}^{LOS} + h_{nm}^{LC} + h_{nm}^{FC} \tag{6.8}$$

Each of the subterms dependencies have been omitted to ease notation. LC stands for Local Cluster, FC stands for Far Clusters and, to state the obvious, LOS stands for Line Of Sight.
It must be remarked that all the Far Clusters will be single-bounce since the multiple-bounce ones were discarded lines above.
Finally, it is observed that the *proportional to* symbol is no longer used, but the ordinary equal symbol. This is because eq. 6.8 on the preceding page is the general expression used to model the scenario in this project. The reason it differs from the expressions above is that the $mn-th$ overall pathloss term L_{mn} will no longer be multiplying the contributions from all the scatterers but inserted into each of the subterms instead:

$$h_{nm}^{LOS} \propto \frac{1}{L_{nm}^{LOS}}$$

$$h_{nm}^{LC} \propto \sum_{p=1}^{N_s^{LC}} \frac{1}{L_{nm}^{p}}$$

$$h_{nm}^{FC} \propto \sum_{c\in\mathcal{FC}} \sum_{p=1}^{N_s^{c}} \frac{1}{L_{nm}^{c,p}}$$

It must be noticed that in the case of the Far Clusters subterm, since the weighting is scatterer-specific, the pathloss distance will depend on each far cluster and each scatterer inside each far cluster. New notation is as follows:

- N_s^{LC} is the number of scatterers in the Local Cluster.
- $\mathcal{FC}$ accounts for the group of visible Far Clusters.
- N_s^c is the number of scatterers in the Far Cluster c.

This approach is used for Visibility Region Gain modelling, removing the need to further control the cluster Visibility Gain. Intuitively, if the cluster is very far away from either the user or the massive array, it is barely visible. Accordingly, two terms account for the Visibility Gain (given in the form of pathloss), now. These are the pathloss seen from the massive array and the pathloss seen from the user.

6.3.4 Shadowing disregard.

Shadowing will be disregarded for all terms, assuming a direct component in the form of LOS is always present, and clusters do not provoke shadowing to either each other or the link between any transmit antenna at the masive array and any receive antenna at any user. This is called Total Free Space. Therefore, shadowing will be ignored in all the terms.

6.3.5 Steering vectors.

Steering vectors $s_m(\phi_{c,p}^m)$ and $s_n(\phi_{c,p}^n)$ are to be used as per the spherical-wave transmission model definition (Near Field). Note that in the Near Field, $s_m(\phi_{c,p}^m)$ and $s_n(\phi_{c,p}^n)$ are complex scalars, as defined below. In a general case, though, they would be defined as for the azimuth angles and the projection of the antennas towards a reference axis, something that can be understood as a Far Field definition (for further understanding and detail, see chap.7 in [25]). In our case, though, and due to the application of the spherical-wave model, each end can effectively distinguish each element at the other end and so, no reference axis for distance projection according to the azimuth angles is to be employed. Thus, the steering vectors will be only distance dependant. Since COST2100 splits them into the transmit and receive signatures, its definition is as follows:

$$
\begin{aligned}
s_m(\phi_{LOS}^m) \cdot s_n(\phi_{LOS}^n) = e^{-jkR_{mn}} = e^{-jkR_{nm}} \\
s_m(\phi_{c,p}^m) \cdot s_n(\phi_{c,p}^n) = e^{-jkR_{mp,c}} \cdot e^{-jkR_{pn,c}}
\end{aligned}
\tag{6.9}
$$

where the symbol $\cdot$ represents the complex multiplication operator, $e^{(\cdot)}$ is the natural exponential function, R_{mn} [m] is the distance from the m$^{\text{th}}$ transmit antenna and the n$^{\text{th}}$ receive antenna, $R_{mp,c}$ [m] is the distance from the m$^{\text{th}}$ transmit antennas and the p^{th} scatterer in cluster c, $R_{pn,c}$ [m] is the distance from the p^{th} scatterer at cluster c to the n$^{\text{th}}$ receive antenna and k [rad/m] is the wavenumber.

It has to be noticed that it has been decided that all antennas at each end be omnidirectional in the XY plane, shared by both ends (2D downgrade).

6.3.6 Subterms definition.

According to the lines above, the definition of each subterm would result in the following expressions:

LOS

$$h_{nm}^{LOS} = \frac{1}{L_{nm}^{LOS}} \cdot e^{-jkR_{nm}} \tag{6.10}$$

Where:

- ${}^1\!/\!_{L_{nm}^{LOS}} = \left({}^1\!/\!_{R_{nm}}\right)^{n_v}$
  being R_{nm} [m] the distance between the m-th transmit antenna and the n-th receive antenna and n_v a dimensionless voltage loss exponent. Since the ends m and n are in each other's Far Field and we assume Free Space between them, this is set to 1 (power loss of 2). This implies there is Total Free Space between each element at all times (no shadowing) and no reflections from the ground, walls or ceiling.

- The steering vectors $s_m(\phi_n^m)$ and $s_n(\phi_m^n)$ collapse into $e^{-jkR_{mn}}$, being k [rad/m] the wavenumber.

All in all, the LOS subterm results in the following expression:

$$h_{nm}^{LOS} = \left(\frac{1}{R_{nm}}\right)^1 \cdot e^{-jkR_{nm}} \tag{6.11}$$

LC

$$h_{nm}^{LC} = \sum_{p=1}^{N_s^{LC}} a_{LC,p} \cdot \frac{1}{L_{nm,p}^{LC}} \cdot e^{-jkR_{mp}} \cdot e^{-jkR_{pn}} \tag{6.12}$$

Where:

- ${}^1\!/\!_{L_{nm,p}^{LC}} = \left({}^1\!/\!_{R_{mp} \cdot R_{pn}}\right)^{n_v}$
  being R_{mp} [m] the distance between the m^{th} transmit antenna and the p^{th} scatterer (seen from the transmitter) and being R_{pn} [m], the distance between the p$^{\text{th}}$ scatterer and the n$^{\text{th}}$ receive antenna. n_v is a dimensionless voltage loss exponent. As done with the LOS component, this is set to 1 (power loss of 2). This implies there is Total Free Space between each element at all times (no shadowing) and no reflections from the ground, walls or ceiling.

- The steering vectors $s_m(\phi_n^m)$ and $s_n(\phi_m^n)$ collapse into $e^{-jkR_{mp,LC}} \cdot e^{-jkR_{pn,LC}}$, where distances as as per the previous bullet point and k [rad/m] is the wavenumber. The subscript LC is reminder for Local Cluster.
- N_s^{LC} is the number of scatterers in the local cluster.
- $a_{LC,p}$ is the complex weighing of the scatterer p in the local cluster. According to COST2100, $a_{LC,p}$ is **complex Gaussian**. This parameter is the most important one modelling a scatterer, since it is responsible for the fading it provides with via the non-coherent phase insertion. Being complex fading, both random amplitude and phase are inserted. Phase incoherency is indispensable but amplitude incoherency is not to such an extent as long as there are enough scatterers to adequately model fading.[1] This lead to the choice of modelling $a_{LC,p}$ as for a complex Gaussian with zero-mean for each component and an equal power introduction, then variance ${}^{0.5}/_{N_s^{LC}}$. This procedure allows to originate a cluster that introduces a mean summed power of 1, as p.eg. done in [29, 30]. Appendix D on page 177 gives full mathematical account of this. In brief, though:

$$\begin{aligned} a_{LC,p} &= \mathrm{Re}(a_{LC,p}) + \mathrm{j}\,\mathrm{Im}(a_{LC,p}) \\ \mathrm{Re}(a_{LC,p}) &\sim \mathcal{N}\left(0, \frac{0.5}{N_s^{LC}}\right) \\ \mathrm{Im}(a_{LC,p}) &\sim \mathcal{N}\left(0, \frac{0.5}{N_s^{LC}}\right) \end{aligned} \tag{6.13}$$

All in all, the Local Cluster (LC) subterm results in the following expression:

$$h_{nm}^{LC} = \sum_{p=1}^{N_s^{LC}} a_{LC,p} \cdot \left(\frac{1}{R_{mp} \cdot R_{pn}}\right)^1 \cdot e^{-jkR_{mp}} \cdot e^{-jkR_{pn}} \tag{6.14}$$

FC

$$h_{nm}^{FC} = \sum_{c \in \aleph} \sum_{p=1}^{N_s^{FC}} a_{FC,p} \cdot \frac{1}{L_{nm,p}^{FC}} \cdot e^{-jkR_{mp}} \cdot e^{-jkR_{pn}} \tag{6.15}$$

Where:

- $\aleph$ is the set of visible far clusters by the mn pair. Since visibility gain is being modelled by means of the pathloss, all far clusters have been decreed to be visible by all pairs at all times, being then $\aleph \equiv all$ in all cases. Should this not be the case hereinafter (e.g., on some simulations), it will be explicitly stated.
- ${}^1/_{L_{nm,p}^{FC}} = \left({}^1/_{R_{mp} \cdot R_{pn}}\right)^{n_v}$
  being R_{mp} [m] the distance between the m^{th} transmit antenna and the p^{th} scatterer (seen from the transmitter) and being R_{pn} [m], the distance between the p^{th} scatterer and the n^{th} receive antenna. n_v is a dimensionless voltage loss exponent. As done with the LOS component, this is set to 1 (power loss of 2). This implies there is Total Free Space between each element at all times (no shadowing) and no reflections from the ground, walls or ceiling.
- The steering vectors $s_m(\phi_n^m)$ and $s_n(\phi_m^n)$ collapse into $e^{-jkR_{mp,FC}} \cdot e^{-jkR_{pn,FC}}$, where distances as as per the previous bullet point and k [rad/m] is the wavenumber. The subscript FC is reminder for Local Cluster.

[1] In conversation with Patrick Eggers [28], the minimum number of scatterers a simulation should consider is 7, so that a realistic fading is obtained. Notwithstanding this, in all our cases, a significantly higher number is used.

- N_s^{FC} is the number of scatterers in the local cluster.
- $a_{FC,p}$ is the complex weighing of the scatterer p in the local cluster. According to COST2100, $a_{FC,p}$ is **complex Gaussian**, as was $a_{LC,p}$. Again, modelling of $a_{FC,p}$ as for a complex Gaussian with zero-mean for each component and an equal power introduction, then variance ${}^{0.5}/_{N_s^{FC}}$. This procedure allows to originate a cluster that introduces a mean summed power of 1, as p.eg. done in [29, 30]. Appendix D on page 177 gives full mathematical account of this. In brief, though:

$$\begin{aligned} a_{FC,p} &= \mathrm{Re}(a_{FC,p}) + \mathrm{j}\,\mathrm{Im}(a_{FC,p}) \\ \mathrm{Re}(a_{FC,p}) &\sim \mathcal{N}\left(0, \frac{0.5}{N_s^{FC}}\right) \\ \mathrm{Im}(a_{FC,p}) &\sim \mathcal{N}\left(0, \frac{0.5}{N_s^{FC}}\right) \end{aligned} \tag{6.16}$$

All in all, the Far Cluster (FC) subterm results in the following expression:

$$h_{nm}^{FC} = \sum_{p=1}^{N_s^{FC}} a_{FC,p} \cdot \left(\frac{1}{R_{mp} \cdot R_{pn}}\right)^1 \cdot e^{-jkR_{mp}} \cdot e^{-jkR_{pn}} \tag{6.17}$$

Chapter 7

Point-to-Point MIMO performance metrics

To conclude on the behaviour of a communication system, the definition of some performance metrics is an essential task. These allow for comparison, both to other systems if the same metrics are applied and to the same system for different situations. Besides, it gives the opportunity to decide if performance expectations are met or not.

The purpose of this chapter is to introduce the performance metrics utilised in this project and argue under which circumstances the system's behaviour meets certain performance goals, in simpler words, when the system behaves well or badly.

The main references to this chapter are [11, 31, 25, 32].

7.1 Single-user and multi-user perspectives

As introduced in chap. 1 on page 1, MIMO is a promising technique to provide higher performance regarding data rates, reliability, etc. Such a MIMO system can be derived in two ways: single-user (or Point-to-Point) and multi-user.

A single-user MIMO system can be understood as a transmitter communicating with only one user, or vice-versa. The user has a receive antenna consisting of an array of two or more antenna elements, enabling the communication system to exploit the advantages of a MIMO technique. In a multi-user scenario, rather than a single user, there exist more, having each of them the same features explained in the lines above.

In general, MIMO systems are expected to achieve higher data rates, whether it being single-user or multi-user. This can measured by means **capacity**. Namely, capacity was computed after optimal power allocation (i.e., waterfilling) for the Point-to-Point case and in the form of sum capacity in the multi-user case.

A deeper attempt to capture the Point-to-Point MIMO system has been carried out throughout this project (yielding the main content of part I). This was mainly due to the will to validate the proposed scattering model as per a simplified version of the COST2100 channel model, as derived in chap. 6 on page 43. Accordingly, a number of additional performance metrics have been defined for the Point-to-Point case. These extra metrics would allow then to comprehend the underlying phenomena that result in the obtained capacity curves, according to the parametrisation of the channel (This had already been introduced in sec. 3.6 on page 24). These additional measures mainly encompass two metrics: (a) the **Condition Number (CN)** [11] (for a two-antenna user case) and a modified version of the **NPCG** [31] (in the more-than-two-antenna user regime); (b) the channel matrix **rank** after the application of optimal power allocation (namely, waterfilling).

Besides the above, and in an attempt to enlighten the analysis of optimal power allocation, i.e. waterfilling, in terms of rank reduction, **conditioning after waterfilling** will also be computed. Although this measure is uncommon in favour of conditioning *before* waterfilling application (measure (a) above), it has been decided to be included for analytical purposes.

On top of the previous, some supplementary analysis was also conducted on the **cumulative distribution function (cdf) curves of the eigenvalues** of the channel matrix $\mathbf{H}$ (before the application of waterfilling). Those curves, though, will only be included for explanatory purposes and will not be shown in a general fashion.

This chapter will only take account of performance metrics as per the single-user (Point-to-Point) scenario. Sum-capacity curves (regarding the multi-user case) will be tackled within the second part of this report, part II on page 87.

7.2 Channel type in the Time Domain recap.

The type of space-time channel has an impact on the derivation of the metrics introduced in sec. 7.1 on the previous page.
As argued in chap. 3 on page 17, the channel that has been modelled is narrowband and fast-fading due to the inherent action of the scatterers present in the environment. Notwithstanding this, it has been explained that instantaneous CSIT is assumed at each time instant (given in the form of simulation realisations).

7.3 Capacity.

Capacity as a metric for Point-to-Point MIMO systems had already been introduced in this report in sec. 3.6 on page 24 as an motivation for the study and delimitation of the space-time channel.
Capacity is defined as the *maximum transmission rate at which reliable communication can be achieved*. If the transmission rate is higher than the channel capacity, then the system breaks down, which means that the receiver makes decoding errors with a non-negligible probability [11].
Definition of capacity varies according to the type of channel. Basically, two factors influence capacity [11]:

1. Knowledge of the channel at the transmitter (CSIT) and at the receiver (CSIR). Commonly, CSIR is taken for granted and CSIT has to be either instantaneously acquired or estimated according to the known channel's distribution.
2. The time-domain nature of the channel: time-invariant or fading.

In the case of slow-fading channels, capacity is not such, but rather a probability of outage is analysed. It is for this reason that we will discard slow-fading channels in this discussion.

Otherwise, CSIR in this project is always assumed.

Lastly, we specify that capacity has been analysed as per the open-loop approach, i.e., discarding eigen-beamforming (pre- and post- coding according to the SVD of the channel matrix $\mathbf{H}$). This lies in the inherent proposal for this project, whose part II analyses beamforming techniques as per robust statistical precoding, then casting eigen-beamforming aside.

The maximum transmission rate $\mathcal{R}_{\max}$ that a system my have at a specific instant t_0 (and then assuming its input covariance matrix $\mathbf{R}_{\text{XX}}$ is fixed) can be evaluated as per eq. 7.1:

$$\mathcal{R}_{\max} = \log_2 \left| \mathbf{I} + \frac{1}{\sigma_n^2} \mathbf{H} \mathbf{R}_{\text{XX}} \mathbf{H}^H \right| \quad [\text{bptx}] \tag{7.1}$$

where $|\ |$ is the determinant operator, $\mathbf{I}$ is the identity matrix, $\mathbf{H}$ is the channel matrix, the superscript ^{H} denotes the Hermitian conjugate, $\mathbf{R}_{\text{XX}}$ is the input covariance matrix, $\mathbf{X}$ is the input vector signal and σ_n^2 is the noise power. Time notation has been ignored to ease readability. Well then, capacity is defined as the maximum value of $\mathcal{R}_{\max}$:

$$\mathrm{C} = \max\left\{\mathcal{R}_{\max}\right\} \quad [\text{bptx}] \tag{7.2}$$

In brief, capacity is defined differently according to the knowledge of lack of knowledge of the instantaneous channel state at the transmitter (CSIT), which eventually comes down to the channel type in the time domain. Capacity definitions are as follows [11, 25, 32] - just to name some - (it must be remarked again that instantaneous CSIR is always assumed):

(a) If instantaneous CSIT can be obtained, optimal power allocation (normally applying waterfilling) is to be done and capacity results in a closed-form expression:

$$\begin{aligned}
\mathrm{C}^{\text{CSIT}} &= \max\left\{\mathcal{R}_{\max}\right\} \\
&= \max_{\mathbf{R}_{\text{XX}}, \text{Tr}(\mathbf{R}_{\text{XX}}) \leq \bar{P}} \left\{\log_2 \left| \mathbf{I} + \frac{1}{\sigma_n^2} \mathbf{H}\mathbf{R}_{\text{XX}}\mathbf{H}^H \right| \right\} \\
&= \log_2 \left| \mathbf{I} + \frac{1}{\sigma_n^2} \mathbf{H}\mathbf{R^o}_{\text{XX}}\mathbf{H}^H \right| \\
&= \sum_{k=1}^{r_{\text{H}}} \log_2 \left(1 + \frac{P_k^o \lambda_k^2}{\sigma_n^2}\right) \quad [\text{bptx}]
\end{aligned} \tag{7.3}$$

Where Tr() is the Trace operator and $\bar{P}$ is the maximum allowed transmit power, $\mathbf{R}^{\mathbf{o}}_{\text{XX}}$ is the input covariance matrix resulting from optimal power allocation, r_{H} is the rank of the channel matrix (the number of eigenvalues greater than zero), P_k^o [W] is the optimal power allocation to eigenchannel k as per waterfilling and λ_k is the k^{th} eigenvalue of the channel matrix. If waterfilling is applied to achieve power optimisation, then eq. 7.3 (showing a closed-from already) results into the equivalent expression below:

$$\mathrm{C}_{\text{WF}}^{\text{CSIT}} = \sum_{k=1}^{r_{\text{WF}}} \log_2 \left(1 + \frac{P_k^{\text{WF}} \lambda_k^2}{\sigma_n^2}\right) \quad [\text{bptx}] \tag{7.4}$$

Where WF stands for waterfilling, r_{WF} is the number of eigenchannels considered by waterfilling, which might be different than the total ones (given by r_{H}), given the requirement $r_{\text{WF}} \leq r_{\text{H}}$. We would like to emphasise the difference between the rank of the channel matrix *before* and *after* waterfilling, i.e. r_{H} and r_{WF}. While r_{H} is the number of parallel independent streams that can be created according to a given channel matrix $\mathbf{H}$, i.e. **multiplexing gain**, r_{WF} accounts for the *strongest ones only*, maximising the capacity of the channel.

Instantaneous CSIT is always the case in time-invariant channels.

Derivation of eq. 7.3 and 7.4 can be found in appendix E on page 181.

(b) If instantaneous CSIT cannot be acquired, normally a distribution may still be obtained. We write this as $\langle\text{CSIT}\rangle$. In this case, the course of action excludes optimal power allocation since that strategy would only fit a specific instantaneous channel. In this case, though, capacity is defined as per the optimal input covariance matrix in accordance with the average channel. Capacity then results into an averaged open-form expression:

$$\mathrm{C}^{\langle\text{CSIT}\rangle} = \max_{\mathbf{R}_{\text{XX}}, \text{Tr}(\mathbf{R}_{\text{XX}}) \leq \bar{P}} \left\{\mathbb{E}_{\mathbf{H}} \left[\log_2 \left| \mathbf{I} + \frac{1}{\sigma_n^2} \mathbf{H}\mathbf{R}_{\text{XX}}\mathbf{H}^H \right| \right] \right\} \quad [\text{bptx}] \tag{7.5}$$

This is the case in fast fading channels. Capacity is averaged over the channel fades during a codeword (so long codewords are preferred) so that fades are averaged out (performance of the codes converges towards a mean performance). Capacity is renamed as *ergodic capacity*. This out-averaging can only be done if fading is modelled as an ergodic process (which is an ordinary assumption), hence ergodic capacity.

As introduced in chap. 3 on page 17, the nature of the space-time channel modelled in this report on the time domain is fast-fading. However, we have argued that, realisation-wise, instantaneous CSIT is assumed. Realisations may be understood as sort of a time-line, among other interpretations (such as the purest conception of realisation as an observation of a stochastic process). Thus, at each realisation, the closed-form expression of capacity can be applied. Capacity results for a set of realisations can be understood as a set of data which may serve as a basis to evaluate capacity of our channel *statistically* via its first and second order moments, namely main and variance values. In lieu of the variance, the standard deviation will be preferred. Fig. 7.1 depicts this procedure.

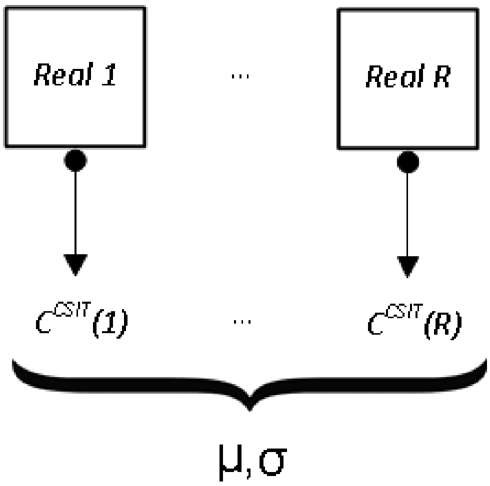

Figure 7.1 *Capacity computation sketch. [*Real *stands for realisation].*

This particular methodology is documented in publications like [32].

7.3.1 Condition Number (CN) and Normalised Parallel Channel Gain (NPCG)

Condition Number (CN)

It is widely known that, due to the expression of capacity assuming instantaneous CSIT (eq. 7.3 on the previous page), capacity is highest when the eigenvalues of the channel matrix **H** are equal to each other, then having all of the eigenchannels the same power (see appendix E on page 181). At high SNR, this means that all eigenchannels are summoned when waterfilling is applied. In this situation, the channel is said to be *perfectly conditioned.* A metric to determine how *well* or *badly* conditioned a channel is called **Condition Number (CN)**. In general, barring the *perfect conditioning* situation, the less spread existing between the channel's eigenvalues, the higher capacity will be. The CN is defined as the ratio of the maximum and minimum eigenvalues of the channel matrix **H**. If the rank of the channel matrix is r_{H}, then there will exist r_{H} non-zero eigenvalues after computing the SVD of **H**, being the complete set $\lambda_{\mathbf{H}}$ defined like $\lambda_{\mathbf{H}} = \{\lambda_1, ..., \lambda_{r_{\mathrm{H}}}\}$. CN is then defined as:

$$\mathrm{CN} = \frac{\max\{|\lambda_{\mathbf{H}}|\}}{\min\{|\lambda_{\mathbf{H}}|\}} \tag{7.6}$$

The power-sense equivalent expression is preferred, though, resulting in the following equation:

$$\mathrm{CN} = \frac{\max\{\lambda_{\mathbf{H}}^2\}}{\min\{\lambda_{\mathbf{H}}^2\}} \tag{7.7}$$

Finally, the logarithmic expression is picked, being the final chosen expression for CN the following:

$$\mathrm{CN} = 10 \cdot \log_{10}\left[\frac{\max\{\lambda_{\mathbf{H}}^2\}}{\min\{\lambda_{\mathbf{H}}^2\}}\right] \text{ [dB]} \tag{7.8}$$

If we rename $\lambda_{\max} = \max\{\lambda_{\mathbf{H}}\}$ and $\lambda_{min} = \min\{\lambda_{\mathbf{H}}\}$, then:

$$\mathrm{CN} = 10 \cdot \log_{10}\left[\frac{\lambda_{\max}^2}{\lambda_{\min}^2}\right] \text{ [dB]} \tag{7.9}$$

And, finally, extracting the square exponents:

$$\mathrm{CN} = 20 \cdot \log_{10}\left[\frac{\lambda_{\max}}{\lambda_{\min}}\right] \text{ [dB]} \tag{7.10}$$

The CN is a parameter able to evaluate a channel's conditioning for any number of antennas at the receiver N. However, it is finest when the number of antennas at the receiver is two, since the maximum rank of the channel matrix is effectively two (we remind the reader about the massive nature of the transmitter in this project - M $\uparrow\uparrow \rightarrow$ M $\gg$ N - and also about the fact the rank of the channel matrix meets $r_{\mathbf{H}} \leq \{$N,M$\}$) and the metric takes into account all of the eigenvalues. For a higher number of antennas at the receiver, though, it has been opted to employ a different metric seeking to lessen the hurdle that the CN possesses to evaluate the evenness of the channel's eigenvalues.

Normalised Parallel Channel Gain (NPCG)

An alternative metric to measure how alike eigenvalues are when the number of antennas at the receiver is greater than two is the Normalised Parallel Channel Gain (NPCG) as follows (based on [31]):

$$\mathrm{NPCG} = \frac{1}{\lambda_{\max}^2}\sum_{i=1}^{r}\lambda_i^2 \tag{7.11}$$

Where r is the number of eigenvalues taken, e.g. r_{H}. We mind the reader that this definition is power-sense.

However, in this project this expression has been altered in order to equate this definition with the CN. Thus, the definition that has been implemented is:

$$\mathrm{NPCG} = \left[\frac{r_{\mathrm{H}}}{\frac{\sum_{i=1}^{r_{\mathrm{H}}}\lambda_i}{\lambda_{\max}}}\right]^2 \tag{7.12}$$

And, in logarithmic units:

$$\begin{aligned}\mathrm{NPCG} &= 10 \cdot \log_{10}\left[\frac{r_{\mathrm{H}}}{\frac{\sum_{i=1}^{r_{\mathrm{H}}}\lambda_i}{\lambda_{\max}}}\right]^2 \\ &= 20 \cdot \log_{10}\left[\frac{r_{\mathrm{H}}}{\frac{\sum_{i=1}^{r_{\mathrm{H}}}\lambda_i}{\lambda_{\max}}}\right] \text{ [dB]}\end{aligned} \tag{7.13}$$

Appendix G on page 189 gives account for proof of validity of this metric and includes its lower and upper bounds.

Joint designation.

Since both the CN and the NPCG provide with information on how much alike the eigenvalues of a channel matrix are, it has been decided to choose a joint denomination for both of them as **Conditioning Metric (CM)**. Notwithstanding this, if the number of antennas at the receiver is exactly two, it is preferred to specify the metric being employed is the CN, instead.

7.3.2 Waterfilling analysis.

Waterfilling rank $r_{\mathbf{WF}}$.

Waterfilling rank r_{WF} is the rank resulting from the application of optimal power allocation, i.e. waterfilling. In other words, it is the number of *strong enough* eigenchannels according to a channel's given SNR. For further understanding of the methodology to evaluate such eigenchannels, see appendix E on page 181. The waterfilling rank is a measure to determine the *effective multiplexing gain* via the effective summoned channels according to waterfilling.

Conditioning after waterfilling

Conditioning after waterfilling will be done as per expressions accounted for in subsec. 7.3.1 on page 58 but according to the *new* rank set by waterfilling, namely r_{WF}, and of course the new set of eigenvalues, accounting for the most powerful first r_{WF} ones.
This analysis is uncommon, being conditioning before the application of optimal power allocation the usual analysis of how well or badly conditioned the channel is. Whether the channel is well or badly conditioned is not an issue in terms of optimal power allocation, as it is how powerful the eigenchannels are. Thus, it may happen that a channel is badly conditioned but at the same time many (or all) of the eigenchannels are summoned (e.g., a high SNR scenario); the channel would still be badly conditioned after waterfilling, although capacity would be maximised.
In other words, the reduction of the effective rank when applying waterfilling might not bring along a significant improvement regarding the channel's conditioning.

The reason to analyse the channel's conditioning *after* waterfilling is precisely to visualise if application of waterfilling *also brings along a conditioning improvement* (which would not necessarily need to happen), if so, when this occurs and to what extent conditioning is upgraded.

7.4 Channels tackled.

In general, the performance metrics explained in the lines above will not only be applied to the channel resulting from the proposed modelling in 6 on page 43. Two more channels will be tackled as an attempt to dekernel the model's behaviour and capture the underlying performance. Those three channels are:

- The LOS channel, resulting from considering the LOS part only at each of the channel matrix terms, then disregarding the NLOS contribution. See eq. 6.8 on page 49. This channel will be identified by the initials **LOS**.

- The NLOS channel, resulting from considering the NLOS part only at each of the channel matrix terms, then disregarding the LOS contribution. See eq. 6.8 on page 49. This channel will be identified by the initials **NLOS**.

- The total channel, resulting from considering both the LOS and NLOS parts at each of the channel matrix terms. See eq. 6.8 on page 49. This channel will be identified by the initials **TOT**.

In order to achieve a fair comparison when applying the performance metrics at each of the channels, the three of them are normalised with their own Frobenius norm $|| \, ||_{\mathbf{F}}$ prior to the metrics application. Then, the total power gain is constrained by its own dimensions N and M [33]:

$$
\begin{aligned}
\mathbf{H}^{\mathrm{LOS}} &\rightarrow \frac{\mathbf{H}^{\mathrm{LOS}}}{||\mathbf{H}^{\mathrm{LOS}}||_{\mathbf{F}}}\sqrt{\mathrm{N}\cdot\mathrm{M}} \\
\mathbf{H}^{\mathrm{NLOS}} &\rightarrow \frac{\mathbf{H}^{\mathrm{NLOS}}}{||\mathbf{H}^{\mathrm{NLOS}}||_{\mathbf{F}}}\sqrt{\mathrm{N}\cdot\mathrm{M}} \\
\mathbf{H}^{\mathrm{TOT}} &\rightarrow \frac{\mathbf{H}^{\mathrm{TOT}}}{||\mathbf{H}^{\mathrm{TOT}}||_{\mathbf{F}}}\sqrt{\mathrm{N}\cdot\mathrm{M}}
\end{aligned}
\tag{7.14}
$$

Chapter **8**

Proposed Point-to-Point MIMO channel model analysis.

The aim of this chapter is to give account of the most significant analysis results on the behaviour of the proposed MIMO channel in chap. 6 on page 43. The analysis of the channel has been conducted according to the performance metrics accounted for in chap. 7 on page 55.
The simulation environment through which the analysis has been carried out is MATLAB.

8.1 Analysis parameters.

This section contains a list of all the parameters whose impact has been analysed via the defined performance metrics.
Those parameters refer to:

- The Channel. Tbl. 8.1.
- The Massive Array. Tbl. 8.2.
- The User. Tbl. 8.3 on the following page.
- The Local Cluster. Tbl. 8.4 on the next page.
- The Far Clusters. Tbl. 8.5 on the following page.

Parameter	Description
Signal-to-Noise Ratio [SNR]	The ratio *transmit power* over *noise power*.

Table 8.1 *Parameters to isolate regarding the channel.*

Parameter	Description
Number of antennas [M]	Influence of the number of antennas at the Massive array.
Antenna spacing [d_A]	Spacing between elements of the massive array.

Table 8.2 *Parameters to isolate at the Massive array.*

Parameter	Description
Distance to origo $[R]$ *(Spherical coordinate)*	Distance from user to the centre of the Massive array (i.e. radial distance).
Echelon angle $[\phi]$ *(Spherical coordinate)*	Echelon angle from origo, i.e. azimuth angle. ϕ is defined like $\phi \in [0°, 180°]$. The subplane defined by the positive values of x (x^+) and y (y^+) contains $\phi \in [0°, 90°]$ while the subplane defined by the positive values of y (y^+) and the negative values of x (x^-) contains $\phi \in [90°, 180°]$. $$[x^+, y^+] \equiv \phi \in [0°, 90°]$$ $$[x^-, y^+] \equiv \phi \in [90°, 180°]$$ $\phi = 90°$ is the y^+ half-line or broadside direction of the massive array. The endfire direction can be either defined by $\phi = 0°$ (x^- half-line) or $\phi = 180°$ (x^+ half-line).
Distance $[x_0]$ *(Cartesian coordinate)*	x-coordinate. Notice that $x_0 = R \cdot \cos(\phi)$
Distance $[y_0]$ *(Cartesian coordinate)*	y-coordinate. Notice that $y_0 = R \cdot \sin(\phi)$
Number of antennas $[N]$	Antennas at the user array.
Antenna spacing $[d_U]$	Spacing between elements at the user array.
Orientation	The user array orientation.

Table 8.3 *Parameters to isolate at the user.*

Parameter	Description
Density $[N_s LC]$	Number of scatterers at the Local Cluster.
Size $[A^{LC}]$	Size of the Local Cluster (area it occupies).
Weighting	Weighting of scatterers in the Local Cluster.

Table 8.4 *Parameters to isolate at the Local Cluster.*

Parameter	Description
Location	xy-positioning of the Far Clusters (p.eg. influence if in between the user and Massive array).
Density $[N_s^{FC}]$	Number of scatterers at the Far Cluster.
Size $[A^{FC}]$	Size of the Far Cluster (area it occupies).
Weighting	Weighting of scatterers at the Far Cluster.
Number $[N^{FC}]$	The number of Far Clusters seen by the user.

Table 8.5 *Parameters to isolate at the Far Cluster.*

8.1.1 Graphical depiction.

Fig. 8.1 depicts graphically the analysis parameters accounted for in tables above (apart from those related to the channel, namely the SNR).

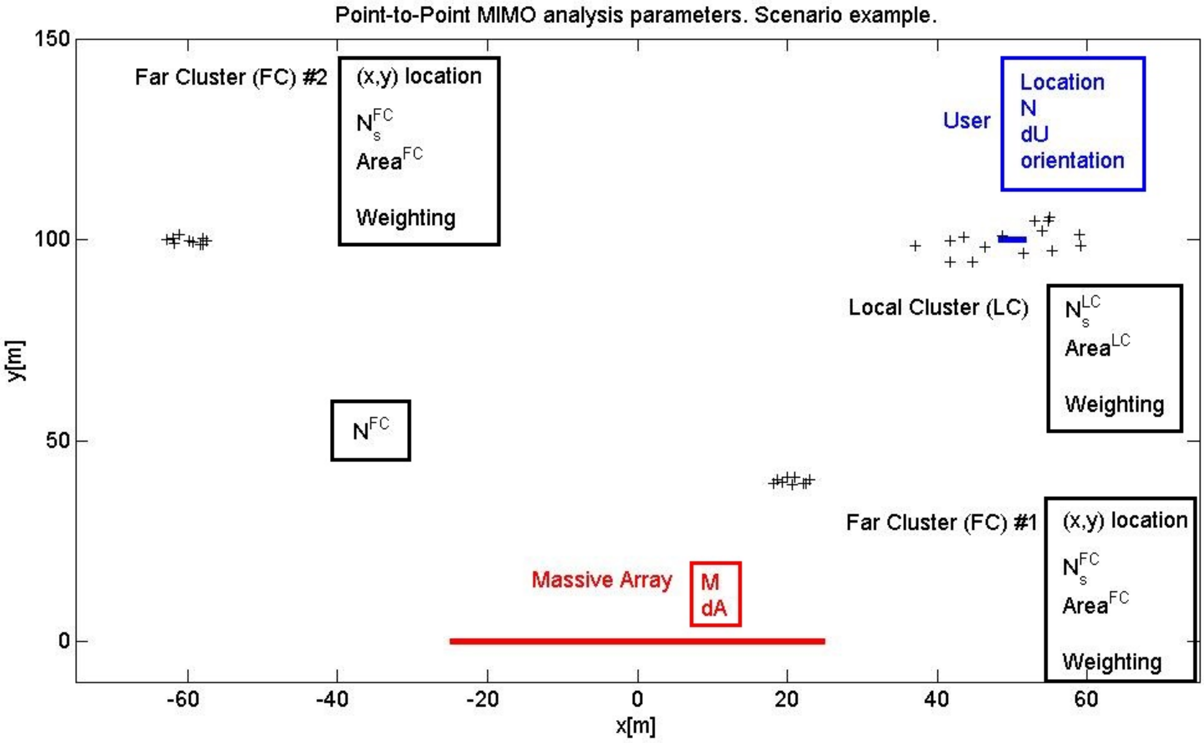

Figure 8.1 *Analysis parameters.*

8.2 Methodology.

The purpose of this analysis is to evaluate the impact on the channel of the parameters listed above through the proposed performance metrics. In this chapter, only the most significant results will be documented.
Unless stated otherwise, the method that has been followed involves isolating the impact of a selected parameter by making it vary, while all the others remain fixed. The ones that remain fixed are called reference parameters, see sec. 8.3. In some situations, though, some of the other parameters are voided. Should this be the case, explicit warning will be made.
For each variation of the isolated parameter, a set of channel realisations will be generated. This will provide the analysis with the sought first and second statistic moments via the mean and std values at all given variations of the selected parameter for all accounted performance metrics (see chap. 7 on page 55).
Resulting curves will be plotted as a function of the isolated parameter. In this chapter, as already stated, only the most significant and meaningful results will be detailed. Thus, not all the isolated parameters will be tackled and on those which are detailed, not all performance metrics might be shown.

8.3 Simulation reference parameters

A complete account of the selected reference parameters (and some additional ones that will never be varied) can be found in the five tables below, considering the channel, massive array, user, local cluster and far cluster in tbls. 8.6, 8.7, 8.8, 8.9 and 8.10,respectively.

Channel parameter	Value	Unit
Power loss exponent	2	[$\cdot$]
No. of users	1	[$\cdot$]
Frequency	4.5	[GHz]
SNR	10	[dB]

Table 8.6 *Channel simulation parameters.*

Tx parameter	Value	Unit
Antenna type	ULA	-
Antenna central location	In origo	-
Antenna orientation	Parallel to x-axis	-
Inter-element separation	3λ=0.2	[m]
Number of elements	251	-
Antenna aperture	50	[m]

Table 8.7 *Massive array simulation parameters.*

Rx parameter	Value	Unit
Antenna type	ULA	-
Antenna central location	[y_0,y_0] or [R_0,ϕ_0]	[m,m] or [m, °]
Antenna orientation	Parallel to x-axis	-
Inter-element separation	6λ=0.4	[m]
Number of elements	2	-
Antenna aperture	0.4	[m]

Table 8.8 *User simulation parameters.*

Local cluster parameter	Value	Unit
No. of scatterers	20	[$\cdot$]
Cluster shape	Elliptic	-
Cluster dimensions	[l,w,h]=[300λ,150λ,0]=[20,10,0]	[m][1]
Scatterers disposition	Inside the ellipse	-
Scatterers distribution	Random (uniformly distributed)	-
Scatterers weighting	None and Random	-

Table 8.9 *Local cluster simulation parameters.*

[1] $\text{Area}^{\text{LC}} = 157.0796[m^2]$

Far cluster parameter	Value	Unit
No. of scatterers	15	[·]
Cluster shape	Elliptic	-
Cluster dimensions	[l,w,h]=[150λ,50λ,0]=[10,3.3333,0]	[m][2]
Scatterers disposition	Inside the ellipse	-
Scatterers distribution	Random (uniformly distributed)	-
Scatterers weighting	None and Random	-

Table 8.10 *Far cluster simulation parameters.*

The following lines take into account the reasoning for some of the selected parameters which have not been examined yet.

- Channel.
  (a) The frequency combined with the aperture of the Massive Array is the one that determines the applications of the spherical wave model. In other words, the Near Field Region ought to be large enough to endorse a spherical wave propagation. On top of that, Massive MIMO appears to be an enabling technology for the upcoming 5G system and a shift to higher frequencies might occur.
  (b) The SNR in an indoors LA-MASS system like the one being tackled in this project is expected to be high. A transmit power of 10 [dBm] employs an SNR being sufficiently high, yet not excessive. While SNR depends on distance and transmit power, depending on the scenario, SNR may vary.
- Massive array
  (a) A number of antennas of $M = 251$ is sufficiently high for a Massive MIMO requirement ($M \gg N$).
  (b) An aperture of 50 [m] is sufficiently large for a Large-Aperture regime.
  (c) As derived in chap. 5 on page 37, a high spacing at both ends is highly beneficial in terms of capacity. A spacing of 3λ is able to meet this requirement.
  A spacing of 3λ and $M = 251$ yields exactly an aperture of 50 [m] at the selected operating frequency.
- User
  (a) A constant orientation of the user along the x-axis, not being the optimal one at a given location (since that one would be the orientation parallel to the massive array, see chap. 5 on page 37), is in turn easier to deal with.
  (b) A number of antennas of $N = 2$ is sufficient to ensure a Point-to-Point MIMO scenario while at the same time CN applies, being that one the most exact conditioning metric (see chap. 7 on page 55).
  (c) While being high for handheld devices, an aperture of 0.4 [m] meets the requirement of a large aperture at the user end for capacity propitiousness.
  (d) The spacing that matches the desired aperture for the given number of antennas is 6λ at the selected operating frequency.
- Local and Far clusters

[2] $\text{Area}^{\text{FC}} = 26.1799[m^2]$

(a) The number of scatterers at the Local and Far clusters, just like their dimensions, are parameters which should be extracted through empirical evaluation at the scenario of interest (COST2100). No relevant parametrisation on the particular scenario tackled in this project has been unearthed by the authors by the time of the edition of this report. Thus, relevant parametrisation had to be computed as per resemblant scenarios. The most related measured scenario was found in [34], where a parametrisation of two different indoor MIMO systems is carried out. However, the Massive nature of this project's MIMO system is missing in this publication in both of them. One of the indoor scenarios modelled in [34] is *"a three-storey office building with a large hall in the middle"*. For this scenario, which may have dimensions comparable to the proposed one in this project, it is stated that the total number of clusters has a mean of 3.69, being 30% of them twin clusters. Barring those yields a resulting mean of 2.58, thus a Local cluster and one or two Far clusters. It has been opted for the former, i.e. one Local cluster and another Far cluster. Regarding the number of scatterers at each cluster, authors in [34] point out that this figure rarely exceeds five (scatterers are referred to as MPCs in this publication). However, owing to the high frequency proposed for Massive MIMO, which would bring along higher resolvability as well, a higher number was selected, namely 20 for the Local cluster and 15 for the Far clusters. This goes in line with conclusions drawn from conversations with [28], who remarks the number of scatterers must be sufficiently high so that a correct propagation model is met. Finally, regarding the dimensions, very few references have been found. Most significantly, it was decided that the Local cluster occupy a larger area than the Far clusters and those were set to 157.0796 [m^2] and 26.1799 [m^2], respectively.

Finally, we let the reader know that the number of channel realisations that has been selected is 500. Realisations are on the channel, namely, on the scatterers random weighting.

8.4 Most significant performance metrics behaviour according to the proposed channel model.

In the following, subsections will contain the name of the isolated parameter whose influence on the channel is to be evaluated as per the proposed performance metrics. The most meaningful results will be contained within.

8.4.1 Channel: SNR

SNR of the channel, namely the ratio *transmit power* P_{Tx} [W] over the noise variance σ_n^2 [W]:

$$\mathrm{SNR} = \frac{P_{\mathrm{Tx}}}{\sigma_n^2} \tag{8.1}$$

Since the channel matrices are unaltered by the value of the SNR, this has no influence over the conditioning of the channel. This is visible in fig. 8.2a on the next page, which shows the CN for the TOT channel for three different user locations, the endfire direction, the broadside direction and an echelon direction given by $\phi = 135°$, at a distance from origo of 50 [m]. Conditioning is very good expect for the endfire case, an expected behaviour since as long as there is not a sufficiently rich scattering environment, antenna elements at both ends become unresolvable due to the nulled effective aperture seen by both ends. However, when optimal power allocation is applied, the higher the SNR is, the more eigenchannels are summoned. This can be seen in fig. 8.2b on the facing page, featuring the rank after waterfilling for the TOT channel for the same users. Notice that at the endfire direction, full rank is only achieved at the highest values of the SNR, due to resolvability achievement. Finally, capacity for the TOT

channel and the same users is shown in fig. 8.3. It must be noticed that the slope of the capacity curves at the high SNR regime matches with the theoretical linear growth of $r_{\mathbf{H}} \cdot \log_2(\text{SNR})$, where the SNR has natural units.
All in all, it can be said that **the effect of a higher SNR results into a higher capacity**.

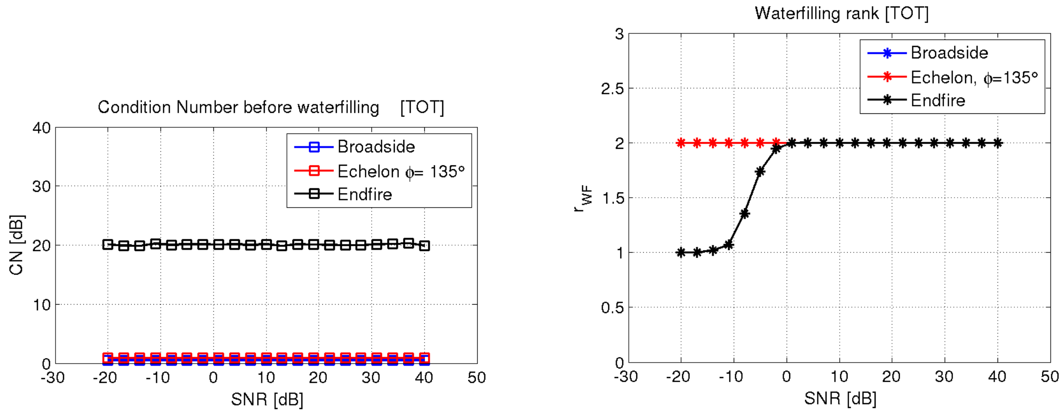

(a) *CN vs SNR.* **(b)** $r_{\mathbf{WF}}$ *vs SNR.*

Figure 8.2 *Conditioning and waterfilling rank.*

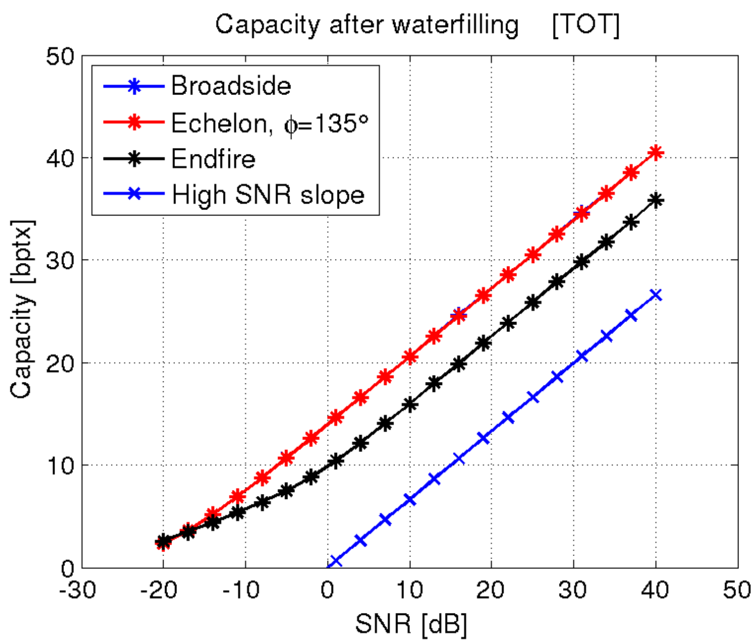

Figure 8.3 *Capacity vs SNR.*

8.4.2 Massive array: number of antennas M

The number of antennas has been varied, maintaining the aperture of the array at a fixed value of 50 [m]. This forcefully implies the spacing varies with the number of antennas M, since the aperture D of a ULA is given by equation:

$$D = (M - 1) \cdot d \ [m] \tag{8.2}$$

Where d is the inter-element spacing.
Results below feature the TOT channel for a user at the broadside direction (radial distance

R=50) with three different number of antennas, N=2, N=4 and N=8. The aperture size has also been maintained at the user side when varying its number of antennas.

Regarding conditioning, the main conclusion is that an increasing number of antennas at the massive array brings along better conditioning, see fig. 8.4a on the facing page. This goes in line with results in literature, p.eg. in [16, p. 13] However, conditioning appears to saturate at an early value of M, approximately between M=25 and M=50 for all N-antenna users. Notice that the highest N-user shows the worst conditioning, something expected as it as well possesses the largest eigenvalue spread and thus, the largest likelihood of unevenness. This is why, conditioning worsens progressively for an increasing number of antennas at the user N. Lastly, the distribution of the eigenvalues is shown in fig. 8.4b on the next page in the form of the Cumulative Distribution Function (CDF) of the the Condition Number for the N=2 user case for three different M values. The CDFs in the LOS cases are totally vertical, meaning very stable eigenvalue spread. However, the TOT curves show some tilting, meaning a larger spread and some added instability. This is due to the NLOS contribution, in which curves clearly slant, pointing towards a much larger spread. In all cases, though, a growing number of antennas at the BS pushes the curves towards better conditioning, confirming the action of an increasing M value.

As regards the rank after waterfilling, it must be noticed that full rank is achieved at all times, meaning that full multiplexing gain is obtained at any M configuration. This is thanks to the scattering environment(LOS ranks are always unit). See fig. 8.4c on the facing page for the TOT channel.

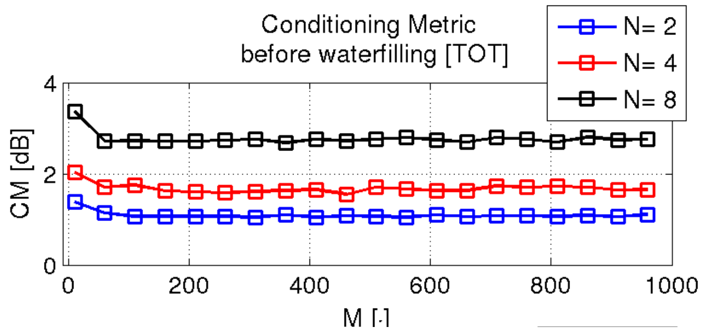

(a) *Conditioning metric versus M, user at broadside direction (R=50 [m] and N=2, N=4 and N=8. TOT channel.*

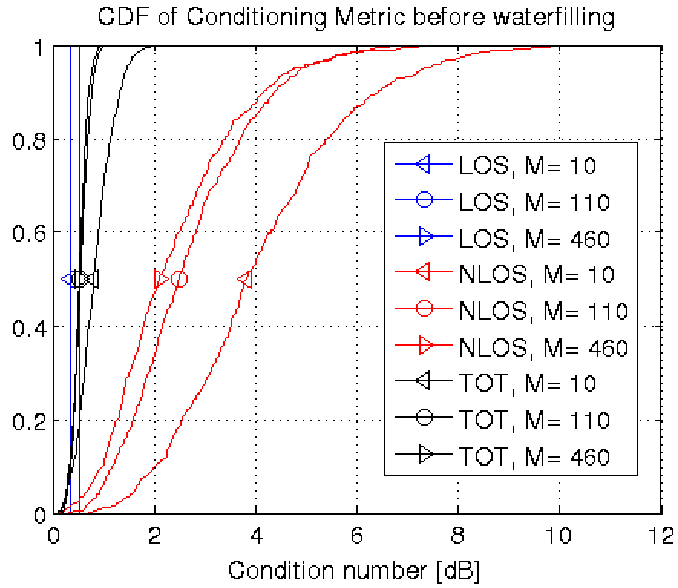

(b) *Eigenvalue for different M values, user at broadside direction (R=50 [m] and N=2 only. LOS, NLOS and TOT channels.*

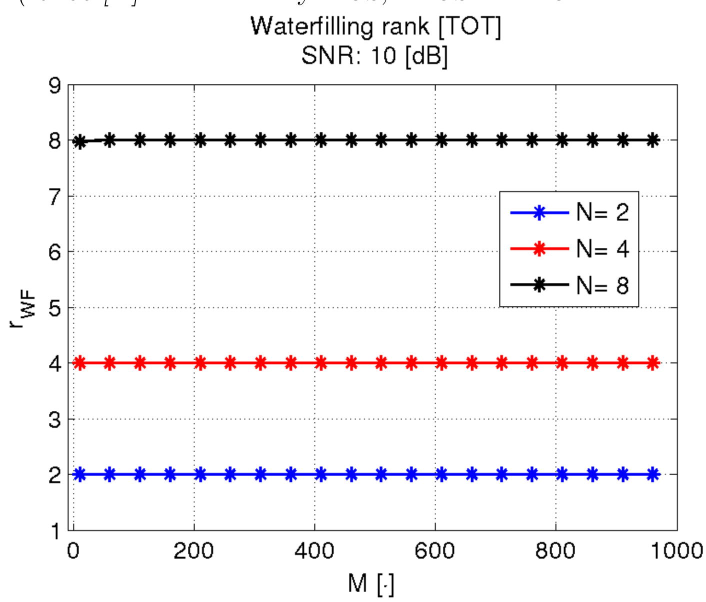

(c) *Waterfilling rank vs M, user at broadside direction (R=50 [m] and N=2, N=4 and N=8. TOT channel.*

Figure 8.4 *Conditioning and waterfilling rank.*

Finally and most interestingly, capacity curves shown in fig. 8.5 on the next page experience

a great improvement with an increasing N (see sec. 8.4.3) and they do so with an increasing M as well. This growth is especially visible for the initial M rise, when capacity grows linearly, which is an expected outcome for the high SNR regime [11]. Then saturation is observed, particularly for the lower N cases. This is due the fixed size of the aperture. For an increasing M, it get to a point where there is no longer angular resolvability, and so Capacity saturates.
All in all, it can be concluded that **a higher number of antennas at the BS results into higher capacity levels**, even for a fixed massive array aperture. **If this is combined with a high number of antennas at the user N, then capacity achievement is larger**.

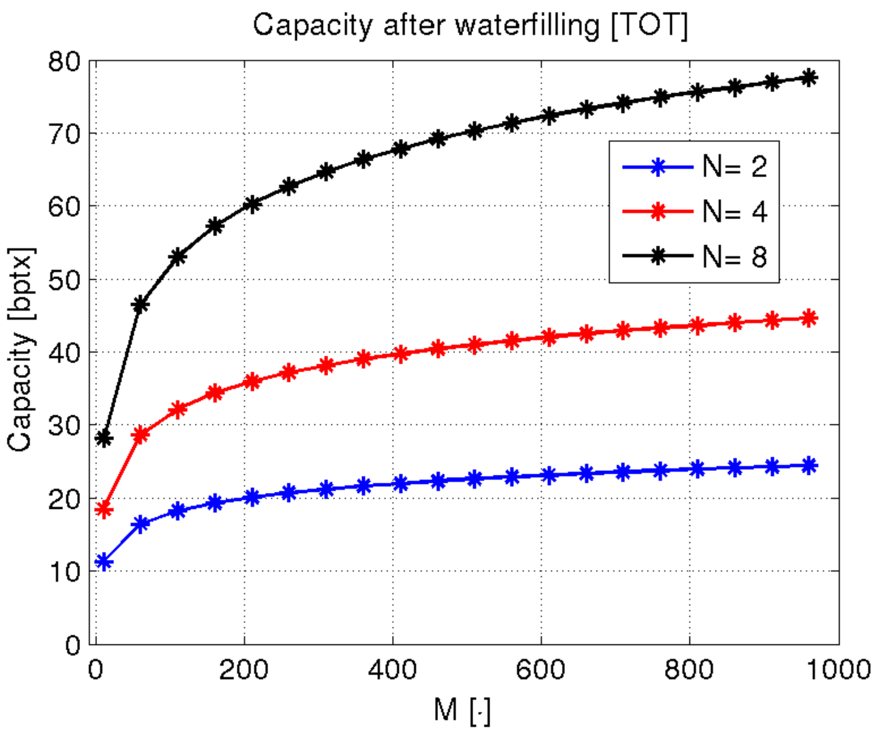

Figure 8.5 *Capacity versus M, user at broadside direction (R=50[m] and N=2, N=4 and N=8. TOT channel.*

8.4.3 User: number of antennas N and aperture D_u

Number of antennas N

The number of antennas N has been varied from one through to 50, fixing the aperture of the user at 0.4 [m]. The user is located at broadside, at $[R, \phi] = [50 \text{ m}, 90°]$. The massive array contains M=251 elements and an aperture of 50 [m]

Fig. 8.6a on the next page exhibits the channel's conditioning for a growing N. Conditioning worsens as N grows, which goes in line with the same behaviour observed for an increasing number of antennas at the massive array M. This is again due to the eigenvalues' enlarged spread as their number gets higher. However, conditioning appears to hold up for the lower N-regime, which would imply this is the area for which a more significant capacity improvement is expected.

With respect to waterfilling rank, seen in fig. 8.6b on the facing page, it can be seen that the rank grows linearly with N until an inflection value of N=14, when its growth rate gets reduced. This goes again in line with the fact multiplexing gain tends to saturate due to antenna elements unresolvability; and since is is the aperture that determines resolvability this behaviour is expected. Thus at some value of N, multiplexing gain considered by waterfilling grows at a much lower rate due to the eigenvalues distribution.

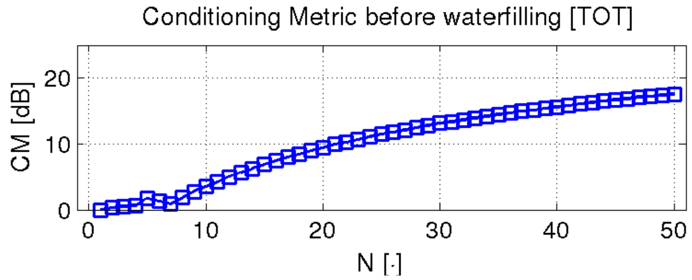

(a) *Conditioning metric vs N, user at broadside direction (R=50 [m]). TOT channel.*

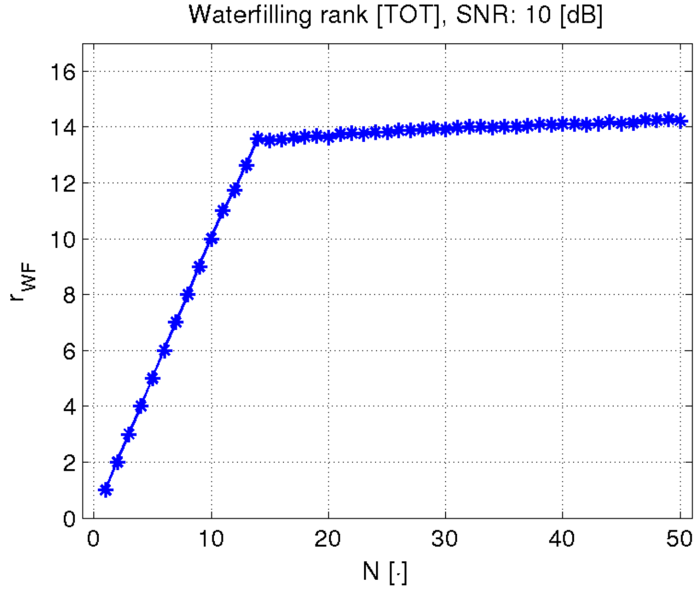

(b) *Waterfilling rank vs N, user at broadside direction (R=50 [m]). TOT channel.*

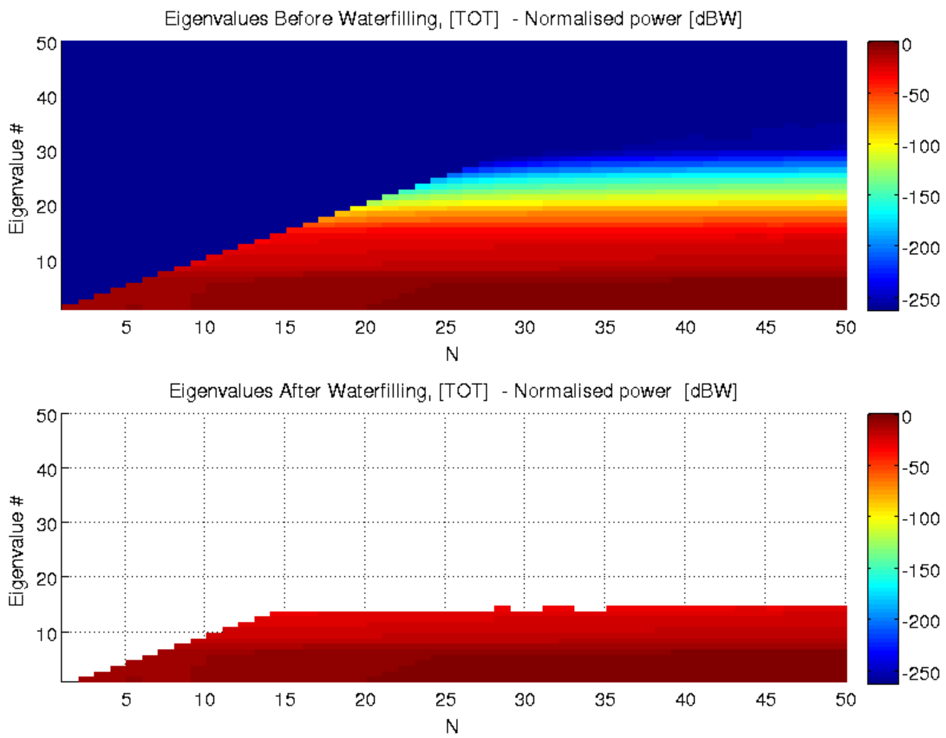

(c) *Eigenvalues normalised power (sorted according to N). TOT channel. After waterfilling application, blank values feature not considered eigenvalues.*

Figure 8.6 *Conditioning, waterfilling rank and eigenvalues nornalised power.*

This can be easily seen in fig. 8.6c on the previous page, which features the normalised power of each eigenvalue (top graph), and the eigenvalues considered by waterfilling (low graph). It can be seen that, considered eigenvalues tend to diminish for an increasing N.

Finally, capacity is drawn in fig. 8.7. The expected value of capacity accounted for above is patent. **Capacity grows linearly with N for the lower levels and then, according to the waterfilling rank, its growth moderates**. Fig. 8.6c on the previous page helps to understand this behaviour. **The main reason why capacity keeps increasing after the waterfilling rank fails to continue increasing significantly is because the considered eigenvalues get more powerful with N**. This goes in line with the surface plot in fig. 8.6c. As N increases, the number of non-zero eigenvalues increases as well up to the point where the linear growth of waterfilling rank fails. Yet **the eigenvalues continue to get stronger**, providing more capacity.

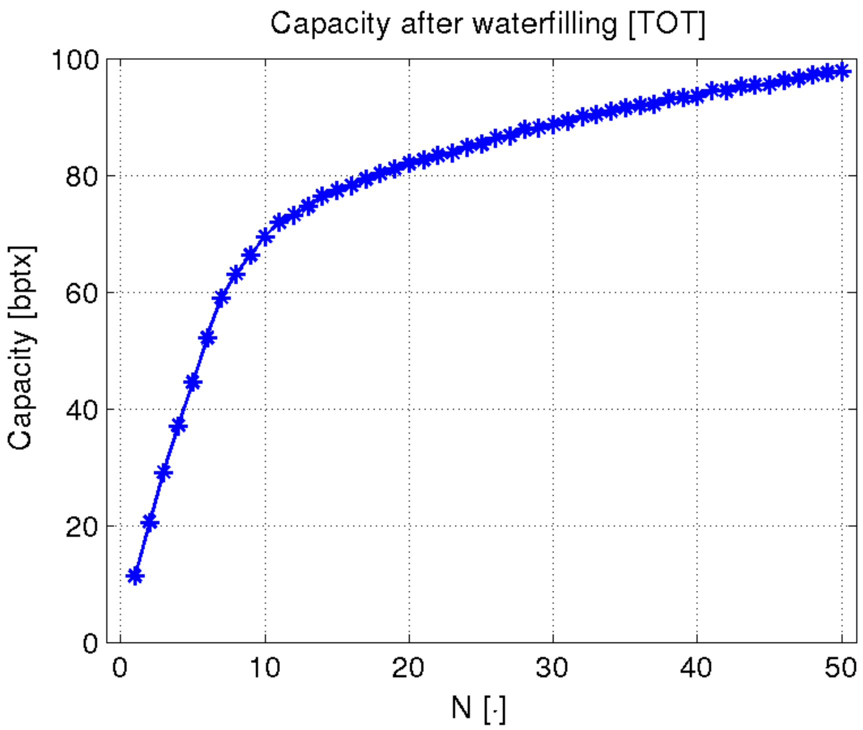

Figure 8.7 *Capacity versus N, user at broadside direction (R=50 [m]). TOT channel.*

Aperture D_u

The aperture of the user D_u has been varied from 0.005[m] to 0.5[m] for the same number of antennas, N=2. The user is located at two locations: (1) at broadside, at $[R, \phi] = [50 \text{ m}, 0°]$; (2) close to the endfire direction, at $[R, \phi] = [50 \text{ m}, 2°]$. We will refer to the latter case as "endfire case", even though that would only be so for an angle of 0°. The massive array has M=251, and an aperture of 50 [m].

Conditioning of the channel is presented in fig. 8.8a on the facing page. As expected, the CN is much higher for the endfire case, since the "effective spacing" is seen low at all times. In contrast, conditioning of the broadside case is in turn adequate at all times, apart from the lowest aperture values (which goes in line with observations for the endfire case, in which the effective aperture seen by the massive array collapses, yielding poor conditioning). These phenomena forecast that the user's aperture will have little impact on capacity.

Otherwise, fluctuations seem to occur on the CN curve for the broadside case. Fluctuations on conditioning are not unique to the variation of D_u and have been observed in some other situations as this chapter will document. In all cases, this phenomenon comes down to

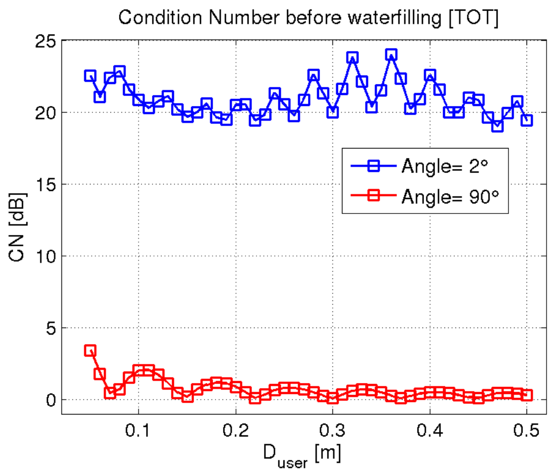

(a) *Condition number vs user aperture. TOT channel.*

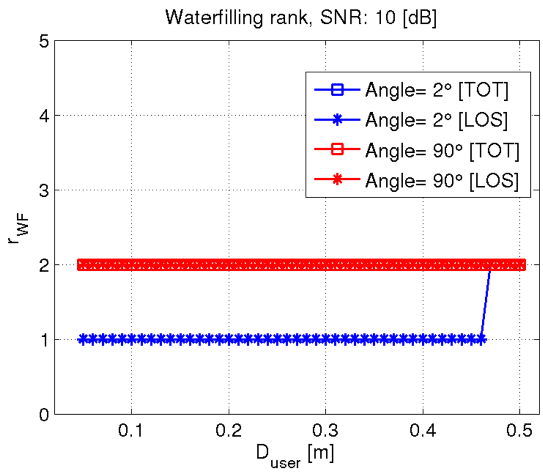

(b) *Waterfilling rank vs user aperture. LOS and TOT channels.*

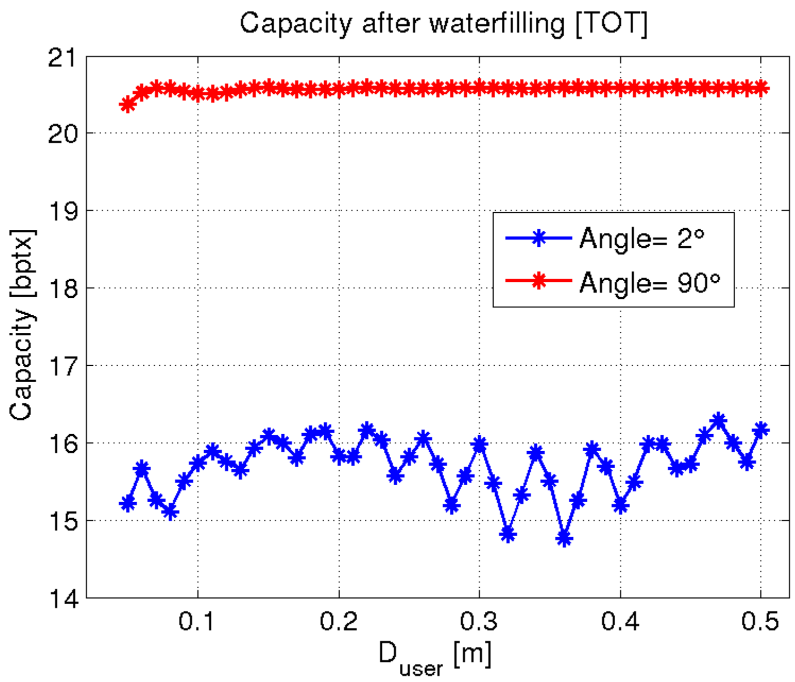

(c) *Capacity vs user aperture. TOT channel.*

Figure 8.8 *Conditioning, waterfilling rank and capacity.*

the propagation signature of the channel matrices, which in turn impinges on the channel's eigenvalue distribution. This is especially noticeable when elements vary their location, such as a modification of D_u. Also, the location of the user itself, see sec. 8.4.4 on the next page.

Regarding the rank after waterfilling, depicted in fig. 8.8b, it must be noticed that in the endfire case and due to poor resolvability, it is only at the highest D_u values that full rank is achieved for the LOS channel, not so for the TOT one.

Finally, capacity plot in fig 8.8c confirms that the growth on the aperture size provokes practically negligible effects on both the broadside and the endfire cases, which supports conditioning observations. On the broadside case, though, a slight initial increase comes down to better conditioning thanks to resolvability provided by the very first aperture increase. To state the obvious, capacity at the endfire case is much poorer than at the broadside.

Joint N+D_u

If the inter-element spacing is maintained when varying N, then the aperture D_u will forcefully do so as well. This joint isolation will be shown next, being the selected spacing of $d_u = 6 \cdot \lambda$ $[m]$. Being this spacing perhaps too high, it will effectively serve to the purpose of this isolation, which aims to verify that a joint variation on N and the aperture is unreservedly beneficial in terms of achieved capacity.
The user is located at broadside, at $[R, \phi] = [50 \text{ m}, 0°]$. Its number of antennas are varied from one to 50, which under the specified spacing yields an aperture ranging from a negligible value (N=1) to almost 20 [m]. It is reiterated that, being such a high aperture for a user totally impractical, this variation will help to understand the expected behaviour of this joint variation. Only the TOT channel will be shown.

Fig. 8.9a features the channel's conditioning, which yields much better results for the joint variation case. As stated before, this comes down directly to the stabilising effect of an increasing number of elements on the statistics of the eigenvalues for an increasing number of elements, as seen for the M isolation [16]. The effect of this is clearly visible in fig. 8.9b, featuring the channel's capacity.

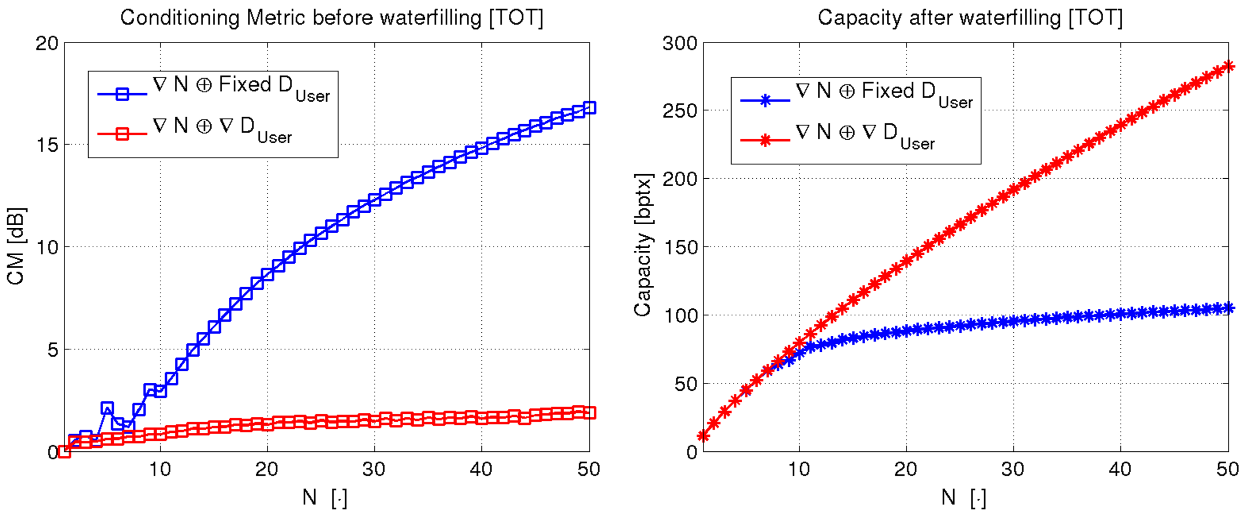

(a) *Condition number vs N (jointly with D_u). TOT channel.*

(b) *Capacity vs N (jointly with D_u). TOT channel.*

Figure 8.9 *Conditioning and capacity for the joint N+D_u isolation.*

8.4.4 User: location

The user's location is one of the key isolated parameters. Isolation of the user's location has been done for a N=2 antenna case, while the massive array contains M=251 antennas and its aperture is set to 33.33 [m] (disobeying this time the reference parameter value). In the first place, the user is located along the broadside direction, varying then the y-coordinate. Finally, a contour plots for all the xy-grid are shown.

Broadside direction

CN curve for the user's location at the broadside direction can be seen in fig. 8.10 on the facing page.
Conditioning is observed to be highly adequate at the close broadside distances of the array, being levels of CN lesser than 1 [dB] up to a distance of y=110 [m], approximately. However, peaks on conditioning are observed at the very close-in distances (y-values lesser than 1 [m]). Although uncertain, it is to our best belief that this might be due to the *reduced effective massive array's aperture* seen by the user at such close-in distances, and goes in line with results of the

kind observed in sec. 8.4.3 on page 74. As ventured in previous subsections, fluctuations appear again. These are due to the wave propagation phase terms' affection on the channel matrix, which in turn act on the eigenvalues distribution. Fluctuations occurrence lessens as distance increases. It has also been observed that, if high resolution simulations are produced, then a higher degree of fluctuations is observed, which goes in line with the reasoning on its cause. Fluctuations yield perfect conditioning at some very specific distances, p.eg. at y=100 [m] and y=200 [m] in fig. 8.10. Those distances would change, should the configuration of the massive array did so as well.

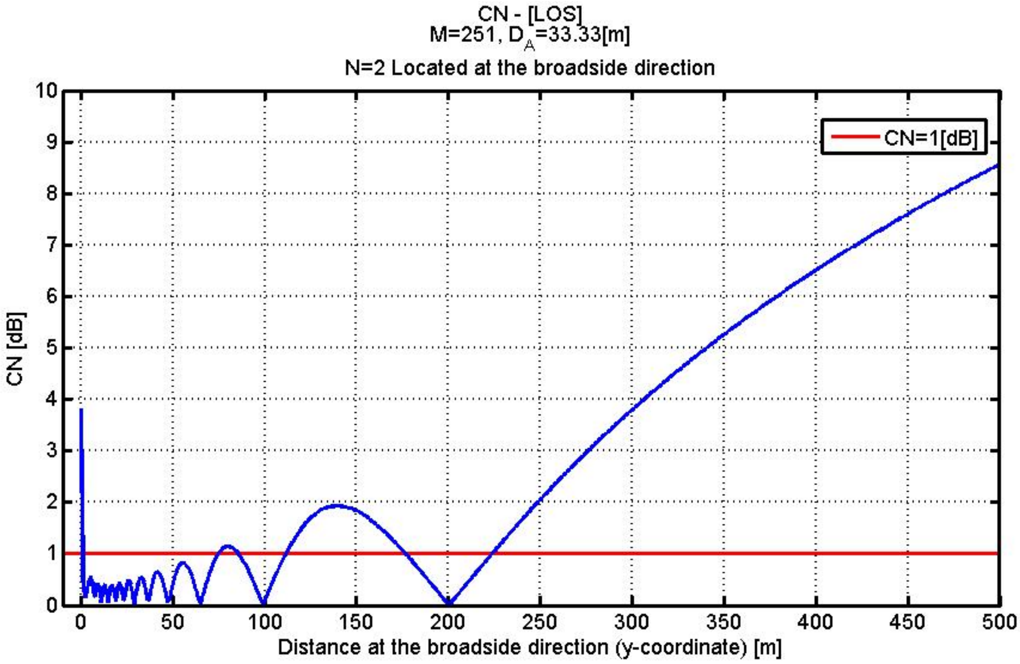

Figure 8.10 *Capacity for an N=2 antenna user, located at several distances from origo along the boradside direction. LOS channel.*

xy grid

Fig. 8.11a on the next page features the channel's conditioning for not only the broadside direction, but for an xy grid of 500 $[m] \times 500$ $[m]$. Notoriously, it can be observed that isocurves follow a quasi-elliptic or oval shape, yielding **the best conditioning at the broadside direction and at closer distances to the massive array**. Fluctuations can be easily confirmed observing the white patches (where CN<1 [dB]) which are surrounded by blue ones. As a matter of fact, an area of CN<1 [dB], unobserved in fig. 8.10, arises on the other hand in fig. 8.11a on the next page. Another significant conclusion is that, **as the user approaches the endfire direction, an important fall on CN occurs**, which comes down to the reduced effective aperture seen by both ends.

In addition, fig. 8.11b on the following page features capacity for the 500 [m] × 500 [m] xy grid. It can be seen that capacity LOS isocurves follow a tendency drawn by the channel's conditioning, being as well maximum in the areas where conditioning is best. Conjunctively, capacity reaches its top values at the broadside direction and at the close-in distances; moreover, a significant drop is observed as soon as the user approaches the endfire direction. In any case, though, capacity levels on the LOS channel are considerably similar to each other.

Conclusively, **the user's location effect on conditioning has a double impingement on the channel's capacity, which varies accordingly**. **Both are better at the broadside direction and at close-in distances to the massive array**.

Lastly, we want to warn the reader that the LOS channel has been selected since it holds the underlying information on capacity behaviour, which is maintained at a high degree in the TOT channel.

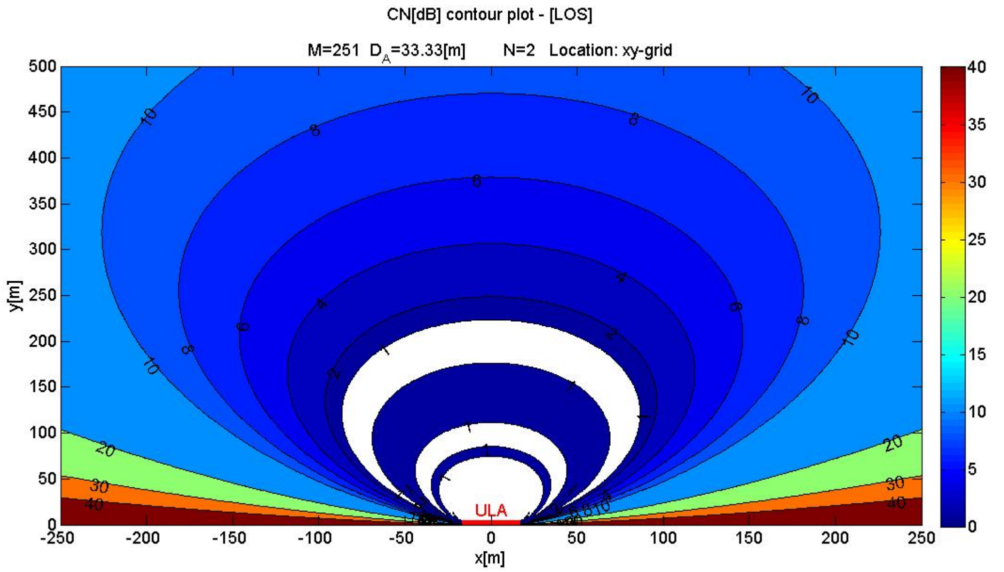

(a) *CN for an N=2 antenna user, located on an xy-grid of* 500 [m] $\times$ 500 [m]. *LOS channel. CN values lower than 1 [dB] are shown in white colour.*

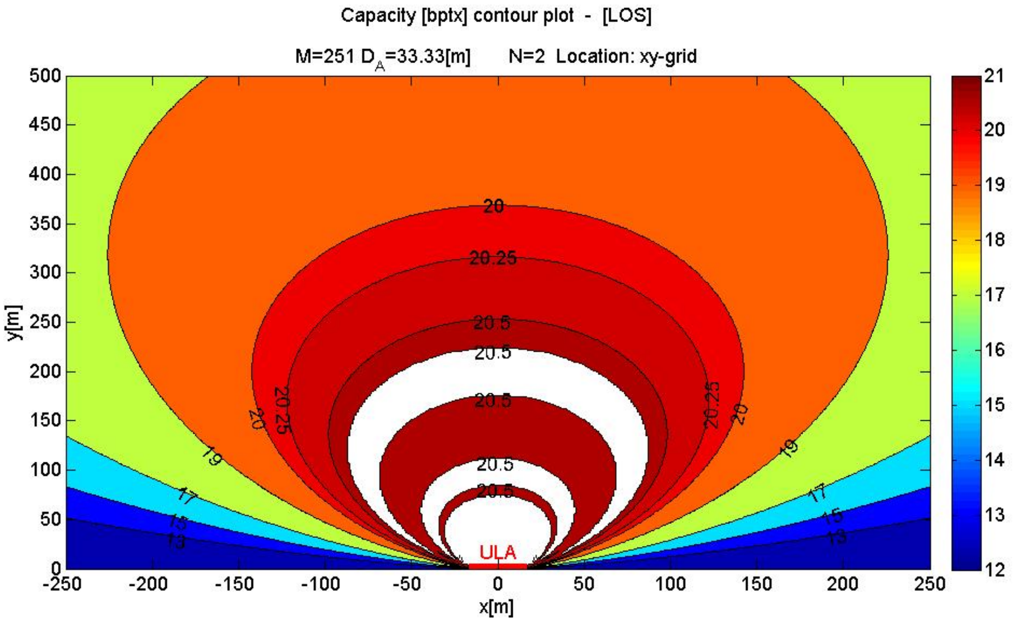

(b) *Capacity for an N=2 antenna user, located on an xy-grid of* 500 [m] $\times$ 500 [m]. *LOS channel. Capacity values greater than 20.57 [bptx] are shown in white colour.*

Figure 8.11 *Conditioning and capacity surface plots vs the user's position. LOS channel.*

8.4.5 User: Antenna orientation

This subsection will be tackled briefly. Its main purpose is to confirm that arguments in chap. 5 on page 37 on the orientation optimality of both ends of the radiolink hold up. To this goal, as the massive array is fixed and oriented along the x-axis, we will ratify that the optimal orientation of the user's array for a specific location is given when the array is parallel to the equivalent broadside array of the massive array (for deeper inspection of the *equivalent broadside array*, we suggest that chap. 4 on page 27 be examined). Or in other words, to verify that the poorest performance occurs when the equivalent broadside array *sees* the user as a source point, something happening when the user's array is perpendicular to the equivalent broadside array of the massive array. This analysis will be done locating the user at both [R,ϕ]=[50 m,5 °] and [R,ϕ]=[50 m,45 °], with N=2. The massive array has M=251 elements and an aperture of 50 [m]. The three channels will be shown, namely LOS, NLOS and TOT channels.

Fig. 8.12a on the next page exhibits the channel's conditioning curves while fig. 8.12b on the following page features the channel's capacity curves at the configuration detailed above.
It can easily be seen that a peak in conditioning together with a dump on the LOS and TOT capacity curves happens twice, coinciding with the orientation angle intervals for which the user's array approaches perpendicularity to the equivalent broadside array; we call each of those intervals *inadequate orientation interval.* **Capacity is minimum when they are exactly perpendicular to each other**. This is evident in the $\phi = 5$ [°] case, where capacity's fall is larger. This echelon direction is much more sensitive to the user's array orientation since, as it is close to the endfire direction, resolvability is handicapped. On the other hand, capacity holds up at orientations off the inadequate orientation intervals; in other words, orientation optimality when both ends are parallel to each other is not that visible, although again it is more obvious for the $\phi = 5$ [°] case. The fact capacity holds up at the non inadequate intervals is explained by the fact that, **as soon as the array is not within the inadequate orientation intervals, quasi-optimality is reached since antenna ends are perfectly resolvable and do not incur any kind of degradation**. However, this is again downgraded at the endfire directions or close. Finally, it must be noted that the NLOS curves do not suffer any downgrade whatsoever at any angles for any of the users. They are even optimal for some orientations. The reason for this is that the scattering environment is rich enough to provide resolvability at any user array orientation. Finally, the reason why the TOT channel is downgraded lies in the fact that it is the LOS component that most significantly influences the channel eigenvalue distribution and thus, conditioning and capacity.

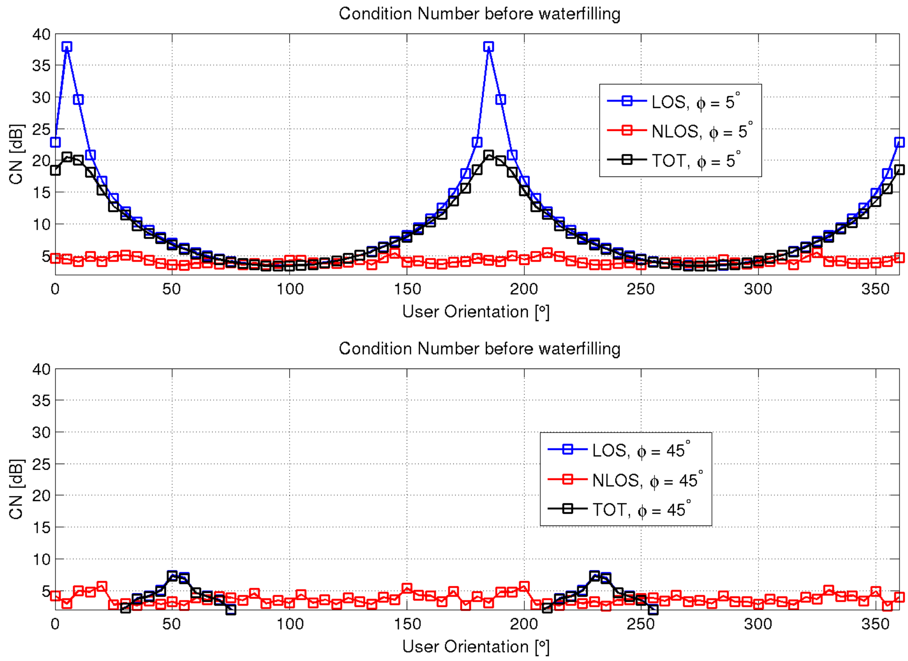

(a) *Conditioning for an N=2 antenna user, located at [R,ϕ]=[50 m,5°] and [R,ϕ]=[50 m,45°]. LOS, NLOS and TOT channels.*

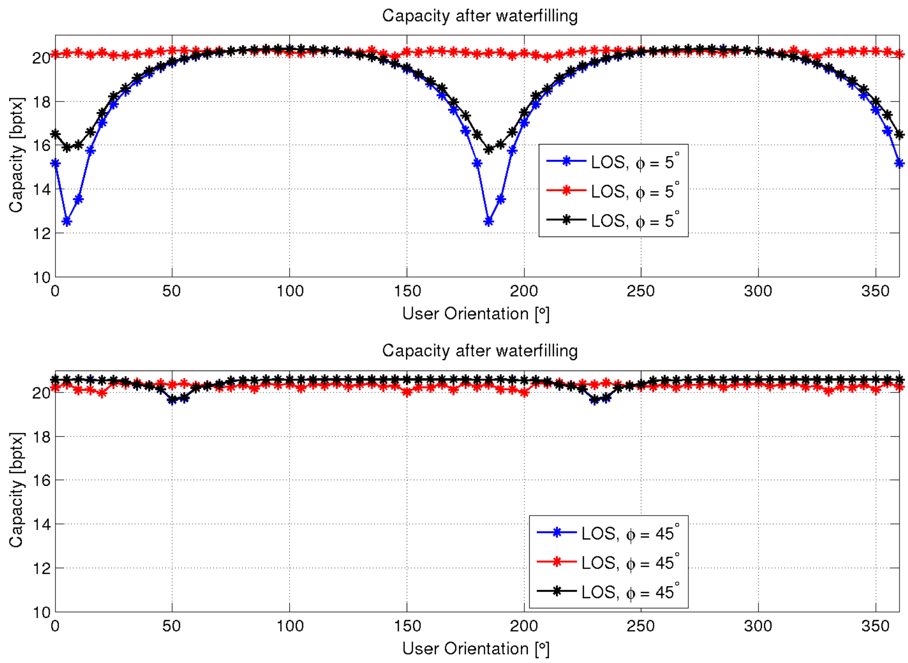

(b) *Capacity for an N=2 antenna user, located at [R,ϕ]=[50 m,5°] and [R,ϕ]=[50 m,45°]. LOS, NLOS and TOT channels.*

8.4.6 Local cluster: scattering density.

Evaluation of the impact that the Local cluster has on the channel has been done setting the number of Far clusters to zero. The number of scatterers at the Local cluster is varied from zero to 25. Its area size is fixed and set to 157.0796 [m^2]. Results are given for an N=2 user being placed at a radial distance to origo of 50 [m] and an echelon angle of 2 [°]. The massive array contains M=251 elements. The three usual channels are analysed, namely LOS, NLOS and TOT channels. Impact of the number of scatterers at the Local cluster on the channel can be examined via the channel's conditioning and capacity.

Fig. 8.13c, fig. 8.13b and fig. 8.13c exhibit the channel's conditioning, rank after waterfilling and capacity. The three figures go in the same line, and explain that, for a high enough number of scatterers, which could range between 7-8 and 12-15, the environment is rich enough to provide an adequate conditioning, and then capacity. Results are given for a user at the endfire, in which the presence of scatterers plays an important role via the enlargement of the "virtual" aperture. The clearest sign in this line can be seen at the curve featuring the rank after waterfilling and capacity, which are lifted by the presence of the scatterers at the initial growth stage.

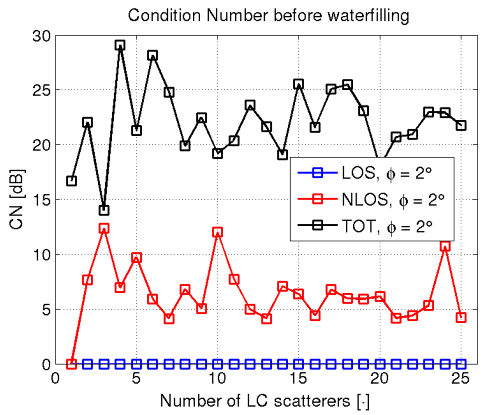

(a) *Conditioning for an N=2 antenna user, located at [R,ϕ]=[50 m,2°]. LOS, NLOS and TOT channels.*

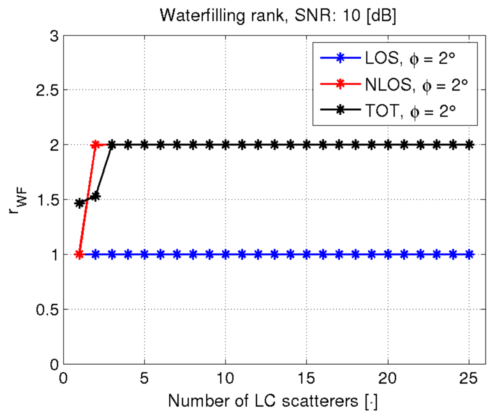

(b) *Rank after waterfilling for an N=2 antenna user, located at [R,ϕ]=[50 m,2°]. LOS, NLOS and TOT channels.*

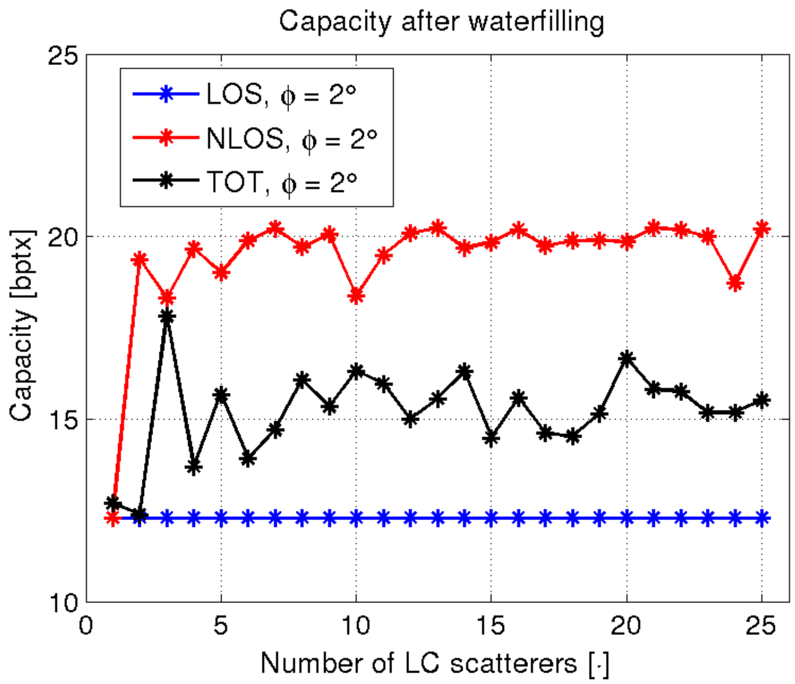

(c) *Capacity for an N=2 antenna user, located at [R,ϕ]=[50 m,2°]. LOS, NLOS and TOT channels.*

Figure 8.13 *Conditioning, rank after waterfilling and capacity.*

8.4.7 Far cluster: number of far clusters.

The far cluster density (number of far clusters in the scenario) is the feature that most influences the channel. In fact, the far clusters have a minor effect in comparison to the local cluster for almost all scenarios, and their effects are only comparable under some circumstances, like the one given by a user being positioned a the endfire direction. This is the case selected for this isolation. The far cluster density has been analysed varying the number of far clusters from 1 to 30, each containing 15 scatterers. It has been decided to place the far clusters at a random position within the chosen scenario. The local cluster has again been voided. The user has been located at 50 [m] from origo at an echelon angle of 0[°].

The channel's conditioning can be analysed with the help of fig. 8.14a on the facing page. Channel capacity is featured in fig. 8.14b on the next page. As expected, conditioning of the LOS channel is very poor at all times, which is natural given the position of the user. The NLOS channel achieves the best conditioning and thus, the highest capacity. The TOT channel lies in between, meaning that the channel gets improved thanks to the action of the scatterers at the far cluster. Once again, this goes in line with the scatterers providing a higher "virtual" aperture: the more far clusters in the scenario, the more enlarged the latter gets. Capacity grows up to some 15 far clusters and then is growth becomes very much gentle, meaning that the additional resolvability of the extra far clusters is not such and provides very little improvement.

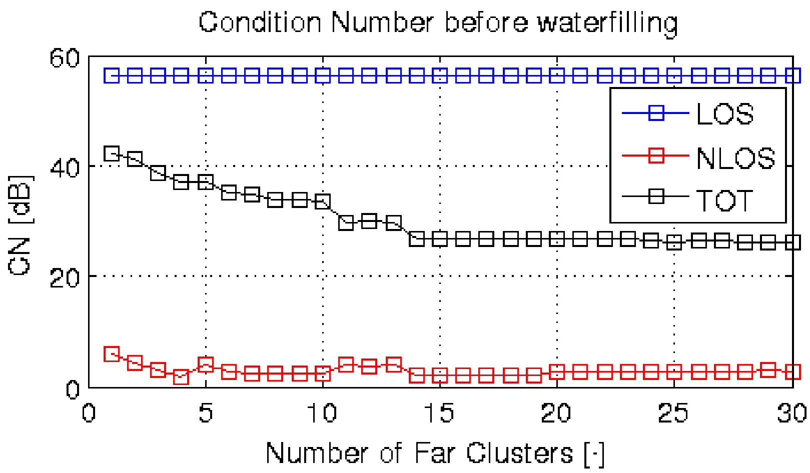

(a) *Condition Number vs the number of far clusters N_{FC}. LOS, NLOS, TOT channels.*

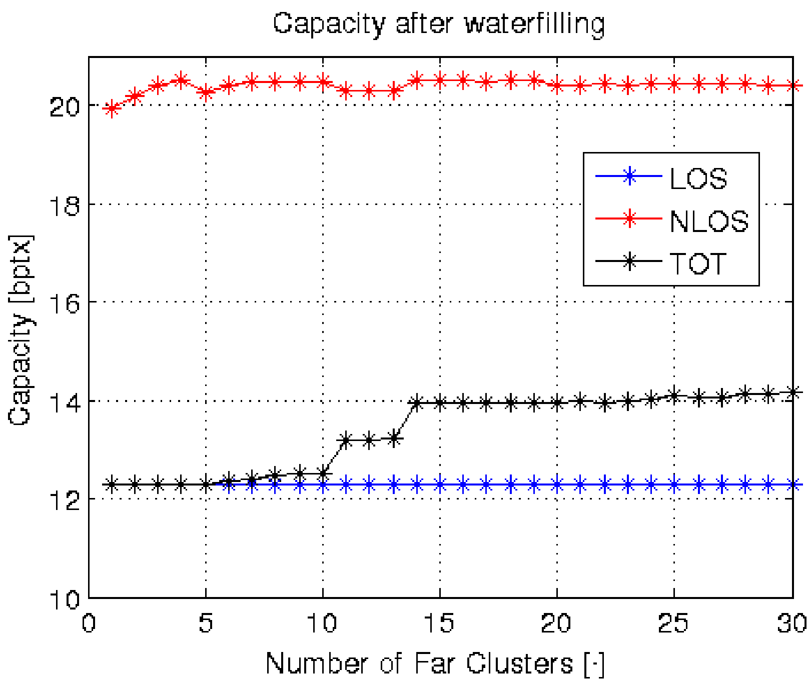

(b) *Capacity vs the number of far clusters N_{FC}. LOS, NLOS, TOT channels.*

Figure 8.14 *Conditioning and capacity vs the number of far clusters. User at enfire.*

8.5 Sub-conclusions

In this chapter, several variables have been isolated regarding the Point-to-Point MIMO case. The purpose of this chapter was to determine the behaviour of the proposed large-aperture massive MIMO channel, whose details are provided in chap. 6 on page 43.

The number of antennas at the BS has been varied while maintaining the size of the aperture at the massive array. An interesting observation was the increase in capacity for increasing M. In the low M regime, capacity would experience a rapid linear growth, before subsiding towards a less significant increase, indicating a point of saturation. This saturation is due to the fixed aperture of the massive Array, and so by increasing M, it gets to a point where angular resolvability is "congested".

Likewise, the effect of N been investigated. By varying N for a fixed M, similar effects in capacity were observed. Capacity would follow a linear growth to a certain N value, from which growth continues with a lesser slope.

So while an increasing the M provides with more capacity, it is mainly the number of antennas at the user, N, that is the limiting factor of the systems multiplexing gains, since capacity scales with min(N,M) and in massive MIMO, $M \gg N$.

Another aspect that plays an important role is the user location. The user has optimal conditions when located at the broadside direction of the massive array. The user is capable of resolving the entire massive array, and so is able to employ all DoF. However, the user will most of the time only have an adequate view of the massive array. However, performance is inadequate when the user is located at the endfire. The reason for this is due to the LOS channel providing the most significant contribution to the channel conditions and being this contribution poor at the endfire direction and close areas. This inadequacy may simply be attributed to the fact that the "virtual" array the user sees is comparable to that of a point-source (or at least it is very much reduced), resulting in the rank of the channel matrix collapsing to unit.

When the user was positioned at different distances from the massive array, p.eg. at the broadside direction, an odd behaviour was observed. Referring back to fig. 8.10, the condition number for a N=2 user at the broadside direction showed fluctuations which were denser at very close-in distances. While increasing the distance from the massive array, these fluctuations would become more defined with increasing size. This effect may be attributable to the wave propagation terms.

The effect of clusters can be seen by the two-part isolation. Firstly, the effect of the local cluster was analysed. Afterwards, focus was directed towards the far clusters.

The main parameter affecting channel conditions regarding the local cluster is the density of the scatterers within the cluster. The higher density, the richer the channel is. However, an interesting observation is that for a certain cluster density, adding more scatterers would not enrich the channel further. Thus based on the the observations, in order to obtain a rich scattering environment, no more than ≈ 10 scatterers are necessary.

As mentioned above, a similar analysis is done for far clusters. In turn, regarding the far clusters it is the number of far clusters that is varied. It is seen for a user at the endfire that for an increasing number of far clusters, the total channel becomes better conditioned. Capacity increases at certain levels of far cluster density[3]. Observing capacity, a conclusion similar to local cluster density may be extracted. For certain numbers of far clusters, adding additional ones would not provide higher capacity, or improve the channel's conditioning, provided the user is at an endfire direction. Locating the user at another location other than endfire would yield much less significant results.

[3]Far Cluster density refers to the number of Far Clusters.

Part II

Beamforming

Chapter 9

MU-Massive MIMO beamforming. Background, goals and proposals.

This chapter briefly addresses both the context of beamforming and its goals within this project's scenario. It includes an introductory section, which concisely confronts the background of MIMO downlink beamforming, a second section stating this project's beamforming goals and a last section containing the proposed approaches to go about them.

9.1 Introduction

Highly data-consuming user devices are growing dramatically, yielding a current exponential growth in data traffic [35]. The future perspective considers an expected 18-fold increase in the next five years, which has caused data providers to both attempt to acquire more frequency spectrum and install more BSs [35]. Nevertheless, and paying no mind to the well-known spectrum scarcity, current cellular networks are single-user oriented systems, which means each user is served at a given resource block: time slot, spectrum channel or code sequence [35].
MIMO systems are considered to be fundamental for the development of future wireless systems, since they would potentially provide with a significant improvement in both performance and bandwidth efficiency, including high capacity achievement, increased diversity and interference elimination [10, 36]. What is more, since MIMO systems are forecast to be employed in scenarios where a single BS communicates with several users simultaneously, like for instance a cellular network, the multi-user case is currently of great interest [10, 37, 36]. It is in fact the simultaneous multiplexing downlink approach opposed to the attempt to heighten the reliability of a single-link, the one that has proven to maximise the channel's performance [38]. Simultaneous multiplexing is often referred to as SDMA. Several techniques have been proposed as a solution to SDMA applied at the BS. They can mainly be grouped into *linear precoding techniques* and *non-linear precoding techniques* [13, 14, 10]. In particular, within the non-linear techniques, Dirty Paper Coding (DPC) has been proven to be the optimal solution, as it achieves the maximum sum rate of the system, although it is as well the most complex and demanding algorithm [10, 36, 38]. In any case, application of these schemes rely on full instantaneous CSIT, which might be an unrealistic assumption or simply prohibitive in some cases, like the FDD channels in which the uplink/downlink reciprocity cannot be applied [38]. Anyway, obtaining instantaneous CSIT could be a very costly and challenging task, however justifiable in multi-user channels [10]. Several approaches to tackle the imperfect CSIT case have been published. We are interested in those attempting to reduce the amount of CSIT via the channel's statistics, normally restricted to the single-antenna user case, being some of them documented in [39, 38]. We also highlight another approach in [36], which uses instantaneous channel data to design an optimised linear precoder for the case in which the user has more than one antenna. Then, account for effects of imperfect CSIT on this last approach is documented in [40].

Massive MIMO approach.

Among other potentials, Massive MIMO systems' expected performance and efficiency increases are dramatic in comparison to ordinary MIMO deployments. This is mainly in the form of capacity growth and energy efficiency. Some recent publications like [16] forecast a ten-fold increase on capacity and a 100-fold on radiated energy-efficiency. This is due to the underlying physics, which would allow both coherent superposition of propagating wavefronts by appropriate beamforming at some intended locations (aiming at intended users) and destructive alignment at other uninteresting locations. This would occur even with low-power antennas at the BS. [16]

Assuming the full CSIT case, interestingly enough, in the massive number of antennas regime linear precoders have been concluded to perform remarkably well with respect to the beamforming task explained above. This is attractive if a design goal is to utilise a low-complexity beamforming approach, since it would cast away the employment of DPC. What is more, recent theoretic research has shown that, as the number of antennas at the BS increases, it is the simplest form of linear precoding, namely *MF* or *conjugate beamforming*, that approaches optimality [41], a statement that goes in line with the first paragraph of this subsection. Nonetheless, more recent work by authors of [15] concludes that, in real systems, MF would only outperform Zero Forcing (ZF) (a traditional multi-user MIMO linear precoding method) in some scenarios and suggests those include the high number of users regime, a high user mobility scenario and the low-capability hardware case.

9.2 Beamforming goals.

As initially proposed in [21], the beamforming goals of this project included the adaptation of the algorithms to the Near Field characteristics of the channel and the analysis of low-complexity approaches. Then, these goals were narrowed down into the design of a robust beamforming algorithm against local movements of the users in the scenario, maintaining the low-complexity profile.

As suggested throughout this project, a Massive MIMO indoor system is tackled. The infrastructure in which this system is to be applied can be of various kinds. It can be argued, though, that in any of those, users can have a certain degree of mobility. Local mobility has been selected for pre-processing design purposes. A user's local movement has been chosen to be within a closed area of 1 [m^2], although different definitions of local movement could be valid and would depend in any case on the scenario's features. For instance, the degree of mobility would be different at a concert than at an airport lounge. The goal is to design a robust precoder which would consider the users' local movement with the lowest complexity possible. An initial study would consider the single-antenna user case, only. Two proposals are suggested in the next section.

9.3 Proposals

9.3.1 Proposal nr. 1: Linear precoding with instantaneous CSIT.

As stated in the introductory section, in the massive number of antennas regime the linear precoders perform very satisfactorily in MIMO systems, now, under the assumption of full instantaneous CSIT. Being able to discard the employment of DPC lowers complexity sufficiently so that this alternative can be evaluated. Since the study of channel state information acquisition overhead is out of the scope of this project, this proposal will serve as reference for optimality as per proposal nr. 2.

9.3.2 Proposal nr. 2: Precoding based on statistical CSIT.

Analysis on imperfect or reduced CSIT in [38, 39, 40], allows to consider an alternative to the perfect CSIT case in which instantaneous feedback is not sought, but rather, work with the statistical channel information is preferred. This would bring along lower complexity at the BS, but at the same time, suboptimality on the channel's achieved sum rates. The enabler lying behind this approach can be found in the nature of Massive MIMO, which could help each user channel to not occupy all of its DoFs, which would go in line with users' separability via beamforming based on different subspaces for each user channel (yielded by the statistics of the different channels, hence precoding based on statistical CSIT). Moreover, the fact channels are expected to be orthogonal to each other [13, 16] serves as motivation to employ statistical precoding, since the impairments found in literature on the resulting precoding matrices as per their inherent correlation might fade away.

Chapter 10

Proposal nr.1: Linear precoding based on instantaneous CSIT.

This chapter addresses the first suggested beamforming proposal according to the beamforming goals within this project's scenario. This proposal's principle lies in the employment of less complex linear precoding, relying on instantaneous CSIT.
The single-antenna user case is considered only.

10.1 Introduction.

As already stated in chap. 9 on page 87, multi-user MIMO systems have the potential to combine MIMO benefits (high capacity, increased diversity, interference suppression) with the advantages of SDMA, which allows the simultaneous transmission of multiple data streams to a number of users, resulting in remarkably high data rates [10, 37, 36]. Barring the user-coordination scenario and restricting ourselves to the downlink channel, the idea of beamforming is to exploit the channel information available at the transmitter, namely CSIT, to grant the users access to the channel simultaneously and at the same frequency [10, 36, 35]. **The main issue lies in the ability to mitigate the inter-user interference**, as depicted in fig. 10.1 for a two-user scenario. Two approaches can be followed in order to meet this goal: doing so at each

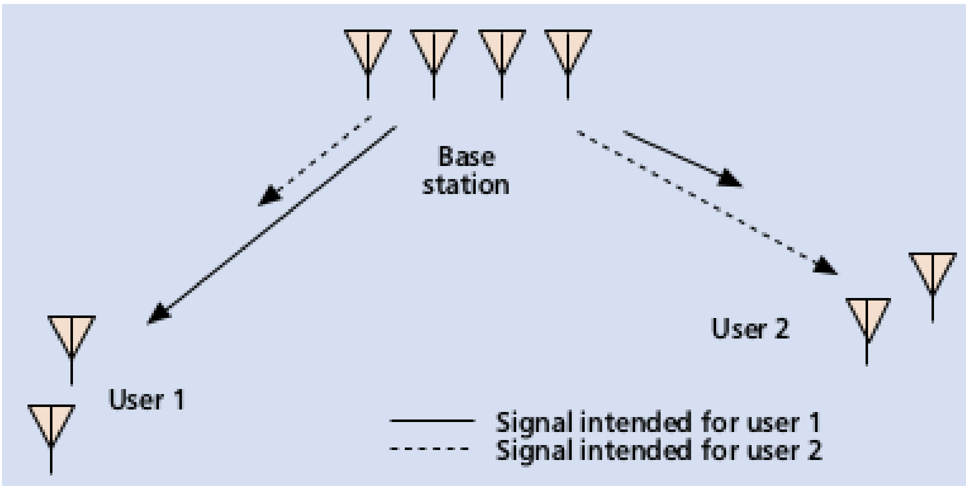

Figure 10.1 *An example of a multi-user MIMO downlink channel. The figure is reproduced from [10].*

user, or designing the transmit signals at the BS with this purpose, via transmit beamforming. Barring the former, which is presumably too complex for a low-profile receiver (such is the case in this project), several beamforming techniques have been proposed to mitigate or even totally eliminate inter-user interference. If instantaneous CSIT can be obtained, then these techniques, as stated in chap. 9 on page 87, can be grouped into [10]:

- Linear precoding techniques, namely MF, ZF and MMSE. [10, 36].
- Non-linear precoding techniques, namely DPC. Also, Tomlinson-Harashima precoding. [36, 42].

Theoretic results suggest that non-linear techniques are optimal, allowing the highest system sum rates. However, they are too costly and complex, and might be unfeasible in real systems. [10, 36, 42]. If a low-complexity goal is to be met, then non-linear techniques are to be discarded in favour of linear ones. What is more, as for instance asserted by authors of [14, 13, 16], in massive MIMO systems, performace of linear precoders is very much satisfactory. These have then been selected as Proposal nr. 1 to meet this project's low complexity goal; robustness on the users' local movement is granted since CSIT is assumed (for deeper inspection on beamforming goals, see chap. 9 on page 87).

10.2 General performance, Massive MIMO.

The employment of a MF-based linear precoders is desired since it does not require any channel matrix inversion, opposed to ZF and MMSE. In other words, it is the simplest linear precoder and thus, the least complex. Ignoring instantaneous CSIT acquisition overhead and cost, channel inversion has a polynomial complexity with regard to both the number of simultaneous users being served and the number of antennas at the BS, while conjugate beamforming's would be negligible, since the computational cost of MF's weight is "trivial", according to [15], as "in hardware, taking the complex conjugate of a signal only needs a bit-flip and an adder". Authors in [13, 41] state that, theoretically, as the number of antennas at the massive array M grows, given an adequate SNR requirement, ZF tends to MF, which would endorse the selection of a MF as the desired precoder. This is thanks to the fact user channels would be more and more uncorrelated to each other, given they are spatially separated. Unlike ZF, MF-based transmit beamforming does not attempt to cancel inter-user interference but instead enhances the symbol power, namely the diagonal of the effective channel (see next section). In a massive MIMO system, channels are expected to be orthogonal to each other asymptotically with M, hence its optimality. [13, 14, 16].

The massive MIMO regime is an added factor to consider the use of MFs instead of ZF precoders, since the weight formation polynomial complexity of ZF-based beamforming would be challenging in multi-use systems with a high number of antennas [35]. However, as published in [15], in real massive MIMO systems, the optimality of conjugate beamforming with respect to ZF should not be taken for granted, since it would only occur in some specific scenarios. MF precoding would only outperform ZF when the number of simultaneous users is very high, the users have high mobility or the hardware capability at the BS were very low. Finally, as this chapter focuses on the single-antenna user (N=1), the MMSE precoder has to be considered, since it is the beamforming type that reaches optimality under any circumstance, thus behaving as a ceiling reference. While ZF completely nulls the inter-user interference by imposing all interference terms be zero, allowing a limited amount of interference as done by the MMSE-based precoding maximises sum capacity in a single-antenna user scenario [10, 36]. Although as yet out of the scope of this chapter, let it be mentioned that, when N>1, MMSE incurs a loss when attempting to reduce the interference between closely spaced receive antennas. A solution to this is proposed in [43] under the name of Block Diagonalization (BD) and in [36] under the name of Regularized Block Diagonalization (RBD).

10.3 System model. Sum rate of linear beamforming schemes.

It has been argued that MF would reach optimality in massive MIMO systems if the number of antennas M is sufficiently high and thus would be the precoding technique that would best match the beamforming goals in this project. Moreover, it has been stated that the complexity of a channel inversion in these systems could be too high for practical implementation. Even so, it has been decided to analyse the three linear precoders in Proposal nr. 1.

In any case, the considered scenario includes K single-antenna (N=1) users that are to be served simultaneously with an M antenna BS which applies transmit linear beamforming, i.e. employing a precoding matrix denoted $\mathbf{W}$. Fig. 10.2 depicts this scenario graphically.

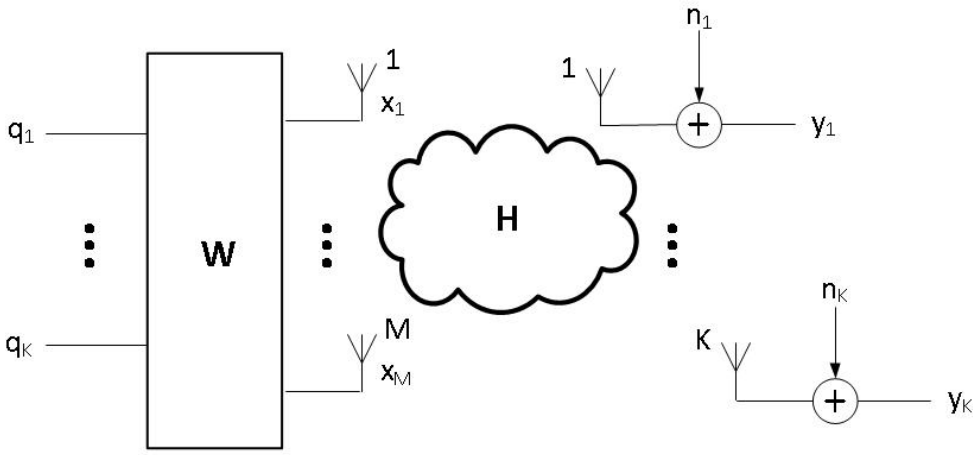

Figure 10.2 *Transmit beamforming scenario for the single-antenna user case. K users. M antennas at the massive array.* $\mathbf{W}$ *is the precoding matrix and* $\mathbf{H}$ *is the channel matrix.*

The normalised precoding matrix is $\mathbf{W} \in \mathbb{C}^{M\times K}$, being the original precoding matrix written like $\mathbf{F} \in \mathbb{C}^{M\times K}$:

$$\mathbf{W} = \alpha_{\mathbf{F}} \cdot \mathbf{F} \tag{10.1}$$

where, $\alpha_{\mathbf{F}}$ is the normalisation factor and is defined considering both that there is a restriction on the maximum allowed transmit power to be $\bar{\mathrm{P}}$ [W]. Appendix K on page 199 derives the normalisation factor, which is reproduced below:

$$\alpha_{\mathbf{F}} \leq \frac{\sqrt{\bar{\mathrm{P}}}}{\sqrt{\mathrm{Tr}\left[\mathbf{F}\mathbf{F}^{\mathrm{H}}\right]}} \tag{10.2}$$

where $\mathrm{Tr}[\cdot]$ is the trace operator and $^{\mathrm{H}}$ the Hermitian operator.
If we choose to transmit the maximum allowed power $\bar{\mathrm{P}}$ [W], then the normalisation factor is unique:

$$\alpha_{\mathbf{F}} = \frac{\sqrt{\bar{\mathrm{P}}}}{\sqrt{\mathrm{Tr}\left[\mathbf{F}\mathbf{F}^{\mathrm{H}}\right]}} \tag{10.3}$$

Otherwise, $\mathbf{X} \in \mathbb{C}^{M\times 1}$ is the transmit signal vector; $\mathbf{q} \in \mathbb{C}^{K\times 1}$ is the set of symbols to be transmitted through the channel; $\mathbf{H} \in \mathbb{C}^{K\times M}$ is the channel matrix; $\mathbf{Y} \in \mathbb{C}^{K\times 1}$ is the set received signals; and $\mathbf{n} \in \mathbb{C}^{K\times 1}$ is the set of additive noise components.

We let certain matrices to be able to be written through concatenation of vectors, in particular:

- $\mathbf{F} = [\mathbf{F}_1 \cdots \mathbf{F}_\mathrm{K}]$, where $\mathbf{F}_k \in \mathbb{C}^{M\times 1}\ \forall\, k \in [1,\ldots,\mathrm{K}]$.
- $\mathbf{H} = [\mathbf{H}_1 \cdots \mathbf{H}_\mathrm{K}]^\mathrm{H}$, where $\mathbf{H}_k \in \mathbb{C}^{1\times M}\ \forall\, k \in [1,\ldots,\mathrm{K}]$.

Under these circumstances, and assuming a flat-fading channel, the transmit signals would have the following expression:

$$\begin{aligned}
\begin{bmatrix} x_1 \\ \vdots \\ x_M \end{bmatrix} &= \mathbf{W} \begin{bmatrix} q_1 \\ \vdots \\ q_K \end{bmatrix} \\
&= \frac{\sqrt{\mathrm{P}}}{\sqrt{\mathrm{Tr}\left[\mathbf{F}\mathbf{F}^\mathrm{H}\right]}}\,\mathbf{F} \begin{bmatrix} q_1 \\ \vdots \\ q_K \end{bmatrix} \\
&= \frac{\sqrt{\mathrm{P}}}{\sqrt{\mathrm{Tr}\left[\mathbf{F}\mathbf{F}^\mathrm{H}\right]}}\,[\mathbf{F}_1 \cdots \mathbf{F}_\mathrm{K}] \begin{bmatrix} q_1 \\ \vdots \\ q_K \end{bmatrix}
\end{aligned} \tag{10.4}$$

And then, the received signals would be written like:

$$\begin{aligned}
\begin{bmatrix} y_1 \\ \vdots \\ y_M \end{bmatrix} &= \mathbf{H}\frac{\sqrt{\mathrm{P}}}{\sqrt{\mathrm{Tr}\left[\mathbf{F}\mathbf{F}^\mathrm{H}\right]}}\,[\mathbf{F}_1 \cdots \mathbf{F}_\mathrm{K}] \begin{bmatrix} q_1 \\ \vdots \\ q_\mathrm{K} \end{bmatrix} + \begin{bmatrix} n_1 \\ \vdots \\ n_\mathrm{K} \end{bmatrix} \\
&= \begin{bmatrix} \mathbf{H}_1 \\ \vdots \\ \mathbf{H}_\mathrm{K} \end{bmatrix} \frac{\sqrt{\mathrm{P}}}{\sqrt{\mathrm{Tr}\left[\mathbf{F}\mathbf{F}^\mathrm{H}\right]}}\,[\mathbf{F}_1 \cdots \mathbf{F}_\mathrm{K}] \begin{bmatrix} q_1 \\ \vdots \\ q_\mathrm{K} \end{bmatrix} + \begin{bmatrix} n_1 \\ \vdots \\ n_\mathrm{K} \end{bmatrix} \\
&= \frac{\sqrt{\mathrm{P}}}{\sqrt{\mathrm{Tr}\left[\mathbf{F}\mathbf{F}^\mathrm{H}\right]}} \underbrace{\begin{bmatrix} \mathbf{H}_1\,\mathbf{F}_1 & \cdots & \mathbf{H}_1\,\mathbf{F}_\mathrm{K} \\ \vdots & \cdots & \vdots \\ \mathbf{H}_\mathrm{K}\,\mathbf{F}_1 & \cdots & \mathbf{H}_\mathrm{K}\,\mathbf{F}_\mathrm{K} \end{bmatrix}}_{\mathbf{H}\,\mathbf{F}\,:\ \text{effective channel}} \begin{bmatrix} q_1 \\ \vdots \\ q_\mathrm{K} \end{bmatrix} + \begin{bmatrix} n_1 \\ \vdots \\ n_\mathrm{K} \end{bmatrix}
\end{aligned} \tag{10.5}$$

The diagonal terms of the effective channel are the symbol terms, i.e. the ones containing the information on the signals intended to each user; the non-diagonal elements are the interference terms, containing the unintended information. Given a user k, its symbol term is the k^th diagonal entry. The interference terms affecting k and due to other users are the k^th row terms, excluding the diagonal term; those will be contained within the k^th user Signal to Interference plus Noise Ratio (SINR) term, i.e. SINR_k. The interference terms due to user k are the k^th column terms, excluding the diagonal term; those will be contained in the other users' SINR terms.
For instance, the symbol term of user k=1 is $\mathbf{H}_1\,\mathbf{F}_1$, the interference terms affecting him and then included in SINR_1 are $[\mathbf{H}_1\,\mathbf{F}_2 \cdots \mathbf{H}_1\,\mathbf{F}_\mathrm{K}]$ and the interfering terms towards other users due to user 1 are $[\mathbf{H}_2\,\mathbf{F}_2 \cdots \mathbf{H}_\mathrm{K}\,\mathbf{F}_1]^\mathrm{H}$.

The received signal at user k is written like:

$$y_k = \frac{\sqrt{\mathrm{P}}}{\sqrt{\mathrm{Tr}\left[\mathbf{F}\mathbf{F}^\mathrm{H}\right]}} \left[\overbrace{\mathbf{H}_k\,\mathbf{F}_k\,q_k}^{\text{symbol term}} + \overbrace{\sum_{\substack{j=1 \\ j\neq k}}^{\mathrm{K}} \mathbf{H}_k\,\mathbf{F}_j\,q_j}^{\text{interference term}} \right] + \overbrace{n_k}^{\text{noise term}} \tag{10.6}$$

And thus, SINR_k would be written like:

$$
\begin{aligned}
\mathrm{SINR}_k &= \frac{P_k^{\text{symbol}}}{P_k^{\text{interference}} + P_k^{\text{noise}}} \\
&= \frac{\frac{\bar{\mathrm{P}}}{\mathrm{Tr}[\mathbf{F}\mathbf{F}^{\mathrm{H}}]} \, |\mathbf{H}_k \, \mathbf{F}_k \, q_k|^2}{\frac{\bar{\mathrm{P}}}{\mathrm{Tr}[\mathbf{F}\mathbf{F}^{\mathrm{H}}]} \, |\sum_{\substack{j=1 \\ j \neq k}}^{\mathrm{K}} \mathbf{H}_k \, \mathbf{F}_j \, q_j|^2 \, + \, \sigma_{n,k}^2}
\end{aligned}
\tag{10.7}
$$

Finally, the system's sum rate would take the expression below:

$$
\mathrm{SR} = \sum_{k=1}^{\mathrm{K}} \log_2 \left(1 \, + \, \mathrm{SINR}_k\right) \ [\mathrm{bptx}] \tag{10.8}
$$

Although inaccurately, on some occasions Sum Rate (SR) will be referred to as *Sum Capacity*, SC.

10.3.1 Simulations proceeding.

On this thesis's simulations, it has been decided to work with the second order moments, namely the mean and std values, on both:

- The SINR of each channel, $\mathrm{SINR}_k \ \forall \, k \in [1, \ldots, \mathrm{K}]$.
- The total SR.

SINR$_k$

For a given precoding matrix $\mathbf{F}$ and channel matrix $\mathbf{H}$, second order moments have been extracted as per a number of realisations of the transmit symbols $\mathbf{q}$. Out of them, only the mean value will be considered for SR computation. The number of realisations that has been selected is 1000. The symbol generation assumes that:

(a) $\mathbb{E}\left[|q_k|^2\right] = 1 \ [\mathrm{W}] \ \forall \, k \in [1, \ldots, \mathrm{K}]$ and

(b) that symbols are independent to each other: symbol q_k is independent to symbol $q_j \ \forall \ j \in [1, \ldots, k-1, \, k+1, \, \ldots, \mathrm{K}]$

Simulations with respect to SINR_k do not consider any other requirement on the transmit symbols.
The noise variance has been set not to vary among users: $\sigma_{n,k}^2 \ = \sigma_n^2 \, \forall \, k \in [1, \ldots, \mathrm{K}]$.
All in all, the resulting SINR will be an averaged value over the transmit symbols:

$$
\mathrm{SINR}_k \rightarrow \mathbb{E}_{\mathbf{q}}\left[\mathrm{SINR}_k\right] = \frac{\mathbb{E}_{\mathbf{q}}\left[P_k^{\text{symbol}}\right]}{\mathbb{E}_{\mathbf{q}}\left[P_k^{\text{interference}}\right] \, + \, \sigma_n^2} \tag{10.9}
$$

where $\mathbb{E}_{\mathbf{q}}[\cdot]$ is the mean value operator with respect to the transmit symbols.

Sum Rate

According to Proposal nr. 1, a given channel matrix realisation determines the precoding matrix $\mathbf{F}$ (hence, reliability on instantaneous CSIT). It has been seen above that for a given channel realisation, an averaging of the SINR for all users occurs. Those averaged SINRs determine the channel's SR. Well then, the channel's resulting SR has in turn been determined as per an averaging of all the resulting SR for different channel realisations, i.e. an averaging over a set of channel realisations. The number of channel realisations that has been produced is 1000.

All in all, the resulting SR will be an averaged value over the channel realisations:

$$\mathrm{SR} \rightarrow \mathbb{E}_{\mathbf{H}}\left[\mathrm{SR}\right] \tag{10.10}$$

where $\mathbb{E}_{\mathbf{H}}[\cdot]$ is the mean value operator with respect to the channel.

10.4 Precoding matrices of MF, ZF and MMSE-based beamforming.

This section includes the different expressions of the precoding matrix $\mathbf{F}$ as per the three linear precoders that have been proposed in this thesis. The system model and procedure to compute the SINR of each channel and the total SR for all of these precoders matches the general scheme accounted for in sec. 10.3 on page 93. However, again just to state the obvious, each of the algorithms has a different precoding matrix $\mathbf{F}$. In all of them, instantaneous CSIT is assumed in the form of the instantaneous channel matrix $\mathbf{H}$.

The reader is reminded that simultaneous beamforming towards K single-antenna users is performed, ant that in this situation the considered downlink channel matrix is $\mathbf{H} \in \mathbb{C}^{K \times M}$ and that the precoding matrix is $\mathbf{F} \in \mathbb{C}^{M \times K}$.

MF

The precoding matrix of the MF-based beamforming reduces to a simple Hermitian operation over the channel matrix [13, 35, 15], hence *conjugate beamforming*:

$$\mathbf{F}^{\mathrm{MF}} = \mathbf{H}^{\mathrm{H}} \tag{10.11}$$

MF's employment of the Hermitian of the channel matrix maximises the diagonal terms of the effective channel $\mathbf{H}\,\mathbf{F}^{\mathrm{MF}}$(see definition of the effective channel in eq. 10.5 on page 94) but conversely, does not tackle interference terms (non-diagonal terms). See eq. 10.12.

$$\begin{aligned}
\begin{bmatrix} y_1 \\ \vdots \\ y_M \end{bmatrix} &= \frac{\sqrt{\mathrm{P}}}{\sqrt{\mathrm{Tr}\left[\mathbf{F}^{\mathrm{MF}}(\mathbf{F}^{\mathrm{MF}})^{\mathrm{H}}\right]}} \underbrace{\begin{bmatrix} \mathbf{H}_1\,\mathbf{F}_1^{\mathrm{MF}} & \cdots & \mathbf{H}_1\,\mathbf{F}_{\mathrm{K}}^{\mathrm{MF}} \\ \vdots & \cdots & \vdots \\ \mathbf{H}_{\mathrm{K}}\,\mathbf{F}_1^{\mathrm{MF}} & \cdots & \mathbf{H}_{\mathrm{K}}\,\mathbf{F}_{\mathrm{K}}^{\mathrm{MF}} \end{bmatrix}}_{\mathbf{H}\,\mathbf{F}^{\mathrm{MF}}\,:\ \text{effective channel}} \begin{bmatrix} q_1 \\ \vdots \\ q_{\mathrm{K}} \end{bmatrix} + \begin{bmatrix} n_1 \\ \vdots \\ n_{\mathrm{K}} \end{bmatrix} \\
&= \frac{\sqrt{\mathrm{P}}}{\sqrt{\mathrm{Tr}\left[\mathbf{H}^{\mathrm{H}}\mathbf{H}\right]}} \underbrace{\begin{bmatrix} \mathbf{H}_1\,\mathbf{H}_1^* & \cdots & \mathbf{H}_1\,\mathbf{H}_{\mathrm{K}}^* \\ \vdots & \cdots & \vdots \\ \mathbf{H}_{\mathrm{K}}\,\mathbf{H}_1^* & \cdots & \mathbf{H}_{\mathrm{K}}\,\mathbf{H}_{\mathrm{K}}^* \end{bmatrix}}_{\mathbf{H}\,\mathbf{H}^{\mathrm{H}}\,:\ \text{effective channel}} \begin{bmatrix} q_1 \\ \vdots \\ q_{\mathrm{K}} \end{bmatrix} + \begin{bmatrix} n_1 \\ \vdots \\ n_{\mathrm{K}} \end{bmatrix} \\
&= \frac{\sqrt{\mathrm{P}}}{\sqrt{\mathrm{Tr}\left[\mathbf{H}\mathbf{H}^{\mathrm{H}}\right]}} \begin{bmatrix} ||\mathbf{H}_1||^2 & \cdots & \mathbf{H}_1\,\mathbf{H}_{\mathrm{K}}^* \\ \vdots & \cdots & \vdots \\ \mathbf{H}_{\mathrm{K}}\,\mathbf{H}_1^* & \cdots & ||\mathbf{H}_{\mathrm{K}}||^2 \end{bmatrix} \begin{bmatrix} q_1 \\ \vdots \\ q_{\mathrm{K}} \end{bmatrix} + \begin{bmatrix} n_1 \\ \vdots \\ n_{\mathrm{K}} \end{bmatrix}
\end{aligned} \tag{10.12}$$

where $||\cdot||^2$ is the vector's square norm. For the k^{th} channel, $\mathbf{H}_k = [h_{k\,1} \cdots h_{k\,M}]$, it is defined as $||\mathbf{H}_k||^2 = \sum_{m=1}^{M} |h_{k\,m}|^2$, where $|\cdot|$ is the absolute value operator.

In a massive MIMO scenario, the different channels are expected to be independent to each other, i.e. to have a high degree of orthogonality to each other, and so, interference terms should tend to zero as the number of antennas at the BS M increases, so a MF ought to be optimal with respect to interference cancellation asymptotically with M. In other words, it should collapse to a ZF beamformer. [13, 16]. Then, the non-diaginal terms in the effective channel in eq. 10.12 on the facing page would tend to zero asymptotically with M:

$$\begin{bmatrix} y_1 \\ \vdots \\ y_M \end{bmatrix} \xrightarrow[M\uparrow\uparrow]{} \frac{\sqrt{\mathrm{P}}}{\sqrt{\mathrm{Tr}\left[\mathbf{H}\mathbf{H}^{\mathrm{H}}\right]}} \begin{bmatrix} ||\mathbf{H}_1||^2 & \cdots & 0 \\ \vdots & \cdots & \vdots \\ 0 & \cdots & ||\mathbf{H}_{\mathrm{K}}||^2 \end{bmatrix} \begin{bmatrix} q_1 \\ \vdots \\ q_{\mathrm{K}} \end{bmatrix} + \begin{bmatrix} n_1 \\ \vdots \\ n_{\mathrm{K}} \end{bmatrix} \tag{10.13}$$

ZF

The precoding matrix of the ZF-based beamforming includes the following channel inversion: [10, 35, 15, 43]:

$$\mathbf{F}^{\mathrm{ZF}} = \mathbf{H}^{\mathrm{H}} \left[\mathbf{H}\,\mathbf{H}^{\mathrm{H}}\right]^{-1} \tag{10.14}$$

This type of inversion is called *pseudoinverse*.

$\mathbf{F}^{\mathrm{ZF}}$ acts on the interference terms, the non-diagonal elements of the effective channel, to completely cancel inter-user interference. Its disadvantage lies in the suboptimal diagonal elements, yielding less symbol power than the MF, yet in a general MIMO system, a higher SINR per user. The employment of ZF would also bring along the use of more transmitted power than the MF case [16]. In any case, ZF beamforming works satisfactorily in any kind of MIMO deployment, including Massive MIMO, while as already stated, MF does not and it is only on massive MIMO systems that performance is adequate, given the tendency of channel responses associated with different users to be nearly orthogonal to each other. Lastly, it must be remarked that ZF is able to completely cancel inter-user interference terms as long as $\mathrm{K} \leq \mathrm{M}$. See the received signal matrix in expression below:

$$\begin{aligned} \begin{bmatrix} y_1 \\ \vdots \\ y_M \end{bmatrix} &= \frac{\sqrt{\mathrm{P}}}{\sqrt{\mathrm{Tr}\left[\mathbf{F}^{\mathrm{ZF}}(\mathbf{F}^{\mathrm{ZF}})^{\mathrm{H}}\right]}} \underbrace{\begin{bmatrix} \mathbf{H}_1\,\mathbf{F}_1^{\mathrm{ZF}} & \cdots & \mathbf{H}_1\,\mathbf{F}_{\mathrm{K}}^{\mathrm{ZF}} \\ \vdots & \cdots & \vdots \\ \mathbf{H}_{\mathrm{K}}\,\mathbf{F}_1^{\mathrm{ZF}} & \cdots & \mathbf{H}_{\mathrm{K}}\,\mathbf{F}_{\mathrm{K}}^{\mathrm{ZF}} \end{bmatrix}}_{\mathbf{H}\,\mathbf{F}^{\mathrm{ZF}}\text{ : effective channel}} \begin{bmatrix} q_1 \\ \vdots \\ q_{\mathrm{K}} \end{bmatrix} + \begin{bmatrix} n_1 \\ \vdots \\ n_{\mathrm{K}} \end{bmatrix} \\ &\underset{\mathrm{K}\leq\mathrm{M}}{=} \frac{\sqrt{\mathrm{P}}}{\sqrt{\mathrm{Tr}\left[\mathbf{F}^{\mathrm{ZF}}(\mathbf{F}^{\mathrm{ZF}})^{\mathrm{H}}\right]}} \begin{bmatrix} \mathbf{H}_1\,\mathbf{F}_1^{\mathrm{ZF}} & \cdots & 0 \\ \vdots & \cdots & \vdots \\ 0 & \cdots & \mathbf{H}_{\mathrm{K}}\,\mathbf{F}_{\mathrm{K}}^{\mathrm{ZF}} \end{bmatrix} \begin{bmatrix} q_1 \\ \vdots \\ q_{\mathrm{K}} \end{bmatrix} + \begin{bmatrix} n_1 \\ \vdots \\ n_{\mathrm{K}} \end{bmatrix} \end{aligned} \tag{10.15}$$

MMSE

Ultimately, the drawbacks experienced by ZF precoding come down to the restriction of zero inter-user interference. Interestingly, allowing a limited amount of interference increases the sum capacity at a given transmit power level. [10]. Fulfilment of this approach can be done via a regularised channel inversion, through a regularisation factor. MMSE regularisation is the one that maximises the SINR at each receiver, being the expression of the so called MMSE precoding matrix $\mathbf{F}^{\mathrm{MMSE}}$ the following [10, 42]:

$$\mathbf{F}^{\mathrm{MMSE}} = \mathbf{H}^{\mathrm{H}} \left[\mathbf{H}\,\mathbf{H}^{\mathrm{H}} + \mathrm{K}\cdot\frac{\sigma_n^2}{\mathrm{P}_{\mathrm{Tx}}}\,\mathbf{I}_{\mathrm{K}}\right]^{-1} \tag{10.16}$$

where $\mathbf{I}_\mathrm{K}$ is the K×K identity matrix and $\mathrm{P_{Tx}}$ [W] is the transmit power. As already covered, $\mathrm{P_{Tx}} = \bar{\mathrm{P}}$ [W]. Moreover, since throughout this thesis the channel's SNR has been defined like $\mathrm{SNR} = {}^{\mathrm{P_{Tx}}}/{\sigma_n^2} = {}^{\bar{\mathrm{P}}}/{\sigma_n^2}$, then eq. 10.16 on the previous page can be rewritten like:

$$\mathbf{F}^{\mathrm{MMSE}} = \mathbf{H}^{\mathrm{H}} \left[\mathbf{H}\,\mathbf{H}^{\mathrm{H}} + \frac{\mathrm{K}}{\mathrm{SNR}}\,\mathbf{I}_\mathrm{K}\right]^{-1} \tag{10.17}$$

MMSE regularisation factor improves performance significantly in comparison to ZF and especially at the low SNR levels [42] and is the optimal solution in any MIMO scenario in which users have only one antenna, achieving capacity linear growth with min(M,K) with the SNR. [10].
For the high-SNR regime, the regularisation factor slumps and MMSE precoding collapses to ZF. However, if the SNR is low, MMSE's performance improves with respect to ZF's.

10.5 Simulation results.

This section is aimed at accounting for the main results yielded by simulations, which would endorse the suggested Proposal nr. 1 as an approach for this project's beamforming goals.
Isolations on several scenario parameters will be carried out. Simple scenarios are preferred in order to give the clearest insight on the performance of the three linear precoders. Finally, it will be proven that, under certain conditions, MF would effectively be the best implementation solution. However, it will be shown that, under some conditions, its application would incur impoverished performance. Being some other factors crucial on this but out of the scope of this thesis, it will be shown that inadequate performance happens mainly due to the users inter-correlation, which gives rise to chap. 11 on page 109, a profound study of correlation within the proposed scenario for a two-user case. We propose an empirical algorithm to determine inter-user correlation on this scenario, which could serve as a basis for decision on MF employment according to the users' rate needs.

Channel matrices

As done with the Point-to-Point MIMO analysis, the channels that have been tackled are the LOS, NLOS and TOT ones. As usual, the channel matrices are normalised by their Frobenius norms $||\cdot||_\mathbf{F}$. Then, by their own dimensions so that the introduction of power is corrected, given in multi-user MIMO by M, K and N. This happens prior to any manipulation on them, i.e. precoding matrices computation, and at each realisation.

$$\begin{aligned}
\mathbf{H}^{\mathrm{LOS}} &\rightarrow \frac{\mathbf{H}^{\mathrm{LOS}}}{||\mathbf{H}^{\mathrm{LOS}}||_\mathbf{F}}\sqrt{\mathrm{K}\cdot\mathrm{N}\cdot\mathrm{M}} \\
\mathbf{H}^{\mathrm{NLOS}} &\rightarrow \frac{\mathbf{H}^{\mathrm{NLOS}}}{||\mathbf{H}^{\mathrm{NLOS}}||_\mathbf{F}}\sqrt{\mathrm{K}\cdot\mathrm{N}\cdot\mathrm{M}} \\
\mathbf{H}^{\mathrm{TOT}} &\rightarrow \frac{\mathbf{H}^{\mathrm{TOT}}}{||\mathbf{H}^{\mathrm{TOT}}||_\mathbf{F}}\sqrt{\mathrm{K}\cdot\mathrm{N}\cdot\mathrm{M}}
\end{aligned} \tag{10.18}$$

As aforementioned, simulations within the current chapter consider N=1 and K=2.

10.5.1 Behaviour with the number of antennas at the BS

The number of antennas at the BS is a key performance issue to determine the predicted goodness of MF with respect to the other linear precoders. It will help to confirm collapse of MF into ZF.
The scenario includes the following:

- The SNR is set to 10 [dB].

- The massive array's aperture is set to 20 [m] and consists M antennas, spaced evenly. M is varied from 10 to 500.
- The users have only one antenna, N=1. Two users are considered, K=2. Their location is fixed. User 1 is located at [x,y]=[-55,60] [m] and User 2 is located at [x,y]=[10,70] [m], as shown in fig. 10.3.
- Each user sees a local cluster and five far clusters. The local cluster contains 30 scatterers, while each of the far clusters has 20 of them.
- Performance of LOS and TOT channels is shown.

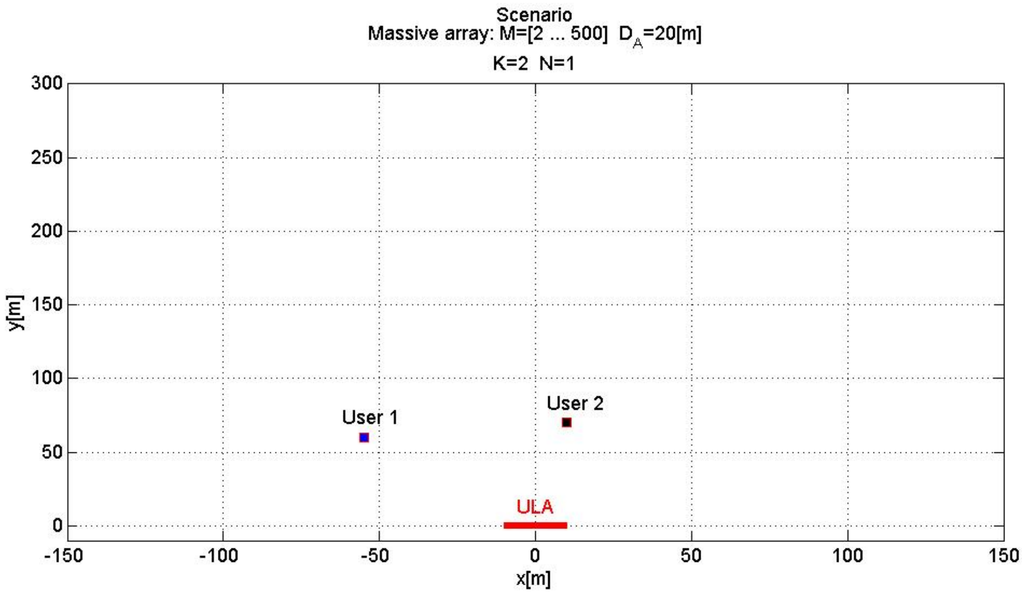

Figure 10.3 *Scenario selected for M variation.*

Fig. 10.4 on the following page features the performance of the channel's SR with respect to M for the three linear precoders considered in Proposal nr. 1.
It can be seen that the MF performs suboptimally for the low M region, and then achieves both ZF and MMSE's levels. This goes in line with its expected optimality behaviour for a large number of antennas, as mentioned before in this document. However, an unexpected drop is experienced at an interval ranging from M=200 through to M=300, roughly. This is indicated in fig. 10.4 on the next page with an annotation tag reading *Slump*. Yet unsupported, it is suggested that this behaviour is directly due to MF's spectral efficiency and particularly, due to impoverished orthogonality [15] (or inter-user interference, see chap. 11 on page 109) at the specified M interval. Moreover, it ought to be noticed that results for the LOS and TOT channels possess a high degree of similarity and if any, the TOT channel seems to lessen MF's lack of optimality. This is especially evident in the area where a drop is observed and would reinforce the argument of inter-user correlation being responsible for it: the scatterers action would help to improve correlation.
Otherwise, both ZF and MMSE appear to behave identically, except for the lowest M values. This is due to the SNR, which is sufficiently high. Both inversion-based precoders are optimal at any M value and yield the highest SR. This is not mainly due to the symbol power achievement, as seen in fig. 10.5 on the next page, but yet rooted in the ability to manage inter-user interference. Fig. 10.6 on page 101 confirms that, while the system is devoid of inter-user interference by ZF employment, this is not the case for the MMSE precoder, which allows a significantly higher amount; Conjugate beamforming's in turn, is the highest.

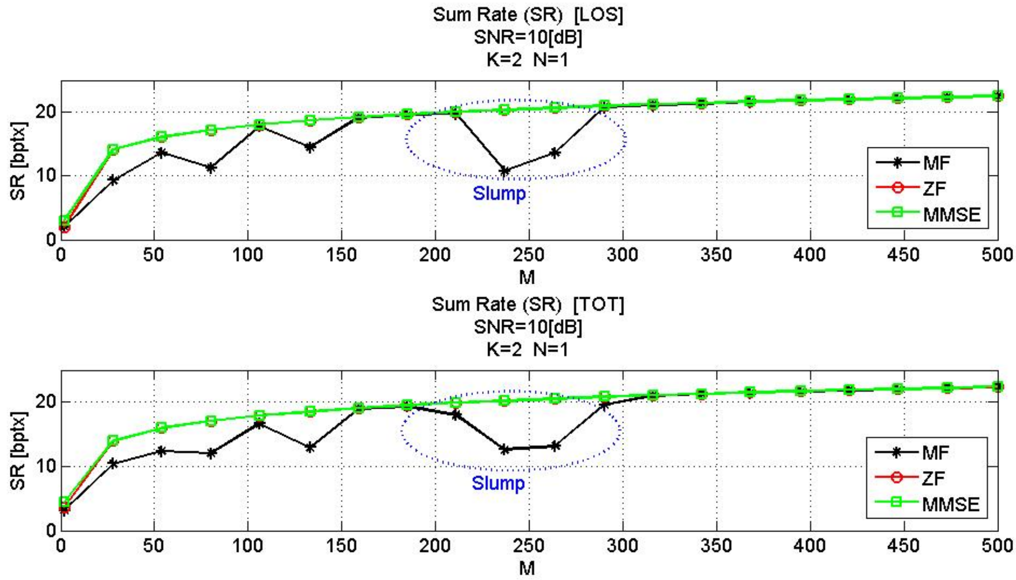

Figure 10.4 *Sum Rate (SR) vs M.*

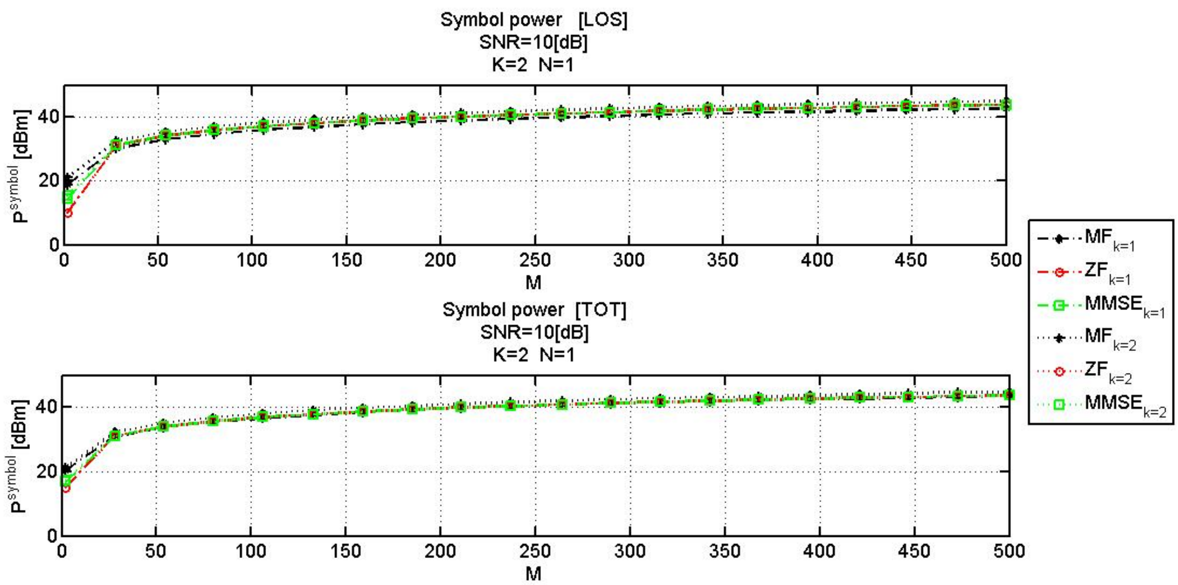

Figure 10.5 *Symbol power vs M.*

10.5.2 Behaviour with the number of antennas at the BS when those are irregularly spaced.

The aim of this subsection is to analyse the behaviour of the SR with respect to the number of antennas at the BS, M, when they are irregularly spaced since unevenness is expected to provide with a higher degree of orthogonality between the channel's vectors. Thus, the falloff on SR observed in fig. 10.4 is expected to lessen.

Fig. 10.7 on the facing page features SR with respect to the variation of M for the irregularity case. All parameters in sec. 10.5.1 on page 98 hold up.

It is first observed that suboptimality of MF is maintained throughout the increasing M up to the very high values, where the SR matches the inversion-based precoders'. This is exhibited in both LOS and TOT cases. However, it must also be noticed that the drop for the M $\approx [200, \cdots, 300]$ interval, although still visible, incurs less penalty, which would go along the lines of improvement

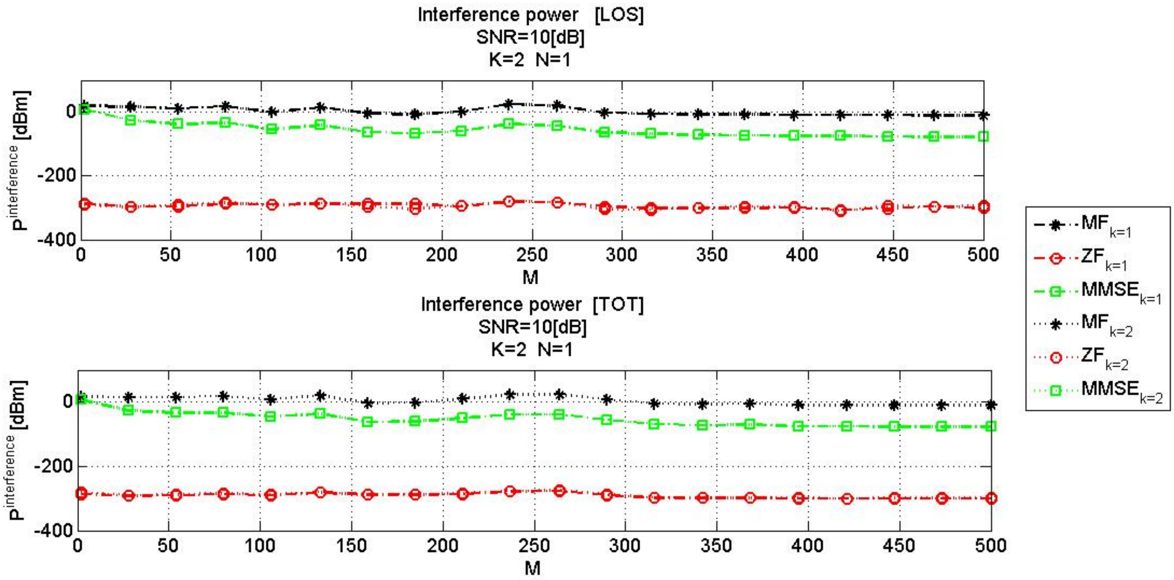

Figure 10.6 *Interference power vs M.*

due to the existence of better orthogonality. This is especially obvious in the TOT channel curve. Also regarding the TOT channel, a much higher degree of coherency is observed on MF's curve tendency. This phenomenon substantiates the hypothesis of the scatterers being responsible for a modification on the inter-user correlation values, in this case in the form of uniformity, which yields coherency on MF's SR tendency.

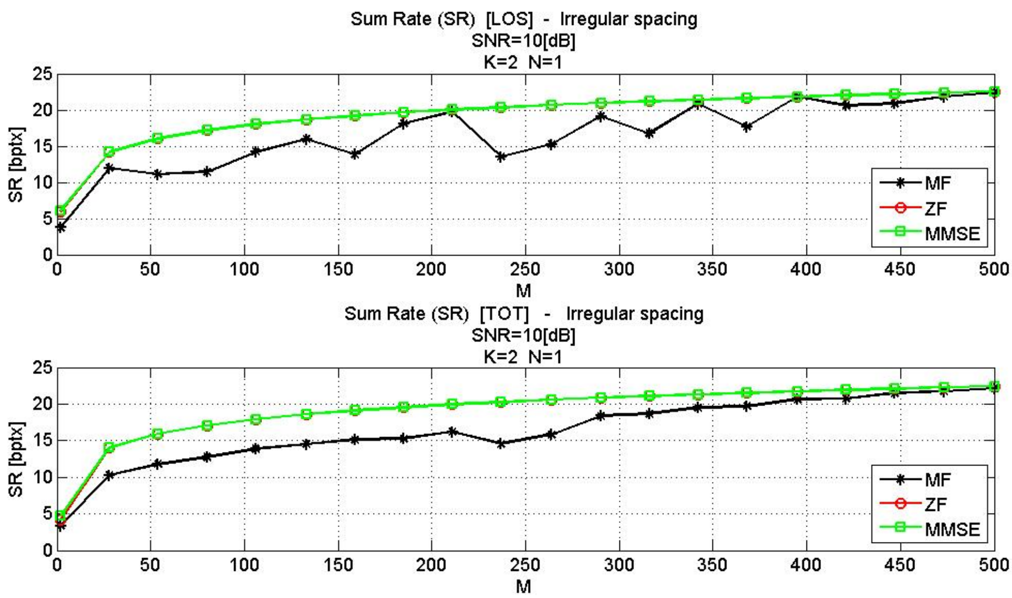

Figure 10.7 *SR vs M. Irregular spacing at the BS.*

10.5.3 Behaviour with the SNR.

The SNR is one of the key parameters on the linear precoders behaviour. For instance, ZF is expected to behave poorly with respect to MMSE, while the latter should keep its optimality for any SNR value. Little has been found in the literature on MF's expected performance with respect to the SNR. However, this subsection will determine that conjugate beamforming is as well SNR-sensitive and that dependence is critical at the very-high SNR regime.

The scenario includes the following:

- The SNR is varied from -30 to 60 [dB].
- The massive array's aperture is set to 20 [m] and consists M=300 antennas, spaced evenly. At a frequency of 4.5 [GHz], this yields a spacing of $\approx 1.5\lambda$ [m].
- The users have only one antenna, N=1. Two users are considered, K=2. Their location is fixed. User 1 is located at [x,y]=[-55,60] [m] and User 2 is located at [x,y]=[10,70] [m], as shown in fig. 10.3 on page 99.
- Each user sees a local cluster and five far clusters. The local cluster contains 30 scatterers, while each of the far clusters have 20 of them.
- Performance of LOS and TOT channels are shown.

Fig. 10.8a on the next page exhibits the channel's SR as per the three linear precoders. The growth of both ZF and MMSE with the SNR is linear as literature reads [10]. Moreover, the expected impoverished performance of ZF at low SNRs seems not to be such at the massive MIMO regime. This is due to the fact the symbol power is high enough at all times (see eq. 10.7 on page 95), whichs allows a high SINR.

Otherwise, MF's growth in massive MIMO is confirmed to be linear as well as the other two precoders'. This goes in line with MF's optimality for the large-number-of-antennas regime. Interestingly, MF's SR fails to continue increasing for a specific value of the SNR, around 20 [dB]. This is due to the asymptotic SINR's behaviour: at some point, $\mathrm{P}^{\mathrm{interference}} > \mathrm{P}^{\mathrm{noise}}$, so the rate at which the SNR grows is much lower than the SINR's. This makes the sum rate saturate for the conjugate beamforming at a given value of the SNR. Proof for this can be seen in fig. 10.8b on the next page, which includes the SR as per the SINR (custom), the Signal to Interference Ratio (SIR)-only (asymptotic behaviour for the very-high SNR regime) and the SNR-only (behaviour up to the inflection point). When $\mathrm{P}^{\mathrm{interference}}$ and $\mathrm{P}^{\mathrm{noise}}$ are comparable, the SR is at a transition interval. This behaviour can also be extracted from fig. 10.9 on page 104, which features the interference power for all precoders and also includes the noise power. If attention is focused towards the MF and the noise power,

- the SNR intervals where $\mathrm{P}^{\mathrm{interference}} < \mathrm{P}^{\mathrm{noise}}$ and the SR is given by SR(SNR)
- where they are comparable and the SR is at a transition zone
- and where $\mathrm{P}^{\mathrm{interference}} > \mathrm{P}^{\mathrm{noise}}$ and the SR is given by SR(SIR)

can be identified.

Finally, we include fig. 10.9 on page 104 in order to give confirmation for the literature's performance statements on MMSE collapsing to a MF for the low SNR and, the other way round, to a ZF precoder for the high-SNR regime.

10.5.4 Behaviour with the SNR for different number of users K.

Another critical aspect on the behaviour of the linear precoders is the number of simultaneous users being served, K. Literature reads that in multi-user massive MIMO systems, the ratio between the number of antennas at the massive array M and the number of users K is high (p.eg. greater than 10), which yields a potential to obtain very high spatial diversity [13]. However, and focusing on beamforming, the employment of MF-based beamforming in real systems would only be optimal in some circumstances. One of the key factors for suboptimality, with regard to spectral efficiency, is the user's channel orthogonality [15]. It will be seen within this section that orthogonality plays an important role in terms of sum capacity values. This is particularly interesting when the number of users K increases.

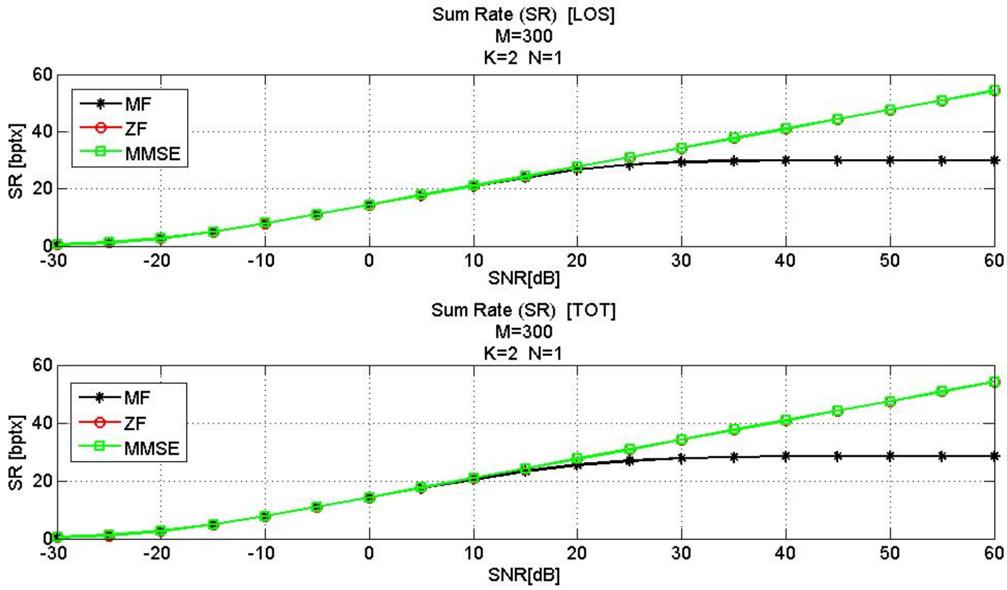

(a) *SR vs SNR.*

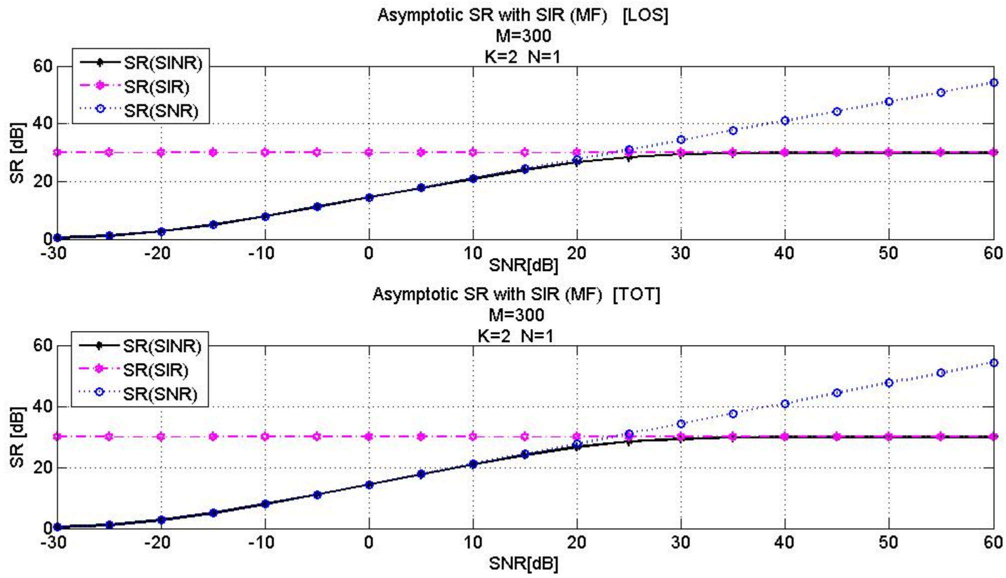

(b) *SR(SINR), SR(SIR) and SR(SNR) vs SNR.*

Figure 10.8 *SR. Behaviour with respect to SNR.*

Fig. 10.11 on page 106 features the achieved SR for a massive array with M=300 antennas and an aperture of D_A=20 [m] for different SNR values and also different number of users being served simultaneously K, namely K=2, K=5, K=15 and K=30. The users are placed at a constant y-value of 100 [m], and different x-values (see fig. 10.10 on the next page). The first user ($k = 1$) is always selected to be one closest to broadside. The rest are picked up randomly to make up the channel matrices corresponding to K=2, K=5, K=15 and K=30. Only the MF and the MMSE precoders are considered. Only the TOT channel is featured. The range of SNR has been narrowed down to SNR=[-20,$\cdots$,20] [dB].
It is of interest to observe that difference in performance between conjugate beamfoming and MMSE in the interval in which $P^{\text{interference}} > P^{\text{noise}}$ is most noticeable as K grows. As the SR is given in this interval by the SIR, this forcefully means that inter-user correlation provokes a downgrade on MF curves via an increase of the interference terms. In other words, conjugate beamforming is unable to create narrow enough beams to cover the different users individually without affecting the others. Extraordinarily, this applies at a much lower extent as we abandon

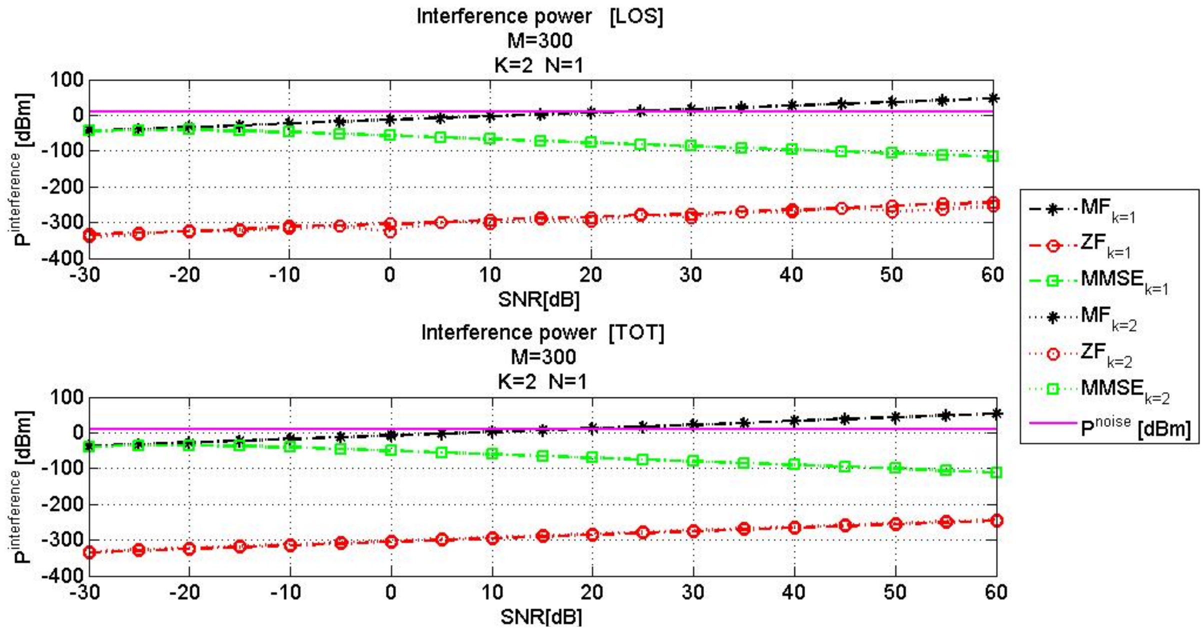

Figure 10.9 *Interference power vs SNR.*

this SNR region heading towards lower values and ceases to appear at the low SNR region, in which interference power is minimised.

It is to our best understanding that this behaviour is directly rooted in the orthogonality of the different channels. If K is low, then the ratio M/K is higher and conjugate beamforming's capability to behave optimally increases. For instance, if K is so high that all users are close to each other, then their channels will be more correlated.

Otherwise, it is likely that the configuration of the massive array in the form of the location of its elements has an impact as well on orthogonality, apart from the aforementioned location of the users. It is for this reason that this analysis has been extended for two additional massive array aperture values. Modifying the antenna aperture for a constant number of antennas causes a change in the spacing, and thus in the location of the different elements. This will in turn influence the channel terms and eventually, orthogonality among the user channels. In total, three different aperture values have been studied: D_A=20 [m], D_A=15 [m] and D_A=10 [m]. The users are located as in fig. 10.10 and the selection procedure is the same as explained above.

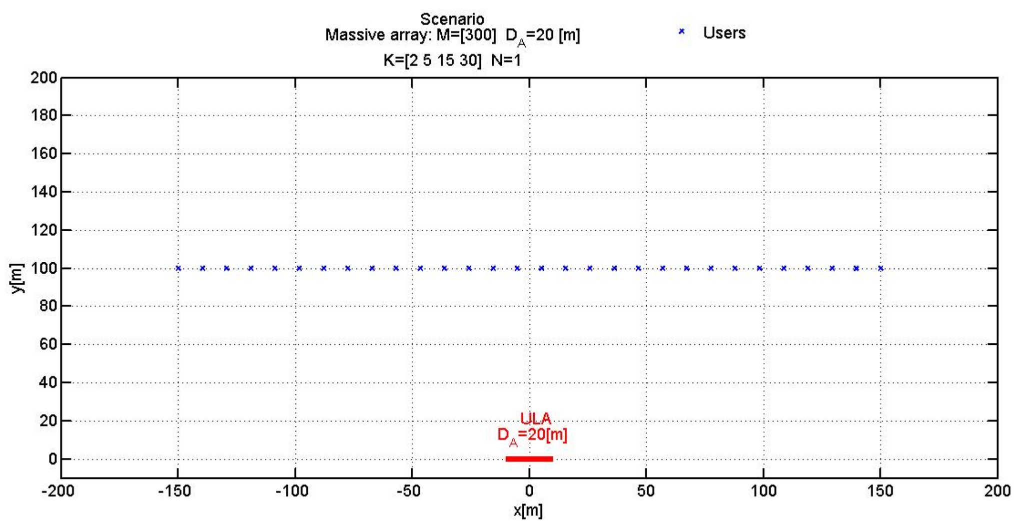

Figure 10.10 *Scenario depicting K=30 users.*

Fig. 10.12 on page 107 exhibits the different behaviour of the beamformers under these circumstances.
Attractively, and barring the K=5 case, which is too low to serve as a basis for tendency on orthogonality (we remind the reader that users are picked up randomly), the performance of the MF appears to improve dramatically as the aperture decreases. This remarkable outcome, together with all the previous findings pointing out at orthogonality as the cause of performance downgrade, is the final incentive for the study of channels orthogonality or inter-user correlation. This will be included in chap. 11 on page 109.

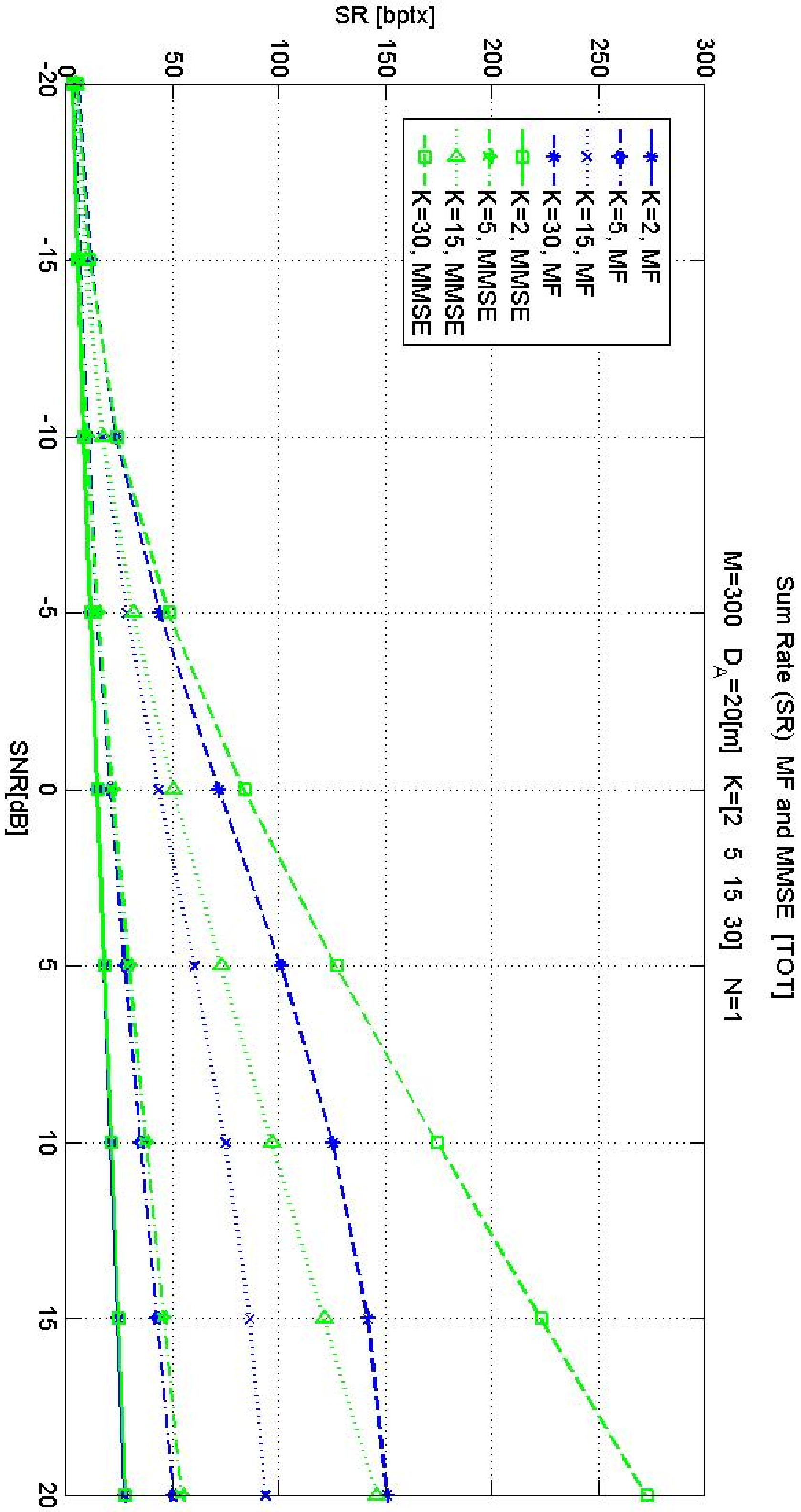

Figure 10.11 *SR vs SNR for different K values. MMSE and MF. TOT channel.*

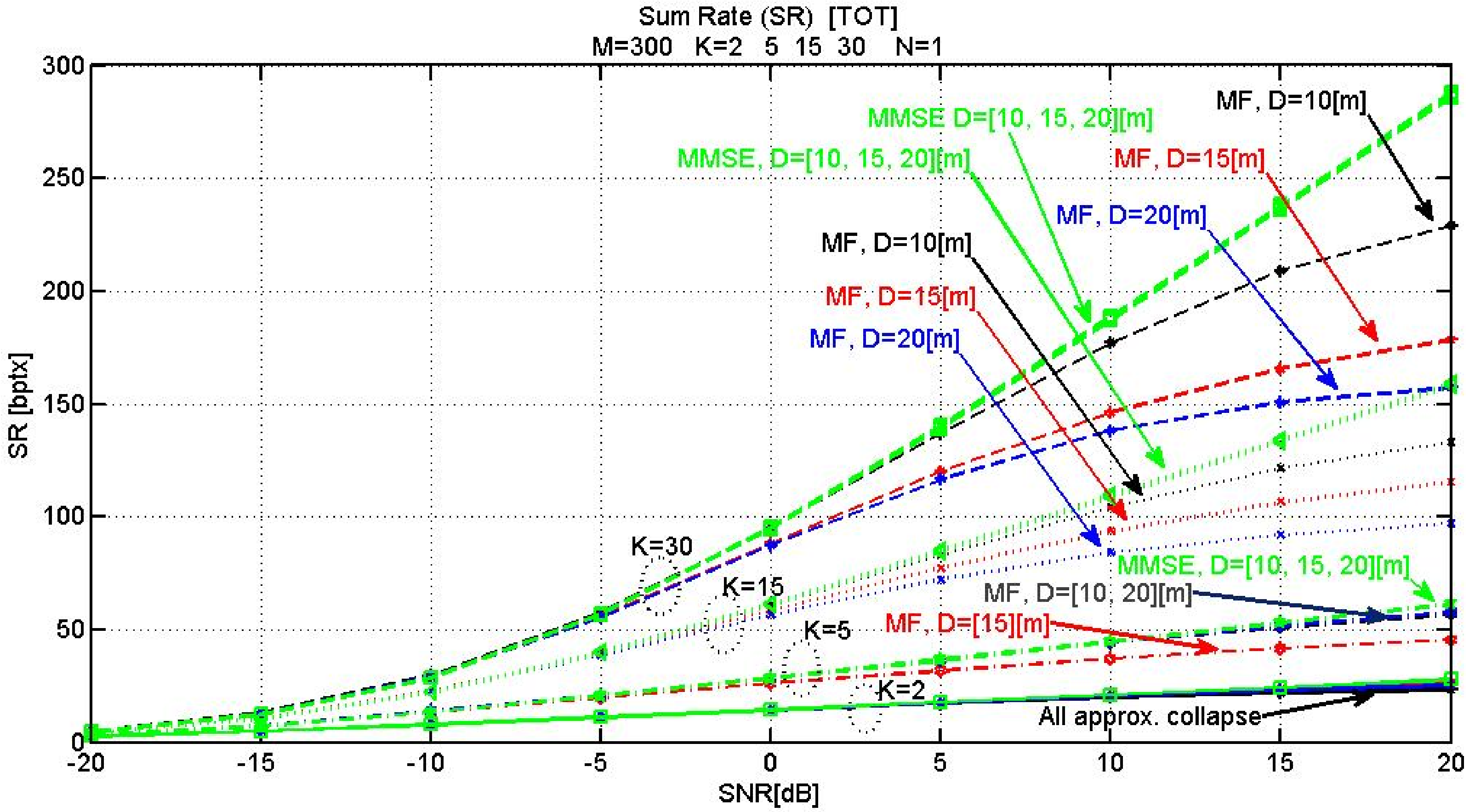

Figure 10.12 *SR vs SNR for different K values and three different apertures, D=20[m], D=15[m] and D=10[m]. MMSE and MF. TOT channel.*

Chapter 11

Orthogonality: analysis and prediction of User separation.

A main difficulty in Massive MIMO is the principle of separating transmissions between users. When having a MU-MIMO scenario, all the different users will interfere with each other, and cause unwanted correlation.

This chapter circles around studying the effect of correlation and orthogonality of channel estimations on performance of a MU-MIMO scenario, and attempt to identify key features so high correlation and low orthogonality may be avoided. Orthogonality will be employed as a unitless metric, and as such be denoted as $\rho_{\perp}$.

11.1 Motivation

We remind the reader that the basic motivation behind Proposal nr. 1, as shown in chap. 10 on page 91 is to reduce the load at the BS, incurring less complexity. This may be done by employing linear precoders, such as the ones analysed in previous chapters. Recalling, these linear precoders are:

- Matched Filter (MF)
- Zero Forcing (ZF)
- Minimum Mean Square Error (MMSE)

Beamforming as for using linear precoders such as MF, ZF, and MMSE, has been shown to yield good results under certain conditions for massive MIMO systems [13, 16]. Furthermore, it has been shown that other non-linear precoding schemes like DPC are unfeasible in practice [36]. In particular, MF has been shown to perform well-enough to match sum capacity rates as those of ZF and MMSE for the massive number of antenna regime [44, 45]. However, as seen in chap. 10 on page 91, it tends to saturate at high SNRs due to the SINR asymptotic dependency. That is, for a growing SINR with fixed noise power, the interference power will grow to a level making the noise power negligible. Thus saying in a sense that the system is interference limited. Moreover, chap. 10 on page 91 has shown that inter-user correlation determining the channel's SINR was dependant on the massive array configuration as well. As all throughout the work presented in this document, the massive array is considered to be a ULA.
In contrast to this, massive MIMO systems are expected to yield very high orthogonality between the different users vectors since channel responses tend to be nearly orthogonal to each other when the number of antennas at the massive array M is very large [16], which would imply MF-based precoding would be optimal.
This yields a contradiction and implies that the single requirement of asymptotically large

number of antennas at the BS might not be enough to determine MF's optimality and that additional issues lying behind the BS's configuration ought to be attended.

On the other hand and barring orthogonality on the conjugate beamformer's performance, ZF and MMSE are more computationally demanding due to the fact that they are based on matrix inversion.

All in all, it is of interest to determine when and where it is possible to use MF, which is simpler than the inversion-based precoders since it is based on matrix conjugation, according to the analysis on orthogonality and inter-user correlation in a massive MIMO system.

Earlier studies have shown that in areas of low orthogonality, an MF precoder will not perform very well. In those areas it would be more beneficial, if high data rates or high sum capacity values are to be obtained, to use the more complex precoders, ZF and MMSE. Interestingly, by using the analysis similar to that of [25], these areas are seen to be related to both the Far Field resolvability and the required channel conditioning. For a uniformly spaced LA-MASS, outthrusts seem to appear, which are shown to be due to the angular resolvability, related to the analysis by [25], and thus a direct result of the uniform spacing between antennas at the BS. The massive array's antenna configuration due to its spacing (and thus, aperture) becomes this way the additional parameter being responsible for MF's performance that focuses our attention. However, in reality this may not be the case. In fact, the antenna separation may be subject to irregular spacings due to some small scale variation. It will be seen that, because of the varying antenna spacing, the outthrusts seem to fade away, replacing the large regions of very good orthogonality with a "patched" area of moderately low orthogonality. Fig. 11.1 shows an example of the effect that different antenna spacings have.

Under certain conditions, though, even with antennas being distributed uniformly, adjusting the Massive array's configuration, the outthrusts can be removed. Particularly, they may be removed from the scenario of interest, by tuning the expression defined by [25], which will be presented in the following chapter.

By studying orthogonality between two channel vectors, and as such two users, it is possible to determine when and where MF precoding can and can not be applied. The main objective is to observe how orthogonality behaves for a scenario consisting of two users with one antenna each, and identify a relation for which areas of low orthogonality may be predicted. This will serve as a basis for other types of scenarios.

Lastly, it must be remarked that it will mainly be the LOS channel that will be tackled in this chapter. This lies behind the fact that it is this channel that most significantly determines orthogonality, as it is rooted in the massive array's configuration, apart from the obvious users' location dependency. Moreover, the TOT channels are highly computationally demanding since they involve the simulation of an elevated number of Monte Carlo simulations in order to provide an indicative representation of the channel's statistics. This yields a particularly high dimension of complexity in the case of the analysis of orthogonality and inter-user correlation, as it involves the extraction of those statistics for a wide range of user locations.

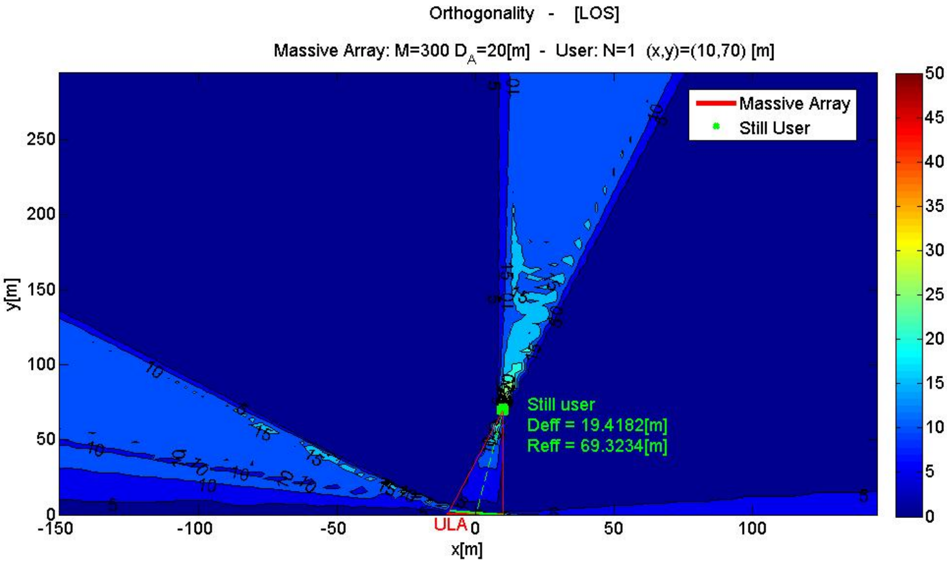

(a) *Two outthrusts occur. The one pertaining the Still User will always be present, no matter the antenna spacing. At the endfire on the left side, and outthrust occurs. This is due to the aperture size of the Massive Array, — and thus directly related to antenna spacing.*

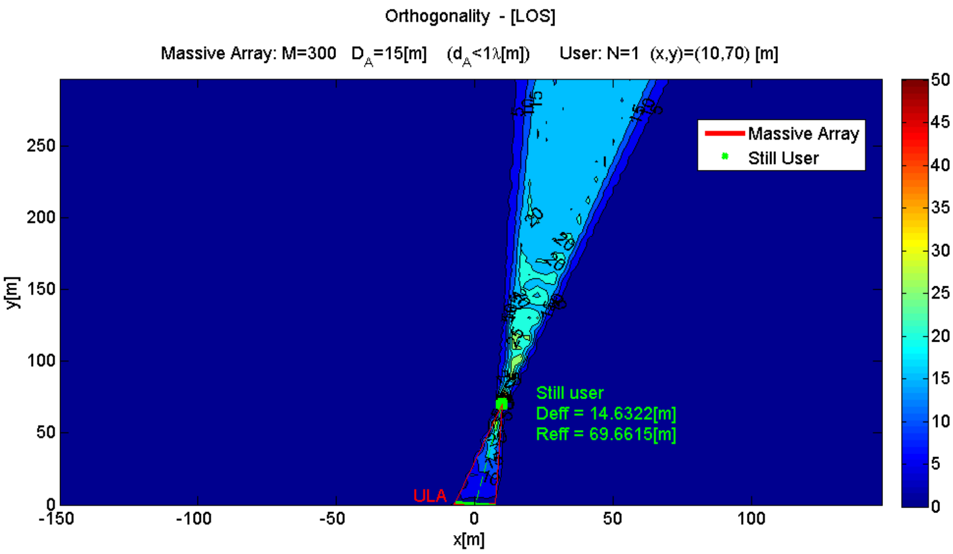

(b) *For the same aperture specifications, the Endfire outthrust now vanishes. The only difference between this figure, and that of fig. (a) is the aperture size.*

Figure 11.1 *A Still User located at (x,y) = (10,70) [m]. Shown are for two aperture sizes of the Massive Array. Fig. (a) shows orthogonality between the Still User and a Mobile User with the Massive Arrays aperture size being 20 [m] and, (b) shows a similar situation with aperture size of the Massive Array being 15 [m].*

11.2 Analysis

In this section, two metrics of seperation between users are defined. These are

- Orthogonality, and
- Correlation Coefficient.

Orthogonality measures the degree of perpendicularity between matrices, or in this case, vectors. Let **A** and **B** be two vectors with dimensions $1 \times N$. Vectors **A** and **B** are orthogonal (or perpendicular) if and only if the dot product of **A** and **B** is 0.

In this context, where **A** and **B** may be channel vectors for two users, if both channel vectors are orthogonal to each other, the two user can be separated. The degree to which they can be separated, measured as $\rho_{\perp}$, ranges from 0 to 1, where 0 means the can be completely separated — users are orthogonal —, and where 1 indicates that users can not be distinguished.

Similar to orthogonality, the correlation coefficient indicates the correlation of two vectors. Correlation is a measure of statistical relationship of two random variables.

It will be shown that for this specific case, orthogonality and correlation coefficient is the same. Because of this, the following study on user separation will only be done, based on orthogonality of channel vectors.

11.2.1 Case definition

For the sake of simplicity[1], the analysis will be based on the following scenario.

A BS with a LA-MASS is serving a bounded area with dimensions (x,y)=(700 [m] × 350 [m]). The BS is serving 2 users with 1 antenna each. User 2, or also referred to as Still User, is positioned at a fixed location. User 1 is positioned at a location and orthogonality between User 1 and 2 is calculated. User 1 is then moved to a new location, and orthogonality is calculated. This is done over the entire grid. The aperture size of the Massive Array is 33.33 [m] and consists of 251 antennas. Fig. 11.2 shows an example of the scenario overview.

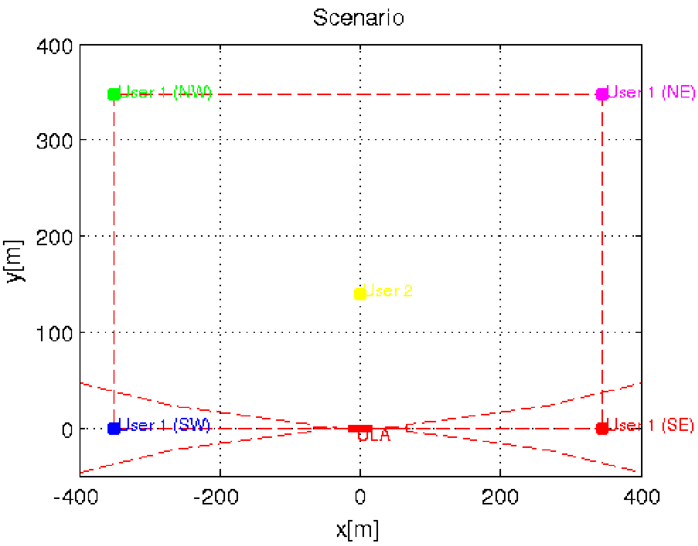

Figure 11.2 *This figure shows the scenario overview, which will form the basis of the Orthogonality study. The Still User, marked in yellow, will be placed at a wide range of locations inside the bounded field marked by the red dashed line. The Massive Array has 251 antennas, with an aperture size of 33.33 [m].*

Several iterations will be done, where User 2 is positioned at different locations.

[1]Also, discussion will mainly be done for LOS case only, except where otherwise noted.

11.2.2 Correlation Coefficient and Orthogonality

Correlation Coefficient and Orthogonality can be directly related to each other, yielding the same results. This is due to the fact that the means employed by the Correlation Coefficient are 0, and so yields the same expression as Orthogonality. For a detailed account of Correlation Coefficient and its relation to Orthogonality, refer to app. H.

Orthogonality as a measure is defined as,

$$\rho_{\perp} = \mathbb{E}\left[\frac{\left|\mathbf{H}_1 \cdot \mathbf{H}_2^{\mathrm{H}}\right|}{\sqrt{\|\mathbf{H}_1\|^2} \cdot \sqrt{\|\mathbf{H}_2\|^2}}\right] \quad [\cdot]\,. \tag{11.1}$$

where $\mathbb{E}[\,]$ is the expectation operator, $|\ |$ is the absolute value operator and $\|\ \|$ is the vector's norm.

Two users are orthogonal if $\rho_{\perp}$ is 0. For the LOS channel and $N = 1$, orthogonality can be considered as the normalised complex scalar product. However, this will still be referred to as Orthogonality for consistency purposes.

11.2.3 Verification

Focusing mainly on LOS, for the mentioned scenario in sec. 11.2.1 on the preceding page, orthogonality between two users is determined.

The transmitter consists of an ULA with M antennas. User 1 and 2 are defined by the M-dimensional channel vector given in eqs. 11.2a and 11.2b, respectively.

$$\mathbf{h}_1 = \begin{bmatrix} h_{1,1} \\ h_{1,2} \\ \vdots \\ h_{1,m} \\ \vdots \\ h_{1,M} \end{bmatrix} \tag{11.2a}$$

$$\mathbf{h}_2 = \begin{bmatrix} h_{2,1} \\ h_{2,2} \\ \vdots \\ h_{2,m} \\ \vdots \\ h_{2,M} \end{bmatrix} \tag{11.2b}$$

The total LOS channel is then,

$$\mathbf{H} = \begin{bmatrix} \mathbf{h}_1^{\mathrm{T}} \\ \mathbf{h}_2^{\mathrm{T}} \end{bmatrix} \tag{11.3}$$

constituting a $K \cdot N \times M$ matrix. The superscript $(\cdot)^{\mathrm{T}}$ denotes the transpose. Since each user only has 1 antenna each, the channel matrix, $\mathbf{H}$ reduces to $K \times M$.

Orthogonality is calculated using eq. H.2, yielding the expression,

$$\rho_{\perp} = \frac{|\mathbf{h}_1 \cdot \mathbf{h}_2|}{\sqrt{\|\mathbf{h}_1\|^2} \cdot \sqrt{\|\mathbf{h}_2\|^2}} \tag{11.4}$$

Using the expression for orthogonality, the level of alignment between two users are shown in fig. 11.3 on the following page. Note that orthogonality is scaled by a factor of 100, thus showing alignment as a percentage.

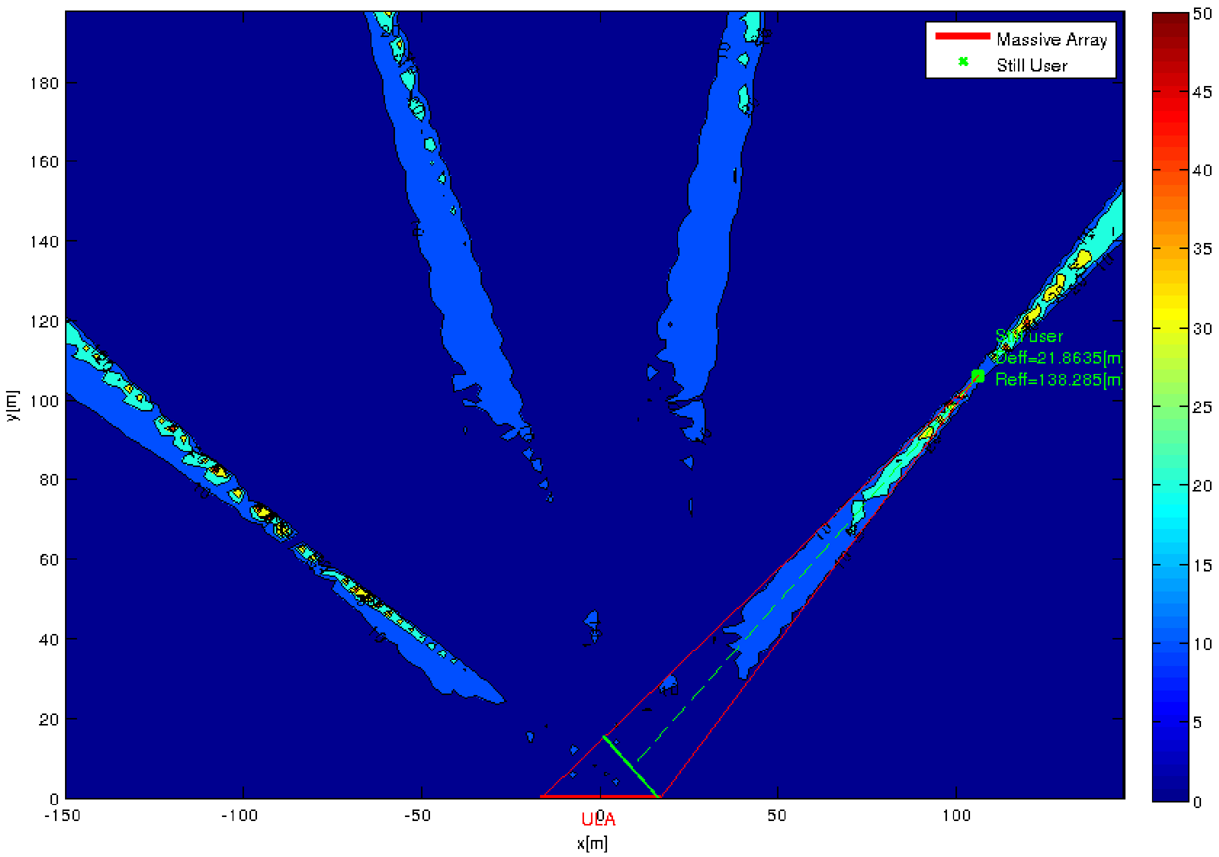

Figure 11.3 *This plot shows the level of Orthogonality between two users. User 1 is located at all places, while User two is located at an Echelon angle of 45° with distance 150 [m] from the centre of the Massive array. Results are scaled with a factor of 100.*

This figure shows a contour plot of the level of Orthognality between two users. User 2, begin the Still User indicated by a green dot, is located at a fixed position. Dark blue indicates area where User 1 and User 2 are completely orthogonal, whereas dark red indicates areas where User 1 and User 2 are very much aligned. Some interesting observations can be made in the aforementioned plot. Several outthrusts appear with some periodicity. The origin of these outthrusts will be explained later, as it is seen that they also appear in the Far Field, and is due to the evenly spaced antennas at the Massive array. In addition to the outthrusts some patches of very low Orthogonality appear around the Still User, as well as the outthrusts. Outside of the low Orthogonality patches, MF can be applied, while inside the specified patches, MF can still be applied, but this will reduce performance. Instead it would be more beneficial to apply ZF or MMSE. The reason why MF would perform unsatisfactorily can be attributed to the fact that the Massive array has difficulty being able to distinguish one user from each other.

With different array configurations at the Massive Array, a variaty of outthrusts would appear. For one configuration, more outthrusts would appear, while for other, there might be less outthrusts. However, while these would come and go, a main outthrust would always be present. This was also related to the location of the Still User. The authors in [25], as will be presented in the following section, confirmed that these outthrusts[2] were due to the number of antennas and the spacing thereof. It should be remarked that analysis in [25] is based on Far Field. To this purpose, orthogonality is calculated, using (a) uniform spacing, and (b) irregular spacing. This is shown in fig. 11.4.

[2] In fact, [25] showed the angular resolvability between radial distances, rather than the outthrusts as mentionend here.

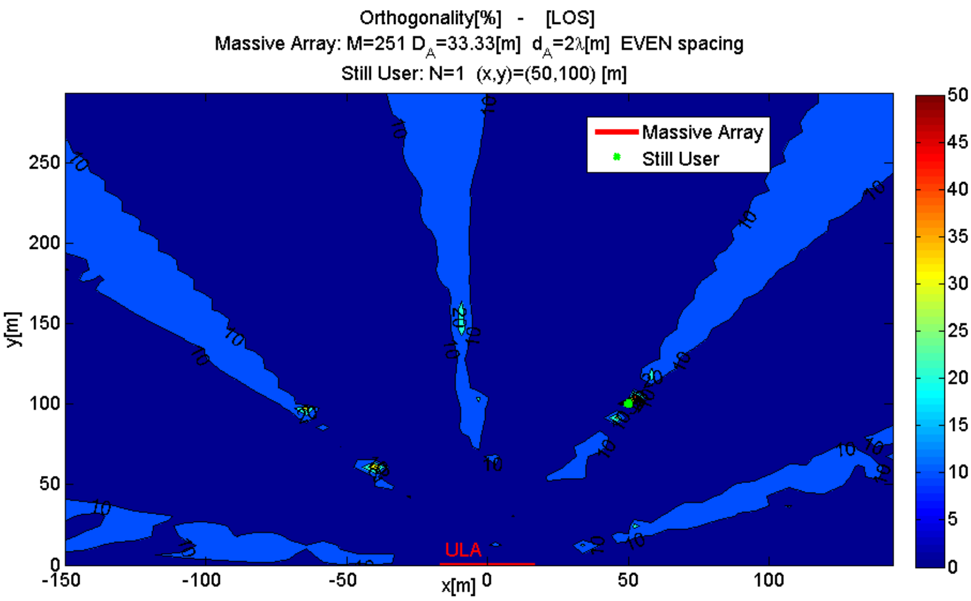

(a) *The Massive Array has a Uniform inter-antenna spacing. Outthrusts tend to an angular periodicity, with one outthrusts pointing in the direction of the still User.*

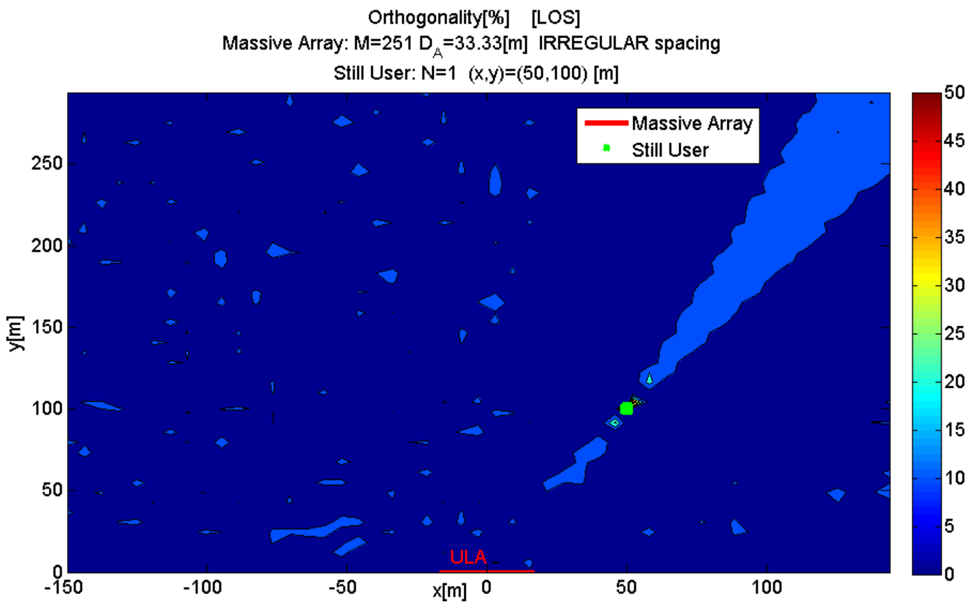

(b) *Reordering the Massive Array to use an irregular spacing results in outthrusts fading away. However, the outthrust where the Still User is located remains present.*

Figure 11.4 *The effect of defining the Massive Array with a uniform spacing contrast an irregular spacing. Both plots are with M=251 and N=1.*

For an evenly spaced Massive Array, the outthrusts would begin to appear for a spacing greater than 1λ. **It is suggested that a spacing below 1λ be the optimal spacing at the massive array so that outthrusts related to the massive array's configuration disappear**, yielding an area like in fig. 11.1b on page 111.

Likewise, using **an irregular spacing for the Massive Array, in turn makes outthrusts fade away**. They are still present, but less defined. Also, in contrast to the homogeneous spacing, the regions with high levels of Orthogonality, are now replaced by a "patched" area of moderate levels of Orthogonality, in some cases perfect orthogonality.

However, the outthrust pointing in the direction of the Still User, pertains in any case. For this reason, focus is mainly directed at the outthrust, that persists, no matter the configuration. This area of interest will be defined by the triangle which constitutes the equivalent broadside array and the Still User location. Drawing a line from the extremes of the equivalent broadside array to infinite, passing through the location of the Still User, defines the two-part areas of interest — lower, and upper triangles. The lower triangle is the one bounded by the extremes of the Massive Array, and Still User location. The vertices extended from the Still User location towards infinite, is the one defining the upper triangle. In practice, this is not possible. For computational simplicity the upper triangle is bounded to a mirror image of the lower triangle of interest in the simulations carried out in this thesis.

11.2.4 Approach by Tse

The whole derivation of approach in [25] in terms of the requirements in this chapter is given in appendix I on page 193.

The outthrusts that were observed in the surface plot of fig. 11.3 on page 114 can also be observed in the Far Field. This has been alluded by Tse and Viswanath [25], who showed how resolvability can be seen in the Far Field. Throughout this section, discussion is mainly based on Tse and Viswanath [25], except where noted otherwise.

Broken down into the basic ideas, Tse and Viswanath [25] apply the Far Field approximations on a MIMO channel, by projecting the antennas onto a reference link. Doing this projects the entire channel matrix onto a single channel term, which is then split into what they call spatial signatures. Afterwards, they break the Far Field assumption by spacing antennas at one end, far apart. Antennas at one end, can no longer be projected onto the reference pair, since incurred inaccuracy will be to great.

A power gain can always be achieved. This is partly due to the projection of the transmitter, which makes the transmit signals be added in-phase at each receiver antenna. Additionally, the projection of the receiver allows the possibility of further combining constructively, such as MRC.

However, DoF gain can not always be achieved. Some DoF will be obtained, however, when either the aperture at the transmitter or at the receiver is large enough. If this is the case, then a DoF gain will be obtained. This happens because of the added angular resolvability the large aperture provides with making the elements of the arrays be resolvable, when in the Far Field.

Applying the analysis made by Tse and Viswanath [25], for the scenario given before, it is anticipated that the noted outthrusts would appear, and be similar to the ones observed during the Orthogonality analysis.

Angular resolvability is described by the following expression.

$$|\cos(\epsilon)| = \left| \frac{\sin(\pi M \Delta_{\mathrm{Tx}} \Omega_{\mathrm{Tx}})}{M \cdot \sin(\pi \Delta_{\mathrm{Tx}} \Omega_{\mathrm{Tx}}} \right| \tag{11.5}$$

where Δ_{Tx} is the massive array's inter-element spacing and Ω_{Tx} is derived in appendix I on page 193.

According to the above equation, if the antenna spacing is large, more peaks and so more periodicity appears. Additionally, channel conditioning may be described by the same equation, since it is based on the angle between two spatial signatures. If $|\cos(\epsilon)| \neq 1$ the channel is well-conditioned, whereas, if $|\cos(\epsilon)| \approx 1$ the channel is ill-conditioned.

In conclusion, according to the analysis by [25], two observations can be made. They are; 1) a larger antenna spacing at the transmitter provokes more outthrusts for an evenly spaced Massive Array, and 2), for an irregular spacing at the Massive Array, outthrusts disappear, except for the main outthrust belonging to the Still User. Based on these two observations, further analysis will focus primarily on the outthrust belonging to the Still User.

11.3 Prediction

The analysis seen in sec. 11.2 focused on why Orthognality as a measure is used. Orthogonality and Correlation was seen to yield same results, and as such Orthogonality was chosen as a metric, since it essentially the inner-product of the two channel vectors. Furthermore, the motivation for investigating Orthogonality, was to identify areas where MF performs well-enough to be utilized, and as such lower complexity at the BS.

In this section, it will be attempted to identify relations between areas of low orthogonality, and known parameters such as User location. Let be defined,

$$\hat{\mathrm{R}}_{\mathrm{Th}} = f(R, \phi)$$

where $\hat{\mathrm{R}}_{\mathrm{Th}}$ is the estimated radius (lying inside the lower triangle) from the User to a boundary where mean orthogonality is lower than some threshold, Th. The radius from the Still User to the centre of the Massive Array is denoted by R, and ϕ is the echelon angle as defined in previous chapters. The aim is simply to know the radial distance that satisfies an area where,

$$\mathbb{E}\left[\rho_{\perp}\right] > \rho_{\perp \mathrm{Th}} \tag{11.6}$$

being that area occupied by the lower triangle. Although reaccounted for later in this chapter, the main motivation is due to simulation complexity. An analogous analysis could be made for the upper triangle.

11.3.1 Method

The overall idea is to find a closed-form relation with respect to the user's location which reveals in which areas orthogonality would be limiting due to the presence of another user.
The employed method relies on the cumulative mean or cumulative average, which is be defined as,

$$\hat{x}_{n+1} = \frac{x_{n+1} + n \cdot \hat{x}_n}{n+1}. \tag{11.7}$$

Essentially, instead of averaging over all points multiple times, the previous mean can be reused for the next iteration. This results in lower computation time, as it is not necessary to re-calculate the average. For this application, it allows the possibility of regularly checking the average $\rho_{\perp}$ to whether or not be within some threshold level.

The Still User is located at a wide range of positions, determined by the echelon angle as well as its radius to the centre of the Massive Array. In other words, the Still User's location is sweeped according to $\phi \in [0°, 180°]$ for all $R \in [50; 320]$ metres[3].

Orthogonality is calculated over the entire scenario area. Afterwards, the points located within the area are singled out, as it is primarily the outthrust pertaining the Still User that is of interest.

The cumulative average is calculated for all the points found within the lower triangle. These points are sorted to distance, in ascending order. That is, the first point is the one situated closest to the Still User.

At this point, Orthogonality has been calculated for many different locations, and as such the following step is to determine the sought closed-form relation. To this purpose, the found R_{Th} are plotted versus ϕ, and curve fitting is performed using MATLAB. By inspection, results indicate to follow a power function. To put it differently, the threshold distance is plotted versus the echelon angle for each threshold level, when the Still User is at one location. The threshold distances are then fitted to one of two curves matching the general expressions,

$$f(x) = \sum_{i=1}^{n+1} p_i x^i \tag{11.8}$$

[3]In some cases, the maximum R is 350 [m].

and

$$f(x) = ax^b + c \tag{11.9}$$

Using $n = 4$, the first expression becomes a 4^{th} order polynomial, whereas the second is a 2^{nd} order power exponential. These two general curve fittings have been chosen since they seem to yield the same tendency when while reviewing the plots, as will be seen later on. However, one has been proven to match better than the other. This will be shown in the following sections.

As mentioned, this is done for several radial distances of the Still User to the centre of the Massive Array. Afterwards, the same information is then fitted to a curve, in order to obtain some relation to location parameters of the Still User.

Results and reasoning is found in the following section.

11.4 Results

Results are based on the following parameters, shown in tbls. 11.1 and 11.2.

Parameter	Setting
x_{Bound}	[-350; 350] [m]
y_{Bound}	[0; 350] [m]

(a) *Scenario parameters.*

Parameter	Setting
Frequency	4.5 [GHz]

(b) *Channel parameters.*

Table 11.1 *Scenario and channel parameters.*

Parameter	Setting
Configuration	ULA
Location	Origo
No. of antennas	251
Aperture size	33.33 [m]

(a) *Massive Array parameters*

Parameter	Setting
Configuration	ULA
No. of Users	2
No. of antennas	1
Antenna spacing	6λ

(b) *User parameters*

Table 11.2 *Parameters related to the Massive Array the the users.*

11.4.1 Fixed R, echelon sweep

The location of the Still User is sweeped over a range of locations, fitting the polar mapping of the x and y coordinates. In polar coordinates, the Still User is at a fixed radial distance from the centre of the Massive Array. Its echelon angle is sweeped from 0° to 90°. Fig. 11.5 shows an example of the scenario, where the Still Useris at 45° echelon angle, and distanced 150 [m] from the centre of the Massive Array.

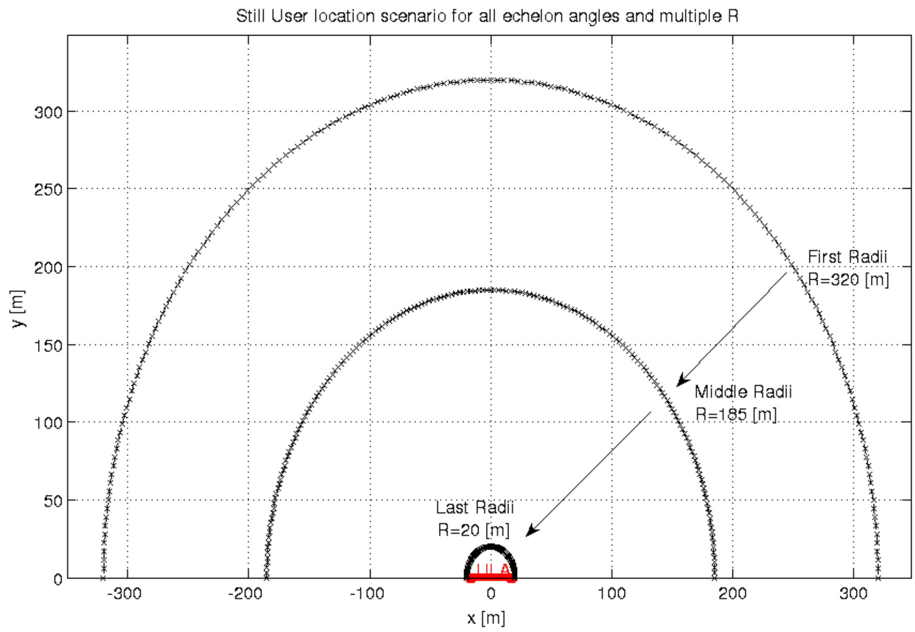

Figure 11.5 *Example of the scenario for the given case. The figure is representative of the simulations. The Still User is located at each point marked with 'x', for a specific radial distance. The Still User is moved closer to the Massive Array, and echelon angles are sweeped once again. The echelon angle is sweeped with a 1 ° resolution, and radius – 15 [m] resolution.*

Fig. 11.6 shows the case for when the Still User is located at an echelon angle of 45° with radial distance of 200 [m].

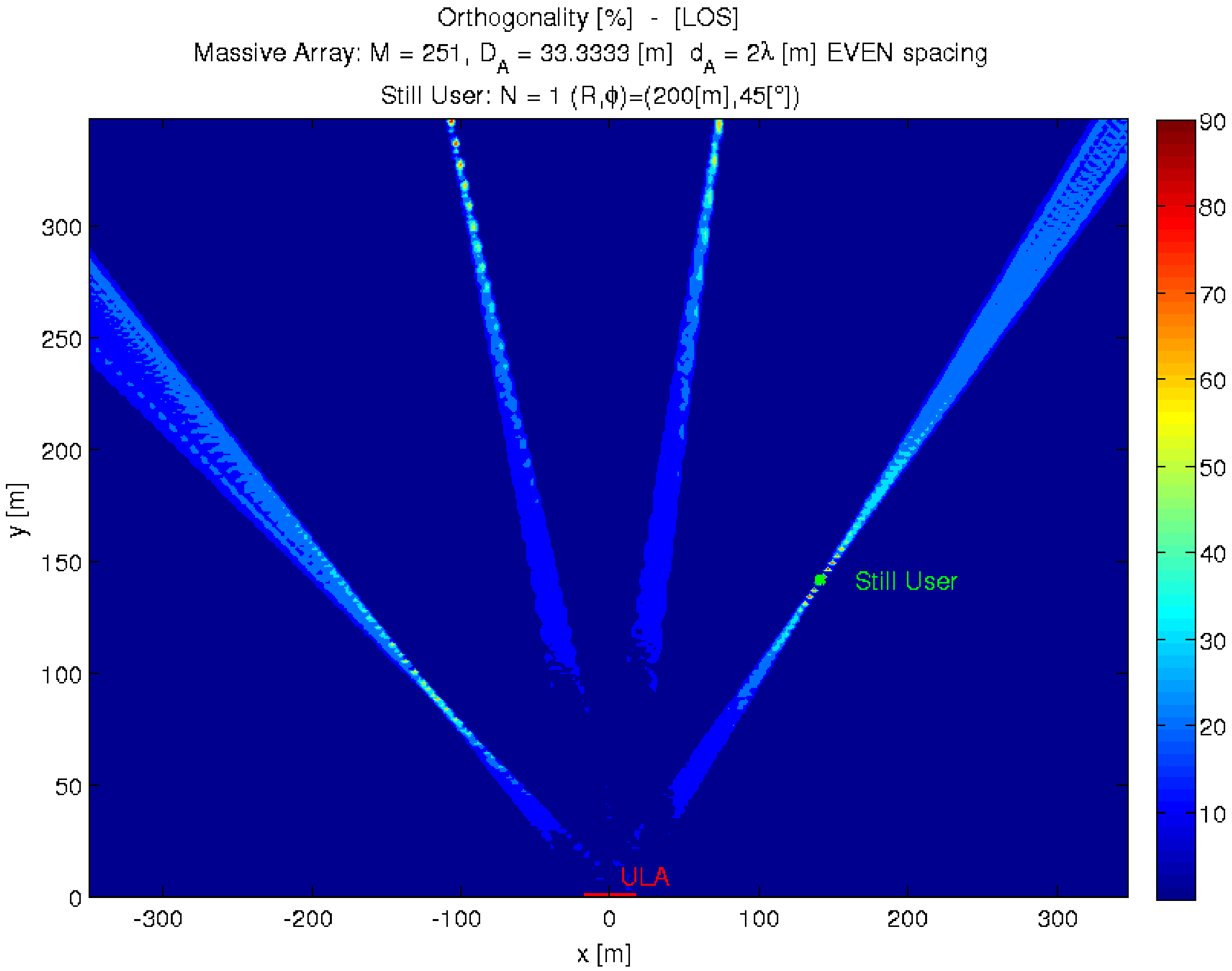

Figure 11.6 *Surface plot of orthogonality. The areas with red indicate areas where there is very little orthogonality. At these locations Matched Filter will not perform well, as the Still User and Mobile User can not be distinguished. Results are scaled by a factor of 100 to yield percentage.*

The figure shows a surface plot of the level of Orthogonality between the Still User and a Mobile User. Patches of red indicate areas where Orthogonality is very low, and as such users can not be distinguished. Instead it would be more beneficial to apply ZF or MMSE at these locations. Dark blue are those locations where MF will perform well enough as with ZF or MMSE. In the surface plot, it can be seen that areas of low orthogonality (i.e. channel vectors are aligned) when the Mobile User is very close to the Still User.

Besides the same as fig. 11.6, fig. 11.7 shows for the same case but along with echelon angles 15° and 75°.

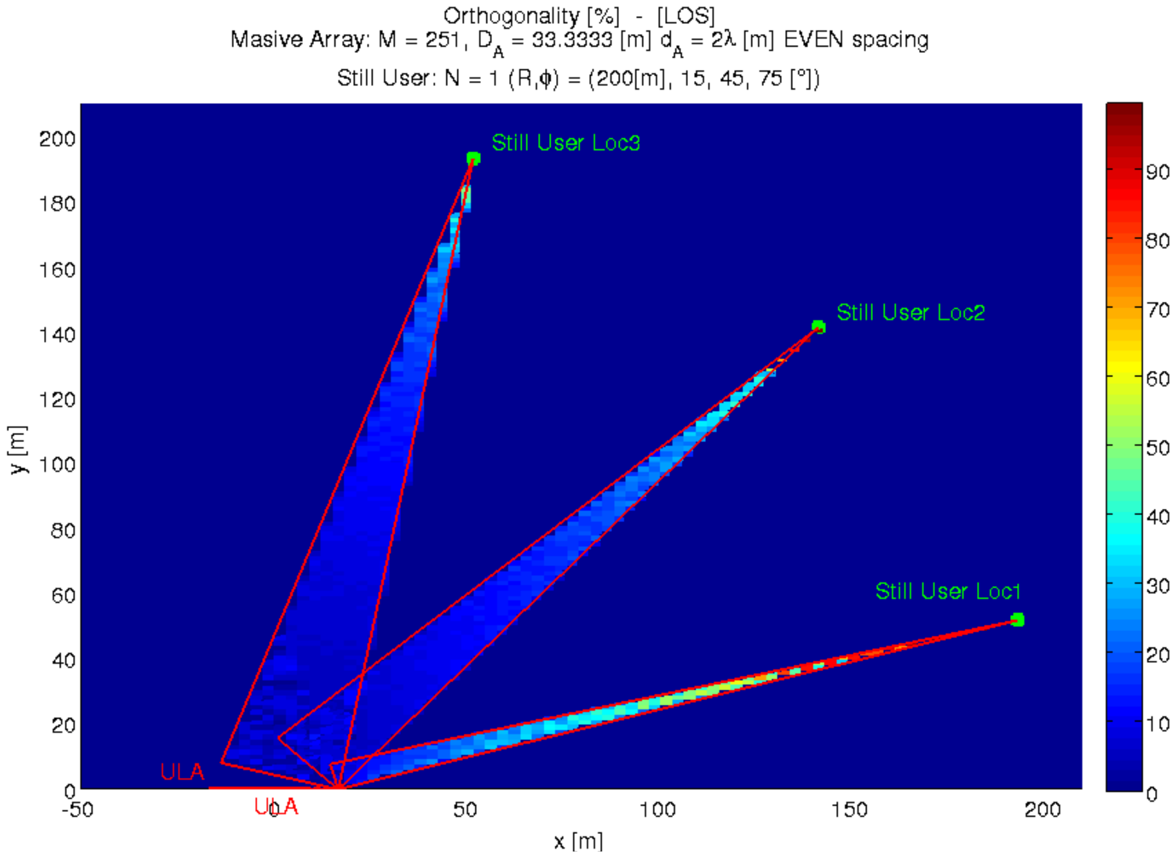

Figure 11.7 *Surface plot showing LOS orthogonality for 15°, 45° and 75° at a radial distance of 200 [m]. Shown is the same plot as in fig. 11.6, however the plot has been zoomed in, Orthogonality is cropped to the triangle of interest.*

Similar to fig. 11.6, it can be seen that very low levels of orthogonality seem to tend around the vicinity of the Still User. Again, this may be contributed to the fact that the Massive Array has difficulty in distinguishing between the two. In this case, as the Still User is located closer towards the broadside direction of the Massive Array, the areas where orthogonality is very low, group closer to the Still User. That is to say, the area where MF can not be applied diminishes.

Fig. 11.8 shows orthogonality for the case where the Still User is at the endfire direction. As it can be seen in the surface plot, for the case where the Still User is located at the endfire direction, Mostly everywhere inbetween the Massive Array and the Still User Orthogonality levels are very low. This is due to the fact that the equivalent broadside array is so small it may be considered a point source.

11.4.2 Threshold Orthogonality using Cumulative Average

All points and their corresponding orthogonality values, are sorted according to the distance from the Still User. Orthogonality is averaged cumulatively in order to search for the distance from the Still User to the point where mean Orthogonality drops below a threshold level. Recall the cumulative average be defined as in eq. 11.7.

Fig. 11.9 shows a similar plot as fig. 11.7. The difference is however that the points have been sorted and the cumulative average of Orthogonality is performed, for 30° echelon angle. The found radii are then shown as points.

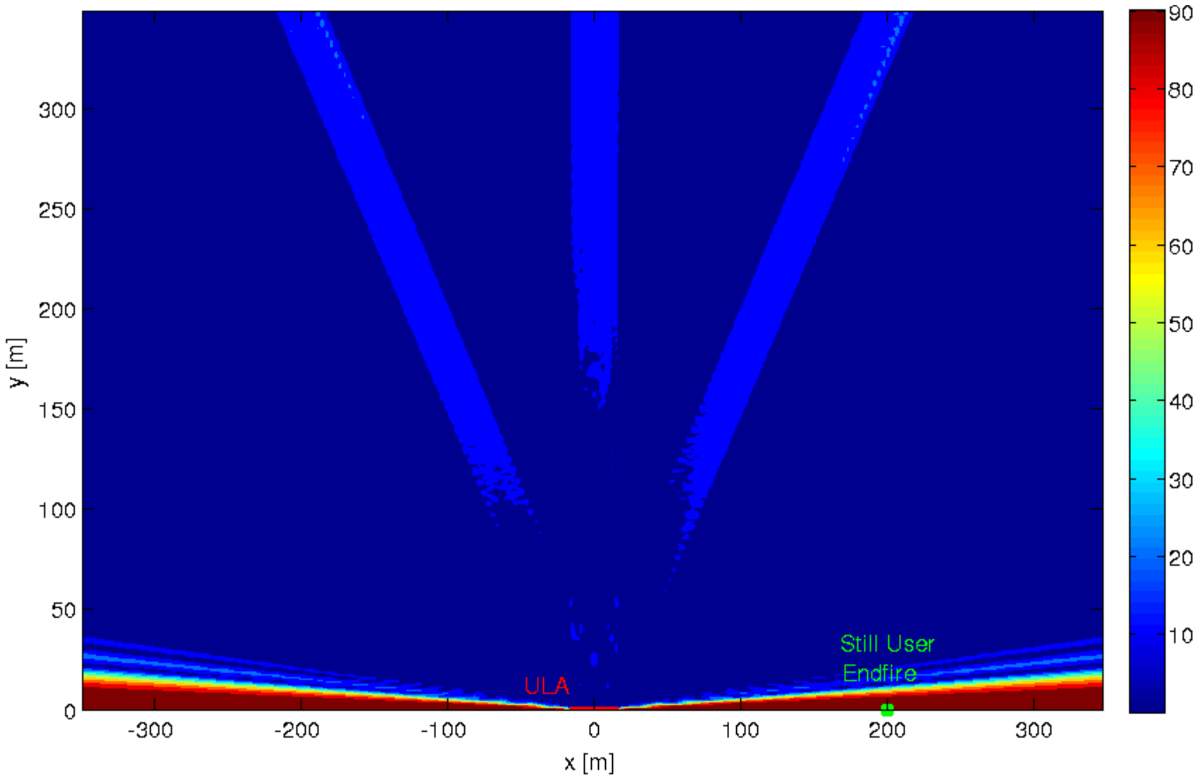

Figure 11.8 *Surface plot showing Orthogonality for the case where the Still User is located in the endfire direction.*

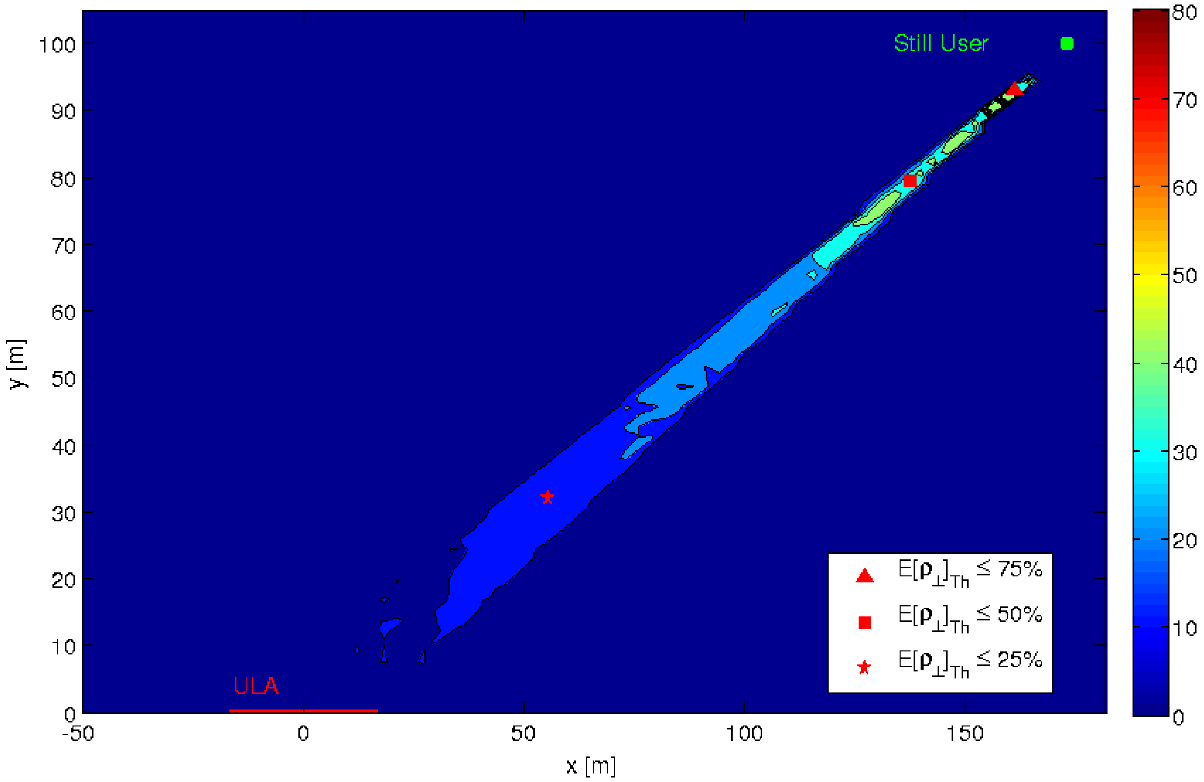

Figure 11.9 *The figure shows a surface plot of three threshold levels and their corresponding radii from the user to where the mean of orthogonality, $\rho_\perp$, is lower than a threshold level. The contour plot is zoomed in, and orthogonality is cropped to only show the triangle of interest.*

A new threshold level is set, and the same procedure starts again. This is done for all echelon angles, and can be seen in fig. 11.10.

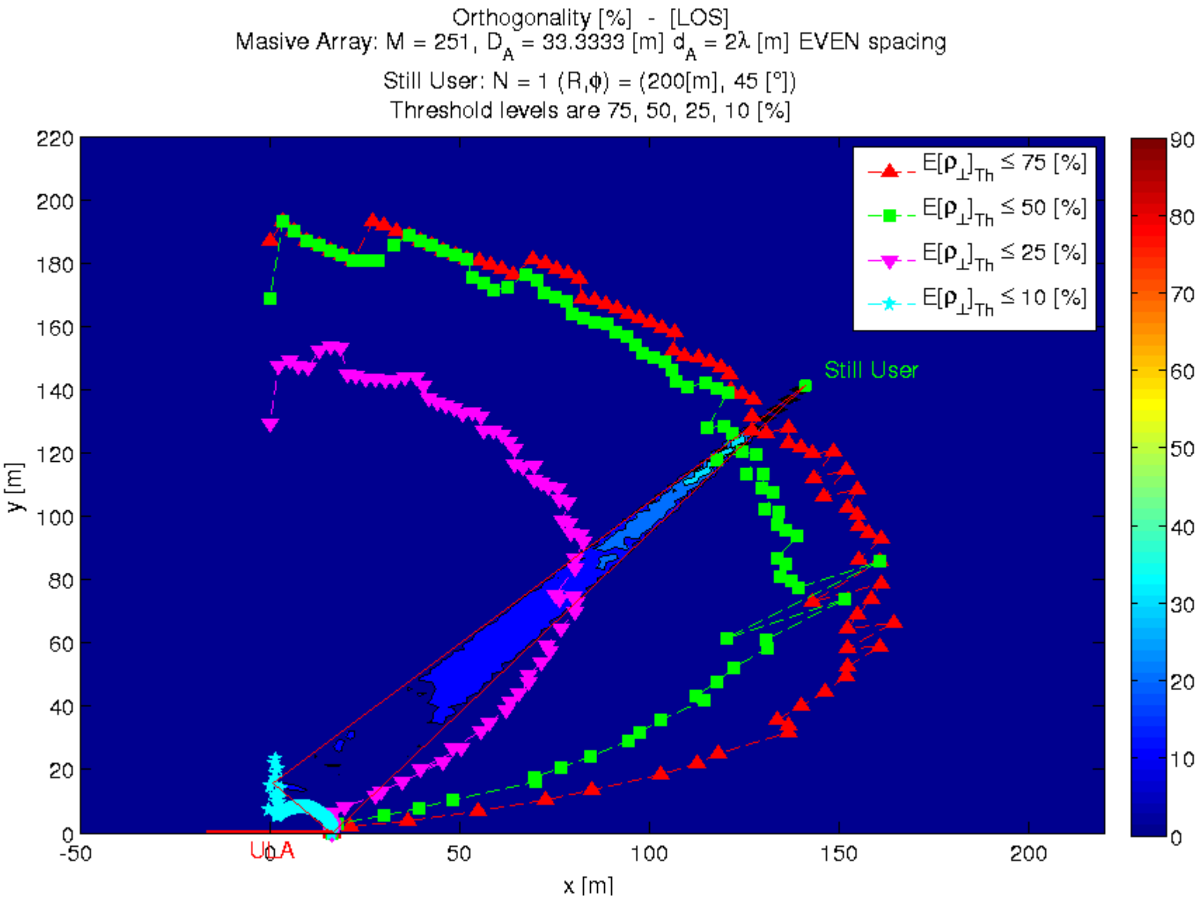

Figure 11.10 *Surface plot of the Still User located at 15°, 45° and 75°, distance 200 [m] from the centre of the Massive Array. Threshold distances have been marked for all echelon angles, in descending order.*

11.4.3 Single Radial Distance: Threshold Curve Fitting

The main goal is to obtain an expression that best predicts areas of low orthogonality, with the Still User as a point of reference. After sweeping all echelon angles, the resulting $\mathrm{R_{Th}}$ is fitted to a 2$^{\mathrm{nd}}$ order power exponential and a 4$^{\mathrm{th}}$ order polynomial. The general expression for the power exponential is given as

$$\hat{\mathrm{R}}_{\mathrm{Th}}(\phi) = a \cdot \phi^b + c, \tag{11.10}$$

where a, b and c are the parameters that best fit the solution. The general expression for the 4$^{\mathrm{th}}$ order polynomial is given as,

$$\hat{\mathrm{R}}_{\mathrm{Th}}(\phi) = p_1 \cdot \phi^4 + p_2 \cdot \phi^3 + p_3 \cdot \phi^2 + p_4 \cdot \phi + p_5 \tag{11.11}$$

where p_1, p_2, p_3, p_4 and p_5 are the parameters that provides the best fitting to the mean orthogonality distances.

Fig. 11.11 shows the marked radial distances, power exponential and polynomial fitting versus echelon angle.

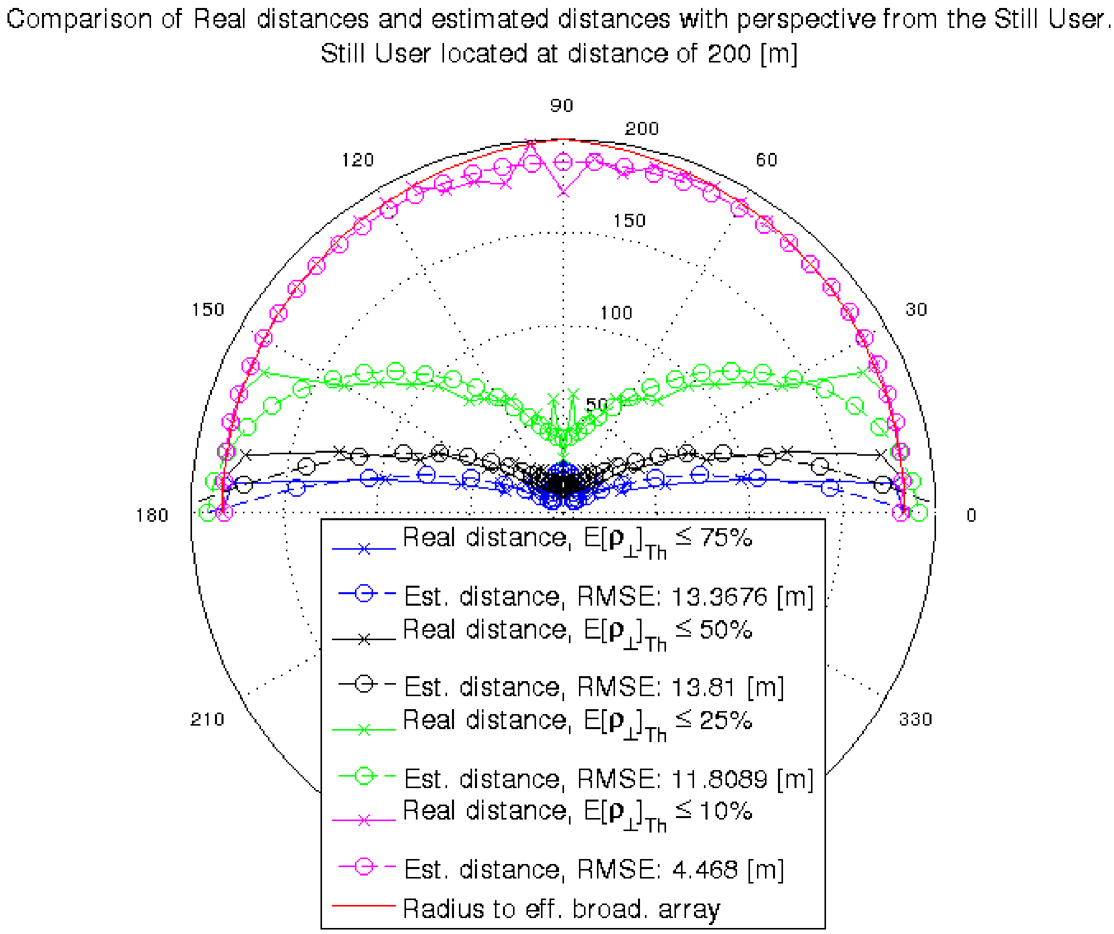

Figure 11.11 *This figure shows the marked radial distances from the Still User to a threshold boundary for all echelon angles. Furthermore it shows the polynomial fitting for the different thresholds. The example is given for the Still User at a distance of 200 [m] from the centre of the Massive Array. In the legends, their respective RMSE is displayed. Its unit is in metres.*

As a figure of goodness, the Root Mean Square Error (RMSE) is extracted. RMSE is a measure that indicates the, on average, error between the observed data and estimated data. See app. J on page 197 for a mathematical account and definition of the RMSE.

Recalling that the expressions given in eqs. 11.10 and 11.11 are only fitted to the echelon angle, results in a different expression for each Still User distance. Instead, it is of interest to have an expression that is a function of both echelon angle and distance. As such, a second fitting is performed on the already fitted terms. These are regressed to a function of R. For the 4^{th} order polynomial, each p_n term is fitted to a 1^{st} order polynomial, having the general form,

$$f(x) = p_1 \cdot x + p_2. \tag{11.12}$$

Similarly, but yet different, the second fitting on eq. 11.10 is performed, by using a mixture of the 1^{st} order polynomial, and a 2^{nd} order power fitting. The second fitting will be established in the following section.

11.4.4 Multiple Radial Distance: Threshold Curve Fitting

As mentioned before, the parameters from in eqs. 11.11 and 11.10 have been further fitted to the expressions,

$$\hat{p}_n = p_1 \cdot R + p_2 \tag{11.13}$$

and

$$\hat{a} = a \cdot R^b + c \tag{11.14}$$
$$\hat{b} = p_1 \cdot R + p_2 \tag{11.15}$$
$$\hat{c} = a \cdot R^b + c \tag{11.16}$$

which in the end will yield the threshold distance as a function of distance and echelon angle, i.e.

$$\hat{\mathrm{R}}_{\mathrm{Th}} = f(R, \phi).$$

The aim is to optain a simple expression in which it is possible to predict radial distances, and in a sense, areas in which MF precoding performance is not a feasible option. In the following are two proposals for such a determination.

Proposal 1: 2^{nd} order power fitting

Combining the 2^{nd} order power exponential and the second fittings given provided in eqs. 11.14–11.16, yield the total estimation function as,

$$\hat{\mathrm{R}}_{\mathrm{Th}}(R, \phi) = \hat{a}(R) \cdot \phi^{\hat{b}(R)} + \hat{c}(R) \tag{11.17}$$
$$= (a_a R^{b_a} + c_a) \cdot \phi^{p_1 R + p_2} + (a_c R^{b_c} + c_c) \tag{11.18}$$

While the power exponential yields a well fitting, with a well-enough RMSE, it is not well defined over the entire echelon angle sweep region. This is evident in fig. 11.11, where real distances tend to follow a parabola type function, which the power exponential does not produce. Thus if the power exponential fitting is to be utilised, echelon angles must be split into a Left Half Plane (LHP) part and a Right Half Plane (RHP) part, so that they form the piecewise function,

$$\hat{\mathrm{R}}_{\mathrm{Th}}(R, \phi) = \begin{cases} \hat{\mathrm{R}}_{\mathrm{Th}}^{\mathrm{RHP}}(R, \phi) & \text{if } 0^\circ \leq \phi \leq 90^\circ \\ \hat{\mathrm{R}}_{\mathrm{Th}}^{\mathrm{LHP}}(R, \phi) & \text{if } 90^\circ < \phi \leq 180^\circ \end{cases} \tag{11.19}$$

Functions $\hat{\mathrm{R}}_{\mathrm{Th}}^{\mathrm{RHP}}$ and $\hat{\mathrm{R}}_{\mathrm{Th}}^{\mathrm{LHP}}$ both have the same general expression, but contains different parameters.

Tbl. 11.3 on the following page shows the parameters for the estimated functions for each threshold level, along with their corresponding RMSE of the second fitting.

	$\mathbb{E}[\rho_\perp]_{\mathrm{Th}}$ [%]	75		50		25		10	
		LHP	RHP	LHP	RHP	LHP	RHP	LHP	RHP
a	a_a	-45476459.4671	4.3686×10^{-10}	$5.6748 \times^{-21}$	8.1744×10^{-21}	1.3816×10^{-17}	-105.9725	2787841968868466	0.0089346
	b_a	-7.1533	4.4379	7.8798	9.2716	7.7642	0.2754	-0.66727	1.338
	c_a	0.00018624	1.0649	0	0	0	318.3898	-289876094152386.8	-7.9852
	RMSE [m/ϕ^b]	0.00038499	4.5591	0.019737	106.7063	25.4137	91.5258	814659317706667.2	4.6967
b	p_1	-0.0072165	-0.00056674	-0.016599	0.0024828	-0.020569	0.0046901	-0.0031805	-0.0040261
	p_2	15.5183	-0.94526	11.8494	-0.91584	6.6619	-0.34291	-3.4881	3.4568
	RMSE [$\cdot$]	3.8192	0.543	2.2042	0.19108	0.8196	0.091546	16.851	2.5645
c	a_c	1.3529	-1.5833×10^{-14}	0.075649	-3.0763×10^{-24}	-2.6532×10^{-16}	17.3449	1.7603	1.0216
	b_c	0.45641	6.1546	0.90166	10.6355	7.2725	0.59624	0.87829	0.99357
	c_c	-0.69792	9.3616	4.1168	0	0	-184.0906	-5.7464	-13.6943
	RMSE [m]	1.2385	4.3991	1.4126	96.8465	29.966	89.3145	30.8623	3.613

Table 11.3 *The parameters listed in this table, are those who satify the best fitting, using a power exponential base expression, for the 4 threshold levels. The RMSE's are based on the second fitting, that is the second column from the left.*

Because it is necessary for the power exponential to be split into two separate expressions defining for the LHP and the RHP, an alternative must be found. Such an alternative must satisfy both the LHP and the RHP using the same expression. This has been found to be the case for the 4^{th} order polynomial.

Proposal 2: 4^{th} order polynomial fitting

Similarly, by combining the first and second fitting, to obtain something that is a function of both distance, R, and echelon angle, ϕ, the complete general expression may be written as,

$$\begin{aligned}\hat{\mathrm{R}}_{\mathrm{Th}}(R,\phi) &= p_1(R)\phi^4 + p_2(R)\phi^3 + p_3(R)\phi^2 + p_4(R)\phi + p_5(R) \qquad (11.20)\\ &= (a_1 \cdot R + b_1)\phi^4 + (a_2 \cdot R + b_2)\phi^3 + (a_3 \cdot R + b_3)\phi^2 \\ &\quad + (a_4 \cdot R + b_4)\phi + (a_5 \cdot R + b_5) \qquad (11.21)\end{aligned}$$

in terms of ϕ, or in terms of R,

$$\begin{aligned}\hat{\mathrm{R}}_{\mathrm{Th}}(R,\phi) &= (a_1 \cdot \phi^4 + a_2 \cdot \phi^3 + a_3 \cdot \phi^2 + a_4 \cdot \phi + a_5)R \\ &\quad + (b_1 \cdot \phi^4 + b_2 \cdot \phi^3 + b_3 \cdot \phi^2 + b_4 \cdot \phi + b_5) \qquad (11.22)\end{aligned}$$

The solution given by the 4^{th} order polynomial, provides a result that is more similar to the parabola type shape for the LHP and RHP, that tends in the mean orthogonality distances. Furthermore, the 4^{th} order polynomial is well defined over the entire range of echelon angles. Thus, taking the 4^{th} order polynomial a step further, by concatenating mean orthogonality distances for both the LHP and the RHP to a single array of data, it is possible for a single general expression, valid of the entire range of echelon angles, to be presented. This is in contrast to the power exponential fitting.

Tbl. 11.4 shows the parameters that best define the closed-form expression which yields $\hat{\mathrm{R}}_{\mathrm{Th}}(R,\phi)$.

		$\mathbb{E}[\rho_\perp]_{\mathrm{Th}}$ [%]			
		75	50	25	10
	a_1	0.25997	0.10139	-0.18912	0.048238
p_1	b_1	-4.842	6.8796	14.9814	-11.1737
	RMSE [$^{\mathrm{m}}/_{\phi^4}$]	3.3976	6.4424	4.3348	3.9255
	a_2	-1.6338	-0.63735	1.1882	-0.30525
p_2	b_2	30.501	-43.148	-94.0783	70.9887
	RMSE [$^{\mathrm{m}}/_{\phi^3}$]	21.3495	40.4947	27.2896	24.9747
	a_3	3.6298	1.7029	-2.0631	0.56669
p_3	b_3	-74.3681	72.6424	188.5209	-135.1605
	RMSE [$^{\mathrm{m}}/_{\phi^2}$]	40.4022	79.2788	57.7107	47.7556
	a_4	-3.3396	-2.2031	0.61836	-0.26433
p_4	b_4	82.7603	-15.6436	-128.2477	70.8388
	RMSE [$^{\mathrm{m}}/_{\phi}$]	22.4261	49.2454	47.4499	25.6112
	a_5	1.1198	1.169	0.98819	1.0197
p_5	b_5	-29.8352	-24.0412	-8.2774	-22.2411
	RMSE [m]	4.7165	2.2426	3.9514	2.2848

Table 11.4 *Parameters listed in this table are those yielding the best fitting of a 4^{th} order polynomial as base fitting with a 1^{st} order polynomial as the secondary fitting. Shown are for the 4 threshold levels of mean orthogonality. The listed RMSE's are for the secondary fitting.*

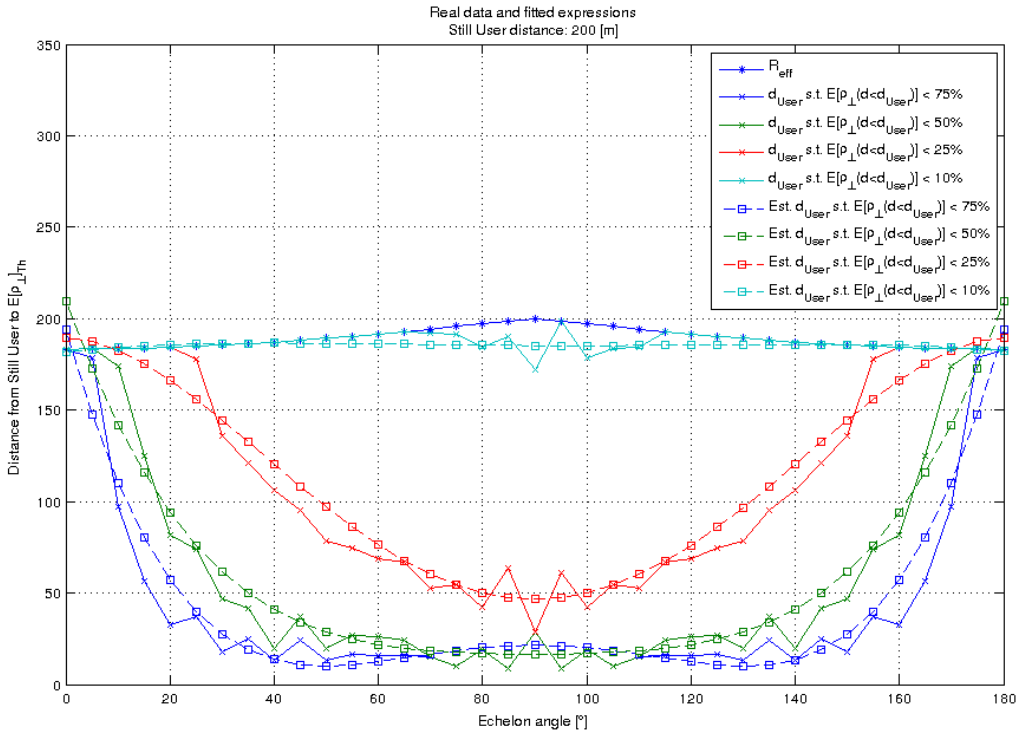

Figure 11.12

In fig. 11.12, the closed-form expression for the Still User distanced 200 [m] from the massive array. The closed-form expression indicate a very well fitting, with a low RMSE. Especially the curve for when the threshold of $\mathbb{E}[\rho_\perp]$ is set to 50 %. The estimated distances, shown with squares, seem to agree very well with the observed distances. In general, compared to the observed distances shown by the x's, the closed-form expression tend to approximate and thus predict distances and so areas, where areas of low orthogonality may appear. It should be remarked that fig. 11.12 is shown as a function of radius and angle — i.e polar coordinates. To better relate the radius and echelon angles, they are related to an xy-grid, using the relations below.

$$R = \sqrt{x^2 + y^2} \qquad\qquad \phi = \arctan\frac{y}{x}$$

These provide the mapping shown in fig. 11.13. Thus, in a sense the location of the point at which mean orthogonality drops below a threshold level, can be expressed as a xy-coordinate, yielding the closed-form expression as,

$$\hat{\mathrm{R}}_{\mathrm{Th}} = f(R,\phi) \Rightarrow \hat{\mathrm{R}}_{\mathrm{Th}} = f(x,y) \tag{11.23}$$

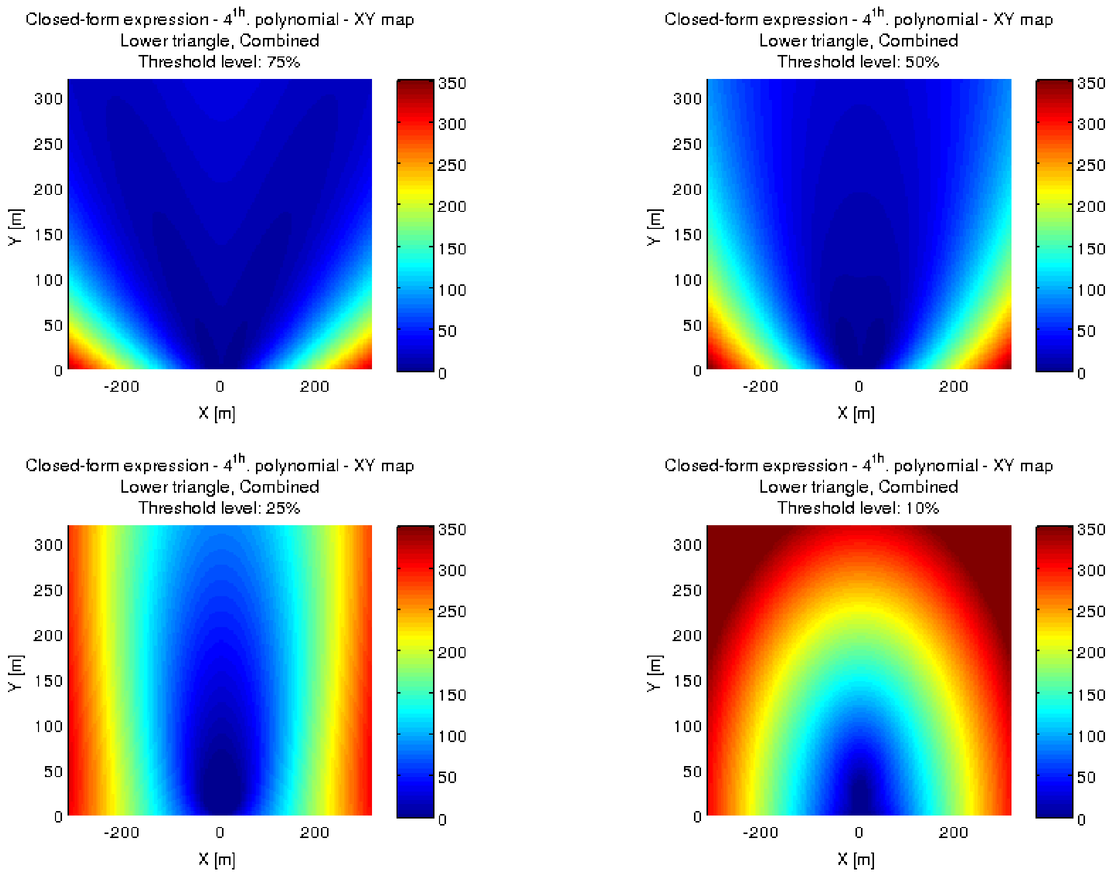

Figure 11.13 *Using the closed-form expression with the parameters listed in tbl. 11.4, yields the prediction shown in the figure. Four threshold levels are produced, 75 %, 50 %, 25 % and 10 %. For a given location in the bounded area, the colors indicate at which distance from the Still User, bad orthogonality is achieved. Rule of thumb, så more blue, thee better. Dark blue means that areas of mean orthogonality greater than a threshold, is closer to the Still User.*

This figure shows the closed-form expression in action, using the parameters listed in tbl. 11.4.

11.5 Sub-conclusion

Correlation coefficient and Orthogonality has been shown to be directly related to each other, given specific circumstances, and as such provides similar results. Due to this relation, Orthogonality was chosen as a metric, in order to identify the possibility of whether or not two (or more) users may be distinguished[4]. Comparing fig. 11.13, to fig. 11.14, shows how the tendencies in the results match with each other.

[4]Analysis has only been done to the $K = 2$ case, i.e. only two users have been simulated.

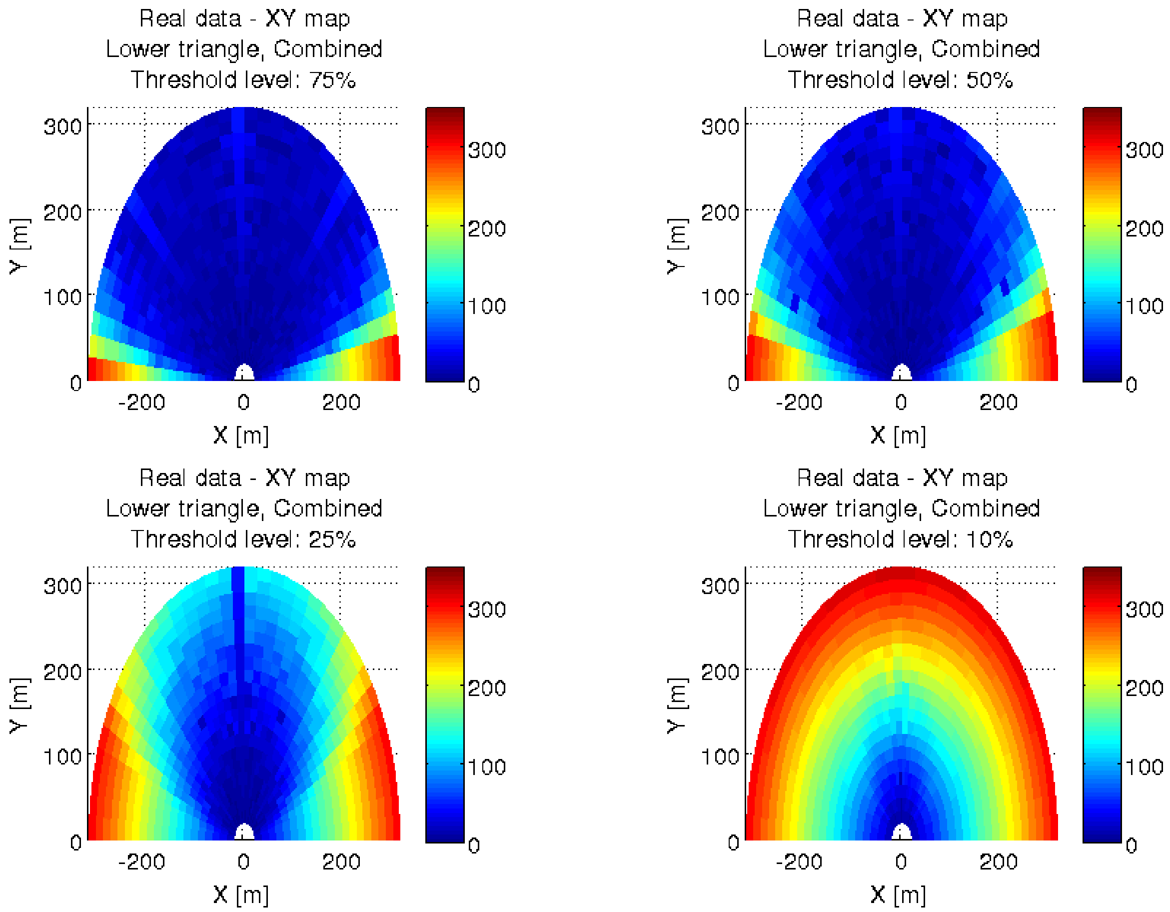

Figure 11.14 *This figure shows a surface plot of the real distances mapped to an xy-grid.*

Prediction of areas with low orthogonality are possible, using the 4^{th} order polynomial presented as proposal no. 2. The estimated distances hereof indicate to fit well with those of the marked distances. The prediction is limited to the triangle of interest, that is defined by the Still User.

To increase precision on the prediction of low Orthogonality areas, a way would be to identify the outliers and ignore them. By outliers, what is meant, is those points of radial distances to threshold that tend to deviate by more a e.g. 1.5σ, where σ is the standard deviation. While this may not be influencing the LOS to much degree, it would be more relevant for the total channel. The total channel introduces more randomness due to the weighting of the scatterers, and as such distances to marked areas would deviate more.

Another way would be to generate several realisations of the total channel, and calculate the channel statistics of marked distances to the areas of low Orthogonality. Including the Non Line Of Sight (NLOS) channel and total channel will increase precision of Orthogonality levels, as well as taking into account the randomness of the channel. Taking the total channel into account, provides a more precise indication of Orthogonality levels, as well as increasing them. Essentially, scatterers benefit Orthogonality. On the other hand, with focus only on the LOS channel, simulations provide a pessimistic view on Orthogonality, by showing threshold distances that may be likely greater than in the TOT channel. Thus it can be said that the LOS channel is the limiting element of Orthogonality.

A Massive Array with a uniform spacing has mainly been the one considered. In reality, due to small scale imperfections, this may not always be the case. To this purpose it may be relevant for a real world scenario to consider arrays with an irregular spacing.

Yet, nonetheless it is the outthrust due to the Still User that remains to effect the possibility of distinguishing between two users. It is this outthrust that, no matter the Massive Array configuration or position of Mobile User, yields the worst Orthogonality levels. Furthermore, this contradicts literature who says that only for an increasing M, channel conditions improve. In this study, it has been shown that it is not only a large M effects the channel, but also the configuration of the Massive Array (effectively inter-antenna spacing) and the location of users.

Chapter 12

Proposal nr. 2: Subspace-based precoding.

This chapter addresses the second suggested beamforming proposal according to the beamforming goals within this project's scenario. This proposal's principle lies in the employment of statistical information-based precoders, thus assuming there is no instantaneous CSIT available.
This proposal considers the single-antenna user case, only.

12.1 Introduction. Considered previous work on statistical-based beamformers.

As seen in chap. 10 on page 91, multi-user MIMO's potential to serve several users simultaneously and at the same frequency, i.e. SDMA, may be achieved with linear precoding techniques relying on instantaneous CSIT. The channel information available at the transmitter is used to create an adequate beamforming that may be able to separate users conveniently. Being one of the goals a low complexity at the BS, within the linear precoders, a MF has been analysed as an enabler to the beamforming needs. This study is included in chaps. 10 and 11.

Imperfect or reduced CSIT would imply that the techniques discussed above be abandoned in favour of other schemes. Those would need focus towards the desired beamforming goals. In this thesis, user mobility is directly tackled since one of the beamforming objectives is to build a precoder robust to the users' local movement. As defined in chap. 9 on page 87, the user's local movement is defined as per a location variation within a closed area of 1 [m^2]. As also mentioned, definition of local movement may vary for different scenarios.

It has been shown that in massive MIMO systems channel responses are more and more mutually orthogonal as the number of antennas at the BS increases [13, 16]. That is to say, they are mutually orthogonal asymptotically with M. This should occur even at the LOS channels, since it is rooted in the propagation terms due to the large number of antennas regime. The main result of this is that the covariance matrix computed as per the users local movement may not occupy all the possible DoF, yielding a finite rank. This property was already studied in literature for massive MIMO systems in the Far Field, concluding that it occurs when the angle spread of incoming signals at the massive array is limited [46]. The aim in this chapter is to find out if this applies as well in the proposed massive MIMO Near Field modelling as per the user's local variation prior to the pre-processing design. Should that happen, this property would serve to develop precoders based on statistical information yielded by the channels' covariance matrices computed for each of the users local movement. As a remark, it must be noticed that, thanks to the study on inter-user correlation in chap. 11 on page 109, it seems that, under certain circumstances, users might be separable even if they share the same or a similar range of incoming paths. It has been seen that orthogonality impairments are mainly subject to the relation between the users location and the massive array's aperture. Moreover, channels appear to be mutually orthogonal at close-in distances to the massive array. So it could happen that two users aligned with each other and with the massive array are separable, even considering channel information yielded by their covariance matrices.

Otherwise, there is no literature information known to the authors of this document on its issue about statistical precoders tackling a beamforming design under the scope of this project's goals. Pieces of work that employ information yielded by the channels covariance matrices, reducing the CSIT feedback, have effectively been found. Authors of [38] rely on a preferred beamforming vector for each user computed as per the channel's covariance matrix, which is forwarded to the BS instead of instantaneous CSIT acquisition, reducing this way the overhead considerably. These preferred beamforming vectors lie within each user's subspace. Optimality would arise if these vectors are mutually orthogonal, when, according to the authors, performance would be asymptotically close to the full CSIT case.
In the same line, authors of [39] build their precoder as from each of the channels' covariance matrices. However, the procedure is slightly more sophisticated than the one in [38]. Bearing in mind this is only part of the work that can be found in this publication, in brief, for each user channel the null subspace where all the other channels lie within is calculated and the user's covariance matrix is projected onto it. Then, the most significant vectors of this projection are considered to build this user's precoder. This process is repeated for all users. This approach implies a serious reduction on the dimension of the CSIT.

Lastly, it is interesting to mention the piece of work carried out by authors of [36]. Although considering full instantaneous CSIT, it roughly relies on transmission in the null subspace occupied by the interferers to each user, for which a cost function is defined. Quoting, "the cost function *[in equation (9) in the publication]* is minimized if each user transmits in the space spanned by the combined matrix of all other users with the power that is inversely proportional to the singular values of the combined channel matrix of these users". This approach constitutes a further modification on the BD precoder, first proposed in [47] and is actually called RBD in [36].

12.2 Covariance matrix rank for a user experiencing local mobility.

The aim of this section is to analyse the rank of the covariance matrices yielded by users experiencing local mobility as it has been defined in this document. Should covariance matrices show finite rankness, then channels would not occupy all their possible DoF. This would serve to build precoders which would allow user separability. Moreover, in massive MIMO systems this property may happen even for the LOS channels, since channel responses have been theoretically proven to be mutually orthogonal, asymptotically with the number of antennas at the BS, M.

To validate this hyptohesis as well as to analyse the impact of the elements of the scenario in the achieved ranks, several tests have been carried out. They include the effect of the scatterers in the scenario.

A single-antenna user has been placed at different locations in a 700 [m]×350 [m] xy-grid. Each of those specific locations are taken as reference locations around which the user will experience local mobility. 1000 Monte Carlo simulations were effectuated. At each of them, a different channel vector $\mathbf{h} \in \mathbb{C}^{M\times 1}$ was obtained. Then, channel vectors were piled up to build an $\mathrm{M} \times 1000$ total matrix, which will be called $\mathbf{H} \in \mathbb{C}^{M\times 1}$. Once the total channel matrix was obtained and normalised as done in previous chapters, the covariance matrix was computed and finally, its rank. A local cluster-only scenario was considered first.
The features being modified at each realisation were:

(a) The user's local movement, only. (Scatterers are unweighted).

(b) The user's local movement together with the scatterer's weighting.

The massive array has 251 elements and an aperture of 33.33 [m]. The selected local cluster contains 25 scatterers and has a size of approximately 157 [m^2].

Fig. 12.1a features isolation nr. (a), while fig. 12.1b does so for isolation nr. (b).

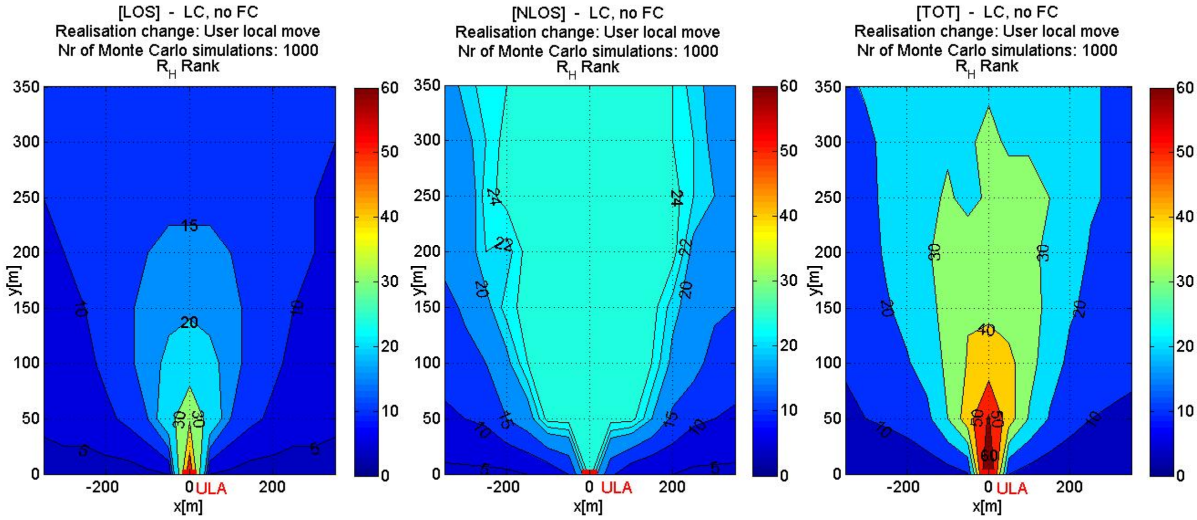

(a) *Channel covariance matrix rank. Isolation (a).*

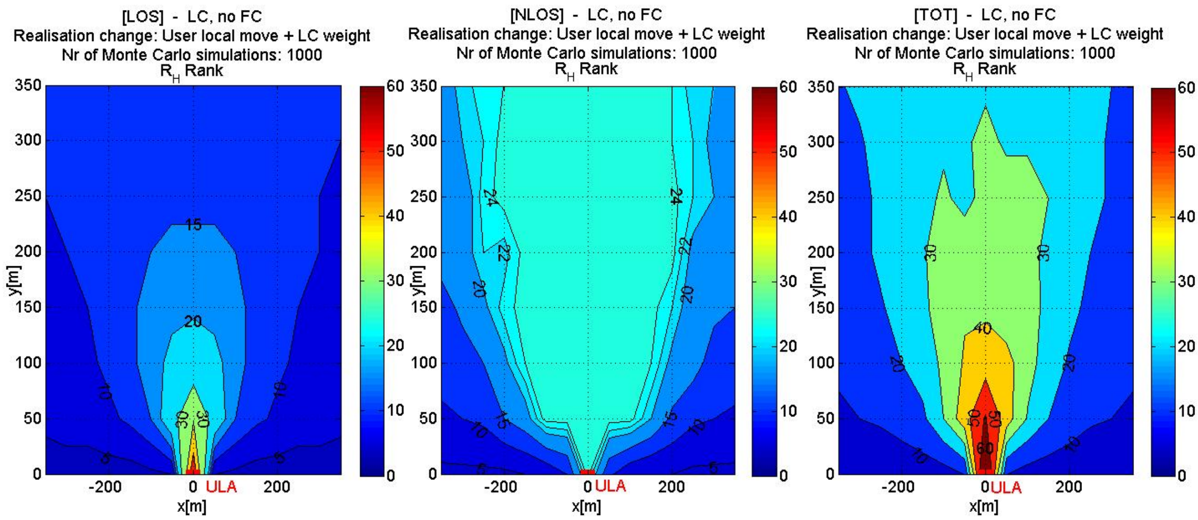

(b) *Channel covariance matrix rank. Isolation (b).*

Figure 12.1 *Covariance matrix rank for a user's local mobility. Several locations.*

The first remarkable conclusion is that, effectively, **not all the DoF are occupied at the LOS channel**. This verifies the hyptohesis in lines above and is significantly important in terms of **potential statistical precoding according to the information yielded by the covariance matrices**. Not only LOS, but all patterns exhibit higher ranks at the broadside and at close-in distances to the massive array, meaning channel realisations are mutually orthogonal at those areas with a higher probability.

As regards the NLOS channel, we observe a lower rank values. Also, the pattern blurs. The lower ranks mean that channel realisations tend to be more correlated on this channel. This is perfectly sensible since scatterers do not suffer any change at all in either location or weighting from realisation to realisation, being only the receive part of the channel matrix the one suffering changes due to the user's different location. Still, user's mobility is able to provide with a non-unit rank at the NLOS. This in turn makes the rank of the TOT channel achieve higher levels than the LOS's.

Finally, it must be noticed that the scatterers' weighing seems not to play any role, whatsoever.

This is due to the fact the number of scatterers is sufficiently high to be able to provide with enough phase randomness, even only due to the propagation terms. The local cluster's impact on the TOT channel is attributable to the enlarged aperture it introduces.

Focus is now directed towards the impact of the far clusters. To this purpose, it has been decided to place a single far cluster between the user and the massive array. The procedure that has been followed is identical to the one described above in this section. The features modified at each of the Monte Carlo simulations were, again:

(c) The user's local movement, only. (Scatterers are unweighted).

(d) The user's local movement together with the scatterer's weighting.

The far cluster has a size of approximately 70 [m^2] and contains 20 scatterers. The massive array's features hold up.

Results are given in fig. 12.2a and fig. 12.2b for isolations (c) and (d), respectively.

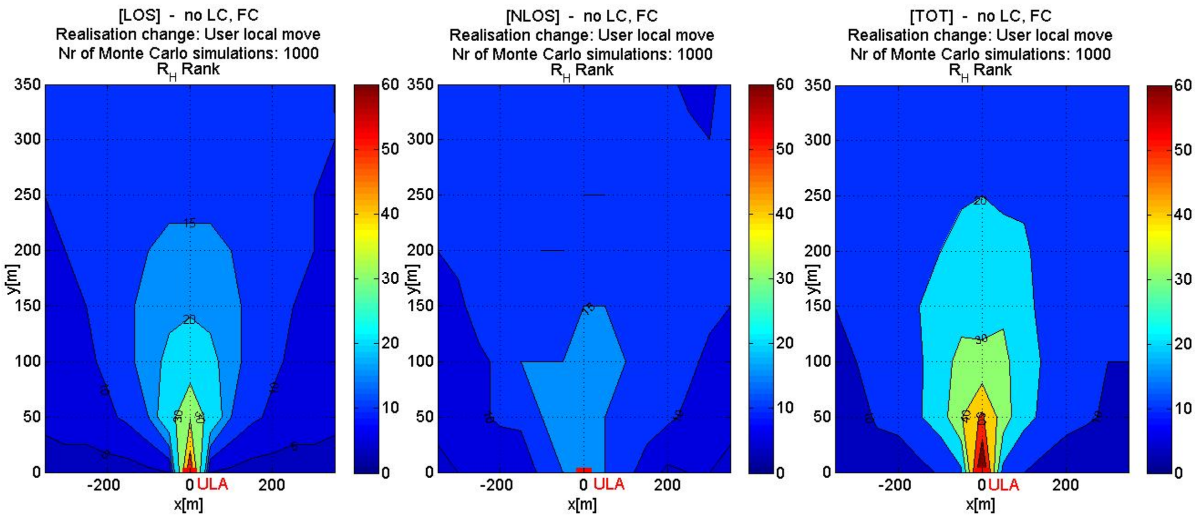

(a) *Channel covariance matrix rank. Isolation (c).*

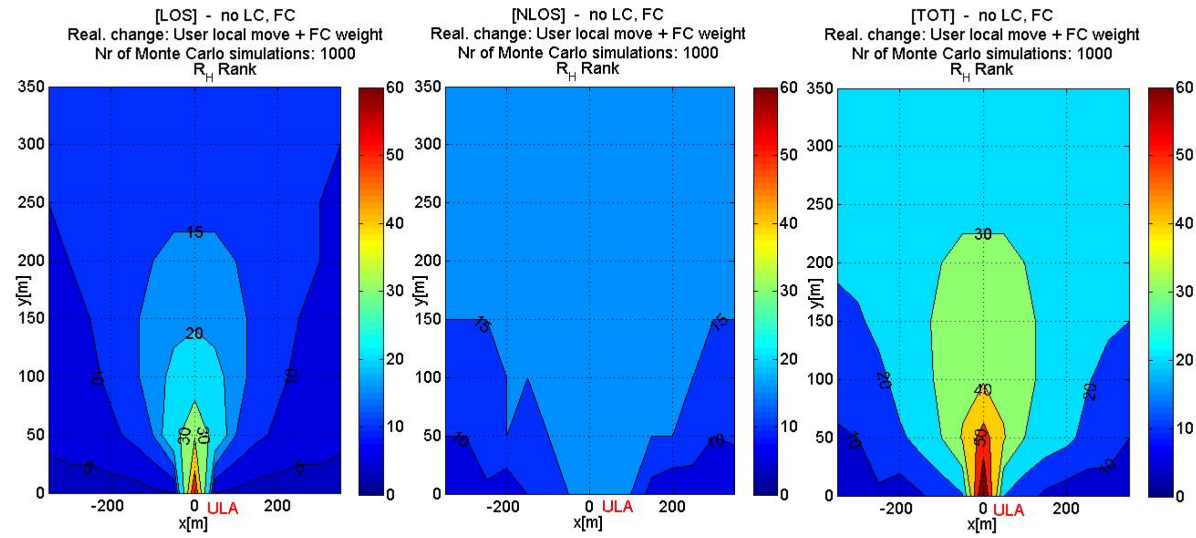

(b) *Channel covariance matrix rank. Isolation (d).*

Figure 12.2 *Covariance matrix rank for a user's local mobility. Several locations.*

The main observation lies in the rank due to the far clusters, which (1) varies if we take the weighing into account and (2) affects the TOT channel at a lesser extent than the local cluster does. (1) is explained by the fact that the receive side is now contributing more to the channel than in (a) and (b) and at the receive side the user's local movement variation is perceived at a much lesser degree. (2) is attributable to the lower level of affect that the far cluster has on the "virtual" aperture seen by the user (since the far cluster is in between the user and the massive array). This concludes that it is the local cluster that most influences the ranks again due to the enlarged "virtual" aperture it provokes.

Conclusions on the covariance matrices ranks as per user local mobility.

Two main conclusions are made on the covariance matrix ranks. These are:

i The low levels of rank seen on the covariance matrices as per the user's local movement defined in this project, for all channels, goes in line with expectations for massive MIMO systems providing asymptotically orthogonal channels. Channels would not occupy all of their degrees of freedom, even in the LOS channel, since channel orthogonality would be provided by the massive nature of the BS and at the same not all channels would be orthogonal to each other, hence not occupying all the DoF. This phenomenon would directly imply that the information on the channel yielded by the covariance matrix of each of the users' channels might serve as a basis for adequate statistical beamforming assuming that the information given by the channel's covariance matrices hold up for a specific coherence time, even when the users experience local mobility.

ii The local cluster influences the ranks of the covariance matrices the most since it provides the user with an enlarged aperture, hence increasing the rank (TOT). Even though this means there are more mutually independent channels with the presence of scatterers, it also implies more DoF are occupied, which would impact the statistical beamformer, as the subspaces they occupy are larger.

12.3 Proposed statistical precoders.

Two approaches have been followed to tackle statistical precoding in this project. Thus, it can be said the Proposal nr. 2 contains two different subproposals. Single-antenna users are regarded and a simple scenario consisting of K=2 users is considered.
A very brief account of the proposals can be seen below.

1. On one hand, beamforming approaches which employ statistical information in the form of the channels covariance matrices have been selected as a basis upon which to build the precoders suggested in this thesis. Those had already been mentioned in sec. 12.1 on page 133 and are repeated below:

   (1-A) Approach based on that by authors of [38].

   (1-B) Approach based on that by authors of [39].

   (1-C) Approach based on that by authors of [36].

   All CSIT overhead which is not related to the covariance matrix forwarding is voided in the mentioned approaches. Thus, all additional steps that any of the algorithms in [38, 39, 36] may take to build their precoders yielded by the latter is disregarded. Also, transmit power optimisation is not considered. Thus, approaches will tackle directly the ability of the built precoders of inter-user interference mitigation, known in literature as multi-user interference (MUI).
   To state the obvious, the covariance matrix employed in this project to develop the beamformers is the one computed as per the users' local mobility.
   Proposals (1-A), (1-B) and (1-C) will be jointly referred to as Proposals nr. 2.1.

2. On the other hand, resulting precoders based on statistical information, i.e. (1-A), (1-B) and (1-C), were modified, yielding the second part of Proposal nr. 2. Modification is fully accounted for further in this document but it consists basically of considering each precoder (1-A), (1-B) and (1-C) as an effective channel matrix and applying linear MMSE beamforming *replacing the channel matrix with the calculated precoding matrices*[1].
   Three modifications conform then this second group of proposals:

   (2-A) Modification of (1-A) as per an MMSE precoder expression.

   (2-B) Modification of (1-B) as per an MMSE precoder expression.

   (2-C) Modification of (1-C) as per an MMSE precoder expression.

   Proposals (2-A), (2-B) and (2-C) will be jointly referred to as Proposals nr. 2.2.

In any of the cases, the precoder will result in an M × K matrix, being M the number of antennas at the BS and K the number of users. Just as for the linear precoders, it is noted as $\mathbf{W}$. This is because the statistical beamforming application presented in this chapter is also linear as per fig. 10.2 on page 93, already introduced in chap. 10 on page 91 and reproduced below:

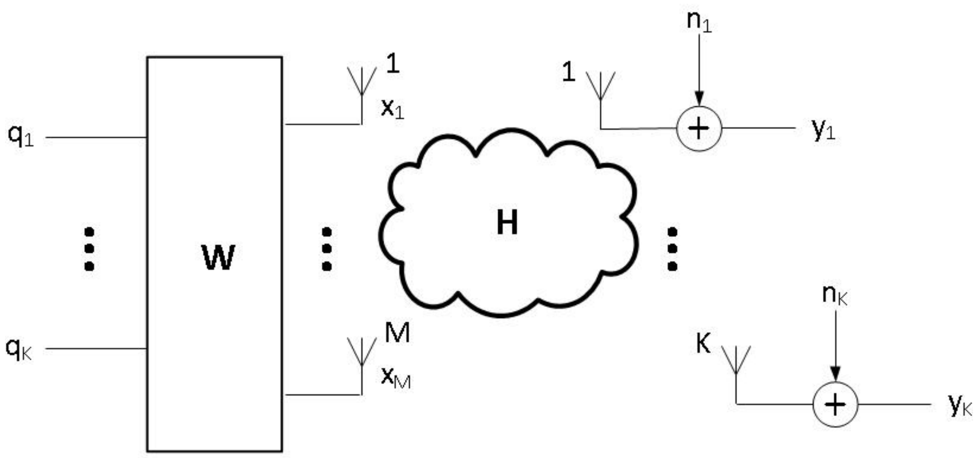

Figure 12.3 *Transmit beamforming scenario for the single-antenna user case. K users. M antennas at the massive array.* $\mathbf{W}$ *is the precoding matrix and* $\mathbf{H}$ *is the channel matrix. Fig. from chap. 10 on page 91.*

The normalised precoding matrix is denoted as, $\mathbf{W} \in \mathbb{C}^{M\times K}$, being the original precoding matrix written like $\mathbf{F} \in \mathbb{C}^{M\times K}$, where $\mathbf{W} = \alpha_{\mathbf{F}} \cdot \mathbf{F}$, and $\alpha_{\mathbf{F}}$ is a normalisation factor derived in app. K on page 199. and that is set to $\alpha_{\mathbf{F}} = \frac{\sqrt{\bar{\mathrm{P}}}}{\sqrt{\mathrm{Tr}[\mathbf{F}\mathbf{F}^{\mathrm{H}}]}}$ to transmit the maximum allowed power, $\bar{\mathrm{P}}$ [W].

12.4 Proposals nr. 2.1.

This section is aimed at the derivation of the group of proposals nr. 2.1., namely (1-A), (1-B) and (1-C).

12.4.1 Proposal (1-A).

Proposal (1-A) is based on work by authors of [38]. The algorithm presented therein relies on a preferred beamforming vector for each user, being that one the one defined by the subspace

[1]Although novel to the authors of this document on issue, in conversation with Elisabeth de Carvalho, supervisor to this thesis, this approach may be found in the literature.

occupied each channel. It does not rely on transmission on the null subspaces of the interfering users, just like the other considered pieces of work. It is stated that optimality is achieved when precoders are orthogonal to each other and counts on some limited instantaneous feedback to select the users that are close to this situation, in which case asymptotic performance would be close to the case of full CSIT. The degree of orthogonality depends on the validity of the initially forwarded precoding vectors. The reduced instantaneous feedback is a metric measuring the degree of alignment of the precoding vector and the instantaneous channel. We repeat that the only CSIT considered by our approaches is in the form of the channel covariance matrices, and thus, all instantaneous feedback is discarded. The full derivation and validity of the algorithm may be found in [38].

The approach suggested here is computed below for a two user scenario, containing a single antenna each.

Each of the channel's covariance matrices assumed to be known at the BS. $\mathbf{R}_1$ is the covariance matrix of user 1 and $\mathbf{R}_2$ is the covariance matrix of user 2. Both covariance matrices can be split up in three different matrices if the SVD is applied.

$$\begin{aligned} \mathbf{R}_1 &= \mathbf{U}_1\,\mathbf{\Lambda}_1\,\mathbf{U}_1{}^{\mathrm{H}} \\ \mathbf{R}_2 &= \mathbf{U}_2\,\mathbf{\Lambda}_2\,\mathbf{U}_2{}^{\mathrm{H}} \end{aligned} \tag{12.1}$$

In general, the covariance matrix of the $\mathrm{k^{th}}$ channel can be written like:

$$\mathbf{R}_k = \mathbf{U}_k\,\mathbf{\Lambda}_k\,\mathbf{U}_k{}^{\mathrm{H}} \tag{12.2}$$

where $^{\mathrm{H}}$ is the Hermitian operator, $\mathbf{U}_k \in \mathbb{C}^{M\times M}$ and $\mathbf{\Lambda}_k \in \mathbb{C}^{M\times M}$, $\forall\, k \in [1,2]$.

The channel covariance matrix can be further expanded like:

$$\mathbf{R}_k = \left[\mathbf{U}_k^{*}\;\mathbf{U}_k^{'}\right]\,\mathbf{\Lambda}_k\,\mathbf{U}_k^{\mathrm{H}} \tag{12.3}$$

where $\mathbf{U}_k^{*}$ are the set of eigenvectors corresponding to the dominant eigenvalues and in turn $\mathbf{U}_k^{'}$ the set of eigenvectors related to the weakest eigenvalues. $\mathbf{U}_k^{*}$ is defined as per the strongest eigenvector, then considering the subspace in which the strongest one lies, only:

$$\mathbf{U}_k^{*} = \mathbf{U}_k^{1} \in \mathbb{C}^{M\times 1} \tag{12.4}$$

The precoder is finally defined like:

$$\begin{aligned} \mathbf{F}^{(\text{1-A})} &= \left[\mathbf{U}_1^{1}\;\cdots\;\mathbf{U}_K^{1}\right] \\ &\overset{\mathrm{K=2}}{=} \left[\mathbf{U}_1^{1}\;\mathbf{U}_2^{1}\right] \end{aligned} \tag{12.5}$$

12.4.2 Proposal (1-B).

Proposal (1-B) is based on work by authors of [39]. In this article, a full multi-user MIMO downlink approach is built exploiting the correlation of the channel vectors. The aim is both to allow for a large number of antennas at the BS and to reduce the CSIT overhead. The approach is given the name "Joint Spatial Division and Multiplexing". It is repeated that the approach proposed in this project voids all the CSIT barring the channels covariance matrices. The aspects based in the work found in [39] which directly tackle the proposal suggested in this chapter require the derivation of the null subspace where all the interfering channels lie, for each user channel. Then, each of the user's covariance matrices is projected onto this null subspace and the most significant vectors of the projection are considered to build each of the user's precoder vectors. This is repeated for all users, resulting in the total precoder. This approach yields a considerable reduction on the dimension of the CSIT. The full derivation and validity of the algorithm may be found in [39].

The approach suggested here and based on [39] is derived below for a general scenario of K users, containing a single antenna each. Then, it will be narrowed down for K=2. Only the aspects in [39] which directly tackle proposal (1-B) are included.

Just as previously, the channel's covariance matrices are assumed to be known at the BS. The covariance matrix of the k$^{\text{th}}$ channel can be written and expanded as such:

$$\begin{aligned}\mathbf{R}_k &= \mathbf{U}_k\,\boldsymbol{\Lambda}_k\,{\mathbf{U}_k}^{\mathrm{H}}\\ &= \left[\mathbf{U}_k^{*}\;\mathbf{U}_k^{'}\right]\,\boldsymbol{\Lambda}_k\,\mathbf{U}_k^{\mathrm{H}}\end{aligned} \tag{12.6}$$

As in (1-A), the matrix $\mathbf{U}_k^{*}$ is selected. Rather than the first column only like in (1-A), a larger number may now be considered. The more columns taken, the more information on the subspace in which $\mathbf{R}_k$ lies is considered. The number of columns that are taken is noted as r_k^{*}, under the requirement that $r_k^{*} \leq r_k$, where r_k is the rank of $\mathbf{R}_k$. This yields that $\mathbf{U}_k^{*} \in \mathbb{C}^{M\times r_k^{*}}$. Different channels may have a different r_k^{*} value. The sum of all channels' r_k^{*} is r^{*}, $r^{*} = \sum_{k=1}^{K} r_k^{*}$. Once this is done for all users, then another iteration must be done, as follows.
For channel k, the matrix containing the interfering $\mathbf{U}^{*}$ matrices is computed. We call this matrix $\boldsymbol{\Theta}_k \in \mathbb{C}^{M\times r^{*}}$:

$$\boldsymbol{\Theta}_k = \left[\mathbf{U}_1^{*}\;\cdots\;\mathbf{U}_{k-1}^{*}\;\mathbf{U}_{k+1}^{*}\;\cdots\;\mathbf{U}_K^{*}\right] \tag{12.7}$$

And its SVD is calculated. Then, the left eigenvectors are split up:

$$\begin{aligned}\boldsymbol{\Theta}_k &= \boldsymbol{\Sigma}_k\;\boldsymbol{\Xi}_k\;\boldsymbol{\Upsilon}_k^{\mathrm{H}}\\ &= \left[\boldsymbol{\Sigma}_k^{(1)}\;\boldsymbol{\Sigma}_k^{(0)}\right]\;\boldsymbol{\Xi}_k\;\boldsymbol{\Upsilon}_k^{\mathrm{H}}\end{aligned} \tag{12.8}$$

Since $\boldsymbol{\Theta}_k$ is a tall matrix, $\boldsymbol{\Sigma}_k \in \mathbb{C}^{M\times M}$, $\boldsymbol{\Xi}_k \in \mathbb{C}^{M\times r^{*}}$ and $\boldsymbol{\Upsilon}_k \in \mathbb{C}^{r^{*}\times r^{*}}$.

The right r^{*} columns of the left eigenvectors are taken, so $\boldsymbol{\Sigma}_k^{(0)} \in \mathbb{C}^{M\times(M-r^{*})}$. $\boldsymbol{\Sigma}_k^{(0)}$ contains the most significant vectors on the null space where the interferers lie. Then, $\mathbf{R}_k$ is projected onto this subspace, which is denoted like $\hat{\mathbf{R}}_k$, and its SVD is performed. Lastly, the left eigenvectors are split up:

$$\begin{aligned}\hat{\mathbf{R}}_k &= \left[\boldsymbol{\Sigma}_k^{(0)}\right]^{\mathrm{H}}\;\mathbf{R}_k\;\boldsymbol{\Sigma}_k^{(0)}\\ &= \mathbf{G}_k\;\boldsymbol{\Phi}_k\;\mathbf{G}_k^{\mathrm{H}}\\ &= \left[\mathbf{G}_k^{(1)}\mathbf{G}_k^{(0)}\right]\;\boldsymbol{\Phi}_k\;\mathbf{G}_k^{\mathrm{H}}\end{aligned} \tag{12.9}$$

Finally, the first b_k columns in $\mathbf{G}_k^{(1)} \in \mathbb{C}^{(M-r^{*})\times b_k}$, which represent the most significant vectors of the projection of the channel's covariance matrix onto the null subspace of all the other interferers, are considered to build the precoder for the k$^{\text{th}}$ user. Columns b_k has to meet the requirement $s_k \leq b_k \leq r_k$, being s_k the number of streams sent to the k$^{\text{th}}$ user. The k$^{\text{th}}$ user's precoding matrix is:

$${\mathbf{F}_k}^{\text{(1-B)}} = \boldsymbol{\Sigma}_k^{(0)}\;\mathbf{G}_k^{(1)} \in \mathbb{C}^{M\times b_k} \tag{12.10}$$

Being $b = \sum_{k=1}^{K} b_k$, the expression of the final matrix is:

$$\mathbf{F}^{(1\text{-B})} = \left[\mathbf{F}_1{}^{(1\text{-B})} \;\cdots\; \mathbf{F}_K{}^{(1\text{-B})}\right] \in \mathbb{C}^{M\times b} \tag{12.11}$$

Once the precoder used in approach (1-A) is derived, it must be noticed that in the N=1 case, as is the one in this chapter, forcefully $b_k = 1\ \forall k \in [1,2]$, since that is the maximum number of streams per user. Then, $\mathbf{F}^{(1\text{-B})} \in \mathbb{C}^{M\times K=M\times 2}$. Moreover, and for simulation fairness with (1-A) and (1-C), $r_k^* = 1\ \forall k \in [1,2]$ is preferred.

12.4.3 Proposal (1-C).

Proposal (1-C) is based on work by authors of [36]. Briefly, in this publication, although considering full instantaneous CSIT, it is relied on transmission in the null subspace occupied by the interferers to each user, just as in the approach by [39]. The algorithm, called RBD, attempts both to perform beamforming so that the loss inherent to the employment of MMSE for users with more than one antenna and due to multi-user interference mitigation is reduced and to eliminate the constraint on the number of antennas at the users. The precoding matrix is computed in two stages: first, MUI is suppressed by designing the precoding matrix under the MMSE criterion. Then, performance is optimised by a means of optimisation of each MIMO channel separately under a transmit power constraint.
The approach suggested in this chapter focuses on the first stage of the algorithm only, i.e. interference suppression. For that, authors of [36] rely on instantaneous CSIT at the BS. The precoding matrix of each user is designed so that each user transmits in the null subspace of its interferers. This is done as per the channel matrices of the interfering channels. The algorithm is completed if transmission is done with the power that is inversely proportional to the singular values of the combined channel matrices of the interfering users (not considered in the suggested approach). The full derivation and validity of the algorithm may be found in [36].

As stated multiple times, all approaches accounted for in this chapter completely disregard instantaneous CSIT in the form of the channel matrices. However, channel covariance matrices are assumed at the BS. We suggest these be used in lieu of the channel matrices to build a precoder under the scope of the MUI stage of an RBD. The approach suggested as proposal nr. (1-C) is explained below.

Once again, each of the user's covariance matrix is assumed at the BS.
The covariance matrix of the $\mathrm{k^{th}}$ channel can be written and expanded like:

$$\begin{aligned}\mathbf{R}_k &= \mathbf{U}_k\,\mathbf{\Lambda}_k\,\mathbf{U}_k{}^{\mathrm{H}}\\ &= \left[\mathbf{U}_k^*\;\mathbf{U}_k^{\prime}\right]\,\mathbf{\Lambda}_k\,\mathbf{U}_k^{\mathrm{H}}\end{aligned} \tag{12.12}$$

At the same time, the covariance matrices of the interferers with user k, $\widetilde{\mathbf{R}}_k \in \mathbb{C}^{M\times K\cdot M}$ can be defined:

$$\begin{aligned}\widetilde{\mathbf{R}}_k &= \left[\mathbf{R}_1\;\cdots\mathbf{R}_{k-1}\;\mathbf{R}_{k+1}\;\cdots\;\mathbf{R}_K\right]\\ &= \widetilde{\mathbf{U}}_k\,\widetilde{\mathbf{\Lambda}}_k\,\widetilde{\mathbf{V}}_k^{\mathrm{H}}\end{aligned} \tag{12.13}$$

Being $\widetilde{\mathbf{R}}_k$ a wide matrix[2], then $\widetilde{\mathbf{U}}_k \in \mathbb{C}^{M\times M}$ and $\widetilde{\mathbf{\Lambda}}_k \in \mathbb{C}^{M\times K\cdot M}$. The last N columns in $\widetilde{\mathbf{U}}_k$ are taken and so is done for $\widetilde{\mathbf{\Lambda}}_k$:

[2] A wide matrix is that of which the nr. of rows are less than the nr. of columns.

$$\begin{aligned}\widetilde{\mathbf{U}}_k &= \left[\widetilde{\mathbf{U}}_k^{(1)}\ \widetilde{\mathbf{U}}_k^{(0)}\right] \\ \widetilde{\mathbf{\Lambda}}_k &= \left[\widetilde{\mathbf{\Lambda}}_k^{(1)}\ \widetilde{\mathbf{\Lambda}}_k^{(0)}\right]\end{aligned} \tag{12.14}$$

where $\widetilde{\mathbf{U}}_k^{(0)} \in \mathbb{C}^{M\times N}$ and $\widetilde{\mathbf{\Lambda}}_k^{(0)} \in \mathbb{C}^{M\times N}$.
The resulting precoder for user k is:

$$\mathbf{F}^{(\text{1-C})} = \widetilde{\mathbf{U}}_k^{(0)} \left[\left[\widetilde{\mathbf{\Lambda}}_k^{(0)}\right]^{\mathrm{T}} \widetilde{\mathbf{\Lambda}}_k^{(0)} + \frac{K\cdot N\sigma_n^2}{\bar{\mathrm{P}}}\cdot \mathbf{I}_N\right]^{-1/2} \tag{12.15}$$

where $\mathbf{I}_N$ is the $\mathrm{N}\times\mathrm{N}$ identity matrix. This is done in the hopes that transmission is carried out in the null subspace of the interferers (given by their covariance matrices).

If we narrow down this approach to the K=2 case in which users have a single antenna, then:

$$\begin{aligned}\widetilde{\mathbf{R}}_1 &= \mathbf{R}_2 \\ &= \mathbf{U}_2\,\mathbf{\Lambda}_2\,\mathbf{U}_2^{\mathrm{H}} \\ \\ \widetilde{\mathbf{R}}_2 &= \mathbf{R}_1 \\ &= \mathbf{U}_1\,\mathbf{\Lambda}_1\,\mathbf{U}_1^{\mathrm{H}}\end{aligned}$$

12.5 Proposals nr. 2.2.

This section is aimed at the derivation of the group of proposals nr. 2.2., namely (2-A), (2-B) and (2-C).

As mentioned earlier in this chapter, derivation of proposals nr. 2.2 rely on considering each precoder (1-A), (1-B) and (1-C) as an effective channel matrix and then applying linear MMSE beamforming *replacing the channel matrix with the calculated precoding matrices.*
This approach is straightaway and so will be defined jointly for all (2-A), (2-B) and (2-C).

For any computed precoder found as per sec. 12.4 on page 138, i.e. (1-A), (1-B) and (1-C), those are taken as channel matrices and the expression for an MMSE precoder is derived. Thus,

$$\mathbf{F}^{(\text{2-A})} = \left[\mathbf{F}^{(\text{1-A})}\right]^{\mathrm{H}} \left[\mathbf{F}^{(\text{1-A})} \left[\mathbf{F}^{(\text{1-A})}\right]^{\mathrm{H}} + \mathrm{K}\cdot\frac{\sigma_n^2}{\mathrm{P}_{\mathrm{Tx}}}\,\mathbf{I}_{\mathrm{K}}\right]^{-1} \tag{12.16}$$

$$\mathbf{F}^{(\text{2-B})} = \left[\mathbf{F}^{(\text{1-B})}\right]^{\mathrm{H}} \left[\mathbf{F}^{(\text{1-B})} \left[\mathbf{F}^{(\text{1-B})}\right]^{\mathrm{H}} + \mathrm{K}\cdot\frac{\sigma_n^2}{\mathrm{P}_{\mathrm{Tx}}}\,\mathbf{I}_{\mathrm{K}}\right]^{-1} \tag{12.17}$$

$$\mathbf{F}^{(\text{2-C})} = \left[\mathbf{F}^{(\text{1-C})}\right]^{\mathrm{H}} \left[\mathbf{F}^{(\text{1-C})} \left[\mathbf{F}^{(\text{1-C})}\right]^{\mathrm{H}} + \mathrm{K}\cdot\frac{\sigma_n^2}{\mathrm{P}_{\mathrm{Tx}}}\,\mathbf{I}_{\mathrm{K}}\right]^{-1} \tag{12.18}$$

12.6 Simulation results.

This section aims to provide with the most significant results on the proposed statistical precoders. It is divided into two subsections, for proposals nr 2.1 and proposals nr 2.2.

The achieved SR was calculated as done for the linear precoders, so considering both a number of channel and transmit symbol Monte Carlo simulations. In both cases this number was set to 1000. The complete procedure is derived in chap. 10 on page 91 and will not be rewritten in this chapter.

12.6.1 Results on proposals nr 2.1

A thousand Monte Carlo channel simulations were considered to build the channel's covariance matrices. We remind the reader that a K=2 scenario is tackled, each user having a single antenna. User 1 was located at [x,y]=[50,60] [m] and User 2 at [x,y]=[-100,20] [m]. Realisation-wise, users suffer local mobility, being the maximum x and y variations of 1 [m], each. A local cluster-only scattering environment was considered. 25 scatterers were considered. The local cluster's area is approximately 70 [m^2]. The scatterers weighting changes as well from realisation to realisation. The massive array was set to M=200 and an aperture of approximately 20.6 [m]. Fig. 12.4 depicts this scenario.

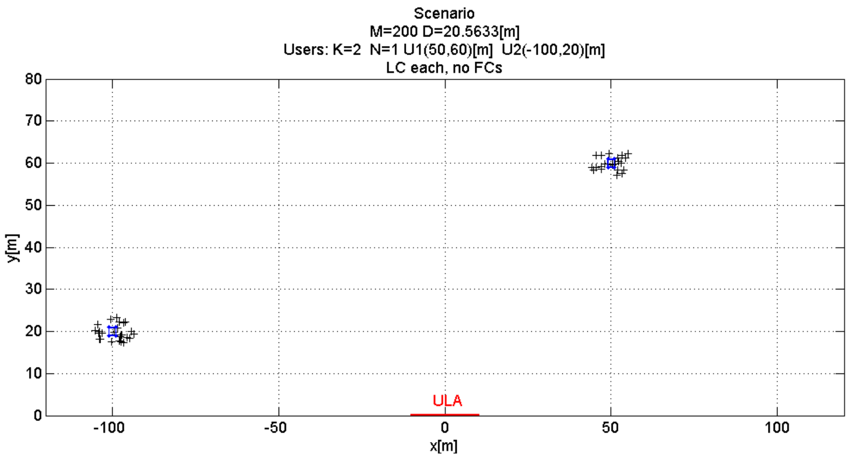

Figure 12.4 *Considered scenario. Users' mobility area is bounded by blue squares. A local cluster surrounds each user.*

Lastly, the performance of the precoders was evaluated according to the achieved SR for different values of the channel's SNR, which was varied from -30 to 90 [dB]. The reason why the upper limit to the SNR was set to such a high value is revealed later. Instantaneous MF and MMSE are included to test the level of suboptimality that the statistical approach would suffer from with respect to the full CSIT case. In graphs, instantaneous MF is indicated as MF_{inst} and instantaneous MMSE, as $MMSE_{inst}$.
Fig. 12.5 features the achieved SR for the LOS and TOT channels.

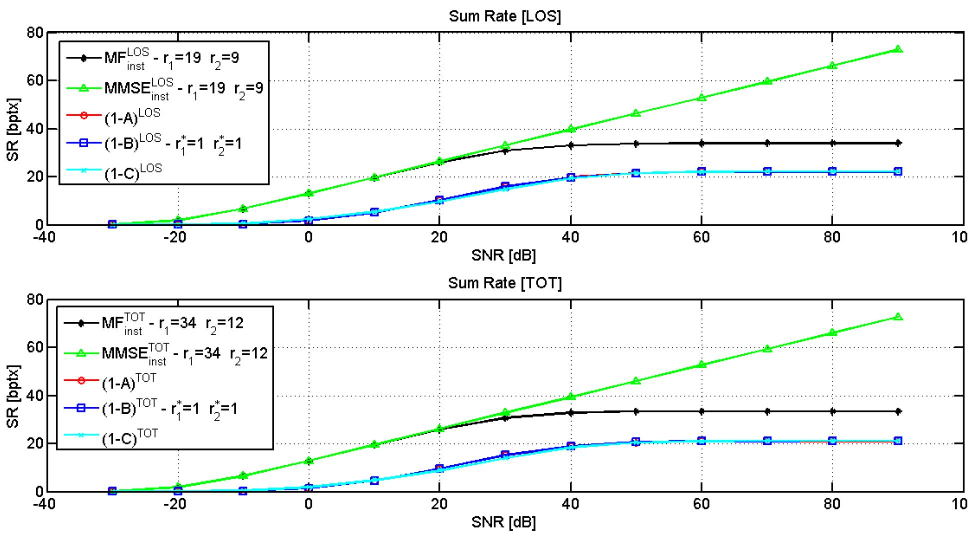

Figure 12.5 *Sum Rates vs SNR. LOS and TOT channels. Covariance matrices ranks are specified. Also,so is done with (1-B)'s r^*_k for $k = 1$ and $k = 2$, set to 1 in both cases.*

All precoders seem to be **equivalent to each other** as they exhibit a very similar behaviour. As it is natural, **they behave suboptimally with regard to the instantaneous precoders**, included for comparison.
Interestingly, **curves exhibit a saturation level**, just the same way conjugate beamforming does. Nonetheless, it occurs at a higher SNR level than with the MF. Note that, while instantaneous MF curves seem to start degrading at an SNR level of approximately 20 or 30 [dB], the statistical precoders do not do so until a level of at least 40 [dB]. This is not due to a major difference in the achieved symbol power, seen in fig. 12.6a on the facing page but rather, lies behind the fact **interference power is lower in the case of the statistical precoders**, something especially noticeable in the case of proposal (1-C). Even though the original proposal (RBD) considered by authors of [36] tackles MUI mitigation, it is certainly attractive to confirm that this occurs as well employing the statistical information suggested in this chapter. Performance in this matter can be confirmed in fig. 12.6b on the next page, which includes the interference power for both users, and more clearly analysed in fig. 12.6c on the facing page, which focuses on the saturation areas.

All in all, though, it must be noticed that, even though more than one DoF would be available for exploitation, the fact fair comparison is sought, together with the fact two of the proposed algorithms can only consider one of them, makes all of them approximately collapse. In the SNR interval of interest, which could range for practical reasons roughly from 0 [dB] to 30 [dB],the difference in the achieved sum rate with respect to the optimal MMSE based on full CSIT is roughly 20 [bptx], slightly less for the lower SNR values. The same applies to conjugate beamforming, although difference is as well narrower at the higher SNR values, due to MF's saturation. However, **although suboptimal, they achieve non-negligible sum rates**. Finally, it must be noticed that in the conditions of the scenario tackled here, (1-A) would be preferred since it is least complex.

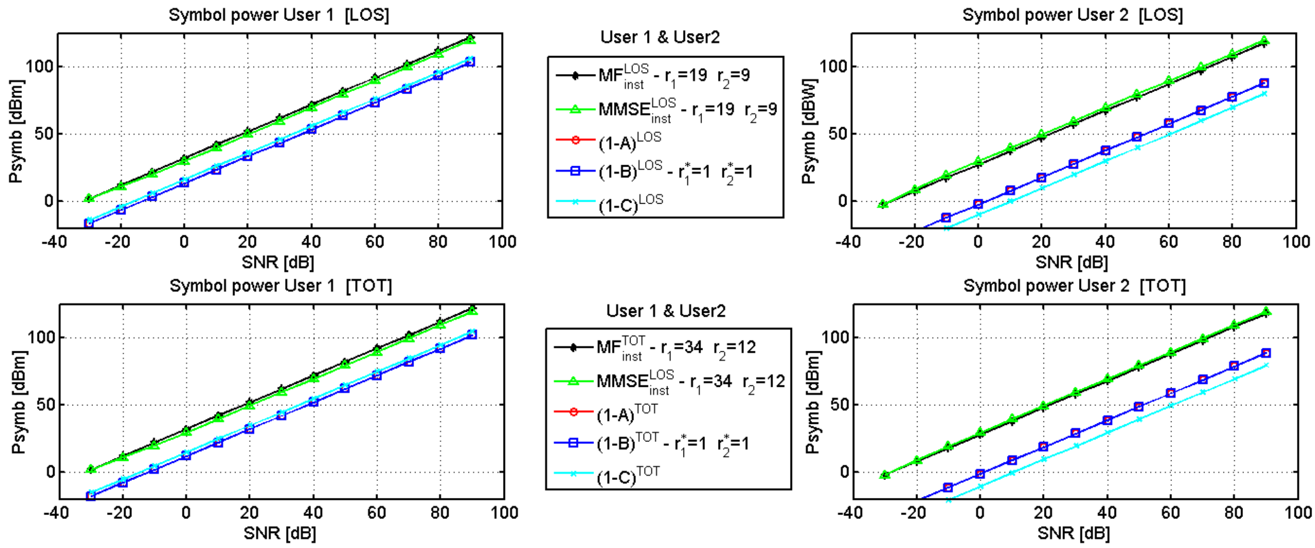

(a) *Symbol power vs SNR. LOS and TOT channels.*

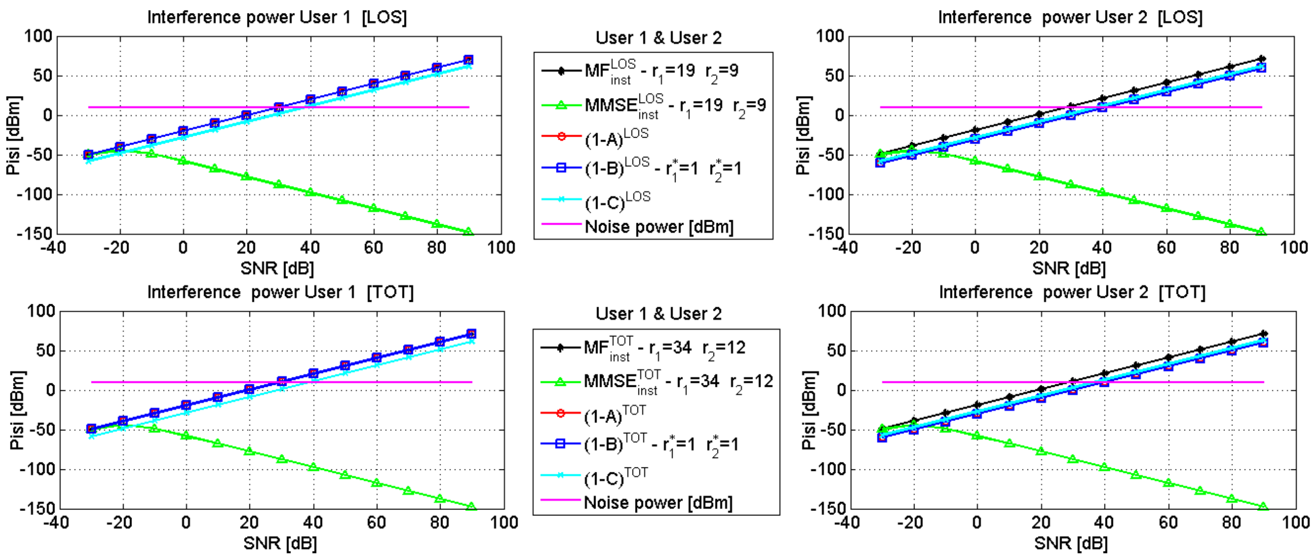

(b) *Interference power vs SNR. LOS and TOT channels.*

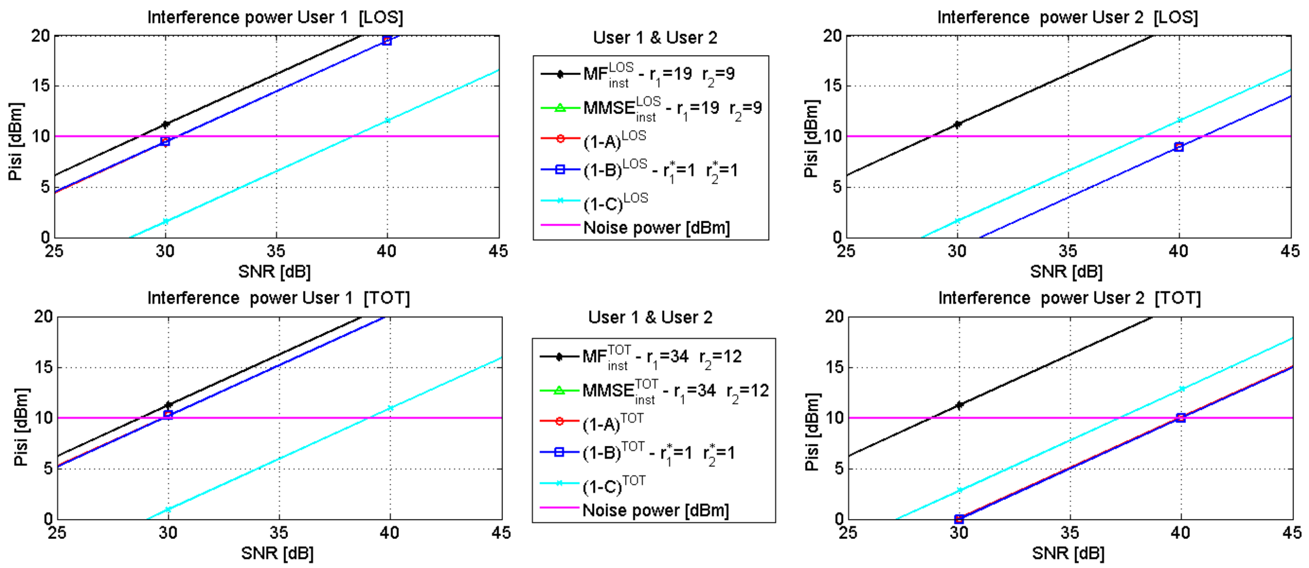

(c) *Interference power vs SNR at the saturation interval. LOS and TOT channels.*

Figure 12.6 *SR, symbol power and interference power.*

Performance according to the user's location.

As seen in sec. 12.2 on page 134, the users location determines the rank of the covariance matrices of the channels, and in turn the number of exploitable DoF. It is expected that the more unconsidered DoF when building a channel's precoding vector, the less accurate if attempting to match the channel's occupied subspace or its interferer's null subspace. This would in turn happen according to the expected scenario's orthogonality pattern since information at the BS is rooted in each of the user's mobility, influenced by orthogonality in the area it moves. This motivated the study of the user's locations. As it has been common throughout this document, a user is placed at a certain fixed location and other one is moved in an xy-grid. In this case, however, at each location, users will suffer local mobility. The still user was positioned at broadside, at (x,y)=(0,50) [m]. The same features as in the line above were assumed, apart from the SNR, which was set to 30 [dB].

Let us first show the orthogonality pattern that the scenario explained above would exhibit. This can be seen in fig. 12.7. It has been calculated according to procedure in chap. 11 on page 109 and corresponds to the real data (resulting from simulations).

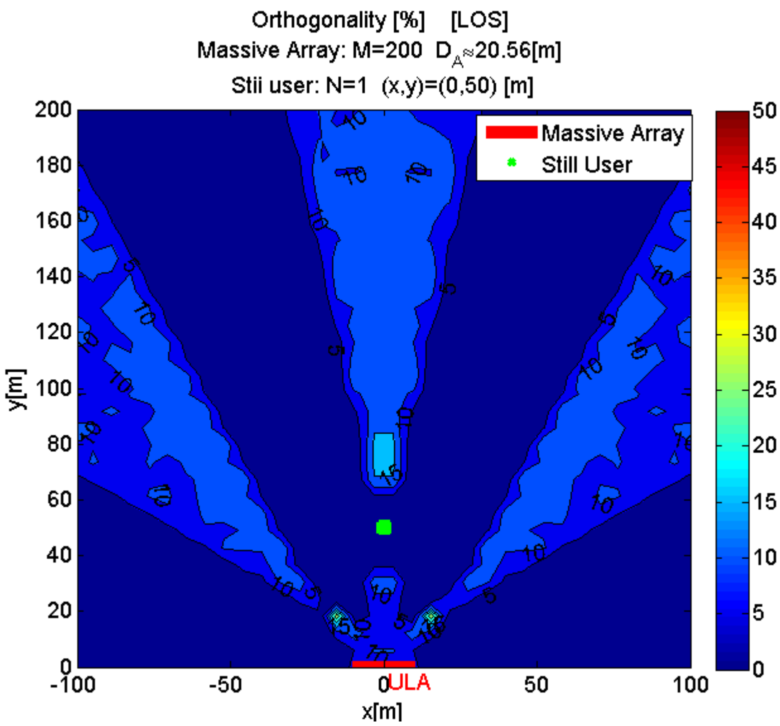

Figure 12.7 *Orthogonality in the suggested scenario. LOS channel.*

Then, the instantaneous precoders' behaviour is shown in fig. 12.8a on the facing page. Notice that the MF's capability is impaired by the orthogonality in the scenario and that its SR pattern goes in accordance, achieving the best results when orthogonality is lower, thus out of the outthrusts. MMSE in turn is able to compensate for this, achieving optimal results mostly everywhere in the grid.

Finally, the surface plots regarding approaches (1-A), (1-B) and (1-C) are exhibited in fig. 12.8b on the next page. It is notable to notice that SR patters go very much in line with the channel's orthogonality, as confirmed for the instantaneous MF case. This is especially evident in the case of approach (1-A). Interestingly enough, while this approach is poorer in the LOS than (1-B) and (1-C), it is the other way round in the TOT channel. To our best reasoning, this is again due to the higher degree of independence achieved in that channel, thanks to the random action of the scatterers. Let us remind the reader that proposal (1-A) acts on each channel's subspaces and not on the null subspaces of the interferers.

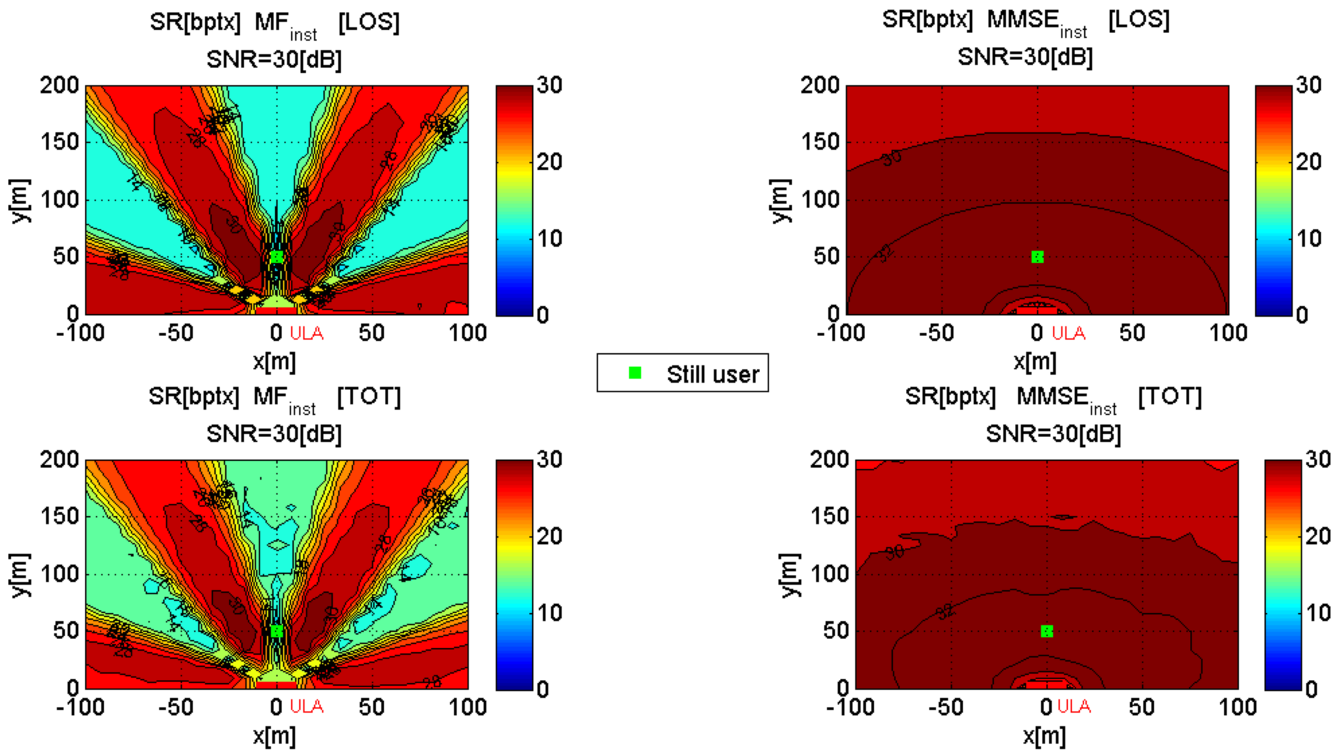

(a) *SR of a MF and MMSE with full instantaneous CSIT. LOS and TOT channels.*

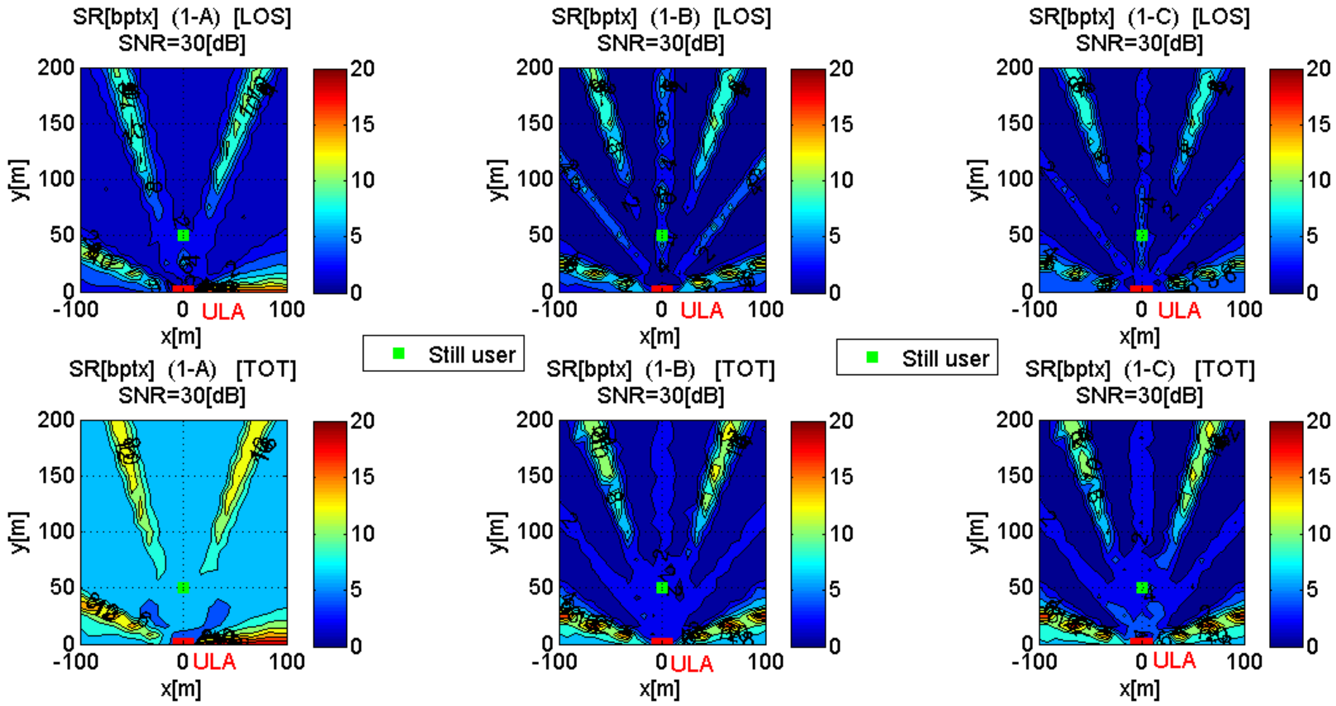

(b) *SR of approaches (1-A), (1-B) and (1-C). LOS and TOT channels.*

Figure 12.8 *Sum rates as per instantaneous MF and MMSE beamforming and proposals nr. 2.1.*

12.6.2 Results on proposals nr 2.2

A thousand Monte Carlo channel simulations were considered to build the channel's covariance matrices. A K=2, multi-user MIMO scenario is considered, having each user a single antenna.

As in sec. 12.6.1 on page 143, User 1 was located at [x,y]=[50,60] [m] and User 2 at [x,y]=[-100,20] [m]. Realisation-wise, users suffer local mobility, being the maximum x and y variations of 1 [m], each. A local cluster-only scattering environment was considered, in which the local cluster contains 25 scatterers. The local cluster's area is approximately 70 [m^2]. The scatterers weighting changes as well from realisation to realisation. The massive array was set to M=200 with an aperture of approximately 20.6 [m]. Fig. 12.4 on page 143 in last subsection depicts this scenario.

Fig. 12.9 features the achieved SR for the LOS and TOT channels.

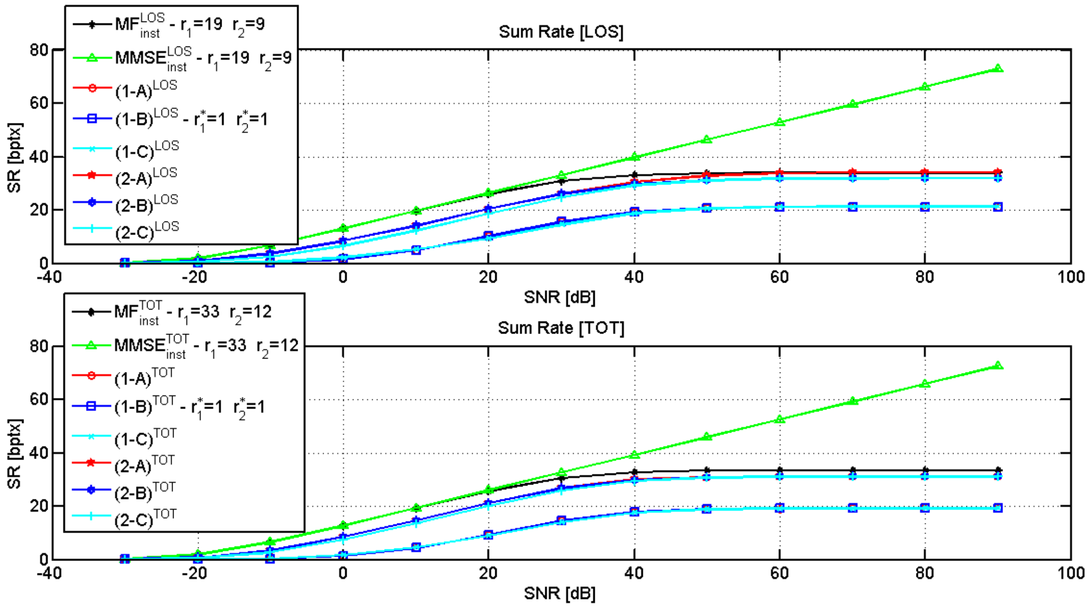

Figure 12.9 *SR vs SNR of approaches (2-A), (2-B) and (2-C). LOS and TOT channels.*

Instantaneous curves and the ones regarding proposals nr 2.1 are also included for comparison. Like proposals nr. 2.1, resulting SR curves tend to collapse to each other. However and **outstandingly, their behaviour is significantly close to the performance of the conjugate beamformer with full instantaneous CSIT**. Even saturation occurs at roughly the same SNR values, rooted in the asymptotic behaviour of the interference power (see chap. 10 on page 91). All in all, **a gain is clearly achieved with respect to proposals 2.1**. Unlike expected, it is an optimisation on the symbol power that lies behind this gain and not on the interference power reduction, as would be expected as per the employment of an MMSE inversion. This can be confirmed in both fig. 12.10a on the facing page and fig. 12.10b on the next page, featuring the symbol power and interference power, respectively.
It must be noticed that this gain **comes at the cost of a matrix inversion**.

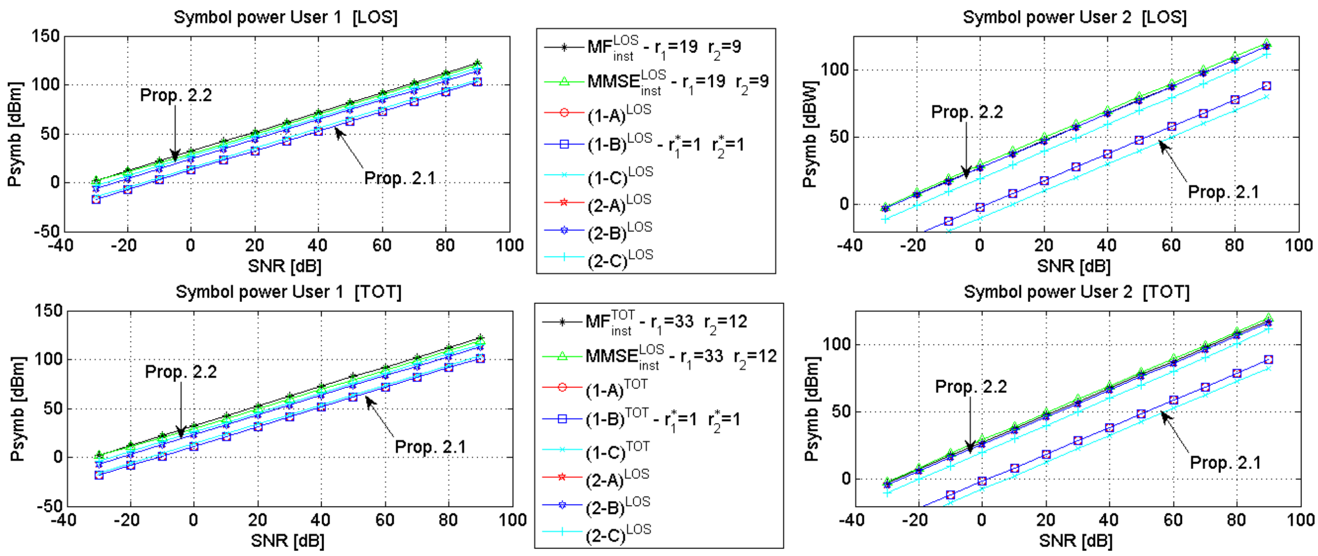

(a) *Symbol power vs SNR at the saturation interval. LOS and TOT channels.*

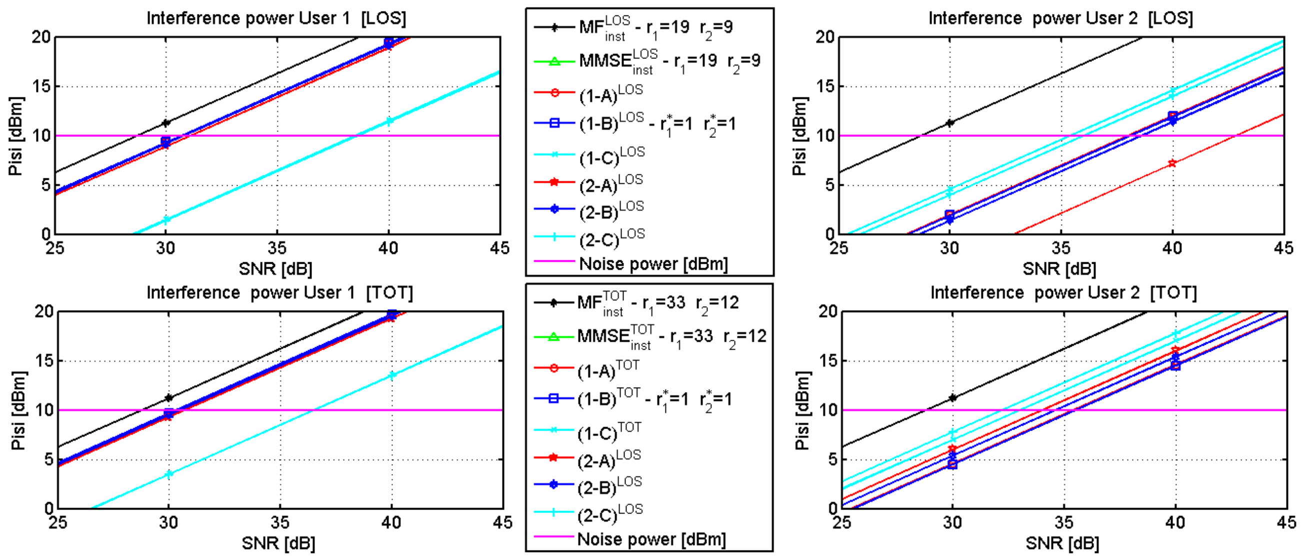

(b) *Interference power vs SNR. LOS and TOT channels.*

Figure 12.10 *Symbol power and interference power.*

Lastly, it is of interest to include the behaviour of (1-B) and (2-B) when (1-B) is calculated with $r_k^* = r_k$ for both channels, so taking the maximum information possible on each of the interferers' null subspaces. Since this has not been done yet for comparison fairness, the results yielded are worth including, especially in terms of (2-B). The sum rate is exhibited in fig 12.11 on the following page.

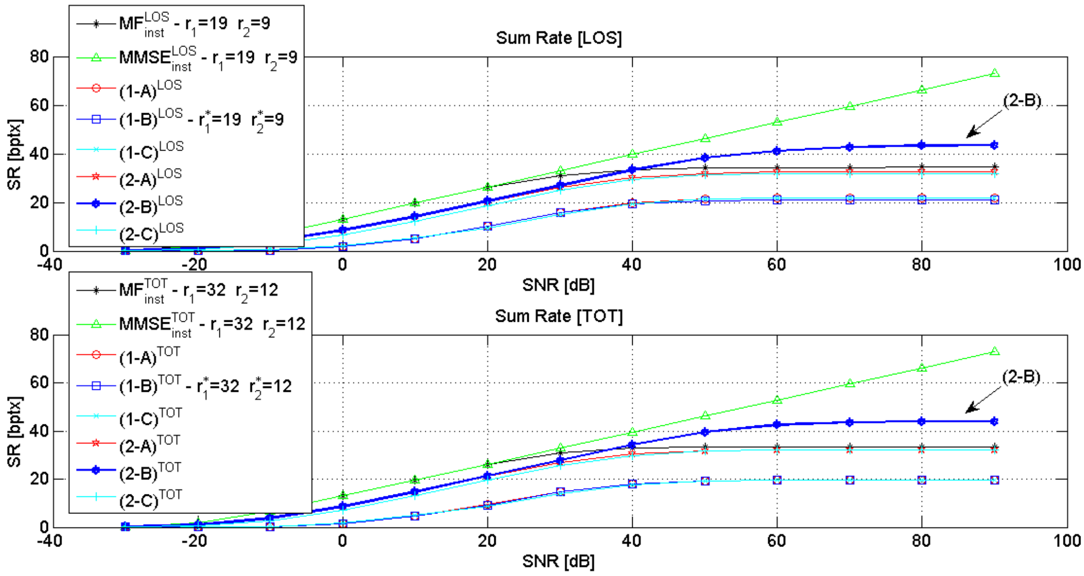

Figure 12.11 *SR vs SNR of approaches (2-A), (2-B) [when (1-B) has $r_k^* = r_k \ \forall k \in [1,2]$] and (2-C). LOS and TOT channels.*

It can be seen that, **while (1-B)'s performance is unaltered, (2-B)'s suffers a significant improvement at the high-SNR interval**, since it continues growing up to very high SNR values, when this process culminates and saturation is observed. Variations at the non-high SNR values are negligible. It is remarkably interesting to notice that performance is significantly closer to the instantaneous beamforming situation given by the MMSE precoder and that at the high SNR values, (2-B) is able to outperform the instantaneous MF case due to its inherent saturation. (2-B) could be regarded as a *suboptimal instantaneous MMSEs*: since the instantaneous conjugate beamforming is seen to start its downgrade at an SNR close to 20 [dB], it is not up to approximately 50 [dB] that (2-B) starts to saturate.
The reason for this improvement is rooted in the **ability of this approach to effectuate MUI mitigation given the possession of enough information on the interferers (yielded by a higher r_k^* for each channel)**, something that can be confirmed in fig. 12.12b on the next page. This is inherent to an MMSE beamformer but again **comes at the cost of a matrix inversion**, which has larger dimensions this time. The symbol power suffers little variation, as shown in fig. 12.12a on the facing page.

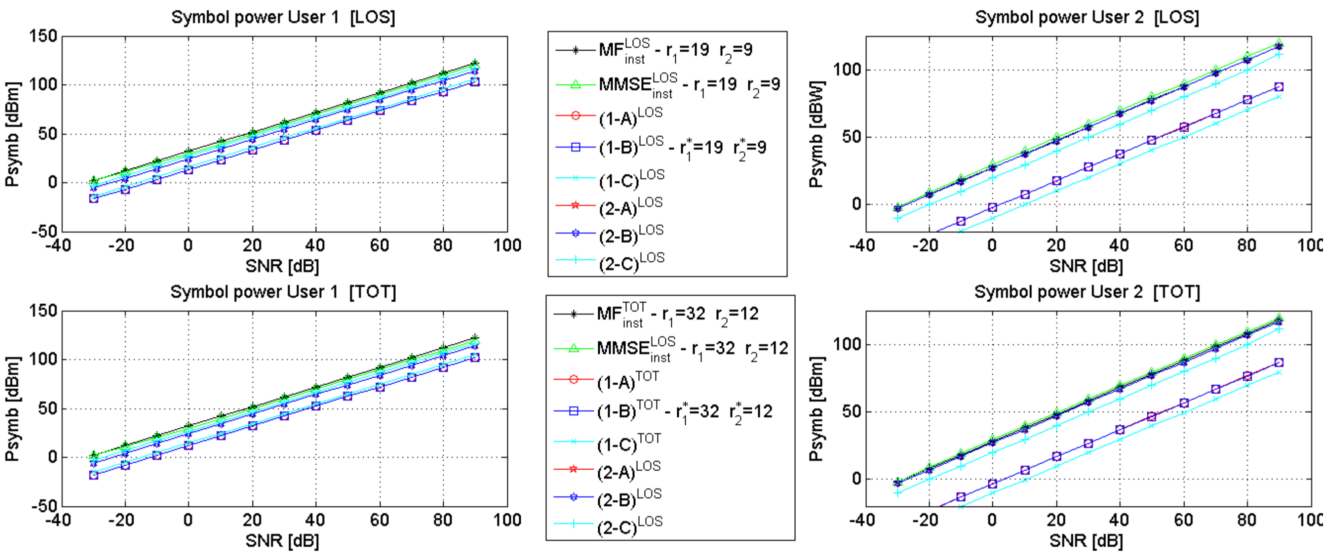

(a) *Symbol power vs SNR at the saturation interval. LOS and TOT channels. (2-B) is calculated with (1-B) having* $r_k^* = r_k \ \forall k \in \ [1, 2]$.

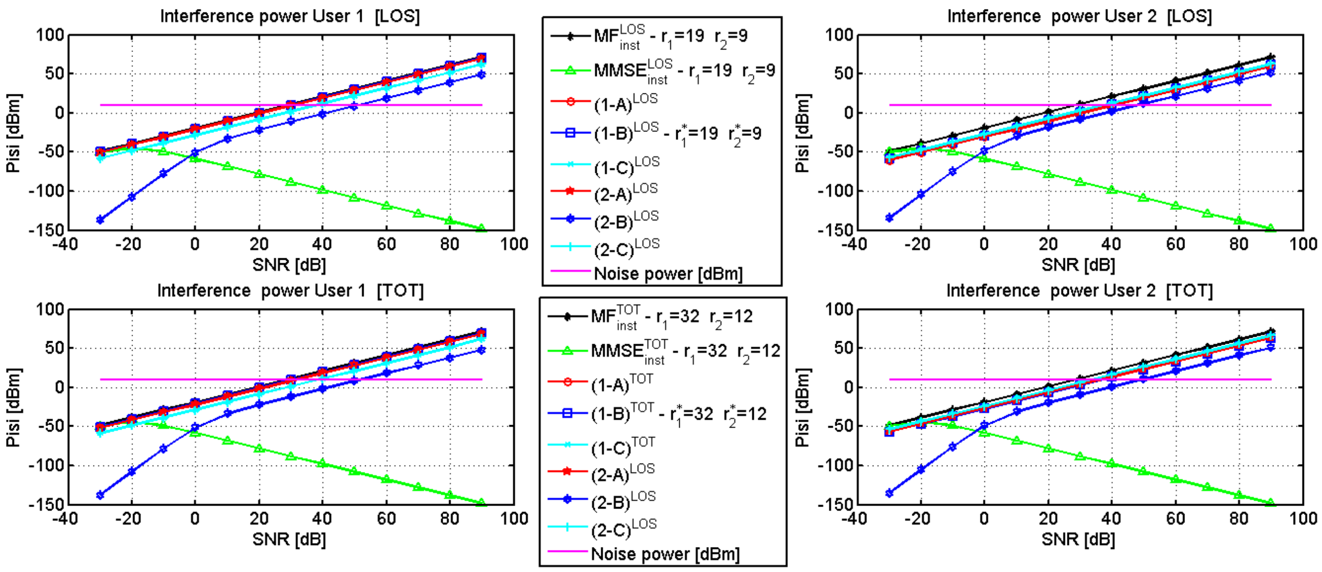

(b) *Interference power vs SNR. LOS and TOT channels. (2-B) is calculated with (1-B) having* $r_k^* = r_k \ \forall k \in \ [1, 2]$.

Figure 12.12 *Symbol and interference power (2-B) is calculated with (1-B) having* $r_k^* = r_k \ \forall k \in \ [1, 2]$.

Performance according to the user's location.

An equivalent analysis to the one carried out in sec. 12.6.1 on page 146 has been done for proposals nr. 2.2 as well. Fig. 12.14a on page 153 shows the achieved SR when (1-B) was computed as per $r_k^* = 1 \ \forall k \in \ [1, 2]$. Fig. 12.14b on page 153 shows the achieved SR when (1-B) was computed as per $r_k^* = 1 \ \forall k \in \ [1, 2]$.

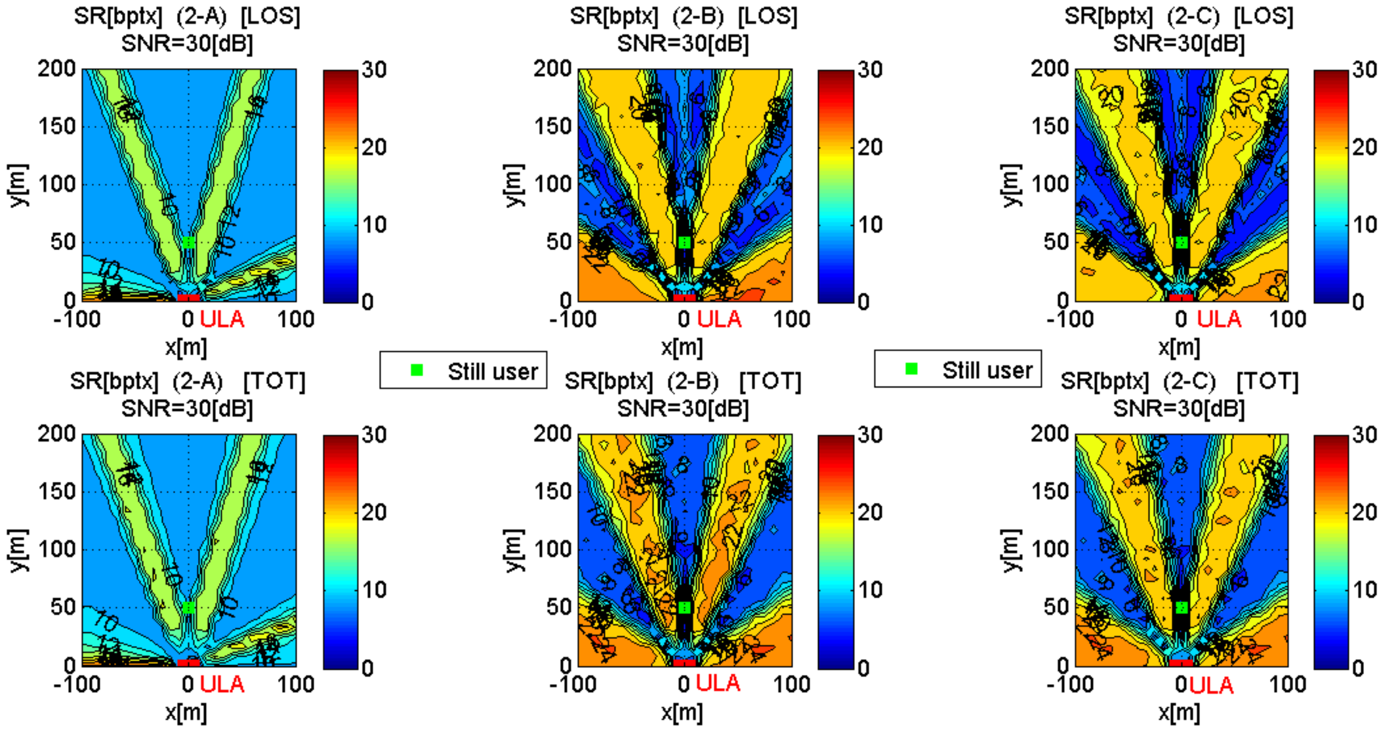

(a) *SR of approaches (2-A), (2-B) and (2-C). LOS and TOT channels. In (1-B),* $r_k^* = 1 \ \forall k \in \ [1, 2]$

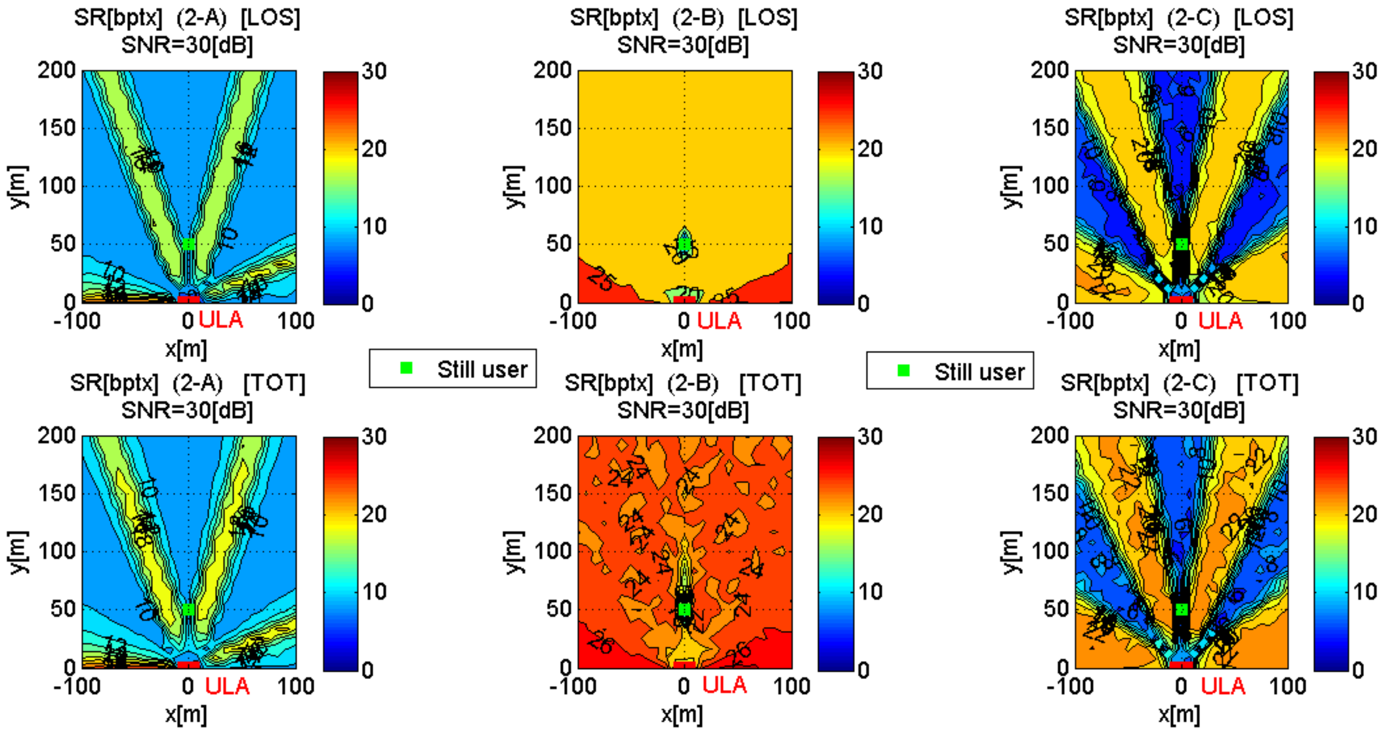

(b) *SR of approaches (2-A), (2-B) and (2-C). LOS and TOT channels. In (1-B),* $r_k^* = r_k \ \forall k \in \ [1, 2]$

Figure 12.13 *Sum rate, proposals nr. 2.2. (2-B) comparison.*

The gain observed earlier in this section is confirmed in this figure as well. Attractively, even with $r_k^* = 1 \ \forall k \in \ [1, 2]$, (2-B) appears to yield the highest SRs, although (2-C)'s performance is significantly close. Again SR patterns seem to behave accordingly to orthogonality, let's not forget that (2-X) approaches are based on the previous calculation of (1-X), which have been shown to depend on it at a high degree. X is specified for A, B and C.

Otherwise, the employment of $r_k^* = r_k \ \forall k \in \ [1,2]$ yields one more time the highest SRs, as already analysed previously.

Finally, comparison of results yielded by taking $r_k^* = 1 \ \forall k \in \ [1,2]$ and $r_k^* = r_k \ \forall k \in \ [1,2]$ only in terms of proposal (1-B) can be seen below in order to confirm that this yields very little additional gain, especially in the TOT. The reason for this is that the improvement of proposals nr 2.1 is seen in the symbol power and not on the interference power, so some additional information on the interferers results in no extra gain, whatsoever.

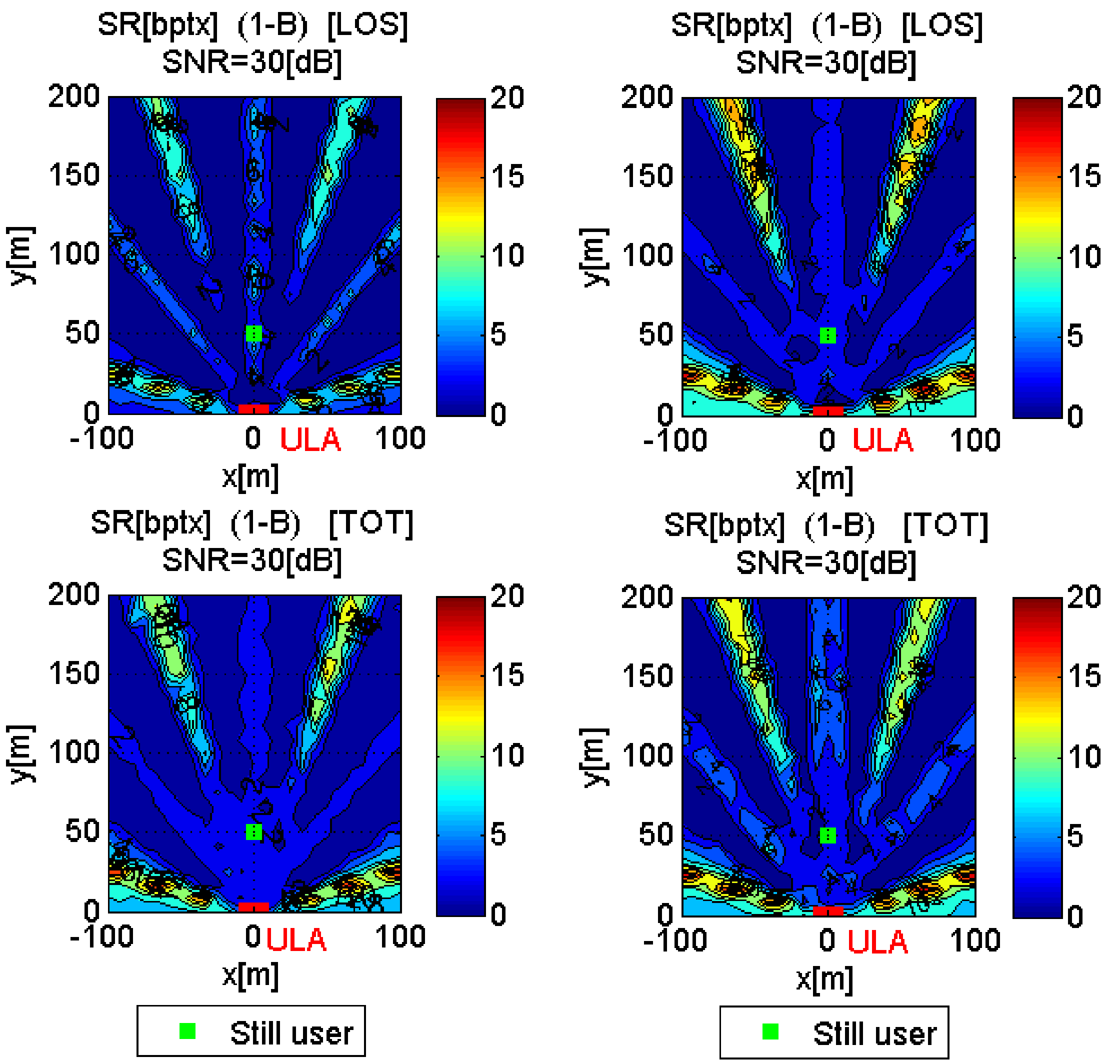

(a) *SR of approaches (1-A), (1-B) and (1-C). LOS and TOT channels. In (1-B),* $r_k^* = 1 \ \forall k \in \ [1,2]$

(b) *SR of approaches (1-A), (1-B) and (1-C). LOS and TOT channels. In (1-B),* $r_k^* = r_k \ \forall k \in \ [1,2]$

Figure 12.14 *Sum rate, proposals nr. 2.1. (1-B) comparison.*

12.7 Main conclusions on statistical precoders.

The low rankness provided by the channel's covariance matrices as per the users' local mobility appears to be an effective enabler for statistical precoding, even in the LOS.

Two approaches have been analysed, obtaining non-negligible SRs with both of them. However, the set of proposals under the denomination of proposals nr. 2.2 exhibit the best performance. This is close to the MF case with full instantaneous CSIT, which is assumed to be optimal

in the massive MIMO regime. As explained in chap. 11 on page 109, though, it is not only this requirement that provokes optimality on this precoder, being inter-user correlation (or orthogonality) limiting as well. This is the case in the scenario tackled in this chapter. This has been done on purpose to test what the impact of limitations due to orthogonality are on the proposed statistical approaches. In any case, the gain observed for proposals nr. 2.2 comes at a cost of matrix inversions, so selection of the desired precoder should take into account the users' needs that are to be covered, together with the level of complexity to be tolerated.
Otherwise, proposal (1-B) may consider some extended information on the channel's covariance matrices. If this is done, a great improvement is observed on (2-B)'s performance at the very-high SNR regime, outperforming the MF precoder, based on instantaneous CSIT information. However, it must be noticed that the cost of channel inversion of (2-B) is enlarged since the matrices to be inverted have larger dimensions.

Part III

Main conclusions and future perspective

Chapter 13

Main conclusions. Future perspective on Massive MIMO.

This final chapter has a two-fold aim.
On the one hand, the main conclusions yielded by this thesis will be briefly tackled. This will be done as per both parts of the project.
On the other hand, the main uncovered issues to the best concern of the authors of this document on its publication will be pointed out, as a reference for future work.

13.1 Main conclusions

13.1.1 Point-to-Point MIMO

The first part of this Master's thesis dealt with the development of a MIMO channel under the massive number of antennas regime and for a very large aperture, which implies a Near Field focus. This was done as per a simplified COST2100 model. The main results yielded that an increased number of antennas at the BS M can significantly improve a P2P MIMO scenario with respect to the maximum achievable rate, previous optimal power allocation. The same goes for the number of antennas at the user N. It is in fact the number of antennas at the user that limits the system's multiplexing gain. The resulting achievable rate is linearly proportional to N in most of the considered scenarios, as long as N is not large enough. If the user's array aperture is varied jointly with its aperture, then growth of capacity can be lifted outstandingly. This is due to the fact that resolvability of elements would not be impaired by the physical space they occupy.
The user's location plays as well an important role on capacity achievement. It has been concluded that the broadside direction to the massive array is optimal. However, most of the user's locations are sufficiently adequate apart from the ones lying along the endfire direction to the array and at close areas to it. This is due to the LOS channel being the most significant contributor to the channel. At the endfire direction, the LOS propagation characteristics fail to yield satisfactory results. This situation can be mitigated if the scattering environment is sufficiently rich, since it would provide the massive array with a larger "virtual" aperture, as seen by the user. In any other situation, the TOT channel (the one considering both the LOS and NLOS propagation terms) is determined most relevantly by the LOS components. However, it is the LOS channel that tends to be optimal. This lies behind the nature of massive MIMO creating what authors like [13, 14] call *favourable propagation conditions*, which come down to all eigenchannels having the same power and thus, maximising capacity. Favourable propagation conditions are yielded if the entries of the channel matrix are i.i.d.[1] and if M$\gg$N.

[1]Independent and identically distributed.

Finally, it must be remarked that work in the high SNR regime is preferred since the linear growth on the achievable rate is achieved for the high SNR values.

13.1.2 Multi-user MIMO beamforming.

The second part of this thesis focuses on a low-complexity beamforming approach under the scope of the users' local mobility. A case study consisting of two single-antenna users was selected as a basis for its development. Two approaches are suggested.

The *first approach* tackles MIMO linear precoders, namely MF, ZF and MMSE, since their complexity is much lower than other non-linear beamformers such as DPC. Instantaneous CSIT is assumed and thus, the users' local mobility goal is met. Capacity in multi-user massive MIMO systems is expected in literature to increase dramatically thanks to the aggressive spatial multiplexing [16]. This would be done as per an adequate pre-processing at the BS or beamforming. Matched filtering in literature appears as an optimal beamformer for massive MIMO systems, since the channel responses in such systems tend to be mutually orthogonal as the number of antennas grows large. However, it has been shown that orthogonality between users' responses (or inter-user correlation), which determines a MF's performance, is poor enough in some cases, motivating an extensive study on orthogonality which has been included in a separate chapter. Basically, it has been proven that it is both the configuration at the massive array and the users location that determine inter-user correlation. On the former, it is particularly the spacing at the massive array that matters. It has been argued that if the massive array has evenly spaced elements, then a spacing lower than 1λ is optimal, since it removes the low-orthogonality areas due to the massive array's configuration. As for the location of the user, it has been justified that the geometry regarding the user and the extremes of the massive array defines an area consisting of two triangles inside which orthogonality of the user's channels is inadequate. These issues arise at the LOS channel since they come down to geometry and get lessened in the total channel (LOS+NLOS). Since the LOS is limiting, it has served as a basis for a vast attempt to provide with a closed-form solution for orthogonality prediction in terms of the users location in the considered scenario.

The *second approach* deals with a beamforming focus that bars the instantaneous CSIT and reduces the assumed channel information at the BS to the covariance matrices of the channels as per the users' local mobility. It is in fact the covariance matrices that enable beamforming as per the information they carry, due to their low rankness. Two sets of proposals are given. In the first place, proposals (1-A), (1-B) and (1-C) are based on analysis in [38], [39] and [36], respectively. These proposed precoders rely on the channel's occupied subspaces -(1-A)- or the null subspaces of the interferers to a user -(1-B) and (1-C)- to build each user's precoding vector. Although suboptimal with respect to the full CSIT case, the achieved sum rates are non-negligible. The second set of proposals, (2-A), (2-B) and (2-C) result from the previous computation of (1-A), (1-B) and (1-C), to which inversion is applied in the fashion of an MMSE beamformer. Resulting precoders perform outstandingly well, reaching the behaviour of a MF under a full CSIT scope. It has been justified that this behaviour is rooted in a maximised symbol power. What is more, it has been shown that, under certain conditions, proposal (2-B) may outperform the behaviour of a full CSIT matched filtering, as the already upgraded symbol power gets combined with a mitigated inter-user interference. As far as the authors of this thesis are concerned, there is no literature dealing with an approach of the kind of the second set of suggested statistical beamformers in this thesis and so validation of simulations has been unattained.

13.2 Future work perspective

This section is aimed at both accounting for some of the delimitations considered in this project that may be tackled as future work and also to suggest other branches of interest.

A simplified model as per the COST2100 scope has been proposed in this thesis. While consistent, this model ought to be completed and/or adjusted to the scattering scenario being examined. Aspects like visibility regions or the presence of multi-bounce clusters might be determinant in some scenarios. Also, the LOS channels might not be available in some scenarios of interest. Lastly, the design of a more dynamic cluster power introduction would be desirable.

One of the main delimitations in this project refers to the fact mainly a two single-antenna user scenario was analysed. In the future, this should be expanded to a higher number of users (regime in which matched filtering is expected to be optimal with respect to channel-inversion precoders [15]). Moreover, validity of the proposed statistical precoders should be examined in the case users have more than one antenna, something we consider to be of significant importance. Otherwise, apart from orthogonality as a limitation to beamforming, other performance factors ought to be analysed. Those may include channel coherence (on CSIT acquisition), precoding delay (particularly for matrix inversion-based pre-processing), channel bandwidth (on channel state forwarding) or hardware imperfections (phase introduction, non-linearities, etc), among others [15].

Bibliography

[1] Werner Weichselberger. *Spatial Structure of Multiple Antenna Radio Channels. A Signal Processing Viewpoint.* PhD thesis, Technischen Universität Wien, 2003.

[2] Jan Mietzner. Multiple-Antenna Systems (lecture), 2008. URL http://www.ece.ubc.ca/~janm/Lectures/lecture_mimo.pdf.

[3] Robert W. Heath Jr. What is the Role of MIMO in Future Cellular Networks: Massive? Coordinated? mmWave?, 2013.

[4] Ed Malyon (Mirror). Sliding floors: West Ham unveil architectural drawings for new stadium, March 2013. URL http://www.mirror.co.uk/sport/football/news/west-ham-olympic-stadium-hammers-1791546#.Ut5_0xC0rIU.

[5] Patrick C. F. Eggers. Antennas & Propagation, 2013. MM9, MM10, MM11, MM12, Lecture Slides.

[6] Constantine A. Balanis. *Antenna Theory: Analysis and Design.* John Wiley and Sons, Ltd, 3rd edition, 2005. ISBN 0-471-66782-7.

[7] Jeng-Shiann Jiang and M.-A. Ingram. Spherical-wave model for short-range MIMO. *IEEE Transactions on Communications*, September 2005.

[8] Lingfeng Liu, C. Oestges, J. Poutanen, K. Haneda, P. Vainikainen, F. Quitin, F. Tufvesson, and P.D. Doncker. The COST2100 MIMO Channel Model. *IEEE Trans. Wirelss Comm.*, 19(6):92–99, December 2012.

[9] Fredrik Tufvesson. Massive MIMO system tutorial. Part II: Propagation apects, 2012. URL http://www.commsys.isy.liu.se/vlm/icc_tutorial_P2.pdf.

[10] Quentin H. Spencer, Christian B. Peel, A. Lee Swindlehurst, and Martin Haart. An Introduction to the Multi-User MIMO Downlink. *IEEE Communications Magazine*, October 2004.

[11] Tim Brown, Elisabeth de Carvalho, and Persefoni Kyritsi. *Practical Guide to the MIMO Radio Channel.* John Wiley & Sons, 2012. ISBN 978-0-470-99449-8.

[12] Patrick C. F. Eggers. Multi-Agent Radio Communications, 2013. MM1, MM2, MM4, MM10 Lecture Slides.

[13] Fredrik Rusek, Daniel Persson, Buon Kiong Lau, Erik G. Larsson, Thomas L. Marzetta, Ove Edfors, and Fredrik Tufvesson. Scaling up MIMO: Opportunities and Challenges with Very Large Arrays. *IEEE Signal Processing*, 30(1), December 2012. URL http://arxiv.org/abs/1201.3210.

[14] Erik G. Larsson. Massive MIMO: Fundamentals, Opportunities and Challenges, June 2013. Presentation slides.

[15] Clayton Shepard, Narendra Anand, and Lin Zhong. Practical Performance of MU-MIMO Precoding in Many-antenna Base Stations. In *Proceeding of the 2013 Workshop on Cellular Networks: Operations, Challenges, and Future Design*, CellNet '13, pages 13–18, New York, NY, USA, 2013. ACM. ISBN 978-1-4503-2074-0. doi: 10.1145/2482985.2482990. URL http://doi.acm.org/10.1145/2482985.2482990.

[16] E. Larsson, O. Edfors, F. Tufvesson, and T. Marzetta. Massive mimo for next generation wireless systems. *Communications Magazine, IEEE*, 52(2):186–195, February 2014. ISSN 0163-6804.

[17] G. J. Foschini and M. J. Gans. On limits of wireless communications in a fading environment when using mulitple antennas. *Wireless Pers. Comm.*, pages 311–335, 1998.

[18] G. G. Raleigh and J. M. Cioffi. Spatio-temporal coding for wireless communication. *IEEE Trans. Comm.*, 46(3):357–366, March 1998.

[19] K. Yu, M. Bengtsson, B. Ottersten, and M. Beach. Narrowband MIMO Channel Modeling for LOS Indoor Scenarios. In *Proceedings XXVIIth Triennial General Assembly of the Internationl Union of Radio Science (URSI)*, August 2002.

[20] L. Cottatellucci and M. Debbeh. On the Capacity of MIMO Rice Channels. In *Proceedings of the 42nd Allerton Conference*, 2004.

[21] Elisabeth de Carvalho. Massive MIMO: Communicating in the Near Field of a Large Aperture Massive Array System, September 2013. Project proposal.

[22] D.-S. Shiu, G. J. Foschini, M. J. Gans, and J. M. Kahn. Fading correlation and its effect on the capacity of multielement antenna systems. *IEEE Trans. Comm.*, 48(3):502–513, March 2000.

[23] D. Chizhik, G. J. Foschini, M. J. Gans, and R. A. Valenzuela. Keyholes, correlations, and capacities of multielement transmit and receive antennas. *IEEE Trans. Wireless Comm.*, 1 (2):361–368, March 2002.

[24] Moray Rumney, editor. *LTE and the Evolution to 4G wireless*. Agilent Technologies, 2nd edition, 2009. ISBN 9789881793515.

[25] David Tse and Pramod Viswanath. *Fundamentals of Wireless Communication*. Cambridge University Press, 2005. ISBN 0521845270.

[26] I. Sarris and A. R. Nix. Maximum MIMO Capacity in Line-of-Sight. *Fifth International Conference on Information, Communications and Signal Processing*, 2005.

[27] Frode Bøhagen, Pål Orten, and Geir E. Øien. On Spherical vs. Plane Wave Modeling of Line-of-Sight MIMO Channels. *IEEE Transactions on Communications*, 57(3):841–849, March 2009.

[28] Patrick C. F. Eggers, 2013. http://personprofil.aau.dk/profil/102698.

[29] Ole Nørklit and Jørgen Bach Andersen. Mobile radio environments and adaptive arrays. In *Personal, Indoor and Mobile Radio Communications. Wireless Networks - Catching the Mobile Future., 5th IEEE International Symposium on*, volume 2, pages 725–728, 1994. doi: 10.1109/WNCMF.1994.529184.

[30] Ole Nørklit, Patrick C. F. Eggers, and Jørgen B. Andersen. Jitter diversity in multipath environments. In *Vehicular Technology Conference, 1995 IEEE 45th*, volume 2, pages 853–857, July 1995. doi: 10.1109/VETEC.1995.504989.

[31] Patrick C. F. Eggers. *Dual directional channel formalisms and descriptions relevant for Tx-Rx diversity and MIMO*. EURO-COST, 2003. COST 273 – TD (03) 044.

[32] Andrea Goldsmith. *Wireless Communications*. Cambridge University Press, 2005. ISBN 0-471-988557-X.

[33] J. B. Andersen and J. Ø. Nielsen. *Multipath Richness – a measure of MIMO capacity in an environment*. EURO-COST, September 2004. COST 273 – TD (04) 157.

[34] J. Poutanen, K. Haneda, Lingfeng Liu, C. Oestges, F. Tufvesson, and P. Vainikainen. Parameterization of the cost 2100 mimo channel model in indoor scenarios. In *Antennas and Propagation (EUCAP), Proceedings of the 5th European Conference on*, pages 3606–3610, April 2011.

[35] Clayton Shepard, Hang Yu, Narendra Anand, Erran Li, Thomas Marzetta, Richard Yang, and Lin Zhong. Argos: Practical many-antenna base stations. In *Proceedings of the 18th Annual International Conference on Mobile Computing and Networking*, Mobicom '12, pages 53–64, 2012. ISBN 978-1-4503-1159-5. URL http://doi.acm.org/10.1145/2348543.2348553.

[36] V. Stankovic and M. Haardt. Generalized design of multi-user mimo precoding matrices. *Wireless Communications, IEEE Transactions on*, 7(3):953–961, March 2008. ISSN 1536-1276.

[37] Veljko Stankovic and Martin Haardt. Multi-user mimo downlink precoding for users with multiple antennas. In *Proc. of the 12-th Meeting of the Wireless World Research Forum (WWRF), Toronto, ON, Canada*, volume 10, pages 12–14, 2004.

[38] M. Kountouris, R. De Francisco, D. Gesbert, D. T M Slock, and T. Salzer. Low complexity scheduling and beamforming for multiuser mimo systems. In *Signal Processing Advances in Wireless Communications, 2006. SPAWC '06. IEEE 7th Workshop on*, pages 1–5, July 2006.

[39] A. Adhikary, J. Nam, J.-Y. Ahn, and G. Caire. Joint Spatial Division and Multiplexing. *ArXiv e-prints*, September 2012.

[40] Bin Song and M. Haardt. Effects of imperfect channel state information on achievable rates of precoded multi-user mimo broadcast channels with limited feedback. In *Communications, 2009. ICC '09. IEEE International Conference on*, pages 1–5, June 2009.

[41] T.L. Marzetta. Noncooperative cellular wireless with unlimited numbers of base station antennas. *Wireless Communications, IEEE Transactions on*, 9(11):3590–3600, November 2010. ISSN 1536-1276.

[42] C.B. Peel, B.M. Hochwald, and A.L. Swindlehurst. A vector-perturbation technique for near-capacity multiantenna multiuser communication-part i: channel inversion and regularization. *Communications, IEEE Transactions on*, 53(1):195–202, Jan 2005. ISSN 0090-6778.

[43] Q.H. Spencer, A.L. Swindlehurst, and M. Haardt. Zero-forcing methods for downlink spatial multiplexing in multiuser mimo channels. *Signal Processing, IEEE Transactions on*, 52(2): 461–471, Feb 2004. ISSN 1053-587X.

[44] Haifan Yin, D. Gesbert, M. Filippou, and Yingzhuang Liu. A coordinated approach to channel estimation in large-scale multiple-antenna systems. *Selected Areas in Communications, IEEE Journal on*, 31(2):264–273, February 2013. ISSN 0733-8716.

[45] Hong Yang and T.L. Marzetta. Performance of conjugate and zero-forcing beamforming in large-scale antenna systems. *Selected Areas in Communications, IEEE Journal on*, 31(2): 172–179, February 2013. ISSN 0733-8716.

[46] Haifan Yin and David Gesbert. Dealing with interference in distributed large-scale mimo systems: A statistical approach. *CoRR*, abs/1310.6674, 2013.

[47] Q.H. Spencer and M. Haardt. Capacity and downlink transmission algorithms for a multi-user mimo channel. In *Signals, Systems and Computers, 2002. Conference Record of the Thirty-Sixth Asilomar Conference on*, volume 2, pages 1384–1388 vol.2, Nov 2002.

[48] Steven Kay. *Intuitive Probability and Random Processes using MATLAB*. Springer, 2006. ISBN 978-0-387-24157-9. doi: 10.1007/b104645.

Part IV

Appendix

Appendix **A**

Mathematics behind Near Field and Far Field boundary distances

A.1 Region boundaries: mathematical background

The mathematical background lying behind the region boundaries can be easily found in classic literature. This subsection relates specifically to [6].
For simplicity, calculations are made as for a linear antenna in origo, placed along the z-axis and with an aperture of D [m], as shown in Fig. A.1. Radiation integrals are dependent on the expression of R, which in turn depends on the position of each of the antenna's charge. In this case, calculated at the point P in the same figure:

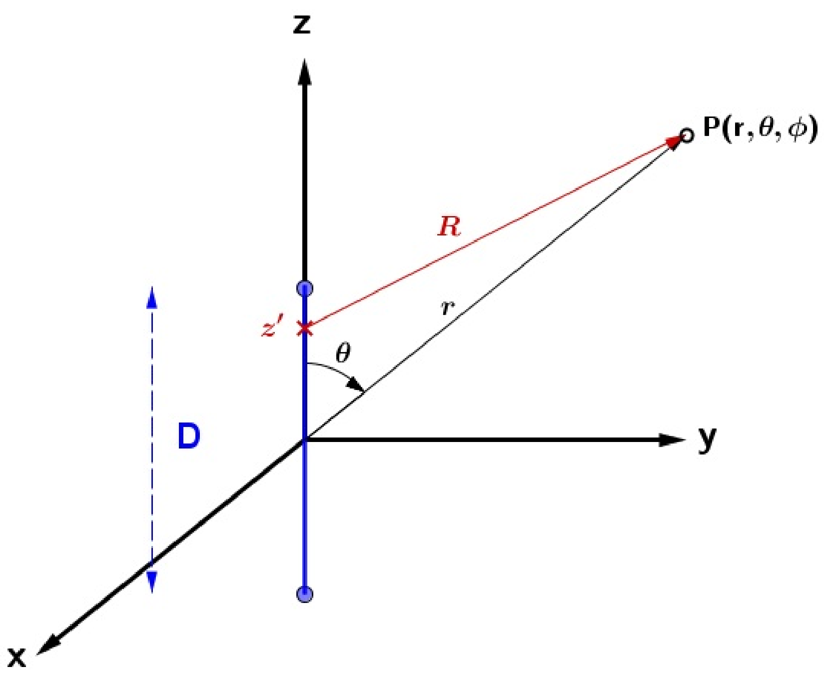

Figure A.1 *Antenna geometry.*

$$R = \sqrt{(x - x')^2 + (y - y')^2 + (z - z')^2} \tag{A.1}$$

$$= \sqrt{x^2 + y^2 + (z - z')^2} \tag{A.2}$$

If Cartesian coordinates are replaced by their Spherical equivalence and P is assumed to be located in the ZY plane, then R becomes:

$$R = \sqrt{r^2 - 2z'r\cos\theta + (z')^2} \tag{A.3}$$

Finally, using the Binomial Theorem, R can be approximated like this:

$$R \cong r - z'\cos\theta + \frac{(z')^2\sin^2\theta}{2r} + \frac{(z')^3\cos\theta\sin^2\theta}{2r^2} + \cdots \tag{A.4}$$

Being the higher order terms negligible if $r \gg z'$.
Both the Reactive-Radiating Near Field and the Radiating Near Field-Far Field boundaries are calculated as for approximations to the last expression regarding the maximum error those approximations can incur. That is to say, in the Far Field, R is taken as for expression A.4 for the electromagnetic field calculation through the radiation integral. Since R appears both in amplitude and phase components within this integral, there will be *amplitude* and *phase* approximations on R, which will produce both *amplitude* and *phase* errors in the integral. Those errors define the region boundaries. Phase errors are critical and are then the ones that are ordinarily considered. According to literature, antennas whose aperture is greater than a wavelength admit a maximum phase error of $\pi/8$ [rad] or 22.5 [°].

A.1.1 Far Field inner boundary: Far Field approximations

In this case,

- The second, third and fourth terms in expression A.4 are neglected for amplitude terms: $R \cong r$.
- Both the third and fourth terms in expression A.4 are neglected for phase terms: $R \cong r - z'\cos\theta$

In the case of the phase approximation, which is the critical one, the second term is much greater than the third one, so it would be the highest error contributor. The distance up to which those terms can be omitted will result in the Radiating Near Field-Far Field boundary expression.
The neglected term

$$\frac{(z')^2\sin^2\theta}{2r} \tag{A.5}$$

takes its maximum when $\theta = \pi/2$ and the maximum value is:

$$\max\left[\frac{(z')^2\sin^2\theta}{2r}\right] = \frac{(z')^2}{2r} \tag{A.6}$$

Thus, the maximum phase error would be a factor of the wavenumber k [rad/m] and must meet the following:

$$\varepsilon_{\text{phase}} = k\frac{(z')^2}{2r} \leq \frac{\pi}{8} \quad \text{[rad]} \tag{A.7}$$

The last expression is maximum when z' is D/2, being D the maximum aperture of the antenna:

$$\max\left[\varepsilon_{\text{phase}}\right] = k\frac{(D/2)^2}{2r} \leq \frac{\pi}{8} \quad \text{[rad]} \tag{A.8}$$

And so the Far Field inner boundary becomes defined like this:

$$r \geq \frac{2D^2}{\lambda} \quad \text{[m]} \tag{A.9}$$

A.1.2 Radiating Near Field inner boundary: Radiating Near Field Approximations

In this case, only the fourth term in expression A.4 on the preceding page is neglected, for phase terms. This omission will produce an error, whose maximum value can be calculated differentiating the neglected term with respect to θ and setting it to zero.

$$\frac{\mathrm{d}}{\mathrm{d}\theta}\left\{\frac{(z')^3\cos\theta\sin^2\theta}{2r^2}\right\}=0 \tag{A.10}$$

This happens when $\theta=\arctan(\pm\sqrt{2})=\theta_{MAX}$, which leads to the maximum phase error allowance:

$$\varepsilon_{\text{phase}}=k\frac{(z')^3\cos(\theta_{MAX})\sin^2(\theta_{MAX})}{2r^2}\leq\frac{\pi}{8}\quad[\text{rad}] \tag{A.11}$$

The phase error will be maximum when z' is D/2, being the result in that case:

$$\{\varepsilon_{\text{phase}}\}_{MAX}=k\frac{(D/2)^3\cos(\theta_{MAX})\sin^2(\theta_{MAX})}{2r^2}\leq\frac{\pi}{8}\quad[\text{rad}] \tag{A.12}$$

And so the Radiating Near Field inner boundary becomes defined like this:

$$r\geq 0.62\sqrt{\frac{D^3}{\lambda}}\quad[\text{m}] \tag{A.13}$$

Appendix **B**

Spherical-wave model optimisation parameters.

B.1 T-R distance.

Both simulations and measurements indicate that the distance between the transmitter and the receiver (T-R distance) determines capacity: a closer distance means higher capacity. Fig. B.1 accounts for capacity variation with respect to T-R distance for several array aperture sizes. Although mentioned below, the array geometry is also determinant to capacity. Precisely, the larger its aperture is, the better performance can be expected.

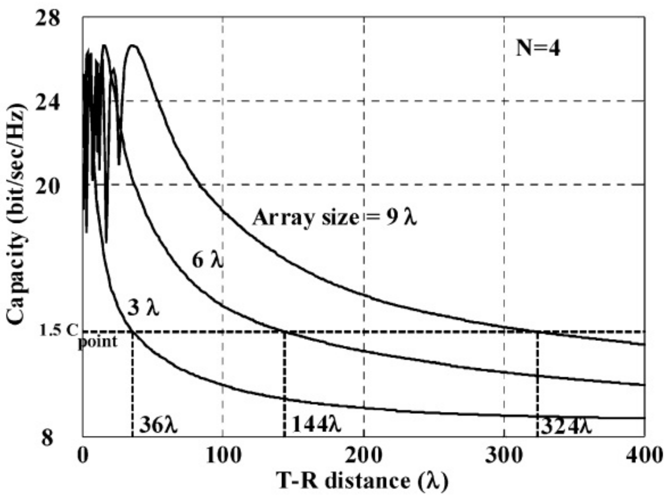

Figure B.1 *Capacity vs T-R distance for several array sizes, being the number of elements fixed to four at both. Ends are at null azimuth angles: at the broadside direction and parallel to each other. [7]*

B.2 Arrays geometry adjustment.

The authors of [7] also claim that the performance of a short-range MIMO system with the presence of LOS given by capacity as per the expression in eq. 5.8 on page 39 can be considerably increased if the proper DOD, DOA and array spacing are adjusted for a given T-R distance. The first two refer to the transmit and receive azimuth angles; the second one, to each end's antenna spacing. It happens that the azimuth angles and the antenna spacing are interrelated. In general, though, a higher antenna separation means a larger aperture, which in turn provokes

higher system capacity (see fig. B.2).
Azimuth angles DOD and DOA ultimately come down to the geometry given by the arrays:

- The relative orientation between the transmit and receive arrays.
- The echelon angle between them (location).

Interrelation is given in thee form of capacity stability: for a given T-R distance, capacity will possess a stable tendency for a range of DOD and DOA for a varying array spacing. However, at a certain spacing, ripples appear. For instance, it is explained in [7] that for a T-R distance of 100λ, for an antenna spacing from 1λ to 5λ, the maximum capacity is achieved when both azimuth angles are null: when both arrays are parallel to each other and at the broadside direction. Although when in general a higher aperture (given by a higher antenna spacing) means higher capacity, from 5λ onwards capacity ceases to be maximum at the broadside direction, since ripples appear. Ripples still reach the maximum capacity value, though.
The last example can be seen in fig. B.2.

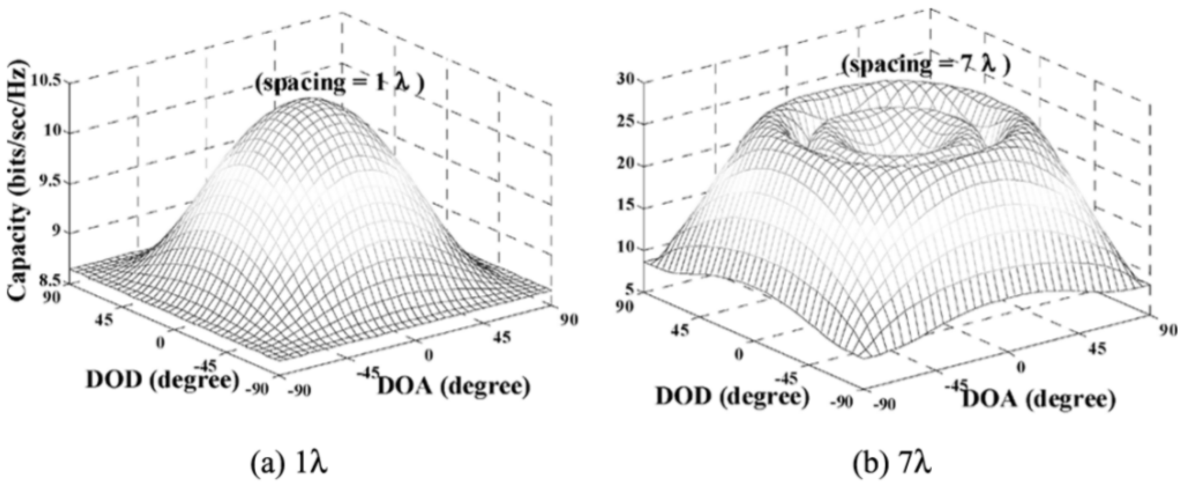

Figure B.2 *Change in MIMO capcity due to antenna spacing, as a function of DOD and DOA. The T-R separation is* 100λ*, and SNR set to 20 [dB]. [7]*

Appendix **C**

COST2100 cluster modelling approach and cluster types.

C.1 Clusters and Large Scale Parameters. Modelling process approaches in GSCMs.

Two aspects constitute the channel models. These are the clusters themselves and some Large Scale Parameter (LSP).

It has been shown, experimentally, that MPCs arrive at a MT in packets. These packets are the result of each object scattering the incoming signals with similar delays and directions. Intuitively, this can be explained by means of a building: if a building acts as an interacting object, it would create several paths due to the scattering features on the building (windows, doors, balconies, corners, etc), which may produce similar delays and directions. The scatterers which result in such a behaviour are grouped together into so-called clusters. Also, sometimes clusters can contain scatterers belonging to different objects.

Where clusters can be parametrised quantities, it is also necessary to allow to model to reflect reality. The LSPs are parameters that reflect the channel parameters globally, such as delay and angular spread at the MT. They are a good measure of how much the model matches experimental observations. However, for this to happen it is necessary to parametrise clusters individually, while at the same time providing global accuracy. To do this, there are two main approaches (see below).

C.1.1 Modelling process approaches in GSCMs.

(a) One approach is to use a **system level approach**. When the stochastic distribution of the LSPs at each instance is known, then the LSPs are defined by their distribution for each channel instance. Then, clusters (and then MPCs) are generated accordingly for any given location of both the BS and MT. An advantage of this is that the LSPs statistics are always guaranteed, and will match experimental results. However, large scale mobility of the MT cannot be simulated, because of the rigid structure of the system level approach, which does not support continuous channel descriptions over intervals larger than the autocorrelation distance. In other words, both the BS and MT have to remain stationary. Also, the addition of new LSPs, such as the inter-link correlation, requires an entire redefinition of the environment.

(b) Another approach is the **cluster-level approach**. This is used when the stochastic properties of the LSPs are not used initially. Then in this case, clusters are generated according to the following procedure.

- First, given the location of the BS, a very large set of clusters are defined throughout the simulation environment, based on their stochastic properties. These are mainly,
  - Attenuation.
  - DOA.
  - DOD.
  - Delay.

  These stochastic properties are given by the scatterers contained in each cluster. **The main feature scatterers have is that they introduce fading in the channel due to the non-coherency provided by their random phase**.
- Secondly, for a given MT location, it is determined which of all clusters are seen by the MT. If seen, then at what extent, i.e. how much they contribute. Clusters seen by a MT are defined by each of the clusters' VRs. An example of a MT in an environment

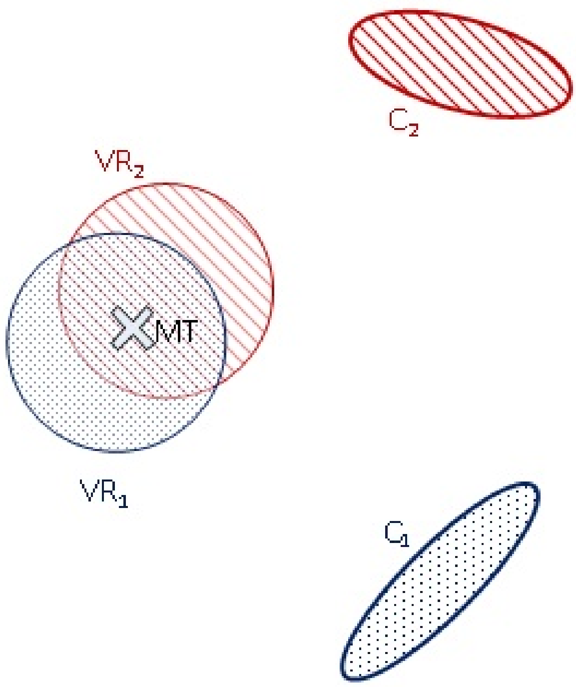

Figure C.1 *Visibility regions.*

  consisting of VRs and clusters is seen in fig. C.1. In this example, the MT is inside VR_1 belonging to cluster C_1 and VR_2 belonging to cluster C_2. Depending on where within each VR the MT is, its cluster's contribution will be greater of lesser. P.eg., in fig. C.1 since it is closer to the centre of VR_1 than it is to the centre of VR_2, the contribution of cluster C_1, given by its Visibility Gain, will be greater. This is namely accounted for by each of the cluster's VR gains.
- Thirdly and finally, the LSPs are synthesised based on the clusters. This is only done once for the entire environment at each time instance.

Contrarily to the system level approach, this model takes into account the mobility of the MT. Additionally, time-invariant channels can be modelled, i.e. clusters' statistics can be modelled differently at each time instance. However, the disadvantage of this approach is that any single realisation of the channel will exhibit large deviations of the LSP statistics compared to a system-level GSCM, but average LSP statistics remain typically consistent.

COST2100 is a cluster-level GSCM.

C.2 Clusters in COST2100.

In the original proposal of the COST2100 model, the aim was to simulate the radio channel between a static multiple-antenna BS and a (mobile) multiple-antenna MT.

Doing this, two types of clusters were defined based on their proximity to the MT. These two types are *local clusters* and *far clusters*; furthermore, far clusters are subdivided into *single-bounce* and *multiple-bounce* clusters. So in the end, COST2100 cluster groups would be:

- Local clusters.
- Single-bounce clusters (far clusters).
- Multiple-bounce clusters (far clusters).

Local clusters are located around the MT or BS, and are characterised by single-bounce scatterers only. They are always visible to either the MT or the BS.

Far clusters are visible to the MT only if this is inside their VRs. They are distributed throughout the simulation area, with an average density following a Poisson distribution.

Characterisation of MPCs depends on whether the MPC originates from a single- or multiple-bounce cluster. Single-bounce clusters can be explicitly mapped to a certain position, according to their delays and angles through a geometric representation. However, multiple-bounce clusters can not explicitly be mapped to a certain point, unless two representations are performed. One of them would correspond to the viewpoint from the BS, while the other to that of the MT. These two representative clusters are necessary single-bounce clusters, because they could not have any geometric mapping otherwise. The multiplicity of the bounces is modelled with a link between the two of them, called inter-link delay. Such two clusters are called *twin clusters*. The reason for this is that geometric mapping of the scatterers inside are identical for both, in the worst scenario, scaled. This can be seen in fig. 6.1 on page 45

Finally, there is the CIR, which has been noted as $\mathbf{H}$ in previous chapters. We remind the reader, that definition of CIR $\mathbf{H}$ of the space-time channel is the main purpose of any wireless transmission model. At a specific time instance, the CIR of a channel is obtained by the superposition of all arriving MPCs at the MT. The amplitude of each MPC is jointly determined by,

- the path loss from the cluster to which it belongs,
- the large-scale properties of the cluster to which it belongs,
- the small-scale properties of each of the scatterers belonging to the specific cluster, which are non-coherent and thus introduce fast fading via their random phase.

On top of this, the CIR must be combined with the antenna steering vectors to complete the MIMO channel matrix [8].

Appendix **D**

Cluster power instroduction as per proposed modelling.

Chap. 6 on page 43 gives account for the Point-to-Point channel model that has been constructed in this project. It is sated that the weighting of each of the scatterers in the system is done as per a Complex Gaussian variable, and that the variances of the real and imaginary parts of this variable are selected so that the mean sum power of the whole cluster yields unity.

D.1 Mathematical computation of the power of a cluster

A scatterer's weighting is defined by COST2100 as a complex Gaussian ($\mathcal{C}N$) variable. For the i$^{\text{th}}$ scatterer of a cluster, if its weighing is written like a_i, then

$$a_i \sim \mathcal{C}N$$

It has been stated in chap. 6 on page 43 what the mean of each of the components is (zero), as well as what their variances are so that a mean sum power of one is achieved ($^{0.5}/_{N_s^c}$, being N_s^c the number of scatterers in cluster c). Let's for this computation assume a priori information on the variances is unknown and let's inversely compute what their value should be to meet this power goal. Let's as well assume their means are zero.
Then, let A_i and B_i be Gaussian distributed random variables with zero mean and different variance according to $\sigma^2_{A_i}$ and $\sigma^2_{B_i}$. That is

$$A_i \sim \mathcal{N}(0, \sigma^2_{A_i}) \qquad B_i \sim \mathcal{N}(0, \sigma^2_{B_i})$$

The complex weighting is then defined like,

$$a_i = A_i + \mathrm{j}B_i \tag{D.1}$$

Taking the expected value of the power of each channel term due to all scatterers in cluster c yields:

$$\mathbb{E}\left[|h^{\mathrm{c}}_{nm}|^2\right] = \mathbb{E}\left[\left|\sum_{i=1}^{N_s^c} a_i \cdot \frac{e^{-\mathrm{j}kR_{mi}}}{(R_{mi})^{n_1}} \cdot \frac{e^{-\mathrm{j}kR_{in}}}{(R_{in})^{n_2}}\right|^2\right] \;[W] \tag{D.2}$$

Rpq [m] is the distance from p to q and vice versa and k [rad/m] is the signal's wavelength.
The components on distances account for the Free Space pathloss of the signal as per th m$^{\text{th}}$ transmit antenna to the n$^{\text{th}}$ receive antenna via the i$^{\text{th}}$ scatterer an due to the location of the scatterers; the exponentials are their signal propagation components. Thus, the power *introduced* by the cluster is due to each of the scatterer's weighting. The aim is to bound the expected

introduced power via the definition of the consequent variances of each of the variables in a_i. Let us define the expected introduced power by cluster c omitting the Free Space pathloss action, $\mathbb{E}\left[\mathrm{P}^c\right]$, like:

$$\mathbb{E}\left[\mathrm{P}^c\right] = \mathbb{E}\left[\left|\sum_{i=1}^{N_s^c} a_i\right|^2\right] \quad [W] \tag{D.3}$$

Applying the expression of the square of a sum:

$$\mathbb{E}\left[\mathrm{P}^c\right] = \mathbb{E}\left[\sum_{i=1}^{N_s^c} |a_i|^2 + \sum_{i\neq j}^{N_s^c} a_i \cdot a_j^*\right] \quad [W] \tag{D.4}$$

where * denotes complex conjugation. Since the Expected Value operator is linear, we may split eq. D.4 into two terms, as follows:

$$\mathbb{E}\left[\mathrm{P}^c\right] = \mathbb{E}\left[\sum_{i=1}^{N_s^c} |a_i|^2\right] + \mathbb{E}\left[\sum_{i\neq j}^{N_s^c} a_i \cdot a_j^*\right] \quad [W] \tag{D.5}$$

Eq. D.5 may be written like:

$$\mathbb{E}\left[\mathrm{P}^c\right] = \mathrm{E}_1 + \mathrm{E}_2 \tag{D.6}$$

$$\mathrm{E}_1 = \mathbb{E}\left[\sum_{i=1}^{N_s^c} |a_i|^2\right] \tag{D.7}$$

$$\mathrm{E}_2 = \mathbb{E}\left[\sum_{i\neq j}^{N_s^c} a_i \cdot a_j^*\right] \tag{D.8}$$

$\mathbf{E}_2$

We now turn our attention to term E_2, given by eq. D.8.
Firstly, we compute the expected value of the random variable given by the product of a_i and a_j. Assuming a_i and a_j are independent to each other, the expected value of their product may become the product of their expected values, which we compute assisted by eq. D.1 on the previous page and then:

$$\begin{aligned}\mathbb{E}\left[a_i \cdot a_j^*\right] &= \mathbb{E}\left[a_i\right] \cdot \mathbb{E}\left[a_j^*\right] \\ &= \mathbb{E}\left[A_i + \mathrm{j}B_i\right] \cdot \mathbb{E}\left[A_j - \mathrm{j}B_j\right] \\ &= \left\{\mathbb{E}\left[A_i\right] + \mathrm{j}\mathbb{E}\left[B_i\right]\right\} \cdot \left\{\mathbb{E}\left[A_j\right] - \mathrm{j}\mathbb{E}\left[B_j\right]\right\} \\ &= 0\end{aligned} \tag{D.9}$$

Finally, applying the Law of Large Numbers (assuming again a_i and a_j are independent to each other, and knowing a priori they are identically distributed, then assuming i.i.d.; and assuming N_s^c is high enough), we may yield a result for E_2:

$$\begin{aligned}\mathrm{E}_2 &= \mathbb{E}\left[\sum_{i\neq j}^{N_s^c} a_i \cdot a_j^*\right] \\ &= \{\text{Law of Large Numbers, weighting is i.i.d. and } \mathrm{N}_s^c \uparrow\uparrow\} \\ &= N_s^c \cdot \mathbb{E}\left[a_i \cdot a_j^*\right] \\ &= 0\end{aligned} \tag{D.10}$$

$\mathbf{E}_1$

We now focus on term E_1, given by eq. D.7 on the facing page and that we reproduce below:

$$\mathrm{E}_1 = \mathbb{E}\left[\sum_{i=1}^{N_s^c} |a_i|^2\right] \tag{D.11}$$

If we split the weighting into the components defined in eq. D.1 on page 177,

$$\begin{aligned}
\mathrm{E}_1 &= \mathbb{E}\left[\sum_{i=1}^{N_s^c} |A_i + \mathrm{j}B_i|^2\right] \\
&= \mathbb{E}\left[\sum_{i=1}^{N_s^c} \left(\sqrt{A_i^2 + B_i^2}\right)^2\right] \\
&= \sum_{i=1}^{N_s^c} \left(\mathbb{E}\left[A_i^2\right] + \mathbb{E}\left[B_i^2\right]\right) \\
&= \sum_{i=1}^{N_s^c} \left(\left[\sigma_{A_i}^2 + \cancelto{0}{(\mathbb{E}[A_i])^2}\right] + \left[\sigma_{B_i}^2 + \cancelto{0}{(\mathbb{E}[B_i])^2}\right]\right) \\
&= \sum_{i=1}^{N_s^c} \left(\sigma_{A_i}^2 + \sigma_{B_i}^2\right) \\
&= N_s^c \cdot \left(\sigma_{A_i}^2 + \sigma_{B_i}^2\right)
\end{aligned} \tag{D.12}$$

$\mathbb{E}[\mathbf{P}^c]$

Finally, $\mathbb{E}[\mathrm{P}^c]$ results in:

$$\begin{aligned}
\mathbb{E}[\mathrm{P}^c] &= \mathrm{E}_1 + \mathrm{E}_2 \\
&= N_s^c \cdot \left(\sigma_{A_i}^2 + \sigma_{B_i}^2\right) + 0 \\
&= N_s^c \cdot \left(\sigma_{A_i}^2 + \sigma_{B_i}^2\right)\ [W]
\end{aligned} \tag{D.13}$$

If we allow the same variance for both weighting components, i.e. $\sigma_{A_i}^2 = \sigma_{B_i}^2 = \sigma^2$, it follows:

$$\mathbb{E}[\mathrm{P}^c] = N_s^c \cdot 2 \cdot \sigma^2 \tag{D.14}$$

It is desired that the expected total power introduced by the cluster c be 1[W]:

$$\mathbb{E}[\mathrm{P}^c] \triangleq 1\ [W] \tag{D.15}$$

Conclusively, the variance value that would meet our purposes is:

$$\sigma^2 \triangleq \frac{1}{2 \cdot N_s^c} = \frac{0.5}{N_s^c} \tag{D.16}$$

Appendix **E**

Closed-form capacity derivations for the instantaneous CSIT aquisition case.

This appendix accounts for the derivation of the closed-form expression of the open-loop capacity under the assumption there is instantaneous CSIT acquisition and particularises that expression to the case in which the optimal power allocation is done as per waterfilling.

E.1 Derivation of the closed-form expression of capacity for instantaneous CSIT

In the case there is instantaneous CSIT acquisition, capacity can be written like:

$$\begin{aligned}
\mathrm{C}^{\mathrm{CSIT}} &= \max\left\{\mathcal{R}_{\max}\right\} \\
&= \max_{\mathbf{R}_{\mathrm{XX}},\mathrm{Tr}(\mathbf{R}_{\mathrm{XX}})\leq\bar{P}}\left\{\log_2\left|\mathbf{I}+\frac{1}{\sigma_n^2}\mathbf{H}\mathbf{R}_{\mathrm{XX}}\mathbf{H}^{\mathrm{H}}\right|\right\} \\
&= \log_2\left|\mathbf{I}+\frac{1}{\sigma_n^2}\mathbf{H}\mathbf{R^o}_{\mathrm{XX}}\mathbf{H}^{\mathrm{H}}\right| \\
&= \sum_{k=1}^{r_{\mathrm{H}}}\log_2\left(1+\frac{P_k^o\lambda_k^2}{\sigma_n^2}\right) \quad \text{[bptx]}
\end{aligned} \tag{E.1}$$

Where $\mathcal{R}_{\max}$ is the maximum transmission rate, $|\quad|$ is the determinant operator, $\mathbf{I}$ is the identity matrix, $\mathbf{H}$ is the channel matrix, the superscript $^{\mathrm{H}}$ denotes the Hermitian conjugate, $\mathbf{R}_{\mathrm{XX}}$ is the input covariance matrix, $\mathbf{X}$ is the input signal vector, σ_n^2 is the noise power, $\mathrm{Tr}(\cdot)$ is the Trace operator, $\bar{P}$ is the maximum allowed transmit power and $\mathbf{R}^{\mathbf{o}}_{\mathrm{XX}}$ is the input covariance matrix resulting from optimal power allocation, r_{H} is the rank of the channel matrix (the number of eigenvalues greater than zero), P_k^o [W] is the optimal power allocation to eigenchannel k as per waterfilling and λ_k is the $\mathrm{k^{th}}$ eigenvalue of the channel matrix.

Throughout this discussion, an MxN MIMO system will be assumed, i.e. formed of an M-antenna transmitter and an N-antenna receiver.

The transmit power from the $\mathrm{i^{th}}$ antenna is $\mathbb{E}\left[|x_i|^2\right]$, where x_i is the $\mathrm{i^{th}}$ transmit signal. The sum of transmit powers is then constrained such that,

$$\sum_{i=1}^{M}\mathbb{E}\left[|x_i|^2\right]\leq\bar{P} \quad \text{[W]} \tag{E.2}$$

Furthermore, as

$$\sum_{i=1}^{M}\mathbb{E}\left[|x_i|^2\right]=\mathrm{Tr}(\mathbf{R}_{XX}) \quad \text{[W]} \tag{E.3}$$

where $\mathbf{R}_{XX}$ is the (auto)covariance matrix of the transmit symbols, transmit power constraint can be rewritten so

$$\mathrm{Tr}(\mathbf{R}_{XX}) \leq \bar{P} \quad [\mathrm{W}] \tag{E.4}$$

applies[1].

Furthermore, since $\mathbb{E}\left[|x_i|^2\right]$ can be regarded as power and assuming the transmit signals are uncorrelated with each other, the (auto)covariance matrix $\mathbf{R}_{XX}$, as derived in app. F on page 187, may be rewritten as,

$$\mathbf{R}_{XX} = \begin{bmatrix} P_1 & 0 & 0 & 0 \\ 0 & P_2 & 0 & 0 \\ \vdots & \vdots & \ddots & \vdots \\ 0 & 0 & 0 & P_M \end{bmatrix} \tag{E.5}$$

In other terms, the SVD of a channel matrix $\mathbf{H}$ is,

$$\mathbf{H} = \mathbf{U}\mathbf{\Lambda}\mathbf{V}^{\mathrm{H}} \tag{E.6}$$

where the superscript ^{H} denotes the hermitian transpose.
To quickly illustrate the principle of the SVD of the channel in MIMO systems, let us reproduce the example of a 2×2 MIMO channel found in [11]. Let the channel matrix of this system be,

$$\mathbf{H} = \begin{bmatrix} h_{11} & h_{12} \\ h_{21} & h_{22} \end{bmatrix}. \tag{E.7}$$

Then its SVD is,

$$\mathbf{H} = \begin{bmatrix} h_{11} & h_{12} \\ h_{21} & h_{22} \end{bmatrix} = \mathbf{U}\mathbf{\Lambda}\mathbf{V}^{\mathrm{H}} = \begin{bmatrix} \mathbf{u}_1 & \mathbf{u}_2 \end{bmatrix} \begin{bmatrix} \lambda_1 & 0 \\ 0 & \lambda_2 \end{bmatrix} \begin{bmatrix} \mathbf{v}_1^{\mathrm{H}} \\ \mathbf{v}_2^{\mathrm{H}} \end{bmatrix} \tag{E.8}$$

where

$$\mathbf{v}_1 = \begin{bmatrix} v_{11} \\ v_{12} \end{bmatrix}, \quad \mathbf{v}_2 = \begin{bmatrix} v_{21} \\ v_{22} \end{bmatrix}, \quad \mathbf{u}_1 = \begin{bmatrix} u_{11} \\ u_{12} \end{bmatrix} \text{ and } \quad \mathbf{u}_2 = \begin{bmatrix} u_{21} \\ u_{22} \end{bmatrix}. \tag{E.9}$$

Based on the SVD of the channel matrix, two observations can be made.

The number of independent streams that can be multiplexed, is determined by the rank of the channel. The rank of channel $\mathbf{H}$ is denoted as r_{H}, and is defined as the number of nonzero singular values of $\mathbf{H}$. Equivalently, the rank is the minimal value between the number of independent row and columns of $\mathbf{H}$, such that $r_{\mathrm{H}} \leq \min(N, M)$.

Furthermore, the relationship between the singular values and channel energy is proven to be useful. The energy in the channel is written as

$$\sum_{i=1}^{N}\sum_{j=1}^{M} |h_{ij}|^2 \tag{E.10}$$

which can be rewritten as $\mathrm{Tr}(\mathbf{H}\mathbf{H}^{\mathrm{H}})$. Using the SVD and the two relationships $\mathbf{H}\mathbf{H}^{\mathrm{H}} = \mathbf{U}\mathbf{\Lambda}^2\mathbf{U}^{\mathrm{H}}$ and $\mathrm{Tr}(\mathbf{H}\mathbf{H}^{\mathrm{H}}) = \mathrm{Tr}(\mathbf{H}^{\mathrm{H}}\mathbf{H})$, the relationship between channel energy and its singular values is,

$$\mathrm{Tr}(\mathbf{H}\mathbf{H}^{\mathrm{H}}) = \sum_{i=1}^{N}\sum_{j=1}^{M} |h_{ij}|^2 = \sum_{i=1}^{r_{\mathrm{H}}} \lambda_i^2 \tag{E.11}$$

[1] To see how this constraint is derived see app. F on page 187.

where $r_H \leq \min(N, M)$. Additionally, since $\mathrm{Tr}(\mathbf{H}\mathbf{R}_{XX}\mathbf{H}^{\mathrm{H}}) = \mathrm{Tr}(\mathbf{H}^{\mathrm{H}}\mathbf{R}_{XX}\mathbf{H})$ also applies then,

$$
\begin{aligned}
\mathrm{C}^{\mathrm{CSIT}} &= \max\{\mathcal{R}_{\max}\} \\
&= \max_{\mathbf{R}_{\mathrm{XX}}, \mathrm{Tr}(\mathbf{R}_{\mathrm{XX}}) \leq \bar{P}} \left\{ \log_2 \left| \mathbf{I} + \frac{1}{\sigma_n^2} \mathbf{H}\mathbf{R}_{\mathrm{XX}}\mathbf{H}^H \right| \right\} \\
&= \log_2 \left| \mathbf{I} + \frac{1}{\sigma_n^2} \mathbf{H}\mathbf{R^o}_{\mathrm{XX}}\mathbf{H}^{\mathrm{H}} \right| \\
&= \log_2 \left| \mathbf{I} + \frac{1}{\sigma_n^2} \mathbf{U}\mathbf{\Lambda}\mathbf{V}^{\mathrm{H}}\mathbf{R^o}_{\mathrm{XX}}\mathbf{U}^{\mathrm{H}}\mathbf{\Lambda}^{\mathrm{H}}\mathbf{V} \right| \\
&= \log_2 \left| \mathbf{I} + \frac{1}{\sigma_n^2} \begin{bmatrix} P_1^o|\lambda_1^2| & 0 & 0 & 0 \\ 0 & P_2^o|\lambda_2^2| & 0 & 0 \\ \vdots & \vdots & \ddots & \vdots \\ 0 & 0 & 0 & P_{r_{\mathrm{H}}}^o|\lambda_{r_{\mathrm{H}}}^2| \end{bmatrix} \right| \\
&= \log_2 \left| \begin{bmatrix} \frac{P_1^o\lambda_1^2}{\sigma_n^2} + 1 & 0 & 0 & 0 \\ 0 & \frac{P_2^o\lambda_2^2}{\sigma_n^2} + 1 & 0 & 0 \\ \vdots & \vdots & \ddots & \vdots \\ 0 & 0 & 0 & \frac{P_{r_{\mathrm{H}}}^o\lambda_{r_{\mathrm{H}}}^2}{\sigma_n^2} + 1 \end{bmatrix} \right| \\
&= \log_2 \left[\prod_{k=1}^{r_{\mathrm{H}}} \left(1 + \frac{P_k^o\lambda_k^2}{\sigma_n^2} \right) \right] \\
&= \sum_{k=1}^{r_{\mathrm{H}}} \log_2 \left(1 + \frac{P_k^o\lambda_k^2}{\sigma_n^2} \right) \quad [\mathrm{bptx}]
\end{aligned} \tag{E.12}
$$

E.2 Waterfilling to achieve optimal power allocation

A method to find the optimal covariance matrix that maximises eq. E.12 is to employ waterfilling, which can be roughly described as rewarding the stronger eigenchannels (with more transmit power) while punishing the weaker ones (with less power, which can even be zero) [11].
Waterfilling redefines the SNR for each eigenmode transmission k,

$$\rho_k = \frac{P_k\lambda_k^2}{\sigma_n^2} \quad [\cdot] \tag{E.13}$$

where λ_k are singular values of the k^{th} eigenchannel, σ_n^2 is the noise power and P_k is the assigned power to each eigenchannel. In addition, a new quantity, γ_k is introduced. γ_k can be understood as the SNR of the k^{th} eigenchannel due to the eigenchannel's gain only (so assuming a transmit power of one, i.e. normalised to the transmit power). It is defined as,

$$\gamma_k = \frac{\lambda_k^2}{\sigma_n^2}, \quad k = 1, \ldots, r_H \quad [\cdot] \tag{E.14}$$

where again r_{H} is the rank of $\mathbf{H}$, defined as the number of nonzero singular values of $\mathbf{H}$ [11]. Thus the eigenmode SNR is defined as,

$$\rho_k = P_k\gamma_k \quad [\cdot] \tag{E.15}$$

for the k^{th} eigenchannel. The capacity of each eigenchannel with transmit power P_k is the capacity of an AWGN channel with SNR $= P_k\gamma_k$, i.e. capacity is equal to $\log_2(1 + P_k\gamma_k)$. To achieve the capacity of the total MIMO channel the power of each eigenchannel is to be adjusted, while complying with the overall power constraint given by,

$$\sum_{k=1}^{r_{\mathrm{H}}} P_k = \bar{P} \quad [W] \tag{E.16}$$

Therefore the capacity of the MIMO channel is the sum of the individual capacities for each eigenchannel, having previously adjusted the power assigned to each eigenchannel optimally:

$$\begin{aligned}
\mathrm{C}^{\mathrm{CSIT}} &= \max_{\sum_{k=1}^{r_\mathrm{H}} P_k \leq \bar{P}} \left\{ \sum_{k=1}^{r_\mathrm{H}} \log_2(1 + P_k \gamma_k) \right\} \\
&= \sum_{k=1}^{r_\mathrm{H}} \log_2(1 + P_k^o \gamma_k) \quad [\text{bptx}] \qquad \text{(E.17)}
\end{aligned}$$

where the superscript ^{o} denotes optimised transmit power. [11]

Method

In waterfilling, power is allocated to eacheigen channel in an iterative way by following,

$$P_k^o = \frac{1}{\gamma_0} - \frac{1}{\gamma_k} \geq 0 \quad [W] \qquad \text{(E.18)}$$

where

$$\frac{1}{\gamma_0} = \frac{1}{r_\mathrm{WF}} \left(\bar{P} + \sum_{k=1}^{r_\mathrm{WF}} \frac{1}{\gamma_k} \right) \quad / \quad \frac{1}{\gamma_0} - \frac{1}{\gamma_k} \geq 0 \quad \forall k \qquad \text{(E.19)}$$

$1/\gamma_k = \sigma_n^2/\lambda_k^2$ is an indication of badness. For each iteration $1/\gamma_k$ is constant, whereas $1/\gamma_0$ varies. Basically what waterfilling does is to assign more power to the best eigenchannel. Let the best possible channel conditions be assumed. If this is the case, each singular value would fulfil

$$\lambda_1 = \lambda_2 = \ldots = \lambda_k = \infty. \qquad \text{(E.20)}$$

Thus if each singular value is infinite, $1/\lambda_k$ is zero, and the sum in eq. E.19 is zero, resulting in

$$\frac{1}{\gamma_0} = \frac{\bar{P}}{r_\mathrm{WF}}. \qquad \text{(E.21)}$$

This means that the average total power is distributed evenly over all eigenchannels (in other words, all the eigenchannels are summoned) and that $r_\mathrm{WF} = r_\mathrm{H}$. This might happen as well in a situation in which the eigenvalues are not infinite, even in a situation in which they are not all equal to each other (see subsec. E.2).
In any case, though, had the singular values not been equal and infinitely large, the requirement in eq. E.18 will come into play. If the badness of an eigenchannel is higher than the level of waterfilling given by $1/\gamma_0$, that eigenchannel is discarded.Generally speaking, waterfilling can be thought of as a method to provide better capacity to the best channels, while discarding the worst channels. Fig. E.1 on the facing page is a pictorial example of waterfilling application, where channels are ordered in descending level of strength. Four channels are taken as an example. Only three of them are summoned after waterfilling application, resulting in a waterfilling rank of three ($P_4^o = 0$).

Performance at high and low SNR levels.

At **high SNR**, the power allocated to each eigenchannel is approximately constant and equal to $\bar{P}/r_\mathrm{H}$ [W]. This is because at a high SNR, the waterfilling threshold $1/\gamma_0 \gg 1/\gamma_k \quad \forall k$. In this case, the capacity of a MIMO channel becomes, [11]

$$\begin{aligned}
\mathrm{C}^{\mathrm{CSIT}} &= \sum_{k=1}^{r_\mathrm{H}} \log_2 \left(1 + \frac{\bar{P}}{r_\mathrm{H}} \gamma_k \right) &\text{(E.22)} \\
&= \sum_{k=1}^{r_\mathrm{H}} \log_2 \left(1 + \frac{\bar{P}}{r_\mathrm{H}} \frac{\lambda_k^2}{\sigma_n^2} \right) &\text{(E.23)} \\
&= \sum_{k=1}^{r_\mathrm{H}} \log_2 \left(1 + \rho \frac{\lambda_k^2}{r_\mathrm{H}} \right) \quad [\text{bptx}] &\text{(E.24)}
\end{aligned}$$

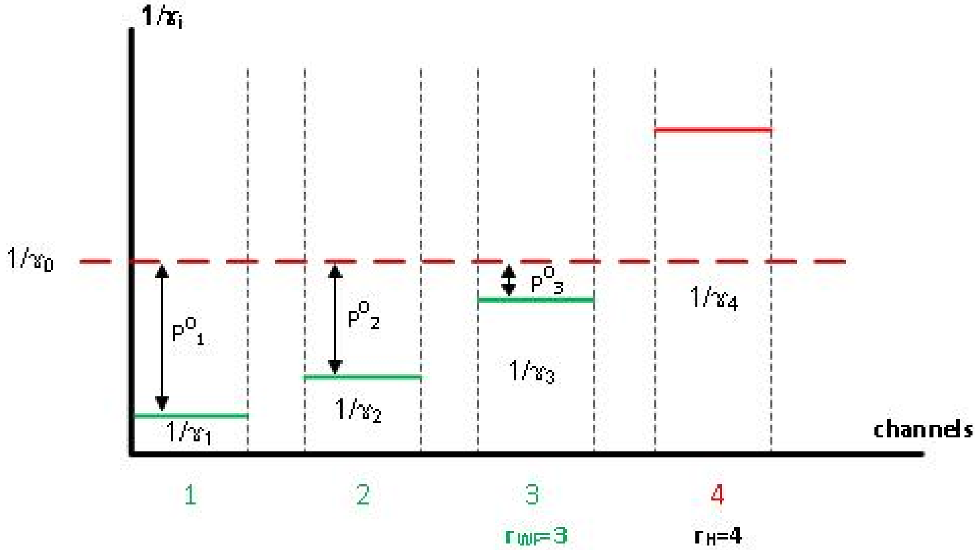

Figure E.1 *Waterfilling application pictorial example.*

Where $\rho = \bar{P}/\sigma_n^2$ is the SNR of the total channel (referred to as simply *SNR* throughout the project).
At high SNR, then, all channels are summoned and the ranks of both the channel matrix and as per watefilling are the same. The best case happens if all eigenchannels are equal to each other (same channel energy), achieving then the maximum level of capacity.

$$\lambda_1 = \lambda_2 = \cdots = \lambda_{r\mathrm{H}} \tag{E.25}$$

As explained in chap. 7 on page 55, a measure to determine how equal the eigenvalues are to each other is the CN. In this project, though, we restrict the use of the CN two the case in which the receiver is made up of two antennas only and use another proposed metric called NPCG in the rest of the cases.

At **low SNR**, the optimal waterfilling strategy is to allocate all power to the strongest eigenmode. Assuming this, capacity becomes,

$$\mathrm{C}^{\mathrm{CSIT}} \approx \log_2\left(1 + \rho\lambda_{\max}^2\right) \quad [\mathrm{bptx}] \tag{E.26}$$

A single stream is now summoned.

Appendix **F**

Input covariance matrix of a MIMO system

F.1 Derivation

For the general case and considering the transmitter consists of M antennas, the (auto)covariance matrix is given as,

$$\mathbf{C}_{XX} = \begin{bmatrix} \mathbb{E}\left[(x_1-\mu_1)(x_1-\mu_1)^{\mathrm{T}}\right] & \cdots & \mathbb{E}\left[(x_1-\mu_1)(x_M-\mu_M)^{\mathrm{T}}\right] \\ \vdots & \ddots & \vdots \\ \mathbb{E}\left[(x_M-\mu_M)(x_1-\mu_1)^{\mathrm{T}}\right] & \cdots & \mathbb{E}\left[(x_M-\mu_M)(x_M-\mu_M)^{\mathrm{T}}\right] \end{bmatrix} \tag{F.1}$$

where x_m is the input signal at the m$^{\mathrm{th}}$ transmit antenna, μ_m is the mean value of x_m and $\mathbb{E}\,[]$ is the expectation operator. If x_m is zero mean for all $m \in [1, \ldots \mathrm{M}]$, $\mathbf{C}_{XX}$ collapses into the (auto)correlation matrix of the input signals $\mathbf{R}_{XX}$, such that

$$\mathbf{R}_{XX} = \begin{bmatrix} \mathbb{E}\left[x_1 x_1^{\mathrm{T}}\right] & \cdots & \mathbb{E}\left[x_1 x_M^{\mathrm{T}}\right] \\ \vdots & \ddots & \vdots \\ \mathbb{E}\left[x_M x_1^{\mathrm{T}}\right] & \cdots & \mathbb{E}\left[x_M x_M^{\mathrm{T}}\right] \end{bmatrix}. \tag{F.2}$$

An alternative expression form of the (auto)correlation matrix is,

$$\mathbf{R}_{XX} = \mathbb{E}\left[\mathbf{X}\mathbf{X}^{\mathrm{H}}\right] \tag{F.3}$$

where $\mathbf{X}$ is the input signal vector: $\mathbf{X} = [x_1 \ldots x_M]^{\mathrm{T}}$, being the superscript $(\cdot)^{\mathrm{T}}$ a transpose operation.

Assuming each transmit signal is not correlated with each other, then their pairwise covariance is zero ($\mathbb{E}\left[x_i x_j^{\mathrm{T}}\right] = 0 \quad \forall\, i, j \mid i \neq j$). This makes $\mathbf{R}_{XX}$ further collapse to,

$$\mathbf{R}_{XX} = \begin{bmatrix} \mathbb{E}\left[|x_1|^2\right] & 0 & 0 & 0 \\ 0 & \mathbb{E}\left[|x_2|^2\right] & 0 & 0 \\ \vdots & \vdots & \ddots & \vdots \\ 0 & 0 & 0 & \mathbb{E}\left[|x_M|^2\right] \end{bmatrix}. \tag{F.4}$$

Uncorrelation can be achieved if the transmit signals are independent to each other since independence implies uncorrelation (although not the other way around). So in that case, we can be certain that $\mathbf{R}_{XX}$ can be written like in expression above (eq. F.4).

Finally, since $\mathbb{E}\left[|x_m|^2\right]$ is a measure of the power of the m$^{\text{th}}$ transmit signal, these terms can be rewritten as per the power of each transmit antenna according to the mean power of each transmit signal (also understood as the *assigned* power at each transmit antenna). And so,

$$\mathbf{R}_{XX} = \begin{bmatrix} P_1 & 0 & 0 & 0 \\ 0 & P_2 & 0 & 0 \\ \vdots & \vdots & \ddots & \vdots \\ 0 & 0 & 0 & P_M \end{bmatrix} \tag{F.5}$$

F.2 Designation

Throughout the project and according to the section above, the input autocovariance matrix may be interchangeably written like:

- $\mathbf{R}_{XX}$ (preferred)
- $\mathbf{C}_{XX}$

Otherwise, it may be interchangeably expressed like:

- Input (auto)covariance matrix (preferred) / (Auto)covariance matrix of the input signals. (preferred)
- Input (auto)correlation matrix (preferred) / (Auto)correlation matrix of the input signals. (preferred)

The word *auto* can be employed to stress that the covariance/correlation matrix is on the transmit signal vector $\mathbf{X}$ with itself.

Appendix G

NPCG validity confirmation as per key channel conditions. Upper and lower bounds.

The aim of this appendix is to provide with a brief proof of validity of the NPCG as an alternative metric to measure the evenness of the channel's eigenvalues in a Point-to-Point MIMO system when the number of antennas at the receiver is greater than two.
It is based on two key extreme channel situations, elaborated below.

G.1 All eigenvalues are equal: perfect channel conditioning. Lower bound

It is trivial to confirm that, if there is null eigenvalue spread ()all the eigenvalues have the same value, i.e. $\lambda_i = \lambda \, \forall \, i \in [1, ..., r_{\mathrm{H}}]$, then:

$$\begin{aligned} \mathrm{NPCG} &= 20 \cdot \log_{10} \left[\frac{r_{\mathrm{H}}}{\frac{\sum_{i=1}^{r_{\mathrm{H}}} \lambda_i}{\lambda_{\max}}} \right] \\ &= 20 \cdot \log_{10} \left[\frac{r_{\mathrm{H}}}{\frac{r_{\mathrm{H}} \cdot \lambda}{\lambda}} \right] \\ &= 20 \cdot \log_{10} \left[\frac{1}{1} \right] \\ &= 0 \text{ [dB]} \end{aligned} \tag{G.1}$$

G.2 Non-perfect channel conditioning.

If the conditioning is not perfect and the eigenchannels have a certain spread, then the sum at the denominator in expression eq. 7.13 on page 59 will be lesser than the rank:

$$\frac{\sum_{i=1}^{r_{\mathrm{H}}} \lambda_i}{\lambda_{\max}} < r_{\mathrm{H}}$$

And then:

$$\begin{aligned} \mathrm{NPCG} &> 20 \cdot \log_{10} \left[\frac{1}{1} \right] \\ &> 0 \text{ [dB]} \end{aligned} \tag{G.2}$$

G.3 Upper bound

Let all the eigenvalues apart from the first one be much lesser than the first one, so that

$$\frac{\sum_{i=2}^{r_{\mathrm{H}}} \lambda_i}{\lambda_{\max}} \ll 1$$

Then,

$$\frac{\sum_{i=1}^{r_{\mathrm{H}}} \lambda_i}{\lambda_{\max}} \approx 1$$

In this situation,

$$\begin{aligned} \mathrm{NPCG} &\approx 20 \cdot \log_{10}\left[\frac{r_{\mathrm{H}}}{1}\right] \\ &\approx 20 \cdot \log_{10}[r_{\mathrm{H}}] \;\; [\mathrm{dB}] \end{aligned} \tag{G.3}$$

Thus, the upper bound is constrained by the logarithmic expression of the channel rank seen above. Fig. G.1 features this upper bound graphically.

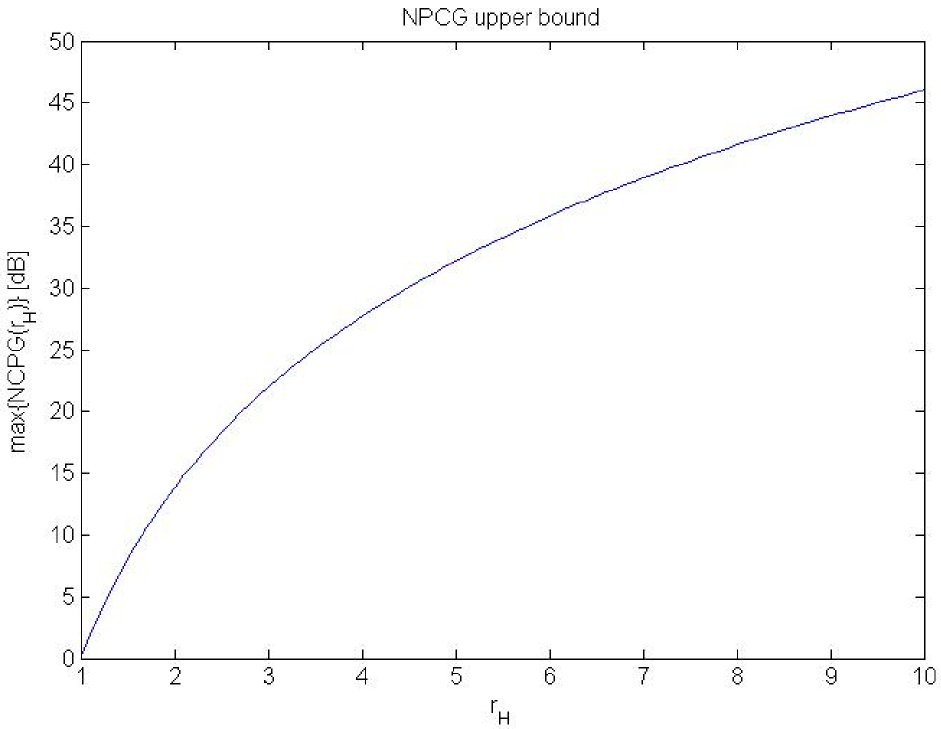

Figure G.1 *NPCG upper bound.*

Appendix **H**

Correlation Coefficient and Orthogonality

H.1 Correlation Coefficient

Assuming $\mathbf{H}_1$ and $\mathbf{H}_2$ are row vectors, i.e. each user has 1 antenna, let two users be defined each by the M-dimension channel vector, $\mathbf{H} = [h_1, h_2, \ldots, h_M]^T$.

The correlation coefficient, denoted by ρ, is given by,

$$\rho_{\mathbf{H}_1,\mathbf{H}_2} = \mathbb{E}\left[\left|\frac{(\mathbf{H}_1 - \mu_{\mathbf{H}_1}) \cdot (\mathbf{H}_2 - \mu_{\mathbf{H}_2})^{\mathrm{H}}}{\sqrt{\sigma^2_{\mathbf{H}_1}} \cdot \sqrt{\sigma^2_{\mathbf{H}_2}}}\right|\right] \quad [\cdot] \tag{H.1}$$

If $\mathbf{H}_1$ and $\mathbf{H}_2$ have $\rho_{\mathbf{H}_1,\mathbf{H}_2} \neq 0$, then $\mathbf{H}_1$ and $\mathbf{H}_2$ are said to be correlated [48]. If $\rho_{\mathbf{H}_1,\mathbf{H}_2} = 0$, then $\mathbf{H}_1$ and $\mathbf{H}_2$ are uncorrelated [48].

The correlation coefficient is a factor that provides information to which degree two random processes may be associated to eachother. That is, if the two channel vectors are positively correlated, if one experiences a fade, the effect will be incurred on the other.

In this situation, the correlation coefficient can be showed to yield the same results as Orthogonality. And as such, mainly orthogonality will be focused upon, throughout this study. This is because the main ambition is to determine how aligned two users are.

H.2 Orthogonality as a metric of User Separation

Orthogonality is a measure of alignment of two vectors. If two users, each with their own channel vector, are orthogonal, then these two users can be separated, and thus MF precoding can be utilized. However, if they are not orthogonal, MF will perform poorly, or in worst cases fail completely. Then ZF or MMSE must be applied.

Two users $\mathbf{H}_1$ and $\mathbf{H}_2$ are orthogonal to each other if,

$$\rho_{\perp} = \mathbb{E}\left[\frac{\left|\mathbf{H}_1 \cdot \mathbf{H}_2^{\mathrm{H}}\right|}{\sqrt{\|\mathbf{H}_1\|^2} \cdot \sqrt{\|\mathbf{H}_2\|^2}}\right] \quad [\cdot] \tag{H.2}$$

is 0.

H.3 Proof Orthogonality matches Correlation Coefficient

Using the case of the same two users given in sec. H.1, by expansion, eq. H.1 yields,

$$\rho = \mathbb{E}\left[\left|\frac{(\mathbf{H}_1 - \mu_{\mathbf{H}_1}) \cdot (\mathbf{H}_2 - \mu_{\mathbf{H}_2})^{\mathrm{H}}}{\sqrt{\mathbb{E}\left[(\mathbf{H}_1 - \mu_{\mathbf{H}_1}) \cdot (\mathbf{H}_1 - \mu_{\mathbf{H}_1})^{\mathrm{H}}\right]} \cdot \sqrt{\mathbb{E}\left[(\mathbf{H}_2 - \mu_{\mathbf{H}_2}) \cdot (\mathbf{H}_2 - \mu_{\mathbf{H}_2})^{\mathrm{H}}\right]}}\right|\right] \tag{H.3}$$

Assuming that $\mathbb{E}[\mathbf{H}_1] \approx \mathbb{E}[\mathbf{H}_2] \approx \mathbb{E}[\mathbf{H}] \approx \mathbf{0}$, then eq. H.3 can be reduced to

$$\rho = \mathbb{E}\left[\frac{|\mathbf{H}_1 \cdot \mathbf{H}_2^{\mathrm{H}}|}{\left|\sqrt{\mathbb{E}\left[\mathbf{H}_1 \cdot \mathbf{H}_1^{\mathrm{H}}\right]} \cdot \sqrt{\mathbb{E}\left[\mathbf{H}_2 \cdot \mathbf{H}_2^{\mathrm{H}}\right]}\right|}\right] \tag{H.4}$$

Eq. H.4 can be further reduced to equal the expression definition of Orthogonality in eq. H.2. For $\mathbf{H}_1$ (and, as well as $\mathbf{H}_2$) it can be written that,

$$\begin{aligned} \mathbb{E}\left[\mathbf{H}_1 \cdot \mathbf{H}_1^{\mathrm{H}}\right] &= \mathbb{E}\left[|h_1|^2 + \ldots + |h_i|^2 + \ldots + |h_M|^2\right] && \text{(H.5)} \\ &= \mathbb{E}\left[\sum_{i=1}^{M} |h_i|^2\right] && \text{(H.6)} \\ &= \mathbb{E}\left[\|\mathbf{H}_1\|^2\right]. && \text{(H.7)} \end{aligned}$$

To abstract from Free-space path loss (FSPL) the normalised channel matrix is applied, and as such the channel matrix will have a mean power or mean gain of 1. And so the following relation holds,

$$\mathbb{E}\left[\|\mathbf{H}_1\|^2\right] = \mathbb{E}\left[\mathbf{H}_1 \cdot \mathbf{H}_1^{\mathrm{H}}\right] = \|\mathbf{H}_1\|^2. \tag{H.8}$$

And using eqs. H.7 and H.8, Orthogonality and the Correlation coefficient can be directly related.

$$\begin{aligned} \rho_{\perp} &= \mathbb{E}\left[\frac{\left|\mathbf{H}_1 \cdot \mathbf{H}_2^{\mathrm{H}}\right|}{\sqrt{\|\mathbf{H}_1\|^2} \cdot \sqrt{\|\mathbf{H}_2\|^2}}\right] && \text{(H.9)} \\ &= \mathbb{E}\left[\left|\frac{(\mathbf{H}_1 - \mu_{\mathbf{H}_1}) \cdot (\mathbf{H}_2 - \mu_{\mathbf{H}_2})^{\mathrm{H}}}{\sqrt{\sigma_{\mathbf{H}_1}^2} \cdot \sqrt{\sigma_{\mathbf{H}_2}^2}}\right|\right] = \rho && \text{(H.10)} \end{aligned}$$

Resolvability in Far Field

This appendix is mainly based on Tse and Viswanath [25]. The transmitter side is the primary focus in this appendix, while the analysis is similar for the receiver side.

For an $N \times M$ MIMO scenario where both the transmitter and receiver are ULAs with M antennas at the transmitter, and N antennas at the receiver. Each antenna is distanced $d_{n,m}$ from eachother. This yields an $N \times M$ channel matrix $\mathbf{H}$ with channel terms,

$$h_{n,m} = a_{n,m} \cdot \mathrm{e}^{-\mathrm{j}kd_{n,m}} . \tag{I.1}$$

This is valid both in Near Field and in Far Field, as long as any delay is $\frac{d_{n,m}}{c} \ll W_{\mathrm{Tx}}^{-1}$. As the reference pair, $d_{1,1}$ is chosen, and so yields,

$$d_{1,1} = d. \tag{I.2}$$

The Far Field happens when,

$$d \gg D_{\mathrm{Tx}} \quad \text{and} \quad d \gg D_{\mathrm{Rx}}$$

where D_{Tx} and D_{Rx} are the aperture sizes at the transmitter and receiver, respectively. Applying the 1st order Far Field approximation, yields,

$$d_{n,m} = d \underbrace{-(m-1)\Delta_{\mathrm{Tx}}\lambda \cdot \cos(\phi_{\mathrm{Tx}})}_{\text{Projection of } \Delta_{\mathrm{Tx}}\lambda \text{ onto d}} \underbrace{+(n-1)\Delta_{\mathrm{Rx}}\lambda \cdot \cos(\phi_{\mathrm{Rx}})}_{\text{Projection of } \Delta_{\mathrm{Rx}}\lambda \text{ onto d}} \tag{I.3}$$

where Δ_{Tx} and Δ_{Rx} are inter element spacing at the transmitter and receiver, respectively, λ is wavelength, and ϕ_{Tx} and ϕ_{Rx} are the angles between transmitter and d, and receiver and d, respectively. This is envisioned as if all antennas at the transmitter and receiver are now aligned on the axis defines by d. And so, a final expression for $h_{n,m}$ can be written as,

$$h_{n,m} = a_{n,m} \cdot \mathrm{e}^{-\mathrm{j}kd_{n,m}} . \tag{I.4}$$

The factor $a_{n,m}$ is the attenuation of the path, and is assumed to be the same for all antenna pairs.

Inserting the Far Field approximation gives,

$$\begin{aligned} h_{n,m} &\cong a_{n,m} \cdot \mathrm{e}^{-\mathrm{j}kd_{n,m}} && \text{(I.5)} \\ &= a \cdot \mathrm{e}^{-\mathrm{j}k(d-(m-1)\Delta_{\mathrm{Tx}}\lambda \cdot \cos\phi_{\mathrm{Tx}} + (n-1)\Delta_{\mathrm{Rx}}\lambda \cdot \cos\phi_{\mathrm{Rx}})} && \text{(I.6)} \\ &= a \cdot \mathrm{e}^{-\mathrm{j}kd} \cdot \underbrace{\mathrm{e}^{\mathrm{j}2\pi(m-1)\Delta_{\mathrm{Tx}}\cos\phi_{\mathrm{Tx}}}}_{\mathbf{e}_{\mathrm{Tx}}(\Delta_{\mathrm{Tx}},\phi_{\mathrm{Tx}})} \cdot \underbrace{\mathrm{e}^{-\mathrm{j}2\pi(n-1)\Delta_{\mathrm{Rx}}\cos\phi_{\mathrm{Rx}}}}_{\mathbf{e}_{\mathrm{Rx}}(\Delta_{\mathrm{Rx}},\phi_{\mathrm{Rx}})} && \text{(I.7)} \end{aligned}$$

Since eq. I.7 is common for all $h_{n,m}$, then the channel matrix $\mathbf{H}$ can be written as,

$$\mathbf{H} = a\sqrt{N \cdot M} \cdot \mathrm{e}^{-\mathrm{j}kd} \cdot \mathbf{e}_{\mathrm{Rx}} \cdot \mathbf{e}_{\mathrm{Tx}}^{\mathrm{H}} \tag{I.8}$$

where,

$$\mathbf{e}_{\mathrm{Tx}}^{\mathrm{H}} = \begin{bmatrix} 1 \\ e^{-\mathrm{j}2\pi(1)\Delta_{\mathrm{Tx}}\cos\phi_{\mathrm{Tx}}} \\ \vdots \\ \mathrm{e}^{-\mathrm{j}2\pi(M-1)\Delta_{\mathrm{Tx}}\cos\phi_{\mathrm{Tx}}} \end{bmatrix}^{H} \quad \text{(I.9a)} \qquad \mathbf{e}_{\mathrm{Rx}} = \begin{bmatrix} 1 \\ e^{-\mathrm{j}2\pi(1)\Delta_{\mathrm{Rx}}\cos\phi_{\mathrm{Tx}}} \\ \vdots \\ \mathrm{e}^{-\mathrm{j}2\pi(N-1)\Delta_{\mathrm{Rx}}\cos\phi_{\mathrm{Tx}}} \end{bmatrix} \quad \text{(I.9b)}$$

The vectors $\mathbf{e}_{\mathrm{Tx}}$ and $\mathbf{e}_{\mathrm{Rx}}$ are steering vectors. The term $h_{n,m}$ is not a spatial signature, as this will always be columns of $\mathbf{H}$. Had this analysis been done for the receiver, $h_{n,m}$ would be spatial signatures.

Power gain will always be achieved. This is because of the projection of the transmitter and the receiver which allows the possiblity of signals being added in-phase, and further combining, constructively using MRC.

On the other hand, a DoF is not always achieved. However, if the aperture at the transmitter or the receiver is large enough, some DoF will be obtained, and thus a DoF gain. This happens because of the added angular resolvability a large aperture provides by making the elements of the arrays resolvable. This is normally not the case in the Far Field.

For a large enough D_{Rx}, projections on to d, at the receiver can no longer be applied, because of the high inaccuracy. Instead, there are now N d's ($d_{n,1}, n \in [1, \ldots, N]$). All M transmit antennas have to be projected on to each $d_{n,1}$ in order to compute $\mathbf{H}$. The channel is then described as,

$$\mathbf{H} = \begin{bmatrix} h_1 \\ h_2 \\ \vdots \\ h_n \\ \vdots \\ h_N \end{bmatrix} \tag{I.10}$$

where each term is defined as,

$$h_n = a_n \cdot \mathrm{e}^{-\mathrm{j}kd_{n,1}} \cdot \mathbf{e}_{\mathrm{Tx}}^{\mathrm{H}}. \tag{I.11}$$

The channel matrix, $\mathbf{H}$ is full rank, if is has distinct and linearly independant rows. This occurs when,

$$\cos(\phi_{\mathrm{Tx},n}) - \cos(\phi_{\mathrm{Tx},n'}) \neq 0 \bmod \frac{1}{\Delta_{\mathrm{Tx}}} \quad \forall[n, n'] \tag{I.12}$$

Alternatively, resolvability may be expressed as,

$$\cos(\phi_{\mathrm{Rx},n}) - \cos(\phi_{\mathrm{Rx},n'}) \gg \frac{1}{M \cdot \Delta_{\mathrm{Tx}}} \tag{I.13}$$

which is the same as,

$$D_{\mathrm{Tx}} \gg \lambda \cdot \frac{1}{\cos(\phi_{\mathrm{Tx},n}) - \cos(\phi_{\mathrm{Tx},n'})} \tag{I.14}$$

This interprets such as resolvability is possible when $\mathbf{H}$ is full rank, and when the aperture at the transmitter is very large, according eq. I.14.

I.1 Conditioning

Eventhough $\mathbf{H}$ is full rank, it may still happen that the channel matrix is ill-conditioned. This is measured by the angle between each pair of spatial signatures. While the spatial signatures are columns of $\mathbf{H}$, and for this analysis $\mathbf{H}$ only has one column, conditioning can still be understood as per the rows of $\mathbf{H}$.

Let ϵ be related to Angle of Departure (AOD) and be defined as,

$$\epsilon \equiv (\phi_{\mathrm{Tx},n}, \phi_{\mathrm{Tx},n'}) \tag{I.15}$$

The AOD is denoted as ϕ_{Tx}, and ϵ is the angular pair of the two largely separated receivers. AOD is known to be directly related to $\phi_{\mathrm{Tx},n}$ and $\phi_{\mathrm{Tx},n'}$, so if one of the angles changes, so the other, and therefore so does ϵ. For a given configuration of the transmitter array[1], then $|\cos(\epsilon)|$, will be periodic with $\cos(\phi_{\mathrm{Tx},n}) - \cos(\phi_{\mathrm{Tx},n'})$, and with period, $1/\Delta_{\mathrm{Tx}}$. Accordingly, for a given configuration, an expression for $\cos(\epsilon)$ for all $\cos(\phi_{\mathrm{Tx},n}) - \cos(\phi_{\mathrm{Tx},n'})$ can be given. This will be called Ω_{Tx}, and defined as,

$$\Omega_{\mathrm{Tx}} = \cos(\phi_{\mathrm{Tx},n}) - \cos(\phi_{\mathrm{Tx},n'}) \tag{I.16}$$

Per derivation it is then possible to write $\cos(\epsilon)$ as,

$$\cos(\epsilon) = \frac{1}{M} \cdot \mathrm{e}^{\mathrm{j}\pi\Delta_{\mathrm{Tx}}\Omega_{\mathrm{Tx}}(M-1)} \frac{\sin(\pi M \Delta_{\mathrm{Tx}}\Omega_{\mathrm{Tx}})}{\sin(\pi\Delta_{\mathrm{Tx}}\Omega_{\mathrm{Tx}})} \tag{I.17}$$

which may be rewritten as,

$$|\cos(\epsilon)| = \left| \frac{\sin(\pi M \Delta_{\mathrm{Tx}}\Omega_{\mathrm{Tx}})}{M \cdot \sin(\pi\Delta_{\mathrm{Tx}}\Omega_{\mathrm{Tx}})} \right| \tag{I.18}$$

Conditioning is given by $|\cos(\epsilon)|$. A channel is well-conditioned when $|\cos(\epsilon)| \neq 1$ and ill-conditioned when $|\cos(\epsilon)| \cong 1$.

By inspection, as Δ_{Tx} is large, eq. I.18 will be highly periodic, and more peaks will appear. Fig. I.1 shows $|\cos(\epsilon)|$ for different transmitter configurations. As the inter-element spacing,

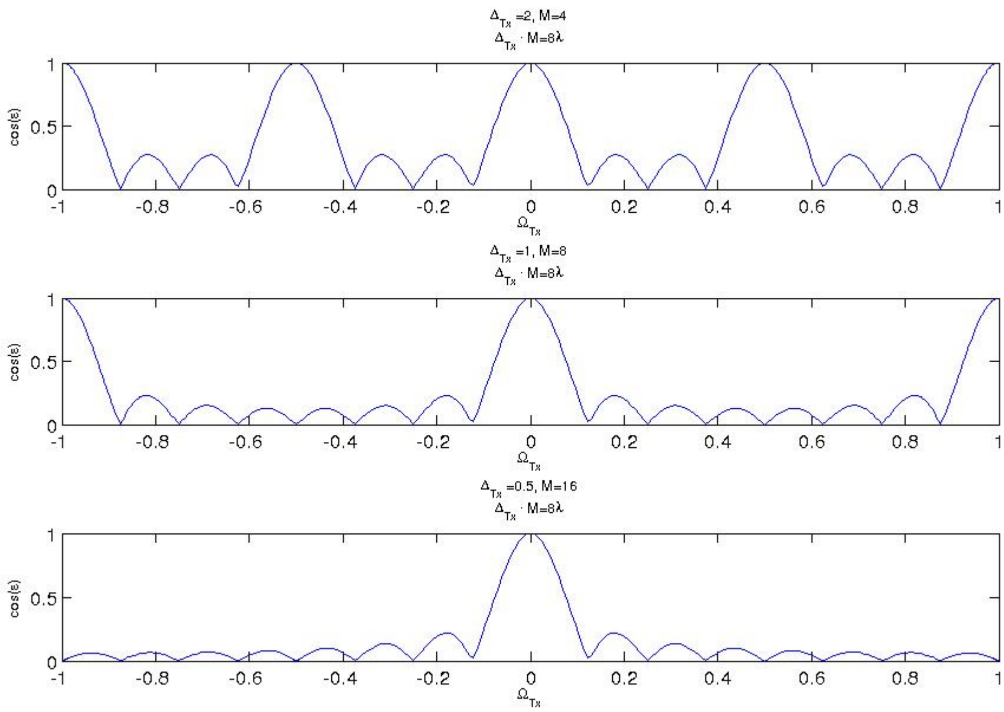

Figure I.1 *Angular periodicity for different transmitter configuration with same aperture. The figure shows for a fixed aperture size, as Δ_{Tx} increases, the angular resolvability decreases.*

Δ_{Tx} is high, more peaks appear.

[1] The configuration is defined by the number of elements, M, and the inter element spacing, Δ_{Tx}.

Appendix J

Definition of Root Mean Square Error (RMSE)

In linear regression, a frequently used meaure of the deviation of estimated data form observed data, is the Root Mean Square Error (RMSE). The RMSE measures the differences between observed data and estimated data based on some linear (or other) prediction model. Essentially, the RMSE can be viewed as the Root Mean Square (RMS) value of the error between observed and estimated data.

Let $\hat{\theta}$ be an estimator, providing estimates based on some model. The error of the estimator, may then be written as the difference $\theta - \hat{\theta}$. The RMS value hereof is then

$$\mathrm{RMSE}[\hat{\theta}] = \sqrt{\frac{1}{n}\sum_{i=1}^{n}\left(\theta_i - \hat{\theta}_i\right)^2} \tag{J.1}$$

If θ is a random variable, then eq. J.1 is,

$$\mathrm{RMSE}[\hat{\theta}] = \sqrt{\mathbb{E}\left[\left(\theta - \hat{\theta}\right)^2\right]} \tag{J.2}$$

where θ is observed measurements, $\hat{\theta}$ is the estimator, and $\mathbb{E}[\cdot]$ is the expectation operator. One remark is that the RMSE is equivalent to,

$$\mathrm{RMSE}[\hat{\theta}] = \sqrt{\sigma_{\hat{\theta}}^2 + \left[\mathrm{Bias}(\theta, \hat{\theta})\right]^2} \tag{J.3}$$

Eq. J.3 shows how the RMSE takes both the variance and the bias on the estimated data, into account.

Appendix **K**

Linear precoding matrix normalisation.

The aim of this appendix is to derive the normalisation factor introduced to adjust the precoding matrix when transmit linear beamforming assuming CSIT is applied, see chap. 9 on page 87.

K.1 Normalisation factor derivation.

The considered scenario contains K single-antenna (N=1) users, which are to be served simultaneously with an M antenna BS which applies transmit linear beamforming, or in other words a precoding matrix that was written like $\mathbf{W}$ in chap 9 on page 87. Fig. 10.2 on page 93 was included to graphically give account for this scenario. Let the following:

- $\mathbf{X} \in \mathbb{C}^{M\times 1}$ is the transmit signal vector.
- $\mathbf{W} \in \mathbb{C}^{M\times K}$ is the normalised precoding matrix.
- $\mathbf{F} \in \mathbb{C}^{M\times K}$ is the unnormalised precoding matrix. $\mathbf{W}$ and $\mathbf{F}$ are linked like this: $\mathbf{W} = \alpha_{\mathbf{F}} \cdot \mathbf{F}$.
- $\mathbf{q} \in \mathbb{C}^{K\times 1}$ is the set of symbols to be transmitted through the channel. It is assumed that
  (a) $\mathbb{E}\left[|q_k|^2\right] = 1\ [W]\ \forall\, k \in [1, \ldots, \mathrm{K}]$ and
  (b) that they are independent to each other.

The transmit power can be calculated like:

$$\mathbb{E}_{\mathbf{q}}\left\{\mathrm{Tr}\left[\mathbf{X}\mathbf{X}^{\mathrm{H}}\right]\right\} \tag{K.1}$$

where $\mathbb{E}_{\mathbf{q}}$ is the expected value operator with respect to the set of transmitted symbols $\mathbf{q}$ and tr [ ] is the trace operator.

If this expression is computed:

$$\begin{aligned}
\mathbb{E}_{\mathbf{q}}\left\{\mathrm{Tr}\left[\mathbf{X}\mathbf{X}^{\mathrm{H}}\right]\right\} &= \mathbb{E}_{\mathbf{q}}\left\{\mathrm{Tr}\left[\alpha_{\mathbf{F}}\mathbf{F}\mathbf{q}\left(\alpha_{\mathbf{F}}\mathbf{F}\mathbf{q}\right)^{\mathrm{H}}\right]\right\} \\
&= \mathbb{E}_{\mathbf{q}}\left\{\alpha_{\mathbf{F}}^2 \cdot \mathrm{Tr}\left[\mathbf{F}\mathbf{q}\mathbf{q}^{\mathrm{H}}\mathbf{F}^{\mathrm{H}}\right]\right\} \\
&= \alpha_{\mathbf{F}}^2 \cdot \mathrm{Tr}\left[\mathbf{F}\mathbb{E}_{\mathbf{q}}\left\{\mathbf{q}\mathbf{q}^{\mathrm{H}}\right\}\mathbf{F}^{\mathrm{H}}\right] \\
&= \text{given (a) and (b)} \\
&= \alpha_{\mathbf{F}}^2 \cdot \mathrm{Tr}\left[\mathbf{F}\mathbb{I}_{\mathrm{K}}\mathbf{F}^{\mathrm{H}}\right] \\
&= \alpha_{\mathbf{F}}^2 \cdot \mathrm{Tr}\left[\mathbf{F}\mathbf{F}^{\mathrm{H}}\right]
\end{aligned} \tag{K.2}$$

If there is a constraint on the maximum transmit power $\bar{\mathrm{P}}$ [W], then:

$$\begin{aligned} \mathbb{E}_{\mathbf{q}}\left\{\mathrm{Tr}\left[\mathbf{X}\mathbf{X}^{\mathrm{H}}\right]\right\} &= \alpha_{\mathbf{F}}^2 \cdot \mathrm{Tr}\left[\mathbf{F}\mathbf{F}^{\mathrm{H}}\right] \\ &\leq \bar{\mathrm{P}}\ [W] \end{aligned} \tag{K.3}$$

Finally, $\alpha_{\mathbf{F}}$ can be solved like this:

$$\alpha_{\mathbf{F}} \leq \frac{\sqrt{\bar{\mathrm{P}}}}{\sqrt{\mathrm{Tr}\left[\mathbf{F}\mathbf{F}^{\mathrm{H}}\right]}} \tag{K.4}$$